PROJECT MOHAVE
FINAL REPORT

March 19, 1999

PREPARED BY:

Marc Pitchford, Ph.D – National Oceanic and Atmospheric Administration
Mark Green, Ph.D and Hampden Kuhns, Ph.D – Desert Research Institute
Ivar Tombach Ph.D – Environmental Consultant
William Malm, Ph.D and Mark Scruggs, Ph.D – National Park Service
Robert Farber, Ph.D and Vince Mirabella – Southern California Edison Co.

WITH CONTRIBUTIONS FROM:

Warren White, Ph.D – Washington University
Charles McDade, Ph.D and Steven Heisler, Ph.D – ENSR Corp.
John Watson, Ph.D; Darko Koracin, Ph.D; Thomas Hoffer, Ph.D (retired), and Doug
        Lowenthal, Ph.D – Desert Research Institute
John Vimont, Ph.D and Kristy Gebhart – National Park Service
John Molenar, Ph.D – Air Resource Specialists
Ronald Henry, Ph.D – University of Southern California
Delbert Eatough, Ph.D – Brigham Young University
Prakash Karamchandani, Ph.D, Yang Zhang, Ph.D., and Christian Seigneur, Ph.D –
        Atmospheric and Environmental Research Inc.
Robert Eldred, Ph.D and Thomas Cahill, Ph.D – University of California at Davis
Pradeep Saxena, Ph.D and Mary Ann Allan – Electric Power Research Institute
Ted Yamada, Ph.D and Danny Lu, Ph.D, Yamada Science & Art Corporation (YSA)

Table of Contents

List of Figures

List of Tables

EXECUTIVE SUMMARY

Purpose

The purpose of this report is to communicate the consensus data interpretation of the principal partners in Project Measurement of Haze and Visual Effects (MOHAVE) concerning the nature, extent, and frequency of the contributions of the Mohave Power Project (MPP) and other sources to haze at the Grand Canyon National Park (GCNP). This executive summary focuses on the primary objective of determining MPP contributions. Th effects of other sources are addressed in the body of the report and in papers published by project investigators.

Introduction

Project MOHAVE was an extensive monitoring, modeling, and data assessment project designed to estimate the contributions of the MPP to haze at GCNP. The field study component of the project was conducted in 1992 and contained two intensive monitoring periods (~30 days in the winter and ~50 days in the summer). Unique, non-depositing, non-reactive perfluorocarbon tracer (PFT) materials were continuously released from the MPP stack during the two intensive periods to enable the tracking of emissions specifically from MPP. Tracer, ambient particulate composition, and SO_2 concentrations were measured at about 30 locations in a four-state region. Figure A is a map of the area showing the locations of MPP, GCNP, and the monitoring sites. Two of these monitoring sites, Hopi Point (HOPO) near the main visitor center at the south rim of the canyon and Meadview (MEAD) near the far western end of the national park were used as key receptor sites representative of GCNP.

Project MOHAVE operated under the joint technical and program management of the Environmental Protection Agency (EPA) and Southern California Edison (SCE) in close partnership with the National Park Service (NPS). Numerous other organizations contributed to the operations and assessment work of the project. Since the end of the field study component of the project, data assessment and modeling efforts were undertaken by the many participants and have led to numerous papers and reports. By design these efforts have been the products of their respective authors and have not been endorsed as findings of Project MOHAVE.

The process of identifying and quantifying the impact of MPP's emissions on Grand Canyon visibility was accomplished using two types of assessment methodologies. The first method, known as receptor modeling, is an empirical assessment of the extensive data collected during the study to estimate the MPP's presence and quantify the resulting atmospheric response, such as an increase in particulate sulfur, MPP tracer, or light scattering. The advantage of this method is that it provides a ground truth and answers the question: do the measurements confirm the presence of the MPP plume? The disadvantages of this method are that measurements cannot be collected everywhere all the time. The second method relies on the application of mathematical models to describe the transport and chemistry of MPP's emissions. Such models also make use of the measurements and can provide predictions at all locations for all times. However, they can provide highly uncertain results due to their lack of complete knowledge of the complex atmospheric transport, dispersion and chemical processes involved in the formation of visibility-
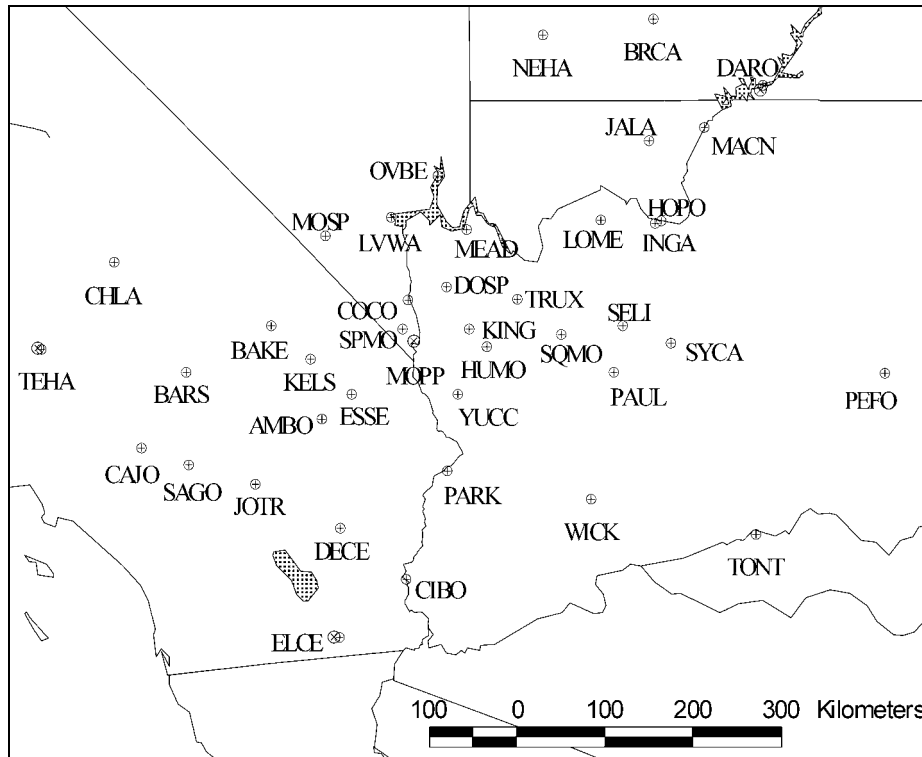
Figure A Project MOHAVE Site Map

Abbreviation	Location	Abbreviation	Location
AMBO	Amboy	LVWA	Las Vegas Wash
BAKE	Baker	MACN	Marble Canyon
BARS	Barstow	MEAD	Meadview
BRCA	Bryce Canyon	MOPP	Mohave Power Plant
CAJO	Cajon Pass	MOSP	Mountain Springs Summit
CHLA	China Lake/Ridgecrest	NEHA	New Harmony
CIBO	Cibola National Wildlife Refuge	OVBE	Overton Beach
COCO	Cottonwood Cove	PARK	Parker
DARO	Dangling Rope	PAUL	Paulden
DECE	Desert Center	PEFO	Petrified Forest National Park
DOSP	Dolan Springs	SAGO	San Gorgonio
ELCE	El Centro	SELI	Seligman
ESSE	Essex	SPMO	Spirit Mountain
HOPO	Hopi Point	SQMO	Squaw Mountain
HUMO	Hualapi Mountain	SYCA	Sycamore Canyon
INGA	Indian Gardens	TEHA	Tehachapi Summit
JALA	Jacob Lake	TONT	Tonto Natational Forest
JOTR	Joshua Tree	TRUX	Truxton
KELS	Kelso	WICK	Wickenburg
KING	Kingman	YUCC	Yucca
LOME	Long Mesa		

impairing aerosols. The summary below examines the results from both of the methodologies discussed above.

Many of the early efforts to estimate the contribution of MPP to haze at GCNP using various models of both types were done prior to the release of the tracer measurement data. This was done to provide a blind method to examine the accuracy of the assessment methods by comparing each method's estimate of tracer concentrations to measurement data at one or both key receptor sites. Correlations between measured tracer concentrations and predicted tracer

concentrations from the original assessments were poor indicating that the initial models could not be used to estimate the MPP impact.

Correlations between measured tracer concentration and both particulate sulfur and light extinction were virtually nil. While this suggests that MPP was not responsible for the majority of visibility impairment at Meadview, it does not indicate that MPP had no impact on visibility in the area. In order to better resolve MPP's contribution to haze at GCNP, a second round of assessments using new and more refined methods was initiated. Most of these methods used the PFT information in their analyses. This report focuses on the results of this second round of assessment methods. These methods are briefly described in Table A. Each of these methods estimates the MPP contribution to sulfate concentrations at one or both of the key receptor sites on a 12-hour or 24-hour basis corresponding to the sample periods for the particulate sample duration (0700 to 1900 MST and 1900 to 0700 MST).

Two of the assessment methods were used solely to estimate bounds between which the actual MPP contributions might lie. The Tracer Max method indicates the absolute maximum contribution of MPP that is physically possible, although such an impact is not considered reasonable. The CALPUFF model was used in two bounding modes – CALPUFF Dry was used to calculate the amount of sulfate attributable to MPP if only the relatively slow gas phase conversion of SO_2 to sulfate took place, while CALPUFF Wet was used to approximate the MPP contribution if every day included 3 hours of in-cloud aqueous conversion at a rate of 20%/hr. By and large the results of the other modeling calculations tended to lie somewhere between those of CALPUFF Dry and CALPUFF Wet.

The results of the various methods have been assessed for reasonableness. For example, the amount of particulate sulfate from MPP should not exceed the total measured amount of sulfate, nor should it exceed an amount corresponding to 100% conversion and no deposition of the MPP SO_2 as determined from the measured tracer concentration (i.e., the Tracer Max calculation). Implicit in the results shown below is the assumption that tracer data are well measured (i.e. with good precision and accuracy) and truly represent the transport and dispersion of the MPP effluent. Collocated precision of the MPP tracer concentrations at Meadview was 7% of the average tracer concentration during the summer period. All of the second round methods with results summarized below have used the tracer concentration data either directly as input or indirectly to optimize or calibrate some aspect of the method.

Findings

Findings below are presented in bullet form and organized into two major categories: overview and specific findings. The overview includes a description of conditions required for MPP visibility impacts at GCNP and describes the process used to generate specific findings. The specific findings contain summaries of the MPP contributions to 12- and 24-hour particulate sulfate, MPP contribution to 12- and 24-hour extinction coefficient, and extrapolation to short-term MPP impacts during the two seasonal intensive monitoring periods and for other times of the year.

Table A Methods Used to Estimate Source Contributions

Method	Description	Inputs	Outputs
Receptor Data Analyses			
Tracer Max (Tracer Scaling)	Estimation of total sulfur impacts by scaling PFT measurements; provides upper bound for potential sulfate impacts	PFT, SO_2, and particulate S concentrations at receptors; emission ratio of SO_2/PFT;	Contribution of PFT source to ambient S; upper bound estimate of contribution to particulate S
Exploratory Data Analysis	Statistical analysis of SO_2, particulate sulfur, and PFT measurements	PFT, SO_2, and particulate S concentrations, and b_{sp} at receptors	Spatial correlations of particulate sulfur, temporal correlations of PFT, SO_2, and particulate S at specific sites
Tracer Regression	Regression of b_{ext} against PFT, industrial methylchloroform, and water vapor mixing ratio	PFT, methylchloroform, and mixing ratio measurements at receptors	Contributions to b_{ext} from emissions in source regions of the chosen tracers
TAGIT	Estimation of sulfate impact by identifying unimpacted sites from PFT measurements	PFT, SO_2, and particulate S concentrations at multiple receptors	SO_2 and particulate S concentrations attributable to sources/source regions where PFT was emitted
Modified CMB	Chemical mass balance receptor modeling, modified to account for conversion and deposition of SO_2 and sulfate	Source/source-regions and receptor concentrations of SO_2, sulfate, and markers -- elements, spherical aluminosilicate, b_{abs}; relative times of travel; ROME estimates of relative conversion rates for emissions from different sources/source-regions.	SO_x and sulfate attributable to sources/source- regions
TMBR	Tracer mass balance regressions of SO_2 against PFT and of particulate S against PFT	Concentrations at receptors of PFT, SO_2, and particulate sulfur	SO_2 and particulate S concentrations attributable to MPP
DMBR	Differential mass balance regression; hybrid of tracer-based dilution calculation with parameterized deposition and conversion	Concentrations at receptors of PFT and SO_2; times of travel from source to receptors; estimates of conversion rates; index of cloud cover	SO_2 and particulate S concentrations attributable to MPP
Source Emissions Simulations			
HAZEPUFF (Modified)	Lagrangian puff model; interpolated wind field; first order sulfate chemistry; modified dispersion classes	Wind profiler soundings, PFT and SO_2 emissions from MPP, relative humidity	Plume locations and concentrations of PFT, SO_2, sulfate, and light scattering attributable to MPP
CALPUFF/ CALMET	Multi-layer Gaussian puff model with parameterized first order chemical conversion; diagnostic meteorological model	Surface and upper air meteorological data, topography, PFT and SO_2 emissions from MPP, solar radiation, ambient O_3	Distribution of concentrations of PFT, SO_2 and sulfate attributable to MPP
ROME/ RAPTAD/ HOTMAC	Lagrangian plume model with explicit reaction chemistry; three-dimensional Lagrangian random puff dispersion; primitive equation meteorological model	Meteorological soundings, topography and land use, solar radiation; MPP emissions of PFT, SO_2, NO_x, and trace metals; background chemical concentrations; PFT concentrations at receptors	Concentrations of PFT, SO_2 and sulfate in MPP plume, at surface and aloft

Overview

- From a meteorological, visibility, and sulfate concentration perspective, the Project MOHAVE study year (1992) is representative of longer periods of record. Minor exceptions to that statement include that the winter of 1992 was somewhat more moist (clouds and precipitation) than the 15 year average; the summer of 1992 was one of the cleaner summers

on record at Hopi Point with less severe conditions for the poor visibility periods; Meadview summer 1992 sulfate concentrations were comparable to summer sulfate levels during the 5-year SCENES monitoring period (1984 - 1989).

- Based on climate records, MPP emissions are usually transported towards the western end of GCNP by wind flow from the south in the summer (April through September) and away from GCNP by flow from the north in the winter (November through February). These wind patterns also cause flow of emissions towards GCNP from source areas to the southwest in the summer such as Southern California, northern Mexico, and the San Joaquin Valley and from sources to the northeast in the winter such as the Navajo Generating Station.

- PFT released from MPP during the winter and summer intensive monitoring periods corroborated the earlier finding that the greatest frequency of transport from MPP to GCNP was during the summer.

- During the summer intensive monitoring period, sites around Lake Mead (Meadview, Overton Beach, and Las Vegas Wash) recorded tracer concentrations above background levels on over 90% of the days; at Hopi Point, tracer was above background concentrations on about half of the days.

- During the winter intensive monitoring period, Meadview recorded MPP tracer concentrations above background levels during about 6% of the days; at Hopi Point, MPP tracer concentration were never measured above background levels.

- Project MOHAVE analysts found negligible correlation between measured MPP tracer concentrations and visibility impairment at Meadview or Hopi Point. The absence of any obvious relationship cannot rule out MPP contributions to haze in GCNP, but strongly suggests that other sources were primarily responsible for the haze.

- Other analyses (summarized in the body of the report), done as part of Project MOHAVE, show that during the summer intensive period there was clear observational evidence linking emissions from distant urban areas such as Southern California to visual impairment at GCNP. These analyses corroborate earlier findings by other investigators who have used techniques designed to specifically identify the presence of the Southern California emission plume.

- From the tracer data and the known ratio of tracer to primary particle emission rates during normal operations of MPP, primary particles from MPP disperse during transport to GCNP to the extent that though they contribute to visibility impacts they alone would not cause noticeable impairment.

- From the tracer data and the known ratio of tracer to SO_2 emission rates for MPP, SO_2 emitted by MPP often reaches Meadview in sufficiently high concentrations to have the potential to cause impairment (See Tracer Max in Table A). Thus, the critical factor in determining the impact of MPP is knowledge of the particulate sulfate production in the atmosphere by conversion of SO_2.

Technical Note - Conversion of SO_2 to sulfate occurs by two different mechanisms: dry or gas-phase chemistry and wet or aqueous-phase chemistry. The rate of dry conversion is slow and greatest during the daylight hours. Wet chemistry is relatively fast but its occurrence is harder to predict since it requires interaction of the SO_2 emissions with liquid water (e.g., in hygroscopic aerosols or cloud droplets) and the presence of oxidants to convert the SO_2 in the liquid phase.

- Project MOHAVE employed a number of methodologies (Table A) to estimate the contribution of MPP to particulate sulfate. With two exceptions (TMBR and TAGIT), these methods had to explicitly determine or use assumed rates of SO_2 to sulfate conversion for each time period during transport from MPP to GCNP. Much of the difference between the various methods is due to the differences in the predicted magnitudes of conversion that derive from assumptions concerning the interactions between emissions and clouds and calculations of emission travel times.

- The various methods do not agree unanimously on which are the most MPP-influenced time periods. The TAGIT method in particular identifies several high impact days that have low estimated MPP impact based upon other methods. The opposite is also true. While logic dictates that not all of the methods can be correct when there are substantial disagreements, there is no consensus concerning which of the methods is more likely to be correct for any particular time period. For these reasons the results from any specific method on any specific date are not ascribed substantial credibility.

- When the results from each of the various methods are sorted by magnitude of MPP impact, the resulting frequency distributions are similar. In other words the various methods tend to agree better concerning the magnitude of a typical MPP contribution (i.e. median or 50th percentile) and for a greater MPP contribution (defined for this report as the 90th percentile) than they do concerning the magnitude for any specific date in 1992. Thus, in order to interpret the attribution results, this report focuses on the range of results for typical and greater MPP contributions as defined by the 50th and 90th percentiles of the frequency distributions of the various methods, while recognizing that such a focus hides the lack of day-to-day agreement between the methods.

- All of the assessment methods except for TAGIT are able to estimate 12-hour MPP particulate sulfate concentrations corresponding to the sample periods at Meadview and Hopi Point. TAGIT is restricted to results for 24-hour duration, corresponding to two sample periods. The relative magnitude of the estimated MPP sulfate is easily determined by dividing the estimated sulfate by the coincident measured total sulfate.

Technical Note - Light extinction coefficient, an optical parameter that increases as visual range decreases and is related to the particulate concentration, is used to quantify visibility in this assessment. The higher the fractional contribution of an emission source to light extinction coefficient the greater is its visibility impact. A CD-ROM with viewing software and computer simulated views is provided with this report to illustrate the appearance of the magnitudes of changes reported in the tables below.

- Estimated relative MPP contribution to the light extinction coefficient was determined by two methods. In both, the first step was to convert each estimated MPP sulfate concentration to a light extinction coefficient value. Based on theoretical analyses of Project MOHAVE measurements, a sulfate extinction efficiency was derived specifically for the sulfate aerosol in the study area. In one method the results of the first step were divided by the corresponding measured light extinction coefficient values, while in the other they were divided by the typically somewhat smaller calculated extinction coefficient values determined from the measured aerosol composition data.[1] In all cases the effects of relative humidity on aerosol size are included in the calculations.

- A number of approaches were used to estimate the ratio of the highest short-term (e.g. 3-hour duration) to 12- or 24-hour duration relative extinction coefficient impacts in order to estimate the short-term impacts. Some of the methods used a limited data set of high time resolution tracer data measured at Meadview, others used the hourly estimated concentrations from the air quality models (e.g. CALPUFF).

- To examine the issue of impacts during the non-intensive monitoring periods, one of the apportionment methods (CALPUFF Dry) that can be implemented without the use of tracer data was used to estimate the particulate sulfate and fraction of extinction coefficient for other times of the year. Ratios of these estimates to corresponding estimates for the months containing the summer intensive period are used to assess the relative importance of MPP during other times of the year.

- One of the most interesting periods during the summer of 1992 was the two days following the discontinuation of tracer release from MPP at 0700 on August 31. Although visibility levels were not unusual, the first two days in September had the highest sulfate measurements recorded throughout the area that summer and represent some of the highest measurements ever made in the area. Winds were light and variable with flow reversals that could have increased the opportunity for SO_2 to sulfate conversion. Because of the lack of tracer data, only a few methods could be used to estimate the contribution of MPP. These are considered to have greater uncertainty than for periods with tracer data and are not included in the specific findings presented below. Some of the results of these showed relatively high MPP contribution to sulfate. However, there are alternative explanations that would indicate other sources are responsible for much of the measured sulfate.

Specific Findings

- The range of estimates by the various methods of MPP sulfate at Meadview and Hopi Point for the summer and winter at the 50th and 90th percentile are shown in Table B for the 12-hour time periods.

---

[1] The calculated extinctions did not match the measurements at times, and so both calculations are shown here.

Table B Range of estimated 12-hour MPP sulfate (ng/m^3) for the 50th and 90th percentile conditions. Model attribution results excluding the bounding estimates of CALPUFF Wet and Dry are shown in bold. Values in parentheses represent the ranges of all attribution results.

	Winter		Summer	
	50th	90th	50th	90th
Meadview	(0.0 to 0.0)	**40** (5 to 50)	**23** to **71** (23 to 93)	**120** to **320** (120 to 540)
Hopi Point	(0.0 to 0.0)	(0.0 to 0.0)	**4** to **27**	**38** to **160**

- Dividing each estimate of MPP sulfate by the measured coincident sulfate results in values shown in Table C that express the range of estimated percent of 12-hour sulfate contributed by MPP at key sites.

Table C Range of estimated 12-hour MPP fraction of measured sulfate (%) for the 50th and 90th percentile conditions. Model attribution results excluding the bounding estimates of CALPUFF Wet and Dry are shown in bold. Values in parentheses represent the ranges of all attribution results.

	Winter		Summer	
	50th	90th	50th	90th
Meadview	(0.0 to 0.0)	**3.5** (0.7 to 4.8)	**1.7** to **3.3** (1.7 to 8.0)	**8.7** to **21** (8.7 to 42)
Hopi Point	(0.0 to 0.0)	(0.0 to 0.0)	**0.4** to **1.6**	**3.1** to **13**

- Converting the 12-hour MPP sulfate estimates to light extinction coefficient and dividing by the coincident measured light extinction coefficient produces the results shown in Table D.

Table D Range of estimated 12-hour MPP fraction (%) of measured light extinction coefficient for the 50th and 90th percentile conditions. Model attribution results excluding the bounding estimates of CALPUFF Wet and Dry are shown in bold. Values in parentheses represent the ranges of all attribution results.

	Winter		Summer	
	50th	90th	50th	90th
Meadview	(0.0 to 0.0)	**0.1** (0.06 to 0.4)	**0.2** to **0.6** (0.2 to 1.0)	**1.3** to **2.8** (1.3 to 5.0)
Hopi Point	(0.0 to 0.0)	(0.0 to 0.0)	**0.1** to **0.4**	**0.5** to **2.6**

- If instead of dividing by the measured extinction coefficient, the estimated MPP light extinction were divided by the somewhat smaller calculated extinction coefficient, the range of values shown in Table E would result.

Table E Range of estimated 12-hour MPP fraction (%) of calculated light extinction coefficient for the 50th and 90th percentile conditions. Model attribution results excluding the bounding estimates of CALPUFF Wet and Dry are shown in bold. Values in parentheses represent the ranges of all attribution results.

	Winter		Summer	
	50th	90th	50th	90th
Meadview	(0.0 to 0.0)	**0.2** (0.1 to 0.4)	**0.3** to **0.8** (0.3 to 1.2)	**1.9** to **4.0** (1.9 to 6.7)
Hopi Point	(0.0 to 0.0)	(0.0 to 0.0)	**0.1** to **0.3**	**0.6** to **2.3**

- One of the methods (TAGIT) could only estimate the MPP contribution on a 24-hour basis. By averaging the 12-hour contributions of the various methods to 24-hour, results of all methods can be used together to estimate the 24-hour MPP contribution to extinction

coefficient. Table F contains the 24-hour average range of estimated MPP extinction coefficient percent of the coincident measured extinction coefficient.

Table F Range of estimated 24-hour MPP fraction (%) of measured light extinction coefficient for the 50th and 90th percentile conditions. Model attribution results excluding the bounding estimates of CALPUFF Wet and Dry are shown in bold. Values in parentheses represent the ranges of all attribution results.

	Winter		Summer	
	50th	90th	50th	90th
Meadview	(0.0 to 0.0)	**0.0** to **0.4**	**0.3** to **0.6** (0.3 to 1.5)	**0.9** to **3.5** (0.9 to 4.8)
Hopi Point	(0.0 to 0.0)	(0.0 to 0.0)	**0.0** to **0.4**	**1.1** to **5.3**[2]

- To examine the relative impacts of MPP on particulate sulfate during non-intensive monitoring periods, MPP estimated sulfate by one of the methods (CALPUFF Dry) which requires only the upper air measurements made at MPP (available from January to September 1992) were compared with corresponding estimates from the same method during the summer intensive period. Table G shows the ratio of the estimates for pairs of month compared to the July and August period that includes the summer intensive.

Table G Ratio of CALPUFF Dry estimated MPP 12-hour sulfate values for 50th and 90th percentile conditions for months not during the intensive monitoring period to corresponding values estimated for July and August.

	January & February		March & April		May & June	
	50th	90th	50th	90th	50th	90th
Meadview	0.0	0.2	0.5	0.8	0.4	0.6

- A similar approach is used to examine the relative impacts of MPP on extinction coefficient during non-intensive monitoring periods. Ratios of the CALPUFF dry estimates of the MPP fractional extinction coefficient for pairs of months to the July and August period that includes the summer intensive are shown in Table H.

Table H Ratio of CALPUFF Dry estimated 12-hour MPP fraction of the light extinction coefficient values for 50th and 90th percentile conditions for months not during the intensive monitoring period to corresponding values estimated for July and August.

	January & February		March & April		May & June	
	50th	90th	50th	90th	50th	90th
Meadview	0.0	0.5	0.7	0.9	0.4	0.7

- The previous two tables show that the CALPUFF estimated MPP contribution of sulfate and fraction of measured light extinction coefficient for March and April 1992 are nearly comparable to the CALPUFF estimated MPP contributions for the summer intensive period (i.e., ratios near 1). Note that because there is no tracer or 12-hour sulfate data during the intervening time periods with which to compare model predictions, the results shown in the last two tables should be treated with caution.

---

[2] The author of the method (TAGIT) that produced this result believes that it has substantial uncertainty as applied to MPP impacts at Hopi Point. The value associated with the next highest method for the 90th percentile is 2.5%, which seems to be a more reasonable upper limit.

- Though results of the various methods to estimate the daily short-term impacts from the 12- or 24-hour average impacts included substantial uncertainties, a ratio of about 2 seems to be a reasonable consensus value at Meadview for periods of greatest MPP impacts. In other words the maximum short-term impacts on any day at the 90th percentile are thought to be about a factor of two higher than the longer-term impacts listed in the tables above for Meadview.

- Some idea of the potential for extreme impacts, beyond the 90th percentiles shown in Table D and Table E above, can be obtained from the greatest individual-day MPP attributions generated over the entire tracer period. The study-maximum estimated MPP contribution to Meadview light extinction during an individual 12-hour monitoring period was from about 2.5% to 8%, depending on the estimation method, with bounding values between 2.5% and 16%. This wide range of estimates underscores the fact that the disagreement among estimates was greatest when estimating infrequent conditions such as those that occur less than 10% of the time.

- The range of 90th percentile values is less than, and therefore consistent with, results of the Tracer Max method that yields an absolute upper bound obtained from the measured tracer concentrations. This method makes the assumption that all of the MPP sulfur emitted is converted to sulfate without depositional loss of either sulfur dioxide or sulfate during transport to Meadview. The approach eliminates any possibility of underestimation (see Tracer Max in Table A). The greatest possible 12-hour impact by this method is about 23%, which is necessarily an overestimate of the greatest actual MPP contribution to Meadview light extinction during the Project MOHAVE tracer period.

- Several different models with their related assumptions were used in this study. There is general agreement among them about the ranges of impacts that may occur 90% of the time. There is less agreement however, about less frequent high-impact events (which occur less than 10% of the time). In any case, empirical data (actual field measurements) show poor correlation between the presence of MPP tracer and visibility impairment in the GCNP. Project MOHAVE analysts were unable to find any data to directly corroborate the extreme values calculated by some of the models, as noted in the results tabulated above.

1. Introduction

Project MOHAVE (<u>M</u>easurement <u>of</u> <u>H</u>aze <u>a</u>nd <u>V</u>isual <u>E</u>ffects) was a source attribution monitoring study designed to determine the contribution of emissions from the Mohave Power Project (MPP) to light extinction at the Grand Canyon National Park (GCNP). Experiments took place throughout 1992 in the southwestern United States and included the release and measurement of perfluorocarbon tracer emitted from MPP. The study was principally funded by the United States Environmental Protection Agency (EPA), the National Park Service (NPS), and Southern California Edison (SCE). This report summarizes the findings of Project MOHAVE.

1.1 Background

In 1977, in Section 169A of the Clean Air Act, Congress set as a national goal, "the prevention of any future and the remedying of any existing impairment of visibility in mandatory Class 1 Federal areas which results from manmade air pollution." Section 169A also required EPA to promulgate regulations to assure reasonable progress toward meeting the national goal for mandatory Class 1 areas where visibility is an important air quality related value. On November 20, 1979, EPA identified 156 areas, including GCNP, where visibility is an important air quality related value. On December 2, 1980, EPA promulgated regulations for managing impairment caused by a single source or a small group of sources.

In 1990, Congress reaffirmed its continuing desire to address visibility issues by adding section 169B to the Clean Air Act. Section 169B, which addresses regional haze, calls for a research program to study regional haze, and required the Administrator of EPA to establish a visibility transport commission for the region affecting the visibility in GCNP.

In January and February, 1987, the NPS, acting in its capacity as the federal land manager for GCNP, conducted a study known as the Winter Haze Intensive Tracer Experiment (WHITEX). WHITEX involved a six-week long intensive monitoring period during which an artificial tracer was released from the Navajo Generating Station (NGS) northeast of GCNP (Malm et al., 1989a). National Park Service analysis of optical, air quality, and meteorological data indicated a significant fraction of the haze in GCNP during this time period was due to sulfates resulting from NGS emissions.

Salt River Project (SRP), the operators of NGS conducted a study during early 1990. The SRP study also indicated a contribution of NGS emissions to haze in GCNP, but at a lower frequency of occurrence. A difference in prevailing meteorological conditions during the years of the NPS and SRP studies would at least partially account for the differences in magnitude and frequency of impacts identified by the two studies.

Based on these studies and additional evidence presented, EPA required substantial reduction of sulfur dioxide emissions from NGS. SRP has begun installing scrubbers on NGS and will complete the installation in 1999. While NGS has been linked to a portion of the haze at GCNP, it is generally recognized that a number of other area and point sources also contribute to haze at GCNP. One potential source is the MPP, a 1580 megawatt, coal-fired steam electric power plant located in Laughlin, Nevada, southwest of GCNP and operated by the SCE. MPP burns low sulfur (0.5% by weight) western coal and has no additional pollution control equipment for

sulfur dioxide. Congress, desirous of additional information concerning the sources of visibility impairment in GCNP, added $2.5 million to the fiscal 1991 appropriation for EPA to conduct "a pollution tracer study at the Mohave Power Plant." Project MOHAVE is EPA's response to the congressional mandate.

Shortly afterwards, Congress created the Grand Canyon Visibility Transport Commission (GCVTC) to advise the U.S. Environmental Protection Agency on comprehensive strategies for protecting visual air quality at national parks and wilderness areas on the Colorado Plateau. The Commission strongly encouraged the EPA to complete Project MOHAVE and to take action consistent with the results of that study within twelve months of its completion (Mathai, 1995).

A brief description of the previous visibility studies relevant to GCNP and how they led to the design of Project MOHAVE follows.

Outage Studies: MPP was inoperable for the seven month period June through December, 1985. The effect of this outage was examined by Murray et al. (1990), using 1984-1987 SCENES data from Spirit Mountain, Meadview, and Hopi Point. The authors concluded that the average relative contribution of MPP to sulfate at Meadview was less than 15%. Using a similar technique, the daily sulfate concentrations at Spirit Mountain and Meadview were compared with MPP power load over the full range of power output (Switzer et al., 1995). The frequency distribution of sulfate at Meadview did not change discernibly based on the power output of MPP. These studies indicated that a source attribution study for MPP would need to be sufficiently precise to resolve a small sulfate signal (<15%) in a variable background.

WHITEX: This study was designed to evaluate the feasibility of attributing single point source emissions to visibility impairment in GCNP. WHITEX was conducted during a six week period in January and February 1987. During this time, an artificial tracer, deuterated methane (CD_4), was released from the NGS at Page, AZ near the eastern end of the Grand Canyon. Aerosol, optical, tracer, and other properties were measured at Hopi Point (on the south rim of the Grand Canyon) and other locations. Using the tracer, 70 to 80% of the sulfate at Hopi Point under certain meteorological conditions in the winter was attributed to the NGS (Malm et al., 1989b). Some controversy arose from this attribution since the ratio of the CD_4 emissions rate to power plant load was not maintained at a stable value (Markowski, 1992). In addition, while the measurement of CD_4 concentrations is quite precise, the analytical costs are high. As a result, only a fraction of the samples collected were ever analyzed. WHITEX demonstrated the potential of tracer techniques for single source attribution. The study also showed that maintaining a stable tracer/power load emission ratio and using a low cost tracer analytical technique could improve the quality of the source attribution.

NGS Visibility Study: The NGS Visibility Study was conducted by the SRP, the operators of NGS, from January 10 through March 31, 1990. Its purpose was to address visibility impairment in GCNP during the winter months and the levels of improvement that might be achieved if SO_2 emissions from NGS were reduced. The study was performed to provide input to the rulemaking process of the EPA regarding NGS SO_2 controls (Richards et al., 1991). Perfluorocarbon tracers (PFT) were released from the three stacks of NGS. Surface and upper air meteorology, particle and gaseous components, and tracer were measured at many sites. The study concluded that the NGS plume was not present at Hopi Point for most of the days. The tracer data quality from this

experiment was insufficient for quantitative source apportionment and the results emphasized the need for better tracer measurements in future studies.

1.2 Project MOHAVE Goals and Objectives

The primary goal of Project MOHAVE is to determine the contribution of the MPP emissions to haze at GCNP and other nearby mandatory Class I areas where visibility is an important air quality related value. This implies a quantitative evaluation of the intensity, spatial extent, frequency, duration and perceptibility of the MPP contribution. The improvement in visibility that would result from control of MPP emissions is included in the primary goal. Secondary goals include an increased knowledge of the contributions of other sources to haze in GCNP and the southwestern United States in general. Because knowledge of regional transport and air quality levels is necessary to separate the effect of MPP from other sources, meeting the primary goal will result in increased knowledge about the impacts from other sources.

These goals are to be attained by completing the following specific objectives:

1. Evaluate the measurements for applicability to modeling and data analysis activities.
2. Describe the visibility, air quality and meteorology during the field study period and to determine the degree to which these measurements represent typical visibility events at the Grand Canyon.
3. Further develop conceptual models of physical and chemical processes which affect visibility impairment at the Grand Canyon.
4. Estimate the contributions from different emissions sources to visibility impairment at the Grand Canyon, and quantitatively evaluate the uncertainties of those estimates.
5. Reconcile different scientific interpretations of the same data and present this reconciliation to policy-makers.

1.3 Guide to Report

The report is divided into 10 sections. This section states the background and objectives of Project MOHAVE. Section 2 describes the study area including the land use, topographical, and meteorological issues that are important to the study. The types of measurements performed as part of the study are documented in Section 3. Section 4 reviews the data quality of these measurements. Section 5 describes the spatial and temporal behavior of light extinction and its components over the study area. Section 6 relates light extinction to airborne chemical composition throughout the region. Section 7 compares the meteorology and air quality during the Project MOHAVE year to previous years. Section 8 summarizes the attribution methods used to attribute light extinction at the Grand Canyon to the Mojave Power Project and other regional sources. Section 9 attempts to reconcile the various attribution methods and presents the range of visibility impairment assessements at Grand Canyon due to the Mojave Power Project. The project accomplishments are compared against its objectives in Section 10 and lessons learned are presented. The appendices describe the MOHAVE database and the unpublished attribution and evaluation methods.

2. Study Setting

This section describes the study domain, major terrain features, land use, meteorology, and regional air quality and visibility.

2.1 The Southwestern United States

Figure 2-1 shows a terrain map of the Southwestern United States. The Colorado river flows from the Northeast corner of the map, through the Grand Canyon, and into Lake Mead. Below the Hoover dam on the western edge of Lake Mead, the Colorado river flows south through the Mohave Valley and toward the Gulf of California.

MPP is located at Laughlin, NV, about 125 km south-southeast of Las Vegas, 350 km northeast of Los Angeles, and 340 km northwest of Phoenix. The MPP is a coal-fired, base loaded generating facility with a 153 m high stack. The base of the stack is at 210 m msl. It uses low sulfur (0.5 % by wt.) Arizona coal delivered by slurry pipeline. Its SO_2 emission rate is approximately 150 tons per day at full operation (Nelson, 1991) and averages 110 tons per day. MPP produces 1580 MW at peak load.

The topography in the vicinity of MPP is complex with sparse vegetation. The Mohave Valley walls are not symmetric with respect to the valley axis. Western slopes rise gradually, while eastern slopes rise slowly for the first few kilometers with steep walls further to the east. The border between Nevada and Arizona also extends along the valley axis. The bottom of the valley is about 200-300 m msl and the ridges reach 1200 m msl. Toward the west, the Mohave Valley extends into a high plateau and toward the east, into the Detrital Valley plateau (600 m msl). The Mohave valley narrows as it approaches Hoover Dam. At Lake Mead the terrain flattens. The western entrance to GCNP is at the end of the eastern arm of Lake Mead (180 m msl).

2.1.1 Land Use

Figure 2-2 is a map of the locations of major cities and roadways in the southwestern United States. The region surrounding the Grand Canyon is sparsely populated. The cities and towns closest to Grand Canyon National Park (GCNP) are Las Vegas, NV to the west, Kingman, AZ and Laughlin, NV to the southwest, Flagstaff, AZ to the south, Page, AZ to the northeast, and St. George, UT to the northwest. Los Angeles and San Diego are major population centers to the southwest with combined populations of approximately 15 million.

In addition to MPP, there are several large coal-fired electric generating facilities near the Grand Canyon National Park. NGS is a 2300 MW plant located near Page, AZ at the eastern end of the Grand Canyon. NGS is currently in the process of installing scrubbers to control its SO_2 emissions. All scrubbers will be on line in 1999. The Reid Gardner coal-fired plant north east of Las Vegas emits approximately 14 tons SO_2 per day. There are two large coal fired power plants in northwestern New Mexico. The plant in Waterflow, NM emits 100 tons SO_2 per day and the plant in Fruitland, NM emits 90 tons SO_2 per day. Emissions data for these facilities was obtained from the EPA AIRS database.
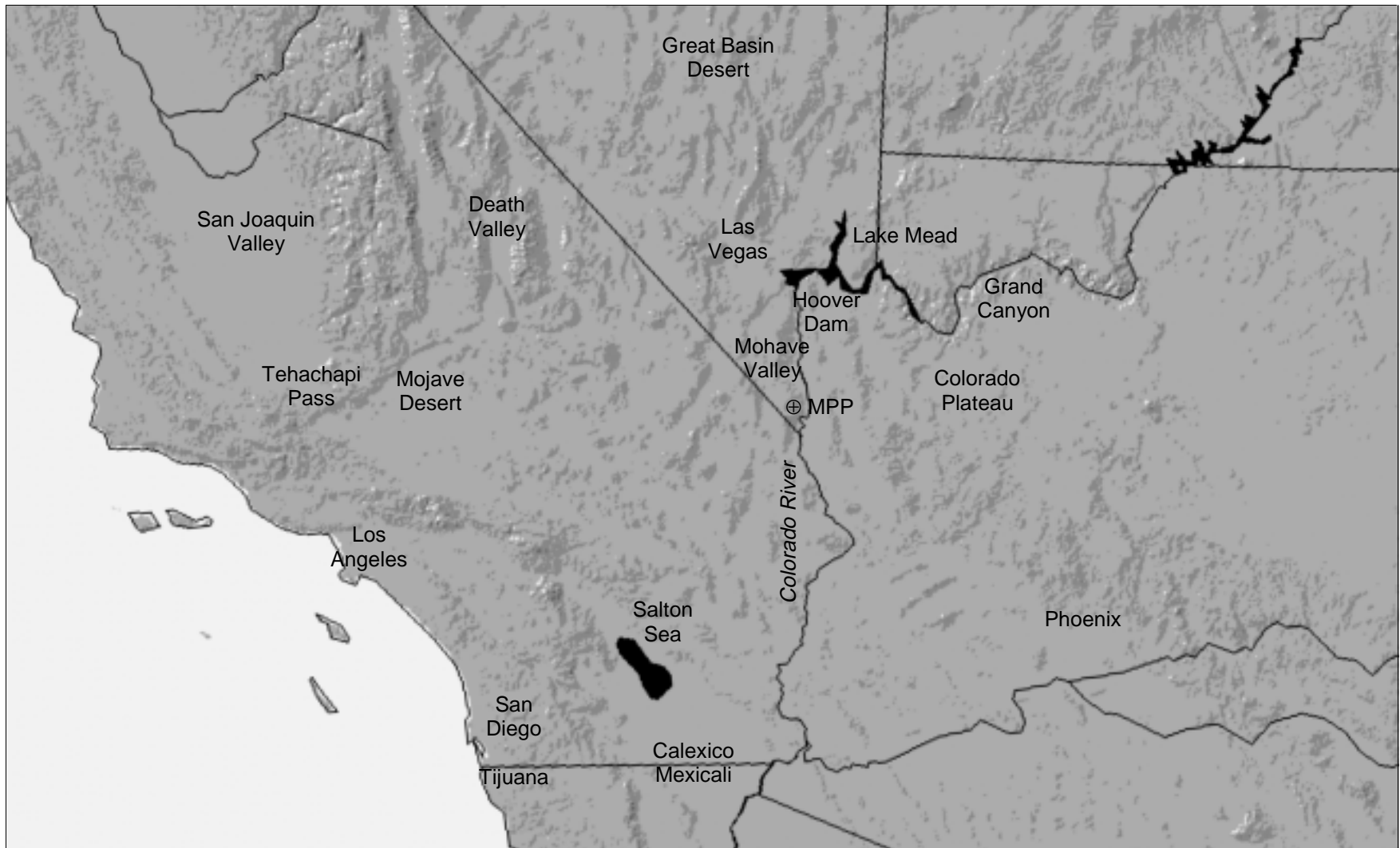
Figure 2-1 Geographic features of the Southwestern U.S.
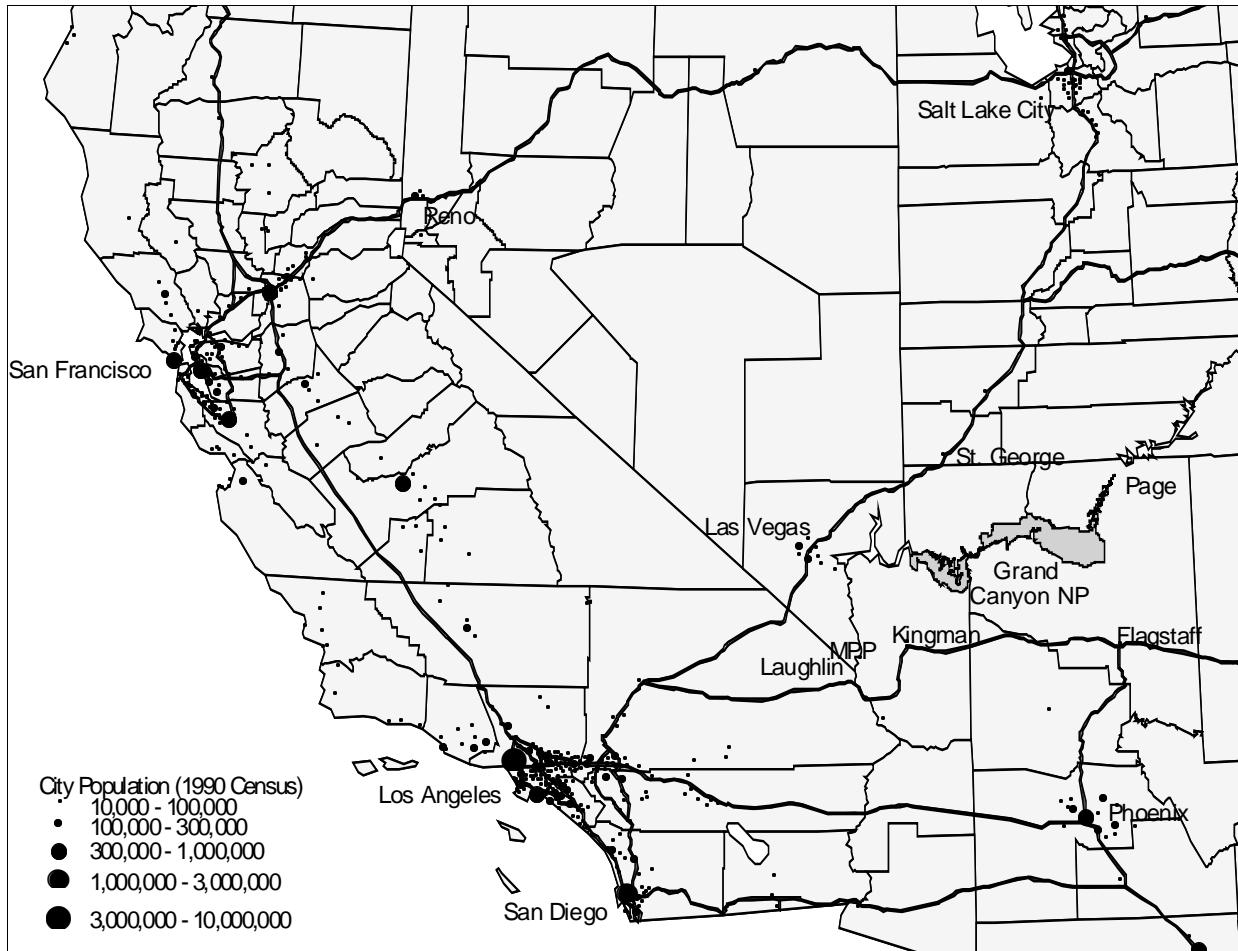
Figure 2-2 Major cities and roadways in the southwestern United States.

The soutwestern United States is the home of several Class I visibility protected areas. Figure 2-3 shows the location of these areas with respect to MPP. GCNP is the closest Class I area to MPP and its western edge is located about 130 km northeast of the facility. Joshua Tree National Monument (approximately 150 km to the southwest) is the next closest Class I area to MPP. Sycamore Canyon and Pine Mountain Wilderness Areas are approximately 200 -250 km east southeast of MPP.

2.2 Meteorology

General meteorological patterns, both synoptic-scale and mesoscale are described here. The effects of these patterns upon pollutant transport are considered in section 7.2.

Substantial differences in meteorological conditions occur across the Project MOHAVE study domain (most of Arizona and the southern parts of California, Nevada, and Utah). Major contributing factors include variations in elevation (3600 m on Mt. Charleston near Las Vegas to –85 m at Death Valley) and the relative importance of maritime versus continental effects. In the western portion of the study area, precipitation falls mostly in the winter months. The eastern portion of the study area experiences winter and summer peaks in precipitation; the summer precipitation is usually from thunderstorms associated with the southwestern or Mexican

monsoon (Douglas et al., 1993). The percentage of annual average rainfall occurring from July-September ranges from less than 10% in the western portion of the study area (western Mojave Desert in California) to greater than 40% in the eastern and southeastern portions of the study area (eastern and southeastern Arizona)(Douglas et. al., 1993).
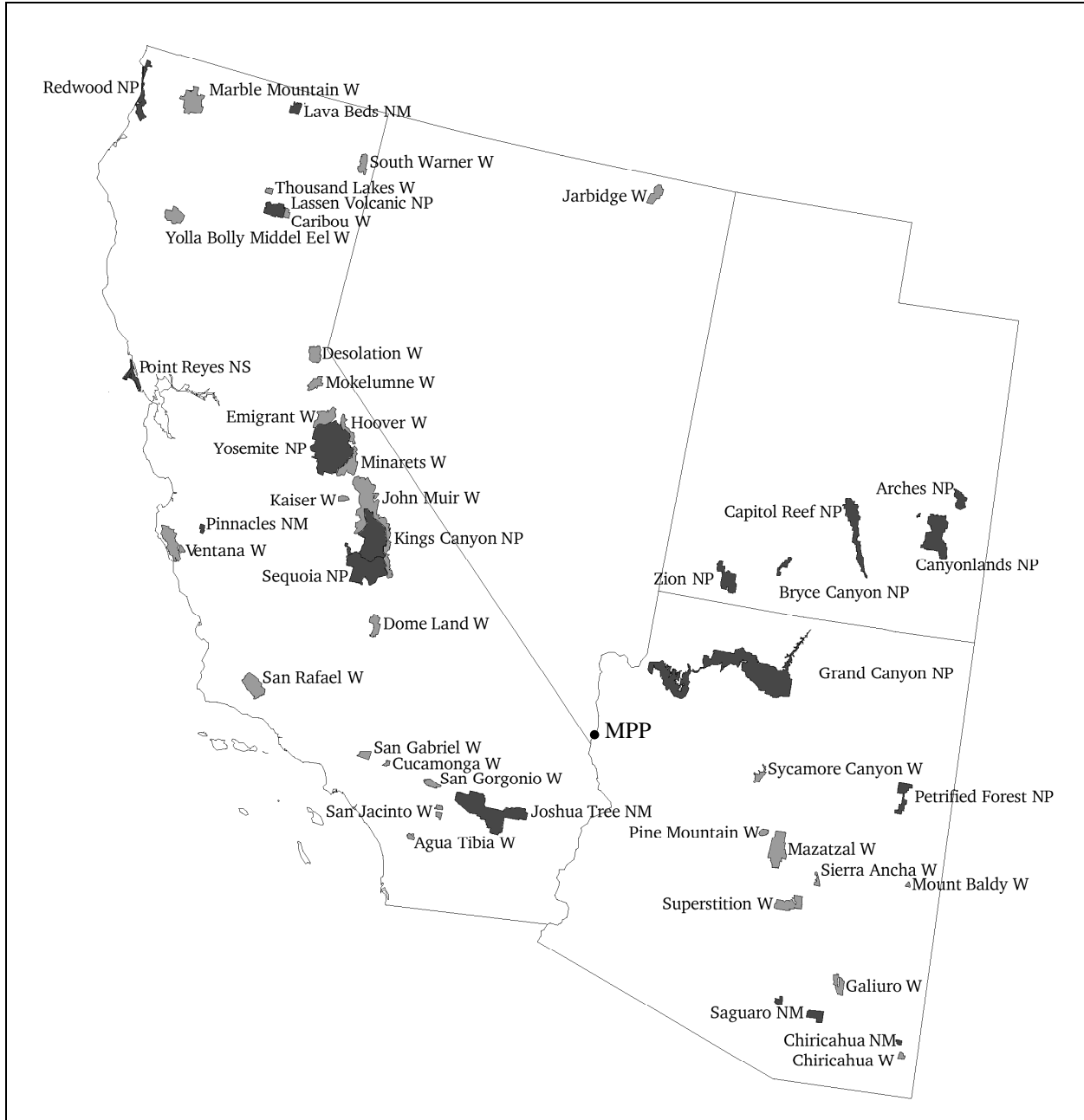
Figure 2-3 Class I areas in California, Nevada, Utah, and Arizona.

Winter storms arrive in the study area from the eastern Pacific Ocean. The winter precipitation falls mainly as snow, sometimes heavy, in the higher elevations and light rain at the lower elevations. In-between the winter storms are periods with clear skies and often light winds from the north or north-east associated with flow of cold air off the Colorado plateau. The frequency

of occurrence of different meteorological patterns varies substantially from month-to-month and year-to-year.

Summer-time patterns are dominated by either dry, southwesterly flow or moist south-southeasterly monsoonal flow. The monsoonal flow is most common during mid-July through early September, while the dry southwesterly flow occurs throughout the warm months, and occurs most regularly in May, June , and September (Green et al., 1992). Low pressure systems over the southwestern U.S. occasionaly pass through the area during summer, most commonly in early (May-June) or late summer (September) (Green et al., 1992; Farber et al. 1997).

Local wind patterns are strongly influenced by terrain features, with channeling within mainly north-south valleys and flows above influenced by synoptic-scale pressure gradients (Green et al., 1998; Farber et al., 1997; and Gaynor and Ping, 1992a). A radar wind profiler was operated at the Mohave Power Project during the Project MOHAVE field study (see section 3.5 for a description of the meteorological monitoring network). During the winter , northerly winds predominated below 1 km AGL (the depth of the Colorado River canyon at MPP), often with a strong jet of 10-15 m s^{-1}. Above about 2 km AGL, winds were in balance with the synoptic scale pressure gradient (Gaynor and Ping, 1992b). The within-canyon jet was especially strong during periods with a high pressure system centered over the Great Basin. For the Great Basin high pattern, rawinsonde measurements near MPP at 5 AM and 5 PM MST showed light winds at the surface in the morning (2 m s^{-1}) with a steady increase to 12-14 m s^{-1} at 800 m AGL and quickly subsiding above this level (Gaynor et. al. 1993). During the afternoon sounding, surface wind speed were higher (6 m s^{-1}) and the peak wind speeds of 10 ms^{-1} occurred over a thicker and lower vertical layer, from about 200-600 m AGL.

Figure 2-4 and Figure 2-5 show the frequency of wind direction as a function of height at MPP and Cottonwood Cove (in the lower Colorado River valley about 40 km north of MPP) during the summer intensive study. Figure 2-4 shows a gradual broadening of the wind direction histogram with height at MPP. Only the last panel shows data for heights above the surrounding mountains. In Figure 2-5, the data are grouped for all heights below 1 km AGL and 1-4 km AGL for morning and afternoon rawinsonde releases; this essentially stratifies the data into within the Colorado River canyon and above the canyon. Within the canyon about 75% of the observations are from the southeast, which corresponds to the local orientation of the valley (wind blowing up-river). Above the canyon, winds are much more variable, with southwesterly winds being the most frequent.

2.3   Air Quality and Visibility

The Project MOHAVE Study area includes some of the best and worst remote area visibility conditions in the western U.S. as measured by the IMPROVE network (Sisler et al., 1996). Emissions from the urban/industrial sources in Southern California and from northwestern Mexico are the cause of a major southwest to northeastern gradient in particulate matter concentrations and visibility across the study area. Table 2-1 below shows the annual, winter and summer average concentrations of PM_{10}, $PM_{2.5}$, coarse mass (PM_{10} - $PM_{2.5}$), and major fine particle components for San Gorgonio (an IMPROVE monitoring site in the mountains that separates the Los Angeles urban area from the Mojave Desert) and for the average of six sites on the Colorado Plateau (Bandelier, Bryce Canyon, Canyonlands, Grand Canyon, Mesa Verde, and

Petrified Forest National Parks). The annual and summer gradient across the study area is apparent for both fine and coarse particle size-ranges. However, the gradient across the study area is much less pronounced in the winter season.
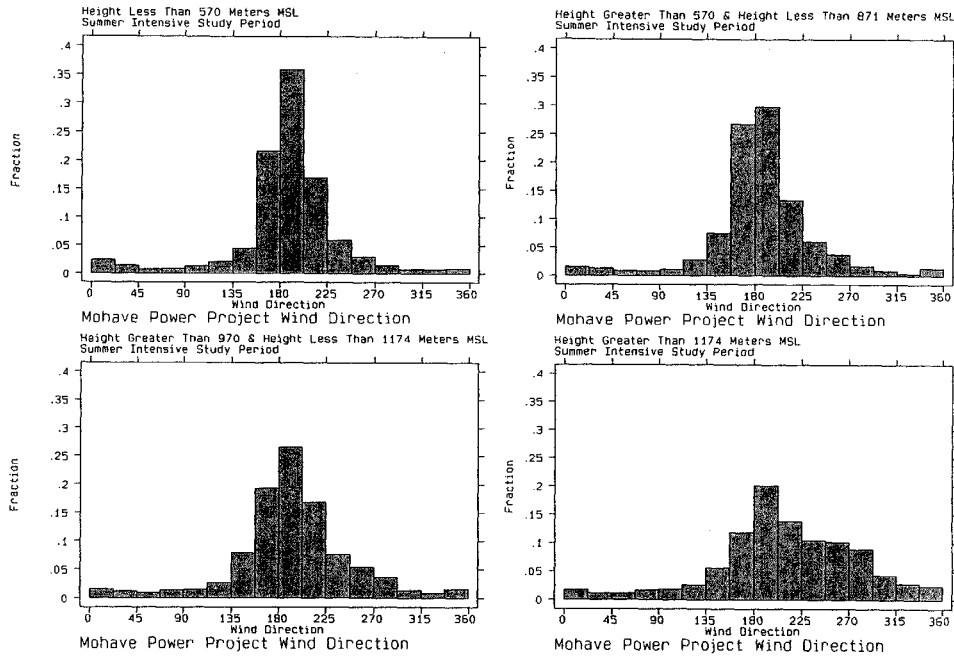
Figure 2-4 Radar wind profiler summary for the summer intensive period at Mohave Power Plant. Data are for all 24 hours of the day.
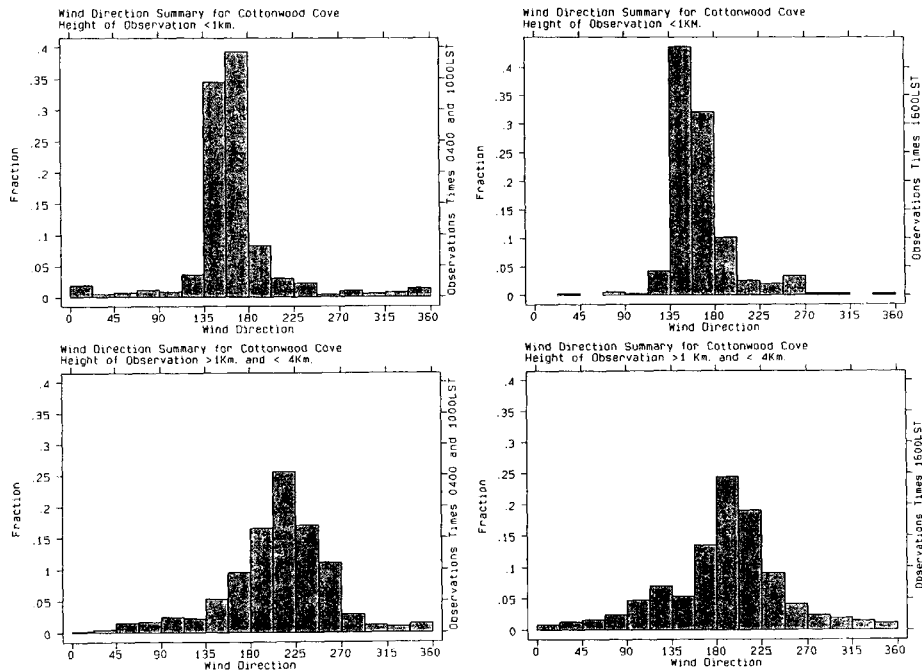
Figure 2-5 Rawinsonde summary for the summer intensive period at Cottonwood Cove. Data are for all 24 hours of the day.

Table 2-1 Annual, winter and summer particulate matter concentrations and fractional contributions of PM$_{2.5}$ for the San Gorgonio and Colorado Plateau IMPROVE monitoring location sites for March 1992 to February 1995.

Location Season	Mass Concentration ($\mu g/m^3$)			Major PM$_{2.5}$ Components ($\mu g/m^3$)				
	PM$_{10}$	PM$_{2.5}$	PM$_{10-2.5}$	Ammonium Sulfate	Ammonium Nitrate	Organic Mass	Elemental Carbon	Crustal Species
San Gorgonio A	16.8	8.3	8.5	1.5	3.7	2.6	0.4	0.7
CO Plateau A	7.4	3.5	3.9	1.1	0.2	1.3	0.2	0.6
San Gorgonio W	6.7	4.1	2.6	0.6	1.3	1.1	0.2	0.2
CO Plateau W	5.4	2.4	3.0	0.8	0.2	1.1	0.2	0.2
San Gorgonio S	22.4	10.4	12..0	2.4	4.2	4.0	0.6	0.7
CO Plateau S	9.2	4.3	4.9	1.3	0.2	1.5	0.2	0.7

The component PM$_{2.5}$ masses do not always sum to the gavimetric PM$_{2.5}$ mass. Differences may be due to the analytical uncertainties of the component and gravimetric measurements. When the sum of components is less than the measured mass, additional material on the filter such as water or seasalt may have been present.

The major components most responsible for the gradient are nitrate and organic carbon, with sulfate and elemental carbon also contributing to the difference between the two regions. Project MOHAVE and other studies have shown the nitrate gradient to be very sharp with much lower concentrations measured at sites only a few tens of kilometers to the east in the Mojave Desert. Notice that during the winter season the Colorado Plateau experiences the same component concentrations as at the San Gorgonio monitoring site with the exception of the nitrate which is considerably higher near Los Angeles and sulfate which is modestly higher on the plateau.

Corresponding visibility levels expressed as calculated light extinction coefficient values are shown in Table 2-2. In this case, light extinction was calculated from chemical measurements with the method used in the IMPROVE report (Sisler et al., 1996). These data reflect a similar seasonal pattern and spatial gradient as seen in the particulate matter concentrations. Fine particle scattering calculated from chemical speciation measurements is responsible for most of the difference between sites with a smaller contribution to the differences from aerosol absorption which is assumed to be caused solely by elemental carbon. Gas molecules that make up the air (e.g. N_2 & O_2) cause the Rayleigh scattering component of the total light extinction, and except for variations caused by air density differences (e.g. altitude changes) is a constant. As a result the relative contribution of Rayleigh scattering to total extinction which is a measure of its importance to visibility is much higher at the Colorado Plateau sites (about 1/3) than at San Gorgonio (about 1/7).

Table 2-2 Annual, winter and summer averages of total calculated extinction and its major components in units of inverse megameters (Mm⁻¹) for San Gorgonio and the Colorado Plateau IMPROVE network sites.

Location Season		Calculated Total Extinction	Fine Scattering	Coarse Scattering	Aerosol Absorption	Rayleigh Scattering
San Gorgonio	Annual	69.7	43.8	5.8	10.2	10.0
CO Plateau	Annual	31.4	13.4	3.0	4.9	10.0
San Gorgonio	Winter	35.6	19.8	1.9	3.9	10.0
CO Plateau	Winter	29.3	13.5	2.0	3.8	10.0
San Gorgonio	Summer	80.3	47.9	7.4	15.0	10.0
CO Plateau	Summer	33.6	13.8	3.9	5.9	10.0

3. Monitoring Network

This section describes the particulate, tracer, and meteorological networks and measurement methods of Project MOHAVE. Table 3-1 lists the locations of all the sites included in the Project MOHAVE database and the measurements performed at each site. The descriptions of the headings in Table 3-1 are provided in Table 3-2. Not all of the measurements summarized were made exclusively for Project MOHAVE. The Project MOHAVE Study Plan (USEPA, 1991) provides the rationale for the observables, sample durations, sampling frequency, and monitoring periods for the study measurements.

3.1 Air Quality Monitoring Network

The Project MOHAVE air quality monitoring network characterized both aerosol and gas phase chemical composition throughout the study region.

3.1.1   Aerosol Measurements

Most aerosol collection was done by the IMPROVE aerosol monitoring samplers, which consist of one or more independent modules (Eldred et al., 1988). The fine particle modules (aerodynamic diameters 0-2.5 µm) consist of an inlet to remove large particles and rain, a cyclone to remove coarse particles, attachments for four filter cassettes and solenoids, a critical orifice for flow control, and a pump. Fine modules used for nitrate measurement have a Na_2CO_3 denuder in the inlet stack to remove HNO_3 gases. The PM_{10} module substitutes a standard PM_{10} inlet for the fine inlet and cyclone. The six types of modules used in Project MOHAVE are listed in Table 3-3. The A/S, D/S, and E/L modules had a Teflon filter followed by an impregnated after filter. The IMPROVE sites had modules A, B, C, and D/S with sample sequencing by a clock timer in a separate module. Meadview had an additional E/L module sequenced by the timer. The background sites had the clock timer inside the A/S module. Sites with a weekly change cycle had a pair of identical samplers.

Additional aerosol filter sampling was performed by researchers from BYU at Spirit Mountain, Meadview, Indian Gardens, Hopi Point, Sycamore Canyon, Dangling Rope, and New Harmony during the winter intensive sampling period and Spirit Mountain, Meadview, Hopi Point, Sycamore Canyon, Dangling Rope, and Painted Desert in the summer intensive sampling period. Measurements conducted by researchers at BYU quantified total sulfur oxides, sulfur dioxide, fine particulate sulfate, total fluoride, and spherical aluminoslicate particles and are discussed in detail in Eatough et al. (1997a) and Eatough et al. (1997b). Samples for the determination of particulate organic material using diffusion denuder techniques (BOSS and BIG BOSS) were collected by BYU researchers at Meadview during the summer. Researchers from the University of Minnesota collected aerosol filter samples for the Harvard School of Public Health at Meadview during the day-time for the summer study. A summary of the samplers used by researchers from BYU and Harvard is shown in Table 3-4.

Table 3-1 Ambient and Meteorological Monitoring Sites in Project MOHAVE

		Position			Aerosol				Tracer		Gaseous								Meteorological										Optical			
SITE	Location	LATF	LONF	ELVM	IO	CC	EL	MS	PFT	TR	DN	HL	HN	NOG	OG	O3	SO2	NH	TA	TD	PR	RH	TS	TU	W1	TV	SG	WW	BA	BS	SVR	BE
ABQN	Albuquerque/Int'L Arpt	35.0500	-106.6167	1619															X	X	X	X	X					X				
ACVN	Arcata - Airport	40.9833	-124.1000	70															X	X	X	X	X					X				
ALSN	Alamosa/Bergman Field	37.4500	-105.8667	2300															X	X	X	X	X					X				
AMAN	Amarillo	35.2333	-101.7000	1095															X	X	X	X						X				
AMBO[1]	Amboy	34.5625	-115.5458	213	X	X	X	X	X								X		X		X								X	X	X	
ASTN	Astoria/Clatsop County Ar	46.1500	-123.8833	3															X	X	X	X	X					X				
BAKE	Baker	35.2833	-116.0667	283	X	X	X	X	X								X											X			
BAND	Bandelier Nat. Mon.	35.7847	-106.2608	2011															X		X										X	X
BANN	Banning Pass	33.9100	-116.9000	730																				X		X				
BAR1	Barstow	34.8400	-117.1200	710																			X				X				
BARS[2]	Barstow	34.9166	-116.9500	590	X	X	X	X	X								X											X			
BCFO	Bullhead City, Field Off.	35.1503	-114.5669	169										X		X	X		X	X	X	X	X	X			X	X				
BCRI	Bullhead City, Riviera	35.1147	-114.6250	167															X	X	X	X						X				
BFLN	Bakersfield/Meadows Field	35.4167	-119.0500	152															X	X	X	X	X					X				
BIBE	Big Bend Nat. Park	29.3439	-103.2067	1082															X		X										X	X
BILN	Billings/Logan Int'L Arpt	45.8000	-108.5333	1092															X	X	X	X	X					X				
BOIN	Boise/Air Terminal	43.5667	-116.2167	876															X	X	X	X	X					X				
BRCA	Bryce Canyon	37.6167	-112.1667	2438	X	X	X	X	X								X											X			
CAJO	Cajon Pass	34.3333	-117.4000	1076	X	X	X	X	X								X		X		X								X	X	X	
CAJC	Cajon Pass - Ucd Coll.	34.3333	-117.4000	1076	X	X	X	X									X											X			
CANY	Canyonlands Nat. Park	38.4639	-109.8217	1806															X		X										X	X
CDCN	Cedar City – FAA Arpt	37.7000	-113.1000	1710															X	X	X	X	X					X				
CEDR	Cedar City	37.6750	-113.0667	1771															X	X	X							X				
CHIR	Chiricahua Nat. Park	32.0097	-109.3883	1567															X		X										X	X
CIBO[2]	Cibola Nwr	33.3000	-114.7000	73	X	X	X	X	X								X											X			
COCE	Cottonwood Cove, East	35.3472	-114.6655	201															X	X	X	X						X				
COCO	Cottonwood Cove, West	35.4833	-114.6833	274	X	X	X	X	X					X		X	X		X	X	X	X	X	X			X	X	X			
COSN	Colorado Springs/Municipa	38.8167	-104.7167	1857															X	X	X	X	X					X				
CPRN	Casper/Natrona Co Int'L A	42.9167	-106.4667	1621															X	X	X	X	X					X				
CYSN	Cheyenne/Municipal Arpt	41.1500	-104.8167	1866															X	X	X	X	X					X				
DAGN	Daggett/FAA Airport	34.8667	-116.7833	585															X	X	X	X	X					X				
DARO	Dangling Rope	37.1333	-111.0500	1158	X	X	X	X		X							X											X			
DECE[2]	Desert Center	33.7000	-115.3666	270	X	X	X	X	X								X											X			
DENN	Denver/Stapleton Int'L Ar	39.7667	-104.8833	1611															X	X	X	X	X					X				
DOS1	Dolan Springs (Tab)	35.5027	-114.2744	1015															X	X	X	X						X				
DOSP	Dolan Springs	35.5833	-114.2833	853	X	X	X	X	X								X											X			
DRAN	Desert Rock	36.6167	-116.0167	1007															X	X	X	X	X					X				
DRMO	Dri Mountain	35.2111	-114.5556	366										X		X	X		X	X	X	X	X	X			X	X				

		Position			Aerosol				Tracer		Gaseous								Meteorological										Optical			
SITE	Location	LATF	LONF	ELVM	IO	CC	EL	MS	PFT	TR	DN	HL	HN	NOG	OG	O3	SO2	NH	TA	TD	PR	RH	TS	TU	W1	TV	SG	WW	BA	BS	SVR	BE
DRTN	Del Rio	29.3667	-100.9167	313															X	X	X	X						X				
EKON	Elko/Municipal Arpt	40.8333	-115.7833	1548															X	X	X	X	X					X				
ELCE[2]	El Centro	32.8333	-115.3833	-4	X	X	X	X		X							X		X		X									X	X	X	
ELC1	El Cajon	32.8100	-116.9800	183																				X				X				
ELPN	El Paso	31.8000	-106.4000	1199															X	X	X	X						X				
ELYN	Ely/Yelland Field	39.2833	-114.8500	1907															X	X	X	X	X					X				
EMPN	Empalme, Mexico	27.9500	-110.8000	11															X	X	X	X						X				
ESSE[2]	Essex	34.7500	-115.2500	520	X	X	X	X	X								X												X			
EUGN	Eugene/Mahlon Sweet Arpt	44.1167	-123.2167	111															X	X	X	X	X					X				
FATN	Fresno/Air Terminal	36.7667	-119.7167	100															X	X	X	X						X				
FCAN	Kalispell/Glacier Pk Int'	48.3000	-114.2667	907															X	X	X	X						X				
FLGN	Flagstaff/Pulliam Arpt	35.1333	-111.6667	2132															X	X	X	X						X				
FOMO	Fort Mohave	35.0406	-114.5989	174										X		X	X		X	X	X	X	X	X			X	X			
GEGN	Spokane/Int'L Arpt	47.6333	-117.5333	719															X	X	X	X	X					X				
GGWN	Glasgow/Int'L Arpt	48.2167	-106.6167	695															X	X	X	X	X					X				
GJTN	Grand Junction/Walker Fie	39.1167	-108.5333	1473															X	X	X	X	X					X				
GLCA	Glen Canyon	36.9400	-111.4900	1128															X		X							X		X		
GRCA	Grandview Point, Gcnp	35.9964	-111.9917	2256															X		X										X	X
GRCW	Yavapai Point, Gcnp	36.0664	-112.1167	2145															X		X										X	X
GTFN	Great Falls/Int'L Arpt	47.4833	-111.3500	1117															X	X	X	X	X					X				
GUMO	Guadalupe Mtns. Np	31.8322	-104.8094	1616															X		X										X	X
GUPN	Gallup/FAA Airport	35.5167	-108.7833	1973															X	X	X	X	X					X				
HESP	Hesperia	34.3800	-117.4100	1166																					X	X		X				
HLNN	Helena/Arpt	46.6000	-112.0000	1188															X	X	X	X	X					X				
HOP5	Hopi Point (12 Hour)	36.0667	-112.1500	2164	X	X	X	X									X												X			
HOPO	Hopi Point	36.0667	-112.1500	2164	X	X	X	X	X								X												X	X		
HOSH	Holiday Shores	35.1164	-114.6056	161										X		X	X		X	X	X	X	X	X			X	X			
HUMO[1]	Hualapi Mountain	35.1167	-113.8667	2408	X	X	X	X	X								X												X			
HVRN	Havre/City-County Arpt	48.5500	-109.7667	788															X	X	X	X	X					X				
ING5[*]	Indian Gardens (12 Hour)	36.0833	-112.1167	1158	X	X	X	X									X												X			
INGA	Indian Gardens	36.0833	-112.1167	1158	X	X	X	X	X								X												X			
INWN	Winslow	35.0167	-110.7333	1487															X	X	X	X						X				
JALA[1]	Jacob Lake	36.7000	-112.2167	2487	X	X	X	X	X								X												X			
JOT2	Joshua Tree (24 Hr Hg Se)	34.0500	-116.2333	1250	X	X	X	X									X												X			
JOTR	Joshua Tree	34.0500	-116.2333	1250	X	X	X	X	X								X		X		X								X	X	X	
KELS[2]	Kelso	34.8995	-115.6533	860	X	X	X	X	X								X		X		X								X	X	X	
KING[2]	Kingman	35.2500	-114.0500	1040	X	X	X	X	X								X												X			
LAGA	Larrea Gardens	35.3000	-114.8000	794											X																	
LASN	Las Vegas/McCarran Int'L	36.0833	-115.1667	664															X	X	X	X	X					X				
LAXN	Los Angeles/Int'L Arpt	33.9333	-118.4000	33															X	X	X	X	X					X				
LBFN	North Platte	41.1333	-100.6833	847															X	X	X	X						X				
LGBN	Long Beach/Wso Airport	33.8167	-118.1500	20															X	X	X	X	X					X				

SITE	Location	Position			Aerosol				Tracer		Gaseous								Meteorological										Optical			
		LATF	LONF	ELVM	IO	CC	EL	MS	PFT	TR	DN	HL	HN	NOG	OG	O3	SO2	NH	TA	TD	PR	RH	TS	TU	W1	TV	SG	WW	BA	BS	SVR	BE
LNDN	Lander/Wso Ap	42.8167	-108.7333	1695															X	X	X	X	X					X				
LOLN	Lovelock - FAA Arpt	40.0667	-118.5500	1190															X	X	X	X	X					X				
LOME	Long Mesa	36.1000	-112.7000	1786					X			X		X	X	X			X	X	X	X	X			X	X			X		
LVWA	Las Vegas Wash	36.1167	-114.8500	457	X	X	X	X	X								X												X			
LWSN	Lewiston/Wso Ap	46.3833	-117.0167	439															X	X	X	X	X					X				
MACN[1]	Marble Canyon	36.8000	-111.6500	1219	X	X	X	X	X								X												X			
MEAD	Meadview	36.0222	-114.0675	905	X	X	X	X	X		X	X	X	X	X	X	X	X	X		X	X		X		X	X	X	X	X	X	X
MED5	Meadview (12 Hour)	35.9833	-114.0667	902	X	X	X	X									X												X			
MED6	Meadview (Ions)	35.9833	-114.0667	902	X	X	X	X									X												X			
MEVE	Mesa Verde Nat. Park	37.2186	-108.4933	2245														X			X									X	X
MFRN	Medford/Jackson County Ar	42.3667	-122.8667	396															X	X	X	X	X					X				
MOJA	Mojave	35.0600	-118.1500	836																				X				X				
MOPP	Mohave Power Plant	35.1453	-114.5906	213						X			X		X	X			X	X	X	X	X	X	X		X	X				
MOSP	Mountain Springs Summit	35.9833	-115.5167	1753	X	X	X	X	X								X												X			
MSON	Missoula/Johnson-Bell Fld	46.9167	-114.0833	976															X	X	X	X	X					X				
NEED	Needles	34.7639	-114.6150	278															X	X	X			X				X				
NEHA	New Harmony	37.5000	-113.3000	1524	X	X	X	X	X								X												X			
NKXN	Miramar Nas	32.8667	-117.1500	147															X	X	X							X				
OAKN	Oakland Int Ap	37.7500	-122.2167	6															X	X	X							X				
OLMN	Olympia/Arpt	46.9667	-122.9000	59															X	X	X	X	X					X				
OTHN	North Bend/FAA Airport	43.4167	-124.2500	1															X	X	X	X	X					X				
OVBE	Overton Beach	36.4333	-114.3667	396	X	X	X	X	X								X												X			
OVER	Overton	36.8080	-114.4644	424																				X				X				
PAGE	Page	36.9300	-111.4500	1326															X	X	X							X				
PALM	Palmdale	34.5900	-118.0400	787																				X				X				
PARK	Parker	34.1500	-114.2667	137	X	X	X	X	X								X												X			
PAUL[1]	Paulden	34.9167	-112.5667	1341	X	X	X	X	X								X												X			
PDTN	Pendleton/Municipal Arpt	45.6833	-118.8500	459															X	X	X	X	X					X				
PDXN	Portland/Int'L Arpt	45.6000	-122.6000	8															X	X	X	X	X					X				
PEFO	Petrified Forest Nat. Prk	34.9139	-109.7958	1690					X										X		X										X	X
PEFR	Petrified Forest	35.1000	-109.7500	1676	X	X	X	X									X												X			
PHXN	Phoenix/Sky Harbor Int'L	33.4333	-112.0167	338															X	X	X	X	X					X				
PIHN	Pocatello/Municipal Arpt	42.9167	-112.6000	1360															X	X	X	X	X					X				
PRCN	Prescott – Municipal	34.6500	-112.4333	1531															X	X	X	X	X					X				
PRES	Prescott	34.5667	-112.2667	1450															X	X	X							X				
PUBN	Pueblo/Memorial Arpt	38.2833	-104.5167	1420															X	X	X	X	X					X				
RDDN	Redding/Municipal Arpt	40.5167	-122.3000	153															X	X	X	X	X					X				
RDMN	Redmond/FAA Airport	44.2667	-121.1500	932															X	X	X	X	X					X				
RKSN	Rock Springs/FAA Airport	41.6000	-109.0667	2055															X	X	X	X	X					X				
RNON	Reno/Cannon Int'L Arpt	39.5000	-119.7833	1341															X	X	X	X	X					X				
ROWN	Roswell/Industrial Air Pa	33.3000	-104.5333	1113															X	X	X	X	X					X				
SACN	Sacramento/Executive Arpt	38.5167	-121.5000	6															X	X	X	X	X					X				

SITE	Location	Position			Aerosol				Tracer		Gaseous								Meteorological										Optical			
		LATF	LONF	ELVM	IO	CC	EL	MS	PFT	TR	DN	HL	HN	NOG	OG	O3	SO2	NH	TA	TD	PR	RH	TS	TU	W1	TV	SG	WW	BA	BS	SVR	BE
SAGO	San Gorgonio Wilderness	34.1933	-116.9133	1710					X										X		X											X	X
SAGR	San Gorgonio	34.2000	-116.9167	1713	X	X	X	X									X													X			
SANB	San Bernardino	34.1800	-117.3800	514																		X	X					X				
SAND	San Diego	34.9700	-117.1600	111																		X	X					X				
SANN	San Diego/Lindbergh Field	32.7333	-117.1667	10														X	X	X	X	X					X				
SBAN	Santa Barbara/FAA Airport	34.4333	-119.8333	2														X	X	X	X	X					X				
SEAN	Seattle/Seattle-Tacoma In	47.4500	-122.3000	137														X	X	X	X	X					X				
SELI	Seligman	35.2833	-112.4833	1661	X	X	X	X	X								X												X			
SFON	San Francisco/Int'L Arpt	37.6167	-122.3833	27														X	X	X	X	X					X				
SHRN	Sheridan/County Arpt	44.7667	-106.9667	1202														X	X	X	X	X					X				
SLCN	Salt Lake City/Int'L Arpt	40.7667	-111.9667	1287														X	X	X	X	X					X				
SLEN	Salem/Mcnary Field	44.9167	-123.0167	60														X	X	X	X	X					X				
SMXN	Santa Maria/Public Arpt	34.9000	-120.4500	82														X	X	X	X	X					X				
SPMC	Spirit Mountain - Colloc	35.2500	-114.7333	1498	X	X	X	X									X												X			
SPMO	Spirit Mountain	35.2500	-114.7333	1498	X	X	X	X	X			X			X	X		X	X	X	X							X	X	X		X
SQMO	Squaw Mountain	35.2167	-113.1000	1981	X	X	X	X	X								X												X			
SYCA	Sycamore Canyon	35.1500	-111.9833	1890	X	X	X	X	X								X												X			
TEBR	Temple Bar	36.0150	-114.3319	485															X			X					X				
TEHA	Tehachapi Summit	35.1000	-118.4333	1280	X	X	X	X	X	X							X		X		X							X	X	X	
TMET	Tonto Plateau, Gcnp	35.0933	-112.0697	1180															X		X	X	X			X	X					
TONT	Tonto Nat. Forest	33.6500	-111.1167	732	X	X	X	X	X								X												X			
TPHN	Tonopah/FAA Airport	38.0667	-117.0833	1654														X	X	X	X	X					X				
TRUX	Truxton	35.4861	-113.5639	1350	X	X	X	X	X								X							X				X	X			
TUSN	Tucson/Int'L Arpt	32.1167	-110.9333	786														X	X	X	X	X					X				
UILN	Quillayute/Wso Airport	47.9500	-124.5500	54														X	X	X	X	X					X				
WICK	Wickenburg	33.9333	-112.8000	732	X	X	X	X	X								X												X			
WMCN	Winnemucca/Wso Airport	40.9000	-117.8000	1310														X	X	X	X	X					X				
WWTR	White Water	33.9000	-116.6800	360																				X				X				
YKMN	Yakima/Air Terminal	46.5667	-120.5333	325														X	X	X	X	X					X				
YUCC	Yucca	34.7500	-114.1667	579	X	X	X	X	X								X												X			
YUM1	Yuma Army Proving Site #1	32.8700	-114.3300	136															X	X	X	X		X				X				
YUM2	Yuma Army Proving Site #2	32.5100	-114.1000	231															X	X	X	X		X				X				
YUMA	Yuma	32.7542	-114.6917	61		X													X	X	X	X					X				

*Supplemental monitoring during winter only
[1]Winter site only
[2]Summer site only

Table 3-2 Field name coding description for the ambient and meteorological observables.

Field Name	Description
BA	Particle optical absorption
BE	Total extinction coefficient
BS	Particle scattering coefficient
CC	Aerosol carbon
DN	Denuders
EL	Elemental composition of aerosol
HL	Gas phase halocarbons
HN	Nitric and Nitrous acid gas
IO	Aerosol anions
MS	Particulate Matter < 10 microns
NH	Ammonia and ammonium
NOG	NOx
O3	Ozone
OG	Gas phase organics
PFT	Tracer
PR	Barometric pressure
RH	Relative humidity
SG	Standard deviation of wind direction
SO2	Sulfur dioxide
SVR	Standard visual range
TA	Ambient temperature
TD	Dew point temperature
TR	Tracer release
TS	Total solar radiation
TU	Turbulence
TV	Virtual temperature
W1	Vertical wind speed
WW	Wind direction

Size-resolved samples were collected at five sites using the *Davis Rotating drum Unit for Monitoring* (DRUM) sampler, a Lundgren-type rotating drum cascade impactor with a single round jet for each stage (Raabe et al., 1988). Each sampler had eight drum stages with 50% collection cut points at aerodynamic diameters of 10, 5, 2.4, 1.1, 0.56, 0.34, 0.24, and 0.069 µm. A Teflon filter behind the last stage collected particles smaller than 0.069 µm. The drums rotated slowly to provide 6-hour time resolution when analyzed with the UCD focused beam Particle Induced X-Ray Emission (PIXE) strip analysis system. The particles are collected on 16.8 cm mylar strips coated with Apiezon L grease to minimize bounce-off. The final orifice provides flow control at 1.1 LPM by operating as a critical orifice.

Table 3-5 summarizes the sampling configurations using IMPROVE and DRUM samplers. For the names of the sites, see Figure 3-1 and Table 3-1. During the routine monitoring periods, 24-hour samples were collected every Wednesday and Saturday as part of the IMPROVE network. During both intensive sampling periods, 12-hour samples were collected continuously at the receptor sites: Meadview, Hopi Point, and Indian Gardens. Meadview had an additional 12-hour fine Teflon/citric acid module to measure ammonium ions and ammonia gas. Hopi Point and Indian Gardens had an additional 24-hour fine module with a Teflon filter. The other IMPROVE and background sites collected 24-hour samples continuously beginning at 0700 MST. Collocated samplers were located at Joshua Tree during the winter intensive sampling period (Teflon only) and at Cajon Summit and Spirit Mountain (Teflon plus carbonate) during the summer intensive sampling period.

Table 3-3 IMPROVE sampler module types used in Project MOHAVE. The B module has a carbonate denuder.

Module	Filter	Aerodynamic Diameter Range	Major Variables
A	Teflon	0 - 2.5 µm	mass, S, organics by H, soil and trace elements, b_{abs}
B	nylon	0 - 2.5 µm	nitrate, sulfate (QA)
C	quartz	0 - 2.5 µm	organic and elemental carbon
D/S	Teflon / carbonate	0 - 10 µm	PM_{10} mass / SO_2
E/L	Teflon / citric acid	0 - 2.5 µm	nitrate, sulfate, ammonium / ammonia
A/S	Teflon / carbonate	0 - 2.5 µm	mass, S, organics by H, soil and trace elements, b_{abs}/SO_2

Table 3-4 Samplers used by BYU and University of Minnesota in Project MOHAVE

Sampler	Denuder	Filter	d_{ae} range	Major variables
BYU Denuder	Carbonate	Teflon/ Nylon	0 - 2.5 μm	Sulfate, nitrate, fluoride, SO_2, HNO_3, HF
BYU Hi Vol	None	Impaction Quartz/ Carbonate	0.5 - 3.5 μm 0 - 0.5μm	Sulfate, nitrate, SAS Sulfate, nitrate, fluoride, SO_2, HF
BYU BOSS	Charcoal	Quartz/ Charcoal	0 - 2.5 μm	Particulate carbonaceous material
Harvard HEADS	Carbonate/Citric acid	Teflon/ Nylon	0 - 2.5 μm	Sulfate, nitrate, ammonium, SO_2, HNO_3, NH_3

Table 3-5 IMPROVE and DRUM sampling configurations for the various periods.

Sites	Frequency	Modules
Fall 1991 Monitoring	*9/4/91 to 1/11/92*	
9 IMPROVE sites	Wed/Sat	A, B, C, D/S
Meadview, Long Mesa	6-hour	DRUM
Winter Intensive	*1/14/92 to 2/15/92*	
Meadview	12-hour	A, B, C, D/S, E/L
Hopi Point, Indian Gardens	12-hour	A, B, C, D/S, 24h A
6 other IMPROVE sites	24-hour	A, B, C, D/S
21 background sites	24-hour	A/S
Joshua Tree	24-hour	collocated A
Meadview, Hopi Point, Indian Gardens, Long Mesa, Spirit Mtn	6-hour	DRUM
Spring 1992 Monitoring	*2/16/92 to 7/11/92*	
9 IMPROVE sites	Wed/Sat	A, B, C, D/S
Hopi Point, Long Mesa	6-hour	DRUM
Summer Intensive	*7/12/92 to 9/2/92*	
Meadview	12-hour	A, B, C, D/S, E/L
Hopi Point	12-hour	A, B, C, D/S, 24h A
Indian Gardens	Wed/Sat	A, B, C, D/S
6 other IMPROVE sites	24-hour	A, B, C, D/S
23 background sites	24-hour	A/S
Cajon Summit, Spirit Mountain	24-hour	collocated A/S
Meadview, Hopi Point, Long Mesa, Spirit Mountain	6-hour	DRUM
Fall 1992 Monitoring	*9/5/92 to 9/31/92*	
7 IMPROVE sites	Wed/Sat	A, B, C, D/S

Three MOUDI size-fractionated impactors were operated the University of Minnesota Particle Technology Laboratory researchers for 12 hours per day (0700 to 1900 MST) from July 17 to August 30, 1992 . The MOUDI samples provided size distributions for sulfate, nitrate, organic carbon, elemental carbon, and elemental concentrations on 8 stages. A cyclone with 1.8 µm cut point was used upstream of the MOUDI sampler. A more detailed description of the methods

and results from both the MOUDI and DRUM experiments is discussed in Pitchford and Green (1997).

3.1.2 Filter Sample Analysis

The IMPROVE sampler filters were analyzed at Davis (UCD), Global Geochemistry (GGC), Desert Research Institute (DRI), and Research Triangle Institute (RTI). The methods and measured variables are summarized in Table 3-6. The Teflon A and carbonate S filters were collected at all sites. The nylon B and quartz C filters were collected at the nine IMPROVE sites. The Teflon E and citric acid impregnated after-filter were collected at Meadview.

Table 3-6 Analytical methods for filter analysis and measured variables

Filter	Lab	Method	Code	Variable	Reference
Teflon A	UCD	gravimetric analysis		mass	Feeney et al., 1984
		integrating plate method	LIPM	coefficient of absorption	Campbell et al., 1989
		proton elastic scattering analysis	PESA	H	Cahill T., 1990
		particle induced X-ray emission	PIXE	Na to Mn, Mo	Cahill T., 1990
		X-ray fluorescence	XRF	Fe to Zr, Pb	Zeng et al., 1993
nylon B	GGC	ion chromatography	IC	nitrate, sulfate, chloride	
quartz C	DRI	thermal optical reflectance (carbon)	TOR	organic and elemental carbon	Chow et al., 1993
Teflon D	UCD	gravimetric analysis		mass	Feeney et al., 1984
Carbonate S	RTI	ion chromatography	IC	SO_2 from sulfate	
Teflon E	GGC	ion chromatography	IC	nitrate, sulfate	
		Technicon colorimetry		ammonium	
citric acid L	GGC	Technicon colorimetry		ammonia from ammonium	

Samples collected by researchers at BYU were analyzed at BYU using a variety of techniques. SO_2, sulfate, and nitrate were analyzed by ion chromatography. Fluoride was analyzed using an ion selective electrode. SAS particles were counted visually on substrates using a scanning electron microscope. Particulate carbonaceous material was analyzed by temperature programmed volatilization analysis. Samples collected by researchers at University of Minnesota were analyzed by ion chromatography at Harvard School of Public Health. Nitric acid vapor was not measured as part of Project MOHAVE.

The DRUM strips for Meadview during the summer intensive were analyzed using the UCD PIXE Strip Analysis System for Na to Pb. Teflon filters from the MOUDI sampler were analyzed using PIXE. The Strip Analysis System was needed to correct for nonuniform deposit on the filters.

3.1.3 Gas Phase Measurements

In addition to the SO_2 concentrations measured by the IMPROVE samplers, several other gas phase measurements were conducted in conjunction with Project MOHAVE. Ozone, NO_x, organic gases, and halocarbons were measured by DRI at multiple sites during the study period. Harvard researchers analyzed samples collected at Meadview for ammonia and ammonium concentrations using annular denuders. BYU researchers also collected and analyzed denuder samples at Hopi Point, Meadview, and Spirit Mountain during both the winter and summer intensive sampling periods.
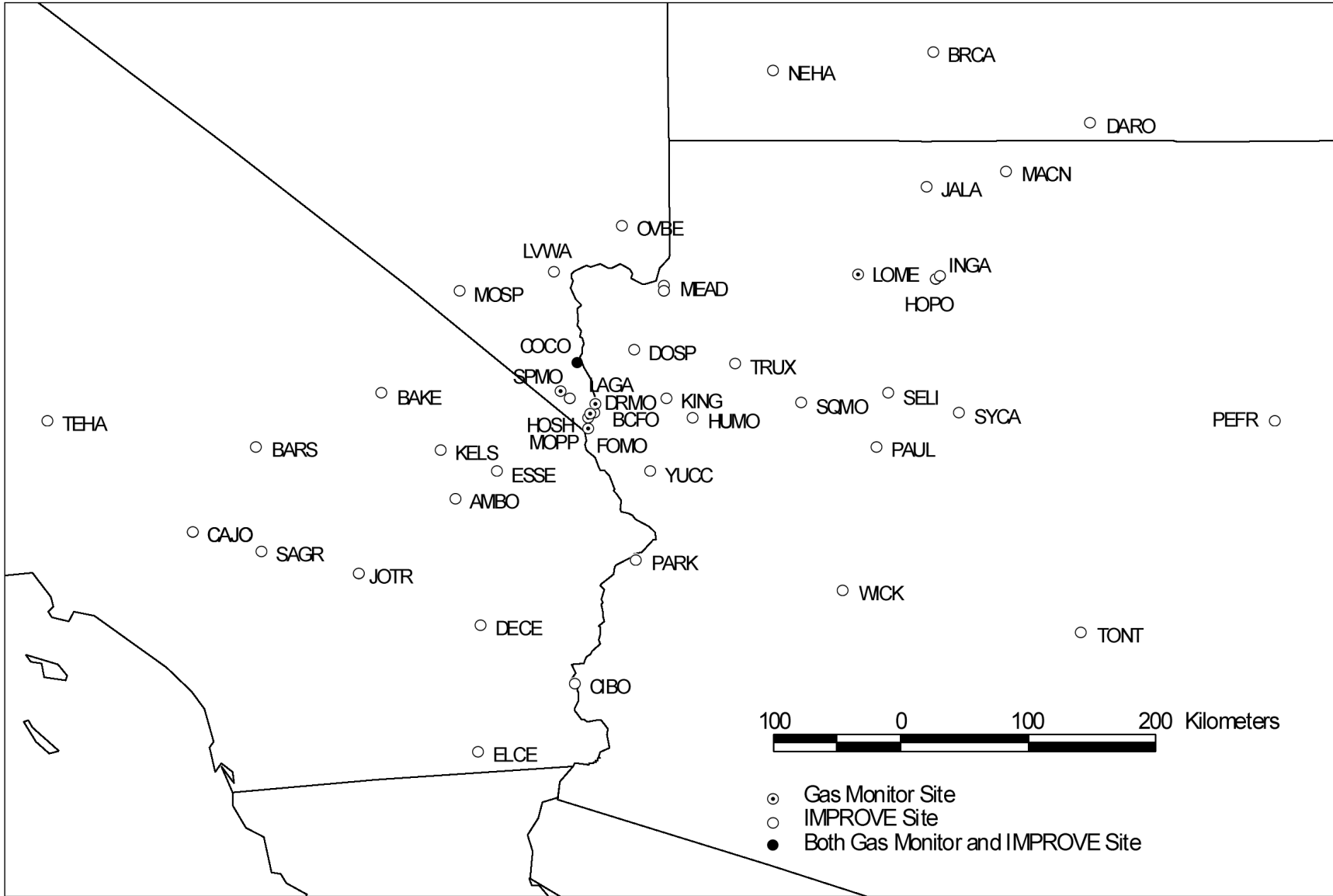
Figure 3-1 Air quality monitoring network for measurements of aerosol composition and gaseous species.

3.2 Tracer Release Network

The locations of the tracer release sites are shown as the open circles in Figure 3-2. Perfluorocarbon tracers (PFT's) used in Project MOHAVE are fully fluorinated hydrocarbons with low solubility in water and moderate vapor pressure, and are therefore inert and non-depositing, as well as non-toxic. At MPP, ortho-perfluorodimethylcyclohexane (oPDCH) tracer was injected into the power plant stack at a height of 20 meters. At the other tracer release locations, tracer was released into the ambient air within a few meters of the surface. The tracer gases were stored in liquid form in stainless steel tanks. A peristaltic metering pump pumped the material from the tank past a linear mass flowmeter and a cumulative mass totalizer onto the surface of a heated disk, which vaporized the tracer. A fan moved the vaporized tracer up a pipe to the atmosphere (or into the MPP stack).

oPDCH was released continuously from the stack of MPP during the 30-day winter and 50-day summer intensive periods. Forty-five percent of the oPDCH consists of the isomer ortho-cis (oc) PDCH, which is measured at the receptor site. The rate of oPDCH release was proportional to power production. This was done to maintain a nearly constant ratio of tracer to SO_2 emissions, which is preferable for receptor and hybrid modeling. This also allows the calculation of the amount of sulfur from the MPP associated with a given tracer concentration. A constant tracer emission rate would have simplified the evaluation of transport and dispersion models used. Sufficient periods of nearly constant tracer emission rates existed to perform these evaluations, thus minimizing the trade-off between tracer release approaches optimized for receptor modeling and deterministic modeling.

Specifically, the tracer release rate was constant when power production stayed within a 10% range of maximum load. For example, if power production was between 90% and 100% of capacity, oPDCH release rates were at their maximum and constant. If the power production dropped to between 40% and 50% of capacity, tracer release rates were reduced to one-half the maximum rate. Figure 3-3 shows the time series of the tracer release rate, power production, and SO_2 emissions from MPP during the winter intensive sampling period. The standard deviation of the ratio of SO_2 emissions (from continuous emission monitors) to oPDCH for the winter was 8.4%; the squared correlation coefficient between oPDCH and SO_2 emissions was 0.95. For the summer, accurate SO_2 emissions measurements were not available; however the winter emissions monitoring showed a high correlation ($r^2=0.99$) of SO_2 emissions with power production. Thus, power production is a good surrogate for SO_2 emission rate. Figure 3-4 shows the oPDCH tracer release rate and power production at MPP during the summer intensive. For the summer, the ratio of power production to tracer release rate had a standard deviation of 6.9% and an r^2 of 0.83.

The average SO_2 to ocPDCH release ratio from MPP was 78.1 g SO_2/mg ocPDCH (488,000 moles SO_2/mole ocPDCH) in winter and 73.3 g SO_2/mg ocPDCH (455,000 moles SO_2/mole ocPDCH) during the summer. The wintertime hourly release ratio remained within 10% of these constants for 84% of the release period. Note that, MPP Unit 1 was off from 1/20/92 at 2100 to 1/28/92 at 1600 and Unit 2 was off from 1/29/92 at 0500 to 2/11/92 at 1800, 7/24/92 at 2000 to 7/27/92 at 0800, and 8/16/92 at 1800 to 8/17/92 at 0400. The tracer release rate was adjusted to account for the resultant changes in SO_2 emissions at these times.

Additional perfluorocarbon tracers were released from other locations to identify times during which emissions from other significant source areas are present throughout the monitoring network. During the winter intensive study, the tracer perfluoromethylcyclopentane (PMCP) was released at Dangling Rope, northeast of the Grand Canyon. This was done to tag the air flow down the Colorado River drainage, which may include emissions from the NGS, other coal-fired power plants in the Colorado River drainage, and from the Salt Lake City urban and industrial area. Prevailing winter mesoscale and nocturnal drainage winds transport emissions from these sources toward GCNP. The time series of PMCP release rates from Dangling Rope is shown in Figure 3-5.

During the summer intensive study, tracer was released from two additional locations in Southern California: Tehachapi Pass and near El Centro in the southern Imperial Valley. Tehachapi Pass separates the San Joaquin Valley from the Mojave Desert and is an important exit route for emissions from oil development and urban areas in the San Joaquin Valley and emissions from the San Francisco Bay area. The El Centro tracer is expected to represent emissions from the San Diego-Tijuana and the Calexico-Mexicali border areas. These two release locations, one to the south of the Los Angeles Basin, and one to the north provide a method for bracketing emissions from the Los Angeles Basin. There are limitations to this approach since emissions from the Los Angeles Basin may impact some sites while neither the Tehachapi or El Centro tracer is detected. This is an inherent difficulty of representing emissions from an area source with one or more point released tracers.

Both PMCP and perfluoromethylcyclohexane (PMCH) were released from Tehachapi Pass using a combination of continuous release and 6-hour pulses every 4 days. PMCP was released continuously from July12 to July 27 during which period three pulses of PMCH were released beginning at 1400 MST. Continuous release of PMCH began on July 27 and continued to the end of August, during which period seven pulses of PMCP were released during selected afternoons. Pulses were designed to time the transport of the PFT through the monitoring network. The hourly average summertime release rates for PMCH and PMCP are shown in Figure 3-6 and Figure 3-7.

Perfluorotrimethylcyclohexane (PTCH) was released from El Centro continuously from July 12 to the end of August with the exception of two 3-day interruptions from August 1 to 4 and from August 22 to 25 (Figure 3-8). The interruptions in tracer release were designed to permit timing of the tracer front through the monitoring network without the need for a second tracer at this site (unavailable for this study). Table 3-7 contains PFT emission rate information for all release locations and seasons. The amount of material available for each of the PFTs for summer and winter was limited. In many cases, released tracer concentrations at receptors were indistinguishable from background concentrations. Due to the large transport distances from the California release locations to the Grand Canyon, it would have been desirable to release more tracer material than was available for these locations in order to improve the signal-to-noise ratio.

Halocarbons, in particular methylchloroform, have been identified as endemic tracers of the greater Los Angeles urban area (White *et al.*, 1990). These compounds are associated with mainly weekday emissions from certain manufacturing facilities such as electronics and aircraft.

Halocarbon measurements for Project MOHAVE were made at Spirit Mountain, Meadview, and Long Mesa.

3.3 Tracer Monitoring Network

Figure 3-2 is a map of the locations of all of the tracer monitoring sites for both the winter and summer intensive sampling periods. The filled circles indicate the locations of the tracer samplers. With the exception of a single monitor operated at Long Mesa, every tracer sampler was collocated with an IMPROVE aerosol sampler (see section 3.1). The sampling periods for both the aerosol and tracer samplers were synchronized to permit direct comparison of aerosol and tracer data.

For the routine tracer monitoring network (Figure 3-2), programmable Brookhaven Atmospheric Tracer Samplers (BATS) were used for sample collection. The sampler consists of two sections: the lid, containing the sample tubes, and the base, containing the power control. The BATS base contained a constant volume flow pumping system which drew sample air through each sampling tube. The flow rate is selected by setting an internal switch to 10,20,30,40, or 50 mL/min of air (at standard temperature and pressure); the switch controls the on/off cycling rate of the pump over a one-minute period. For Project MOHAVE, the sampling rate was 50 mL/min. The sample air flows consecutively through the tubes by means of a multiple port switching valve. A digital printer and integrated circuit memory module recorded the start time, day of week, and the tube number for each sample. The BATS removable lid held 23 stainless steel sampling tubes, each packed with approximately 150 mg of Ambersorb adsorbent. The Ambersorb adsorbed the tracers from the sample air flowing through the tube. Breakthrough of the perfluorocarbon tracer gases was less than 0.1%. The tracer gases remain adsorbed until heat is applied to desorb the tracers during analysis.

In addition to the 24- and 12-hour sampling, higher time resolution monitoring of PFTs was conducted for limited periods of time at the Meadview and Dolan Springs sites. A field version of the electron capture gas chromatograph with a dual trap (one sampling while the other is analyzed) was employed at Meadview to collect and analyze on-site the PFT concentrations with 15 minute time resolution for a two week period from July 28 to August 11, 1992. Occasional electrical power interruptions meant that this system was not operated continuously during this period. The Department of Energy collocated a BATS system programmed for two-hour sampling at the Dolan Springs site to take advantage of the nearby release of tracer at MPP. This higher temporal resolution data is available from DOE for a three week period from July 9 to July 31, 1992.

The PFT samples were analyzed at Brookhaven National Laboratory using electron capture gas chromatography. For analysis, the PFTs, retained on the adsorbent in the BATS tubes, were desorbed by resistance heating of the tubes to $460\,°C$. The sample was passed through a precut column and a Pb catalyst bed before being reconstituted in an in situ Florisil trap. Once the trap was thermally desorbed, the sample again passed through the same catalyst bed, and then through a permeation dryer. The sample was then passed into the main column of the gas chromatograph where it was separated into the various perfluorocarbon constituents and ultimately into the electron capture detector. The experimental procedure is described in more detail by Dietz (1996).
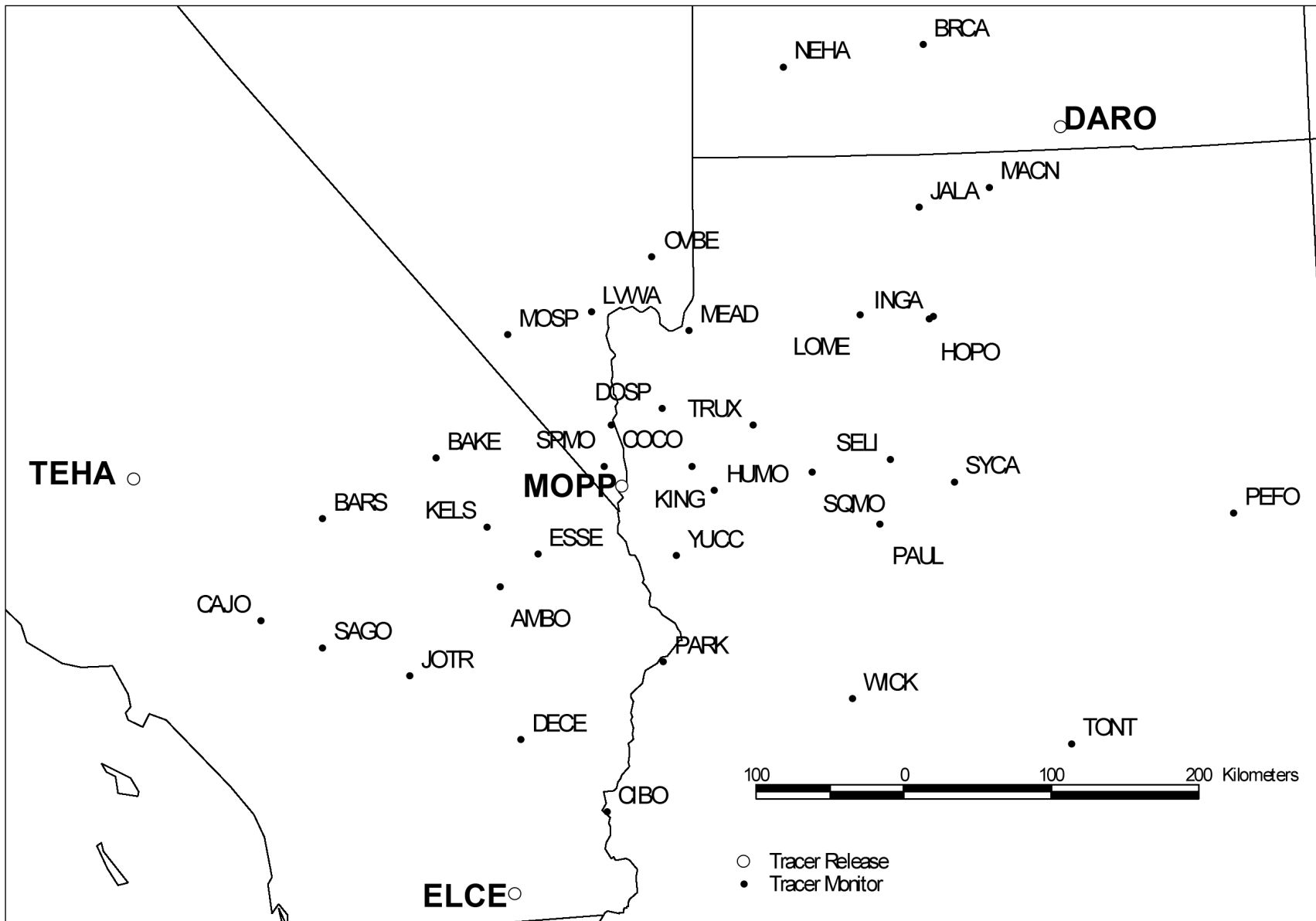
Figure 3-2 Tracer release and monitoring network.
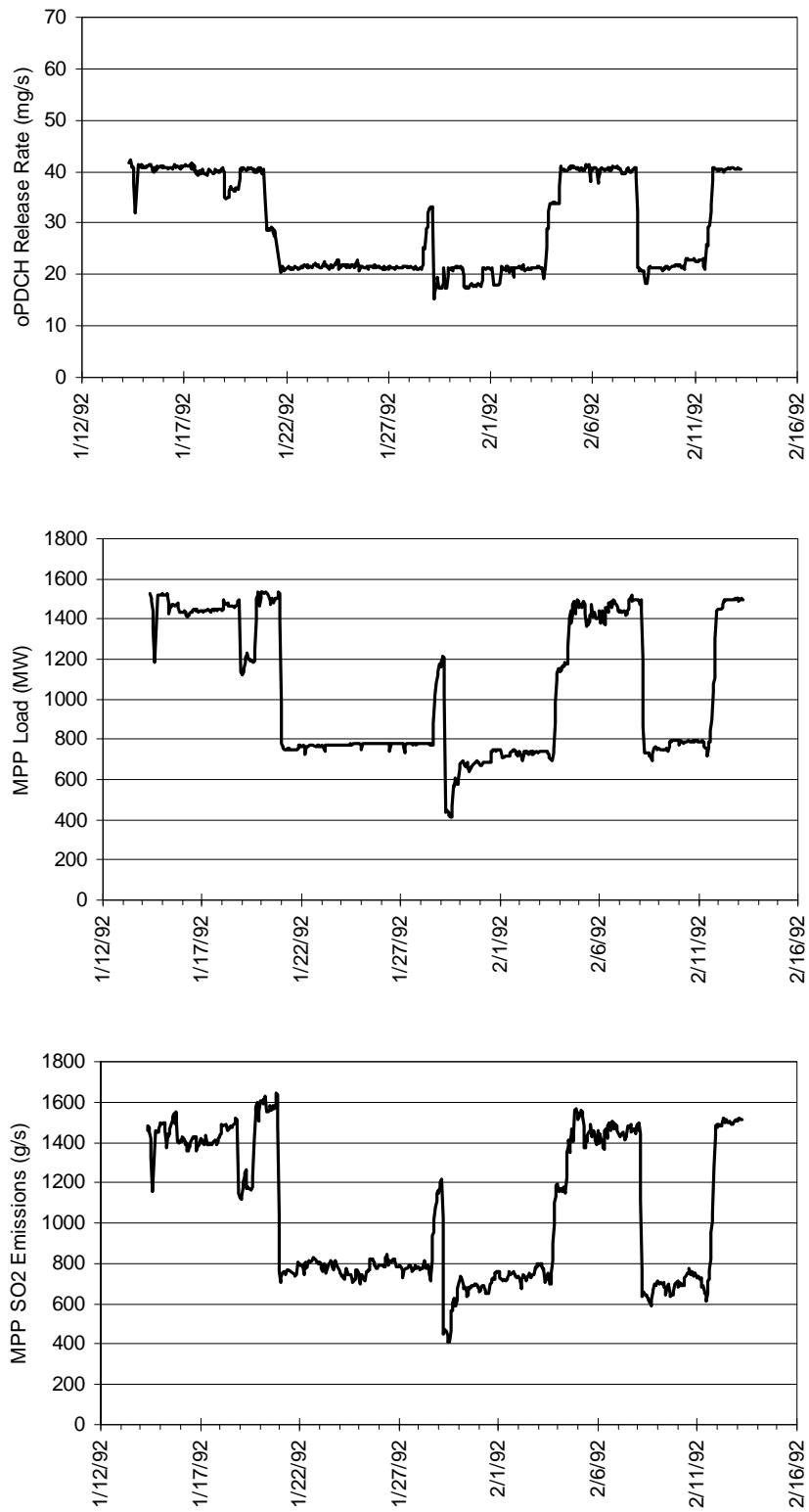
Figure 3-3 Time series of oPDCH tracer release rate, power load, and SO$_2$ emission at MPP during the winter intensive.
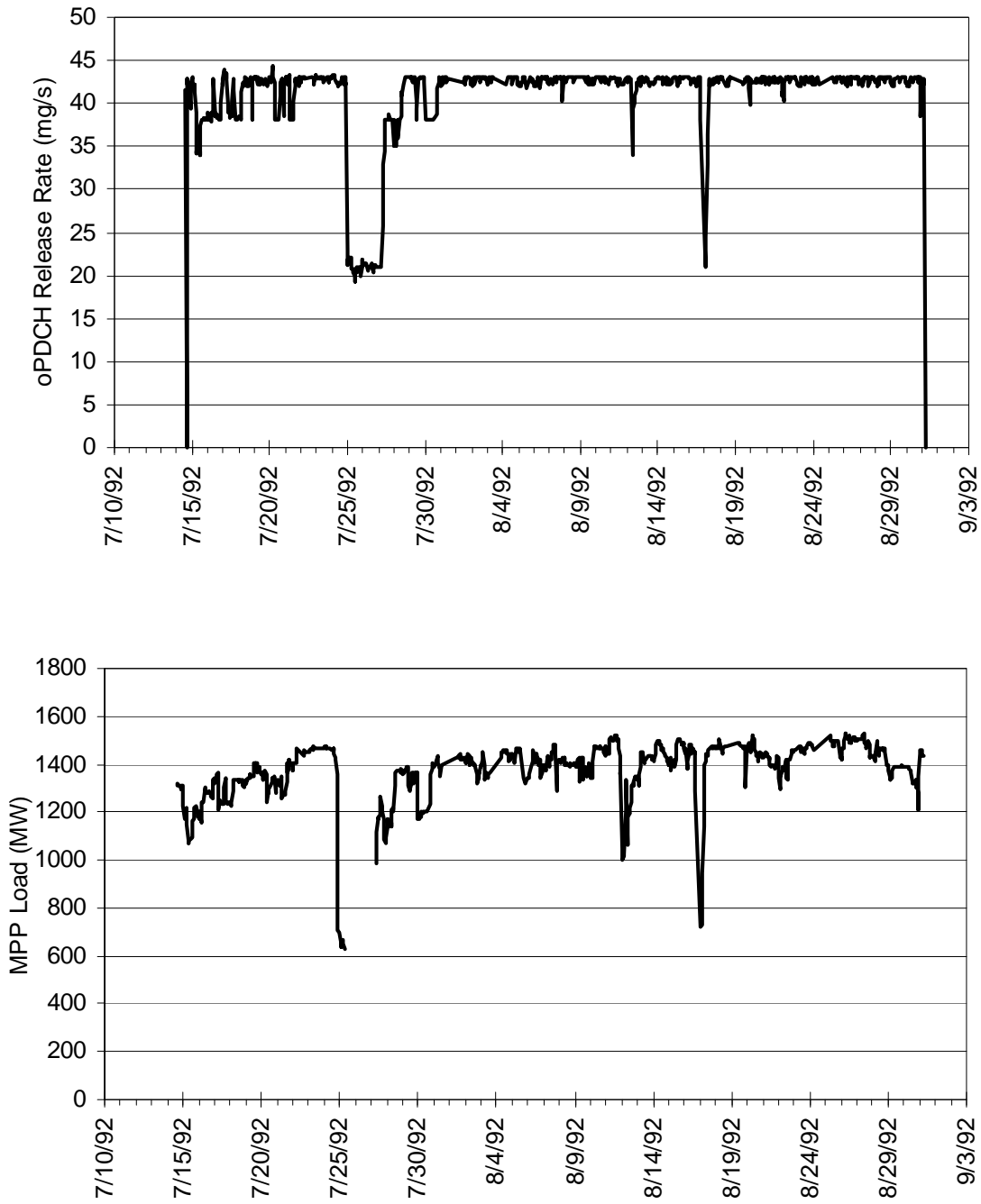
Figure 3-4 Time series of oPDCH tracer release rate and power production at MPP during the summer intensive.
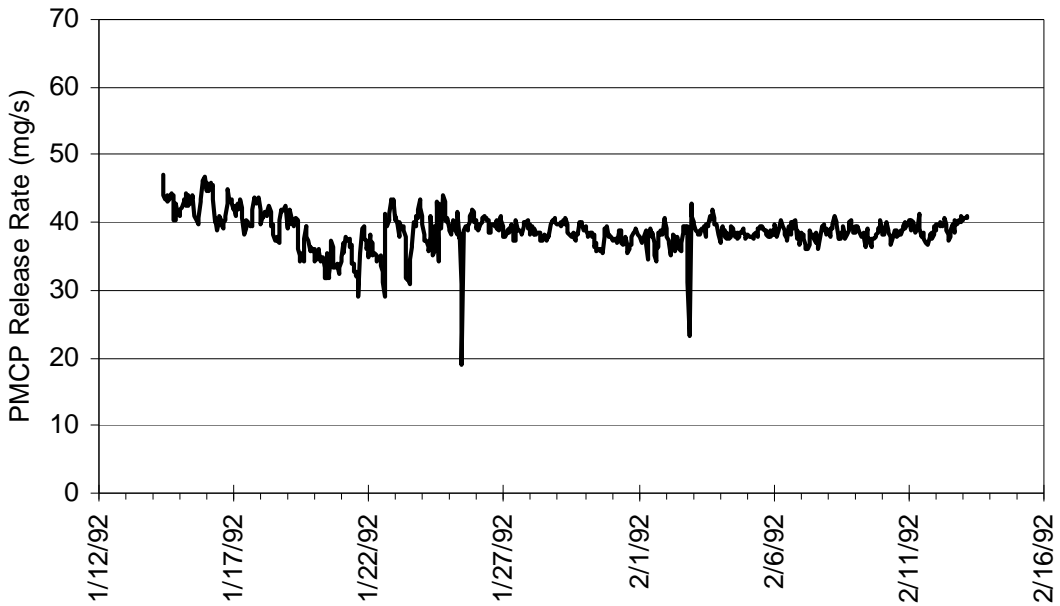
Figure 3-5 Time series of hourly average PMCP tracer release rate from Dangling Rope during the winter intensive.
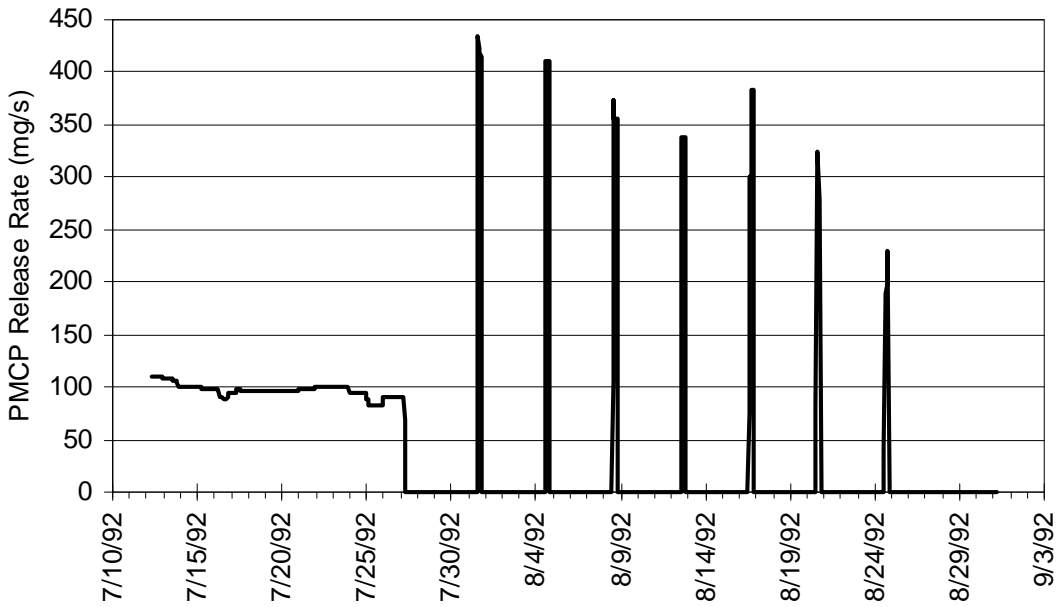
*Figure 3-6 Time series of hourly average PMCP tracer release rate from Tehac**h**api Summit during the summer intensive.*
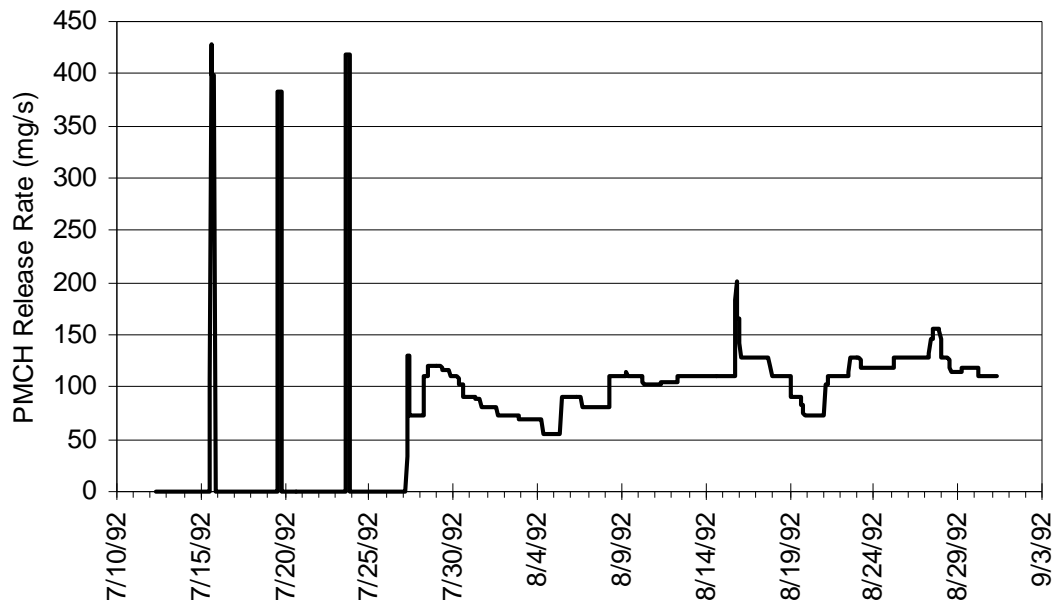
Figure 3-7 Time series of hourly average PMCH tracer release rate from Tehachapi Summit during the summer intensive.
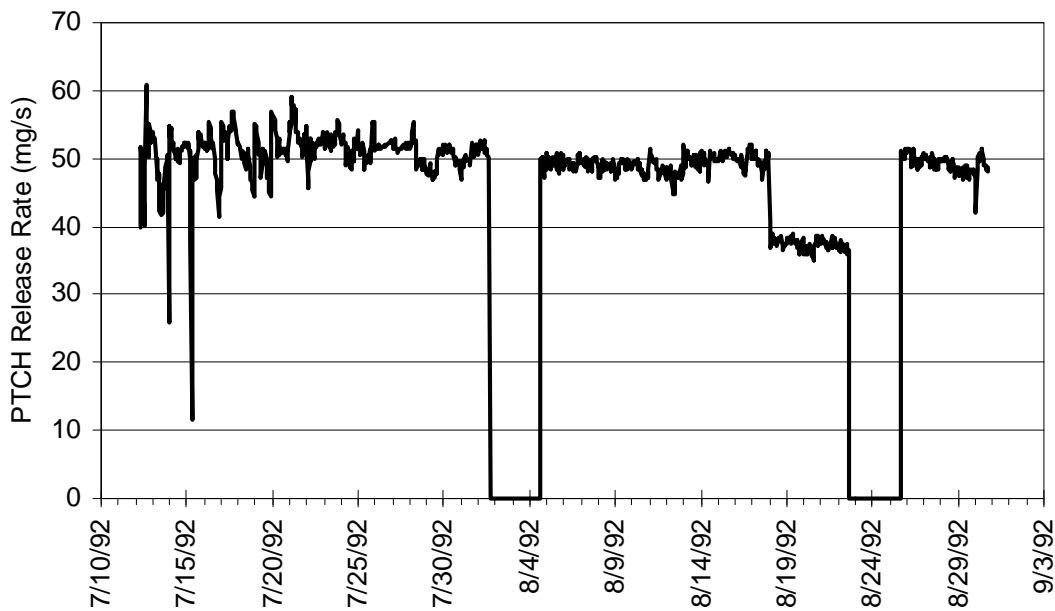
Figure 3-8 Time series of hourly average PTCH tracer release rate from El Centro during the summer intensive.

3-17

Table 3-7 Summary of the location and quantity of PFT's released during Project MOHAVE

PFT	Release Location	Total Released (kg)	Start Date (MST)	Stop Date (MST)
PMCP	Dangling Rope	100	1/14/92 0900	2/13/92 0500
PMCP	Tehachapi Summit	125	7/12/92 0700	7/27/92 0700
PMCP	Tehachapi Summit	9	7/31/92 1400	7/31/92 2000
PMCP	Tehachapi Summit	9	8/4/92 1300	8/4/92 2000
PMCP	Tehachapi Summit	8	8/8/92 1300	8/8/92 2000
PMCP	Tehachapi Summit	8	8/12/92 1400	8/12/92 2100
PMCP	Tehachapi Summit	7	8/16/92 1300	8/16/92 2000
PMCP	Tehachapi Summit	7	8/20/92 1300	8/20/92 2000
PMCP	Tehachapi Summit	5	8/24/92 1300	8/24/92 2000
oPDCH	Mohave Power Project	73	1/14/92 0700	2/13/92 0700
oPDCH	Mohave Power Project	176	7/12/92 0700	8/31/92 0700
PMCH	Tehachapi Summit	9	7/15/92 1300	7/15/92 2000
PMCH	Tehachapi Summit	9	7/19/92 1300	7/19/92 2000
PMCH	Tehachapi Summit	9	7/23/92 1400	7/23/92 2000
PMCH	Tehachapi Summit	315	7/27/92 0600	8/31/92 0700
PTCH	El Centro	90	7/12/92 0700	8/1/92 1600
PTCH	El Centro	72	8/4/92 1600	8/22/92 1600
PTCH	El Centro	22	8/25/92 1600	8/30/92 2000

3.3.1   Calculation of Ambient PFT Concentrations

Prior to the winter tracer study, during November and December 1991, a background study was conducted in the study area for a period of 10 days at each site. The BATS samplers were deployed at 27 sites. Each sampling period was 12 hours. The pump flow rates for each sampler were measured at Brookhaven National Laboratory before and after the background study and standardized to standard temperature and pressure conditions. The volume sampled depends on the density of air at the sampling location, so density was estimated at each location.   At two sites, hourly temperature, pressure, and humidity data was available to calculate atmospheric density. At the other sites, density was calculated using hourly virtual temperature and pressure estimates from measured data and application of the hydrostatic equation. Standards were run on each of the two gas chromatographs to determine the response curve of the instrument. Each sample run could then be determined to represent a quantity of perfluorocarbon in femtoliters (10^{-15} l). The atmospheric concentration was then obtained by dividing by the sample volume.

Average background concentrations for each perfluorocarbon were calculated. For ocPDCH, one episode of elevated concentrations up to 50% above background occurred at many sites during the background study. These elevated values had an insignificant effect upon the average background concentration (less than 0.01 fl/l ocPDCH). Calculated ambient backgrounds of the released PFTs were: ocPDCH, 0.52 fL/L; PMCP, 5.45 fL/L; PMCH, 4.83 fL/L; PTCH, 0.61 fL/L.

For the winter and summer intensive sampling periods, sample volumes were not explicitly determined. To determine concentrations of released PFTs, ratios of the chromatogram peak

heights of each released PFT to ptPDCH (not released) were compared to the pre-release ratio. By correcting for non-linearities in the chromatograph response curve and some response change between the pre-release study and the winter and summer studies, the sample concentrations can be calculated as:

$$C_{T,S} = \frac{\left(\dfrac{H_{T,S}}{H_{R,S}}\right)}{\left(\dfrac{H_{T,BG}}{H_{R,BG}}\right)} \; x \; C_{T,BG} \; x \; F_{CAL}$$

(3–1)

where $C_{T,S}$ = tracer concentration in sample; $H_{T,S}$ and $H_{R,S}$ = peak heights of released and reference (ptPDCH) tracers in sample; $H_{T,BG}$ and $H_{R,BG}$ = peak heights of released tracer and reference tracer from background study; $C_{T,BG}$ is the concentration of the released tracer from the background study; and F_{CAL} is a factor that accounts for changes in the chromatograph response to the released and reference tracer from the background study. The tracer concentration due to the release is then given by $C_{T,S}$ minus a background concentration.

Rather than subtracting the concentrations determined from the background study, the concentrations due to the Project MOHAVE releases were calculated by subtracting average concentrations for the few days of sampling immediately before tracer release for the winter and summer studies. This data set contained 105 values for the winter and 132 values for the summer. For the released tracers, calculated concentrations rose slightly between the background and winter studies and more between the winter and summer studies. The increase in calculated background between the background and summer studies was 8% for ocPDCH, 9% for PMCH, and 15% for PMCP. PFT samples were collected during the interim period between the winter and summer intensive sampling periods at Long Mesa and Hopi Point. Background levels and standard deviations are shown in Table 3-8. It should be noted that the winter and summer backgrounds were not calculated using measured volumes as in the background study; they were calculated using the ratio to ptPDCH method described above. The ptPDCH concentration was assumed to be invariant during all three studies. It is expected that the true background values did not rise as much as the 8%,9%, and 15% amounts; rather, variability in the analytical methods and assumptions used in the concentration calculations are more likely the reason for the increase. The variability, of course, increases the uncertainty in the calculated PFT concentrations.

Increases in background could occur due to releases associated with Project MOHAVE and through manufacturing and use of the PFTs for other purposes. In an article on background PFT measurements taken in 1994 in Austria in support of the European tracer experiment (ETEX) Piringer et. al. (1997) suggest that atmospheric levels of PFTs have been increasing over the last decade or so. The approximate increase in atmospheric PFT levels due to Project MOHAVE can be estimated by comparing the mass of PFTs released by Project MOHAVE to the estimated atmospheric mass of PFTs. Assuming the mass of the atmosphere is 5.2×10^{18} kg (Warneck, 1988), the troposphere contains 80% of the mass of the atmosphere (Wallace and Hobbs, 1977), and the PFTs are well mixed through the troposphere, the increase in PFTs due to Project MOHAVE releases is 0.13% for PMCP; 0.14% for PMCH, 0.38% for ocPDCH and 0.47% for PTCH.

Table 3-8 Background perfluorocarbon concentrations (fL/L). Uncertainties are the standard deviation of the background measurements.

PFT	Background study (Nov 25-Dec 5, 1991)	Winter study (Jan 11-13, 1992)	Interim Period (Feb 22-Jun 26, 1992)	Summer study (Jul 5-11, 1992)
ocPDCH	0.52 ± 0.06	0.53 ± 0.05	0.52 ± 0.04	0.56 ± 0.06
PMCP	5.5 ± 0.3	5.7 ± 0.8	5.3 ± 0.6	6.3 ± 0.6
PMCH	4.8 ± 0.3	4.9 ± 0.4	5.0 ± 0.3	5.3 ± 0.3
PTCH	0.61 ± 0.16	Not determined	Not determined	0.6 ± 0.6

3.4 Optical Monitoring Network

During the winter intensive sampling period (1/11/92 – 2/13/92), three Optec, Inc. Next Generation Nephelometers (NGN's) were installed by Air Resources Specialists at Amboy, Cajon Pass, and Joshua Tree National Monument. Nephelometers measure the scattering of light by particles which is an important component of the total extinction budget. Each nephelometer was equipped with sensors to measure chamber temperature, ambient temperature, and relative humidity. In addition to the particle scattering coefficient, the total extinction coefficient was also measured using transmissometers at the following locations: Meadview, Bandelier National Monument, Big Bend National Park, Canyonlands National Park, Chiricahua National Monument, Grand Canyon National Park (South Rim and West In-Canyon), Guadalupe Mountains National Park, Mesa Verde National Park, Petrified Forest National Park, and San Gorgonio Wilderness Area. The transmissometers measure the average irradiance of a light source of known intensity over the path length of the instrument.

For the summer intensive sampling period (7/12/92 – 9/3/92), six nephelometers were deployed at Cajon Pass, El Centro, Joshua Tree National Monument, Kelso, Tehachapi, and Meadview. The same network of transmissometers used during the winter intensive sampling remained in operation through the end of the summer intensive sampling period. A map of the locations of each of these monitors is shown in Figure 3-9.

3.5 Meteorological Monitoring Network

Meteorological monitoring is necessary to characterize the speed, direction, and depth of air mass transport in the region and for model validation and initialization. The existing network of National Weather Service and other monitoring sites in the region was insufficient to characterize the complex meteorological setting of the study area. Additionally, for the sparse network of NWS upper air measurement sites, vertical profiles are taken only twice per day. Thus, they do not capture potentially important changes in meteorological conditions, such as the full resolution of a diurnal cycle. While it was recognized that it would be impossible with available funds to set up a meteorological monitoring network to capture all flows of interest, the existing network was supplemented with additional measurement sites.
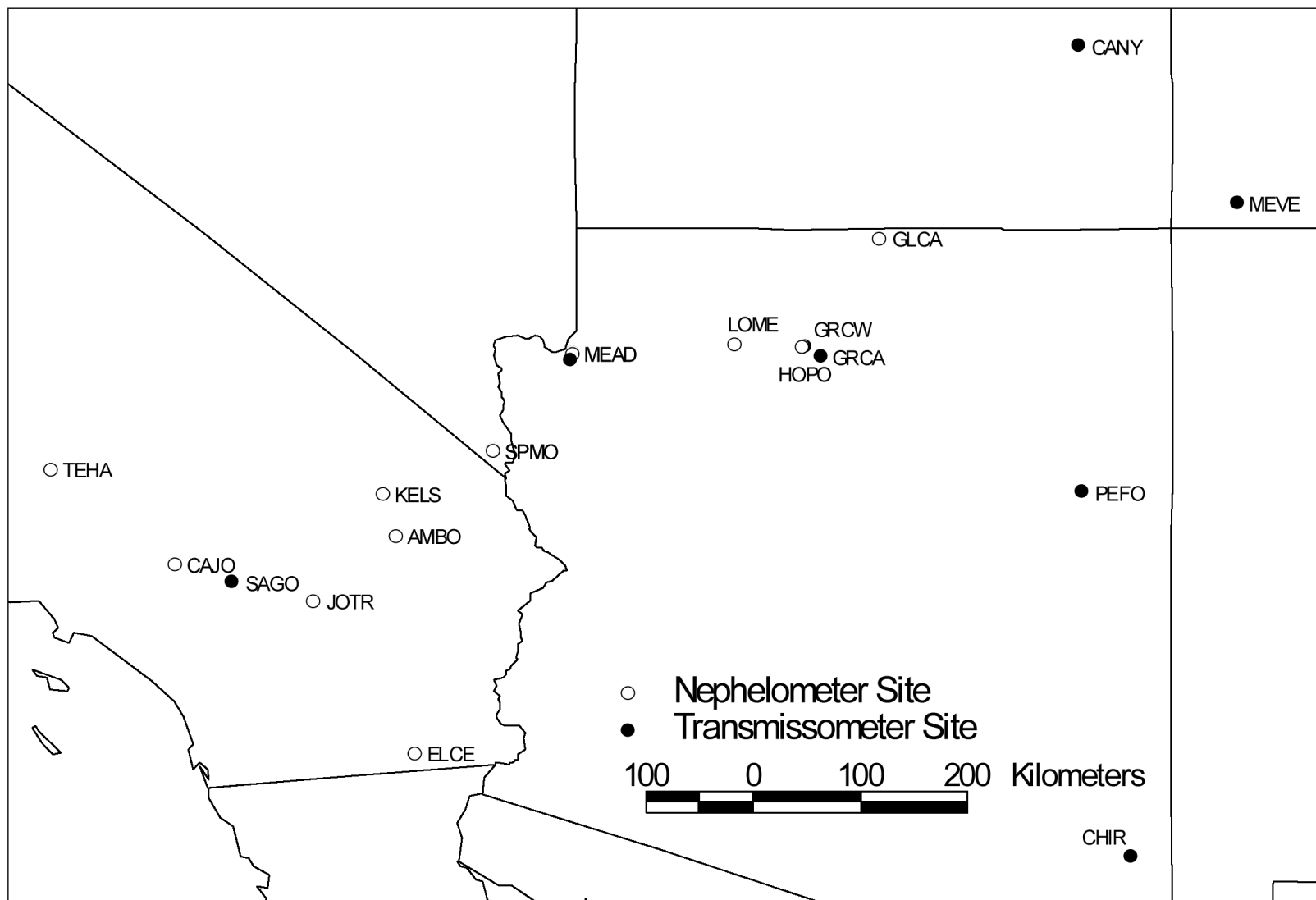
Figure 3-9 Optical properties network from Project MOHAVE including total extinction coefficient and particle scattering coefficient.

The additional sites had both surface and upper-air measurements. They consisted of doppler wind profiling radars (915 MHz), Radio Acoustic Sounding Systems (RASS), doppler sodars, and rawinsondes for upper air measurements and typically, wind speed and direction, temperature, relative humidity, and pressure for surface measurements. The radar wind profilers allow for continuous remote sensing of the three components of wind (u, v, and w) from about 100 m to approximately 3-4 km above the surface, with the maximum height being roughly proportional to absolute humidity. Data are reported as hourly averaged values of horizontal wind speed and direction and vertical velocity for 100 m thick layers at the high resolution mode and 400 m thick layers at the low resolution mode. At the higher levels, the 400 m mode provides greater data recovery than the 100 m mode. The RASS gives virtual temperature profiles by measuring the vertical distribution of the speed of sound using the scatter of radar waves from the vertically propagating acoustic waves (Neff, 1990). The RASS has a range of about 150 m to 600 m with a resolution of about 50 m.

The rawinsondes used for the study use balloon-borne instruments to measure wind speed, wind direction, temperature, relative humidity (RH), and pressure from near the surface to 5000- 6000 m AGL. The resolution for wind speed and direction measurements was typically 50-100 m, while the resolution of the temperature, RH, and pressure measurements was generally 20-30 m. The measurements were usually twice per day, although three times per day measurements were also made. Surface meteorological measurements were also made at the optical monitoring sites and SCE's long-term air quality monitoring sites. Data from all National Weather Service monitoring sites in the study region were also archived and added to the Project MOHAVE database. During the summer, the US Army radiosondes at Yuma, normally used only 5 days per week were augmented to 7 days per week operation. Although they were not sponsored by Project MOHAVE, additional radar wind profilers were also operated in Southern California during the summer intensive study; data from these profilers is included in the Project MOHAVE database. Additional upper air monitoring locations, instrumentation used, and purposes are shown in Table 3-9. The locations of meteorological stations are shown in Figure 3-10.

Table 3-9 Locations and purposes of supplemental upper-air meteorological monitoring for Project MOHAVE.

Location	Instrument	Season	Purpose
MPP	WP,RASS,S	Y	Initial transport of MPP emissions; stability
MPP	R	W	Evaluation of collocated wind profiler; wind, stability, and moisture profiles
Truxton	WP, RASS	Y	Open terrain site representative of regional flow patterns
Meadview	WP, RASS	W, S	Grand Canyon receptor site closest to MPP
Cedar City, Prescott, Yuma	R	W	Fill in gaps in NWS radiosonde network
Needles	WP, R	W	Along Colorado River, downwind of MPP in winter
Overton Beach	S	S	Monitor drainage flow from Reid Gardner power plant toward lower Grand Canyon
Page	R	Y	Monitor transport from northeast of Navajo power plant and other sources
Cottonwood Cove, Dolan Springs	R	S	Possible Colorado River Valley exit locations for MPP plume
WP= Radar Wind Profiler, S= Sodar, R= Radiosonde, Y= Year-round, W= Winter, S= Summer			
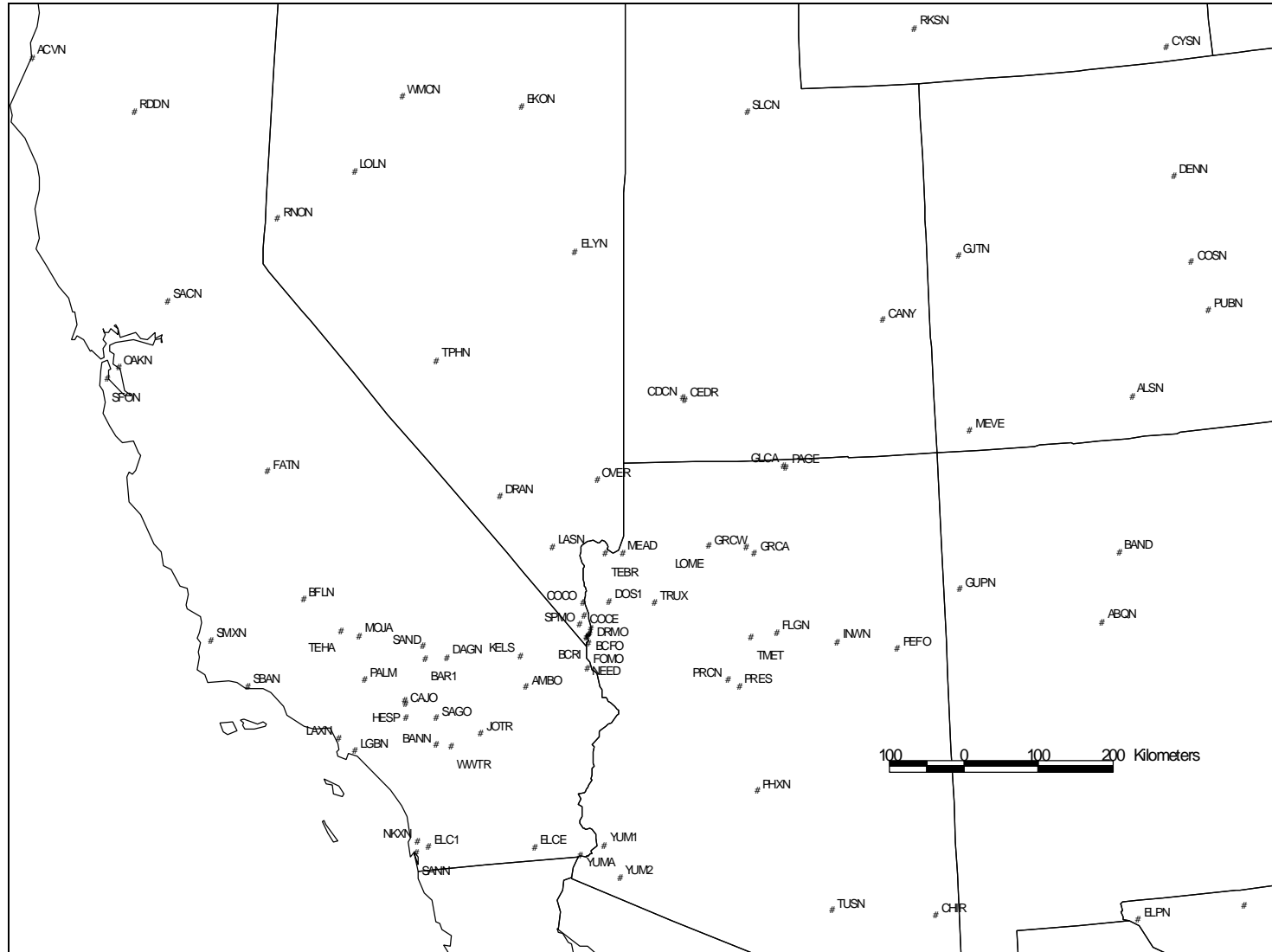
Figure 3-10 Meteorological observation sites.

4. Measurement Evaluation

This section evaluates the measurements taken during the study and determines the degree of confidence that is associated with each one. Most of the measurements were characterized in terms of their completeness, precision, lower quantifiable limit, and accuracy. The specific approaches for determining these parameters for each measurement are described in the following subsections. Generally, however, they can be defined as follows:

Completeness reflects the percentage of valid Level-1 data obtained, as compared to the maximum amount that could have been obtained. Level 1 (univariate) validation involves checking the data for outliers, unrealistic rates of change, and proper indication of time and location of data.

Precision is a measure of mutual agreement among individual measurements of the same observable under similar prescribed conditions. Precision is estimated by repeated measurements with the same monitor and calibration system.

The lower quantifiable limit (LQL) is the lowest value that can be distinguished in the ambient atmosphere. Sources of variability that influence the LQL can include instrument noise and variability.

Accuracy represents the extent to which a measurement differs from its true value. Accuracy is evaluated by the deviation of a measurement from a reference value which is provided by known or standard reference materials.

4.1 Optical Data Quality

Visual air quality was monitored during Project MOHAVE using integrating nephelometers to measure light scattering and transmissometers to measure total light extinction. The details of these measurements were described in Section 3.4.

4.1.1 Nephelometers

Optec, Inc. NGN nephelometers were used for the light scattering measurements. The quality of the nephelometer data is summarized below.

4.1.1.1 Completeness

Data completeness for the nephelometer is defined as the percent of hours each instrument was collecting valid Level-1 data throughout its complete period of operation. Data completeness exceeded 90% for all sites during the winter intensive and for four of the six sites during the summer. The sites falling below 90% completeness during the summer were Meadview (81.3%) and Cajon Pass (60.3%). Data recovery exceeded 95% during both intensives for all of the ambient temperature and relative humidity sensors that were collocated with the nephelometers.

4.1.1.2 Precision and Lower Quantifiable Limit

The precision of the NGN nephelometers was determined from the drift of the slope of the calibration line based on multiple manual zero air checks and span checks using Freon-22. The estimated precisions during the winter intensive were all within ±20%, determined at 95% confidence from the standard deviation of repeated calibrations. Nephelometer performance during the summer intensive was variable. For three instruments (Joshua Tree, Cajon Pass, and Meadview), precision was within ±15%. Two other instruments suffered poorer precision, Meadview #1 at 25.5% and Kelso (an NGN-1 nephelometer) at 41.1%. For the remaining three instruments (El Centro, Tehachapi, and Cajon Pass #1), only two calibration checks were conducted during the course of the study, so insufficient data were available for statistical analysis.

For the NGN nephelometer, the LQL is ±1 count, the maximum resolution of the electronics of the instrument, which represents approximately ±1 Mm^{-1}.

4.1.1.3 Accuracy

The NGN nephelometer accuracy was judged against instrument response to a separate supply of Freon-22 gas, supplied by an independent auditor. Audits were conducted at three sites during the summer intensive (Cajon Pass, Joshua Tree, and Meadview). The accuracy of all instruments was judged to be within ±4% at the Freon-22 calibration level of approximately 80 Mm^{-1}.

4.1.1.3.1   Sampling Bias

The NGN nephelometer was designed to minimize sampling biases, compared to older model nephelometers. Still, some small biases remain which would cause the measured scattering to underestimate ambient scattering. First, a perfect nephelometer would measure scattering throughout the entire field of view of the instrument, from 0 to 180°. The integration angles for the NGN are 5 to 175°. For small particles ($PM_{2.5}$), this truncation error is less than 10%.

Next, the measured scattering corresponds to a nominal wavelength of 550 nm for the NGN nephelometer. The actual spectral response of the instrument's light detector can cause an error of less than 2%, again determined for fine particles.

Finally, heating of the air sample in the nephelometer chamber can cause volatile aerosol components such as water to be lost, thereby reducing the measured scattering. However, the open-air design of the NGN nephelometer reduces chamber heating to less than 1°C in most cases. At the low relative humidities common in Project MOHAVE, the effects of such heating are minimal, well within the precision of the measurement.

4.1.2   Transmissometers

Total light extinction was determined using transmissometers, which measure the average irradiance of a light source of known intensity over the path length of the instrument. The quality of the transmissometer data is summarized below.

4.1.2.1 Completeness

Data completeness for the transmissometer is defined as the percent of hours each instrument was collecting valid Level-1 data throughout its complete period of operation. Data completeness exceeded 95% for most sites and 85% for all sites during the winter intensive, the summer intensive, and the interim period between intensives. Data completeness for the transmissometer is also reported in terms of the number of valid 1-hour averages obtained during periods not influenced by meteorological events such as fog, rain, and blowing dust. Weather-modified completeness exceeded 70% for many sites and exceeded 50% for most sites, with the exception of Big Bend (45%), Canyonlands (35%), Chiricahua (41%), and Petrified Forest (23%) during the winter intensive, and Chiricahua (37%) during the summer intensive. These lower values reflect adverse weather events and are not necessarily indicative of poor instrument performance.

4.1.2.2 Precision and Lower Quantifiable Limit

For the transmissometers, the precision of the light extinction measurements, determined from the variability of light extinction within a single hour, varied from ±2% without optical interference to ±20% with optical interference, such as clouds passing through the sight path.

For transmissometer measurements, the LQL represents the resolution of the instrument, or the smallest change in extinction that can be distinguished. The LQL for the instrument is approximately 0.3% transmittance, which corresponds to an extinction change of ±1.5 Mm^{-1} under clear conditions of around 10 Mm^{-1}. At the other end of the range, the ability of the instrument to quantify hazy conditions is determined by values at low transmittance (i.e., high extinction, or low visibility). For every transmissometer sight path, a maximum usable b_{ext} was calculated that corresponds to a 5% transmittance for the path. All sight paths were selected such that, based on historical visibility data, extinction greater than this maximum b_{ext} occurs less than 1% of the time. When the measured b_{ext} was greater than this maximum value, it was assumed that meteorological or optical interferences, not ambient aerosols, were causing the high extinction. All measurements greater than the calculated site-specific maximum threshold are flagged in the data file.

4.1.2.3 Accuracy

The accuracy of the transmissometer measurements was determined through pre- and post-study lamp calibrations and through routine field checks which verified instrument alignment and cleanliness. Accuracy of ±3% transmittance was met throughout the study. Independent system audits of several transmissometers revealed no problems with instrument alignment or settings.

4.1.2.3.1   Measurement Bias

During validation, all transmissometer data were subjected to checks to identify meteorological or optical interferences. The intensity of the light in the sight path can be modified not only by the intervening aerosol, but also by:

- The presence of condensed water vapor in the form of fog, clouds, and precipitation.

- Condensation, frost, snow, or ice on the shelter windows.

- Reduction in light intensity by insects, birds, animals, or vegetation along the sight path, or on the optical surfaces of the instrumentation or shelter windows.

- Fluctuations in light intensity due to optical turbulence, beam wander, atmospheric lensing, and miraging caused by variations in the atmospheric index of refraction, and by the known drift in lamp intensity.

Validation checks based on expected minimum and maximum values and rates of change were applied to identify these anomalous conditions. Data failing the checks are flagged with identifier codes in the data base.

Large diurnal fluctuations in the transmissometer values at Meadview were observed during the winter intensive. It was determined that a cold air drainage flow in the sight path was apparently broadening the beam at nighttime due to density discontinuities in the atmosphere. The transmissometer sight path was changed prior to the summer intensive in order to alleviate this problem.

4.1.3 Light Absorption

Light absorption (b_{abs}) measurements in Project MOHAVE were conducted using the Laser Integrating Plate Method (LIPM) on the IMPROVE sampler Teflon filters collected for gravimetric mass and elemental analysis. Data quality for these measurements is described in detail in Section 4.2, which covers the filter-based measurements, and will be summarized here.

The overall sample recovery rate was 94% during the winter intensive and 92% during the summer intensive. Sites that did not achieve at least 80% recovery are listed in Section 4.2.

The mean relative precision for the b_{abs} measurements was 13% for the winter intensive and 15% for the summer intensive. In the winter intensive, 98% of samples registered b_{abs} values above the LQL, compared with 100% of samples in the summer.

The LIPM used for b_{abs} measurements was subjected to a calibration check after every fifth sample, using a set of ten control filters. The average standard deviation of these calibration checks during Project MOHAVE was 1.5%.

Differing interpretations of the light absorption measurement (b_{abs}) can lead to a discrepancy of a factor of two in the reported b_{abs} values. In reporting b_{abs} for IMPROVE and Project MOHAVE, UC Davis (UCD) applies a correction factor to account for shadowing of absorbing particles by other particles captured on the filter (UC Davis, 1994). This shadowing correction typically increases the reported b_{abs} value by about a factor of two over the LIPM measurement. Other groups, such as DRI, apply no correction to the measured b_{abs}, and still others (Weiss, 1989; Waggoner, 1995) argue that the measured b_{abs} should be decreased by up to a factor of two to account for filter matrix effects. Heintzenberg et al. (1997) conclude that the b_{abs} methods used in IMPROVE appear to yield values that are high, perhaps by large amounts. This conclusion is supported by laboratory experiments conducted by Horvath (1993). To date, the b_{abs} correction

discrepancy has not been resolved, so the numbers reported in the Project MOHAVE data base can be considered to be an upper bound to the possible range of values.

4.2 Aerosol Data Quality

The aerosol measurement methods were described in Section 3.1.1. Most of the filter sampling measurements were conducted using the IMPROVE aerosol sampler and various samplers operated by BYU. Additional, specialized aerosol measurements were also conducted by the University of Minnesota and Aerosol Dynamics, Inc.

4.2.1 UCD IMPROVE Samplers

Aerosol sampling at most sites was conducted using the IMPROVE sampler. The quality of the IMPROVE aerosol data is summarized below.

4.2.1.1 Completeness

Sample recovery rates and observed ranges for flow rate and particle cut point are summarized below. The recovery rate is based on the number of samples in the final database with valid analysis of the Teflon A filters. The flow rate and particle cut point are for the A modules. There were 33 sampling days in winter and 53 in summer.

The overall recovery rate during the winter intensive was 94%. Three of the 33 samplers had less than 80% recovery. The Indian Gardens 12-hour sampler had a defective relay that caused the loss of every third sample at times, so recovery was 77%. Fortunately, the 24-hour Teflon A sampler at Indian Gardens had a 97% recovery rate. The Overton Beach site was vandalized twice, so only 70% recovery was achieved. A week of samples at New Harmony was lost when water collected in the cyclone, resulting in 79% recovery.

The overall recovery rate during the summer intensive was 92%. Six of the 34 samplers had less than 80% recovery. The low recoveries at four of these sites (Petrified Forest: 74%, Wickenburg: 75%, Cibola: 60%, and New Harmony: 75%) appear to have been associated with summer electrical storms and related high winds, power outages, and power surges. Six clocks were damaged by power surges at these sites and two samplers were blown over. Overton Beach again had vandalism, losing the last two weeks and achieving 72% recovery overall. Operator problems at El Centro resulted in 70% recovery.

The IMPROVE sampler is designed such that a 50% capture particle size cutpoint of 2.5 μm is achieved at a flow rate of approximately 22.8 lpm (actual volume, not corrected to STP). The equation used to calculate the D_{50} cut point of the sampler is

$$D_{50} = 2.5 - 0.334(Q - 22.8) \tag{4-1}$$

where Q is the flow rate in lpm. At most sites the mean flow rate over each intensive period was between 21.1 and 24.1 lpm, yielding cutpoints between 3.0 and 2.0 μm, respectively. The exceptions during the winter were Joshua Tree (21.0 lpm, 3.1 μm), Hualapai Mountain (20.9 lpm, 3.1 μm), Jacob Lake (21.0 lpm, 3.1 μm), Las Vegas Wash (19.2 lpm, 3.7 μm), Mountain

Springs (18.2 lpm, 4.0 μm), New Harmony (20.7 lpm, 3.2 μm), and Wickenburg (27.3 lpm, 1.0 μm). The exceptions during the summer were Baker (20.8 lpm, 3.1 μm), Cottonwood Cove (20.9 lpm, 3.1 μm), and Mountain Springs (20.8, 3.1 μm). In all but one of these cases, the flow deviation resulted in a cutpoint exceeding the design value, which would allow somewhat more coarse material to pass but, for most aerosols, would not alter the measured concentration of secondary particles appreciably. At Wickenburg in the wintertime, however, the 1.0 μm cutpoint might cause some of the secondary material to be missed.

4.2.1.2 Precision

The concentrations for gravimetric mass, carbon, and ions were calculated from the measured mass of the component, M, the mean field blank value, B, and the sampled volume, V, using the equation:

$$C = \frac{M - B}{V} \qquad (4\text{-}2)$$

For gravimetric analysis, M is the difference between the mass measurements before and after sampling. Similarly for light absorption (b_{abs}) measurements, M represents the difference between light transmittance through the filter before and after sampling. For carbon and ions, M is the amount of the component measured on the filter.

The equations for PIXE, PESA, and XRF differ from those above for two reasons. First, the analytical methods measure areal density in ng/cm^2, so that the collection area, A, enters into the equation for concentration. Second, a blank filter is used during analysis to estimate spectral background, which is subtracted before the instrumental values are reported, so no field blank values are subtracted for any variable. The concentrations are calculated using:

$$C = \frac{A}{V}\left(\text{areal density}\right) \qquad (4\text{-}3)$$

The precision in the concentration will thus depend on the fractional precision of the analysis associated with calibration (f_{cal}), the fractional precision in volume (f_v, typically around 5%), and for all but the elements, the standard deviation of the field blanks (σ_{fb}). The constant analytical precision drops out because it is included in σ_{fb}. The equation for carbon and ions is:

$$\sigma^2(C) = \left(\frac{\sigma_{fb}}{V}\right)^2 + \left(\frac{2B}{V}\right)f_{cal}^2\, C + \left(f_{cal}^2 + f_v^2\right)C^2 \qquad (4\text{-}4)$$

The equation for mass and b_{abs} is:

$$\sigma^2(C) = \left(\frac{\sigma_{fb}}{V}\right)^2 + \left(f_v\, C\right)^2 \qquad (4\text{-}5)$$

The calibration term (f_{cal}) is not included because both mass and b_{abs} are determined from small differences between two measured values.

For PIXE, PESA, and XRF, there are two sources of uncertainty: the fractional calibration error (f_{cal}), and the statistical precision determined from the number of counts in the peak and background (f_s), based on standard Poisson statistics. The calibration uncertainty is the same for every element. It is monitored every analytical session from the precision for sulfur, hydrogen, and iron for a group of around 25 reanalyzed samples. The statistical precision is determined for every variable from the actual spectrum. The equation for precision for elemental measurements is:

$$\sigma^2(C) = \left(f_s^2 + f_{cal}^2 + f_v^2 \right) C^2 \qquad (\text{4-6})$$

For small concentrations, below around 10 times the minimum detectable limit (mdl), the precision is generally a constant $\mu g/m^3$, with a value of one-half the mdl. For large concentrations, above 10 mdl, the uncertainty due to counting statistics becomes unimportant, and the precision is generally a constant fraction of the concentration. This fraction is the quadratic sum of the volume and calibration precisions; for most variables, this is around 5%.

The mean relative precision was reported for each season, determined as the mean precision divided by the mean concentration for the season. These values are listed in Table 4-1 and Table 4-2. The variables beginning with OC and EC represent various fractions of organic and elemental carbon from TOR analysis. OCLT (organic carbon low temperature) is operationally defined as carbon evolved from filters at temperatures < 140 deg C in the absence of oxygen. OCHT (organic carbon high temperature) is carbon evolved from filters at temperatures between 140 and 550 deg C in the absence of oxygen plus pyrolyzed carbon. OC tot is the sum of OCLT and OCHT. ECLT (elemental carbon low temperature) is the non-pyrolyzed carbon evolved from filters at temperatures of 550 deg C in the presence of 2% oxygen. ECHT (elemental carbon high temperature) is the carbon evolved from filters at temperatures of 550 – 800 deg C in the presence of 2% oxygen. LAC (light absorbing carbon) is the sum of ECLT and ECHT.

Relative precision was generally under about 20% for gravimetric mass, light absorption (b_{abs}), most of the ions, and about half of the elements. Precision generally exceeded 20% for organic and elemental carbon, largelly due to high blank variability, and for elements with small concentrations. Precision was worse for 12-hour samples than for 24-hour samples because less material was collected on the filters.

Precision was also quantified at a few sites from collocated sampling using identical measurement systems. Precision determined in this manner accounts for all aspects of uncertainty, both in the field and in the laboratory.

A special study was conducted at Meadview in November 1991, just prior to the winter intensive, which included 14 fine IMPROVE modules with Teflon filters. Some modules had denuders and some did not, but it was assumed that the denuders would have no effect on the concentrations of elements on Teflon. The standard deviations of the collocated measurements were approximately equal to the propagated precisions for S, H, Zn, and b_{abs}, indicating that the propagated values accounted for all of the principal aspects of precision for these observables. However, the standard deviations of the soil elements (Si, K, Ca, Fe) exceeded the propagated precisions by over a factor of two. This difference may be attributable to a combination of particles near the cutpoint of the cyclone (recall the dependence of cutpoint on flow rate) and

possible inhomogeneities in the ambient concentrations, neither of which are incorporated into the propagated precision.

During the winter intensive sampling period collocated modules with Teflon filters were operated at Joshua Tree. During the summer intensive sampling period collocated modules with Teflon filters and carbonate impregnated afterfilters were operated at Cajon Summit and Spirit Mountain. Here, again, collocated precision for the soil elements, especially Fe, exceeded the propagated precisions, as did precisions for SO_2 determined on the impregnated filters, presumably due to the variability of loss of SO_2 in the sampler inlet.

Table 4-1 Mean relative precisions for variables measured by PIXE, PESA, XRF, and LIPM on the Teflon A filter.

Variable	Winter	Summer	Variable	Winter	Summer
H	7%	12%	Fe	5%	5%
Na	35%	46%	Ni	65%	38%
Si	6%	6%	Cu	8%	8%
S	5%	5%	Zn	7%	7%
Cl	79%	21%	As	44%	50%
K	7%	7%	Se	11%	11%
Ca	6%	6%	Br	7%	7%
Ti	12%	17%	Sr	17%	12%
V	71%	79%	Zr	54%	54%
Cr	64%	79%	Pb	11%	12%
Mn	24%	60%	b_{abs}	13%	15%

4.2.1.3 Lower Quantifiable Limit

For particulate matter measurements, the LQL is defined as the concentration equal to twice the precision. It is considered to be the lowest concentration that can be measured reliably. For low concentrations (at or near the LQL), the precision is dominated by the counting uncertainty for elemental analyses and by the blank variability for all other analyses. The other components of precision, flow rate and analytical calibration uncertainty, contribute little at low concentrations.

Table 4-2 Mean relative precisions for mass, carbon, ion, and SO_2

Variable	substrate	winter 24-hour	summer 24-hour	winter 12-hour	summer 12-hour
Mass	Teflon	6%	4%	17%	7%
OCLT	quartz	>100%	46%	>100%	>100%
OCHT	quartz	23%	12%	39%	43%
OC tot	quartz	24%	12%	39%	44%
ECLT	quartz	55%	13%	>100%	59%
ECHT	quartz	36%	25%	58%	49%
LAC (EC tot)	quartz	31%	13%	65%	38%
SO_4^{2-}	nylon	5%	5%	5%	7%
NO_3^-	nylon	5%	5%	11%	8%
Cl^-	nylon	57%	89%	>100%	>100%
SO_4^{2-}	Teflon	NA	NA	5%	5%
NO_3^-	Teflon	NA	NA	93%	9%
NH_4^+	Teflon	NA	NA	9%	8%
NH_3	citric acid	NA	NA	13%	35%
SO_2	carbonate	10%	7%	24%	7%

The chemical components whose concentrations fell above the LQL for more than 90% of the samples were, for the most part, those whose mean relative precisions fell below 10% (see Table 4-1 and Table 4-2). Thus, for example, elemental sulfur was detected in all samples, whereas organic and elemental carbon were detected in only about half of the samples.

4.2.1.4 Accuracy

Two components of the measurement are critical in assessing the accuracy of aerosol concentrations determined on filters: the accuracy of the flow measurement in the field and the accuracy of the analytical measurement in the laboratory.

Flow measurement accuracy is determined through flow checks using a metering device independent of that used for routine flow measurements. In Project MOHAVE, these checks were conducted during independent performance audits, which were conducted during each of the two intensives. Flow audits were performed on 28 IMPROVE modules at seven sites during the winter intensive, and on 37 modules at ten sites during the summer.

IMPROVE sampler flow rates were measured accurately during both intensives. During the winter, all but two of the 28 sampler flow rates agreed with the audit flow rate within 5%, and all but one agreed within 10%, the exception being the 24-hour A module at Indian Gardens, which read high by 11.6%. During the summer, all but five of the 37 sampler flow rates agreed with the audit flow rate within 5%, and all but two agreed within 10%, the exceptions being the two D modules at Joshua Tree, one of which read high by 18.8% and the other low by 20.6%.

Analytical accuracy is determined through regular (typically daily) instrument checks using independent standards. Standards are analyzed after each batch of filters, and the filters in that batch are reanalyzed if the response to the standards deviates from the accuracy goal, which is typically ±10%. Thus, analytical accuracy was maintained within ±10% for all analytical values.

4.2.1.4.1 Sampling Bias

Beyond these readily quantifiable components of accuracy, some measurements are subject to biases due to the design of the sampling device or assumptions applied to the data. Several of these biases, and their implications to measurement accuracy, are described here.

Sulfur Dioxide: The IMPROVE sampler was designed originally to collect particulate matter only, so the materials in the flow system were not selected to minimize losses of gases. Before reaching the impregnated filter, the sample stream passes through an aluminum inlet, a metal cyclone, and the particulate-matter filter.

Tests by UCD have shown that the metallic surfaces of the inlet and cyclone adsorb some of the SO_2 in the sample. UCD concluded that approximately 20 percent of the SO_2 is lost in the fine inlet and 40 percent in the PM_{10} inlet, but losses but can be substantially greater or smaller for any individual sample. Ambient relative humidity has also been shown to influence the deposition of SO_2 in the sampler inlet. The actual loss for any given sample could often range from 0 to 50 percent, with an even wider margin for some samples. As a further complication in the Project MOHAVE network, SO_2 was determined using a PM_{10} head at the full IMPROVE sites (such as Meadview) but using a $PM_{2.5}$ head at the outlying sites.

Although these tests have provided evidence for the loss of SO_2 in the IMPROVE sampler inlet, these losses have not yet been precisely quantified, and the physical conditions which lead to losses have not been fully characterized. Thus, the magnitude of the loss cannot be predicted or quantified for a specified sampling period, and individual concentration values cannot be reliably adjusted to account for inlet losses. Because the SO_2 inlet losses cannot be predicted reliably for a given sample, the IMPROVE SO_2 data have been used as they exist for data analysis, acknowledging that SO_2 concentrations may have been underestimated.

The implications of this SO_2 bias on the study conclusions are varied. Table 8-2 indicates which techniques used ambient SO_2 concentrations as part of the analysis. Only methods that rely on the IMPROVE SO_2 data would be affected (i.e. Exploratory Data Analysis (Mirabella and Farber, 1998), Tracer Mass Balance Regression (Ames and Malm, 1998), and Differential Mass Balance Regression (Ames and Malm, 1998)). Note, the Modified CMB analysis used SO_2 data collected by researchers from BYU and not the IMPROVE SO_2.

Sulfate: The other potentially significant bias in the measurement of sulfur compounds involves adsorption of gaseous SO_2 by particles already collected on the filter, which would result in a loss of SO_2 and a concomitant gain in particulate sulfate on the filter. Such a conversion mechanism has been presented as a hypothesis by BYU to explain their observations that particulate sulfate concentrations determined following an annular denuder (to remove SO_2) are smaller than sulfate concentrations measured with no denuder for about 25% of samples collected in the desert Southwest. The observed artifact can approach 0.4 $\mu g/m^3$ for the collection of particles <3.5 μm. However, for collection of <2.5 μm particles, the observed difference is smaller, typically less than 0.1 $\mu g /m^3$, and, for all samples, averaging close to 0.02 $\mu g /m^3$ (Eatough et al., 1997b, 1995, Lewis et al., 1991).

Measurements using the IMPROVE sampler, however, provide no evidence for this sampling bias. As part of the routine IMPROVE network, UC Davis has collected thousands of parallel $PM_{2.5}$ samples on completely independent Teflon and nylon filters. Particles are collected on a Teflon filter with no denuder and on a parallel nylon filter following a carbonate denuder which is believed to remove SO_2, but whose efficiency has not been established. The Teflon filters are analyzed for sulfur using PIXE and the nylon filters are analyzed for sulfate by ion chromatography. Their data show good agreement between 3xS on Teflon (PIXE) and sulfate on Nylon (IC), suggesting that removing SO_2 prior to the filter does not alter the measured particulate sulfur concentration.

In the Project MOHAVE data analyses, the measured IMPROVE sulfate concentrations have not been modified to account for the sampling artifact that BYU has proposed, although a possible sulfate oversampling of 0.1 to 0.4 $\mu g/m^3$ was considered by analysts when interpreting the data. Interpretation of the data with and without accounting for this effect would represent the upper and lower bounds of sulfate measurement uncertainty. Although BYU's findings are intriguing and suggest that further research is warranted to better understand the sampling differences, their data are not sufficient to quantify the artifact nor to demonstrate conclusively that it exists. BYU's findings suggest that there is an artifact, but we do not yet understand why it occurs and we cannot predict it or quantify it reliably.

Volatile Organic Carbon: Filter collection of particulate organic carbon is complicated by adsorption and volatilization of organic material. Compounds which exist as gases in the atmosphere can be adsorbed on the quartz filter, resulting in oversampling of organic carbon. Conversely, semi-volatile particulate material on the filter can be lost due to volatilization during sampling, resulting in undersampling.

Organic carbon in Project MOHAVE was determined using quartz filters in the IMPROVE sampler, followed by analysis using the Thermal Optical Reflectance (TOR) method. Quartz filters were collected in tandem in a filter pack, with the afterfilter designed to capture volatile organic material. In calculating ambient concentrations, it was assumed that volatilization of the particulate matter on the front filter was minimal, so that the material on the afterfilter was due only to the collection of atmospheric organic gases. Thus, the afterfilter values were subtracted from the front filter values to determine ambient concentrations.

During the summer, a single average afterfilter value was used to represent the entire network. During the winter, separate afterfilter values were used to represent the average for each of the three field laboratories where filters were loaded and distributed.

Approximately 20 percent of the Project MOHAVE afterfilters were analyzed, and the average values were subtracted from the front filter values to determine ambient concentrations. For the summer period, the average afterfilter loading of 13 µg/filter represented approximately 0.8 µg/m^3 for 12-hour samples and 0.4 µg/m^3 for 24-hour samples. Similar values were observed at most sites during the winter, with a separate value used for each of the monitoring sites.

By comparison, reported ambient organic carbon concentrations typically ranged from about 0.5 to 4 µg/m^3. Thus, the afterfilter correction ranged from around 100 percent at small concentrations to around 10 percent or less at higher concentrations

Other studies in the desert Southwest, principally by BYU, have provided evidence that the collection of gas-phase organic compounds by a quartz filter may produce a small positive artifact, but that a much larger negative error results from the loss of 20-80 percent of the particulate-phase organic material during sampling (Eatough *et al*., 1993; Cui *et al*., 1997). Tests conducted using a sampling system employing diffusion denuders, quartz filters, and sorbent filters have indicated that concentrations of particulate-phase organic compounds in the southwestern U.S. have been underestimated by collection of particles with only quartz filters.

The magnitude and chemical nature of particulate volatilization have not been fully characterized, nor has its variability. But, there is good evidence that volatilization exists, and that particulate carbon may be underestimated by up to about a factor of two if it is not considered. Consequently, it is likely that the IMPROVE sampler values represent a lower bound on particulate carbon concentration. If the organic carbon values are biased low, some likely ramifications include:

- For mass balance calculations, carbon is probably underrepresented. However, the same volatilization losses would occur in the measurement of gravimetric mass on Teflon filters, so the mass balance may appear complete.

- For Mie calculations, the extinction contribution of organic carbon is probably underestimated, unless typical volatilization losses are accounted for.

- For light extinction budgets (LEB) based on Multiple Linear Regression (MLR), the regression slope for carbon (i.e., the apparent extinction efficiency) will probably be underestimated and the intercept will be over estimated. These biases occur because the loss of semi-volitile particulate organic material is variable, with the uncertainty in the values driven by variations in temperature and particle concentration.

Elemental Carbon and Light Absorption: Uncertainty in the IMPROVE sampler carbon measurements can arise from the apportionment of organic carbon (OC) versus elemental carbon (EC) by the Thermal Optical Reflectance (TOR) analysis method. Huffman (1996) conducted a statistical comparison of the organic and elemental carbon data with light absorption data from the Teflon filters in the IMPROVE network, assuming a light absorption efficiency of 10 m^2/g for EC. He suggested that the TOR assignment overestimates organic and underestimates elemental carbon. Huffman's statistical model indicated that a portion of the TOR organic carbon should be in the elemental category, typically decreasing the reported total organic carbon by around 20% and doubling the total elemental carbon.

Horvath (1996) offers an alternate explanation for the discrepancy between measured elemental carbon and light absorbtion. Using laboratory generated aerosol, he found that non absorbing aerosols could interfere with and positively bias the LIPM measurement.

Differing interpretations of the light absorption measurement (b_{abs}) can also lead to a discrepancy of a factor of two in the reported b_{abs} values, as described in Section 4.1.3. To date, neither the OC/EC discrepancy nor the b_{abs} correction discrepancy has been resolved. Hence, there is no clear consensus to guide the Project MOHAVE data analysis. The bounds of disagreement in the measurement of EC and b_{abs} can be summarized as follows:

- EC (or, more accurately, light absorbing carbon, LAC) can differ by about a factor of two, depending on the interpretation of the TOR thermograms. EC as reported by DRI includes only the EC peaks. Huffman and others have suggested that a portion of the OC is light absorbing (perhaps even chemically elemental), so that the LAC should be larger than that reported by DRI, by about a factor of two.

- The integrating plate method as applied by UCD (with the shading adjustment) yields higher b_{abs} values than does densitometry as applied by DRI. The difference depends on the filter loading correction, but on average is about a factor of two. In comparison tests UCD and DRI uncorrected b_{abs} values agree very well, so any differences lie in the interpretation (i.e., adjustment) of the data.

In practice, two combinations of these interpretations of EC and b_{abs} are used:

- IMPROVE and Project MOHAVE have used UCD's b_{abs} (with the shadowing correction) and TOR EC. This combination results in an absorption efficiency of 20 m^2/g. However, there is some support among the IMPROVE community for interpreting LAC as EC plus a portion of the (presumably) light absorbing OC, which would yield an effective efficiency of 10 m^2/g.

The Grand Canyon Visibility Transport Commission (GCVTC) elected to use b_{abs} with no shadowing or matrix correction, along with TOR EC. This combination has also been used by DRI and others in many other studies such as the Phoenix, Tucson, and Dallas urban haze studies. This approach is consistent with an absorption efficiency of 10 m^2/g, which agrees with theoretical estimates based on Mie theory.

The questions surrounding the interpretation of EC and b_{abs} measurements have yet to be resolved. Therefore, the bounds on the Project MOHAVE conclusions are defined by the combinations of interpretations that could be used. The base case for Project MOHAVE, as described above, uses UCD's b_{abs} and TOR EC. The uncertainty bounds can be summarized as follows:

- Modifying the base case by assigning a portion of the OC to the EC fraction would typically decrease OC by about 20% and double the EC concentration. b_{abs} would be unchanged.

- Using the GCVTC approach would decrease b_{abs} by about a factor of two. OC and EC would be unchanged.

One combination that has not been used in practice is DRI b_{abs} (uncorrected) combined with LAC increased by adding a portion of the OC. This combination would result in an absorption efficiency of 5 m^2/g, which is too low to meet theoretical expectations. Thus, it need not be considered in assessing the bounds of the Project MOHAVE conclusions.

One complicating factor related to this topic is that some soil oxides also absorb light. The contribution of such crustal fine material should be considered when comparing b_{abs} with EC.

4.2.1.4.2   Method Intercomparisons

Several method intercomparisons were conducted during data validation. These intercomparisons employed two different measurements which should be expected to yield the same quantity, which can provide an indication of sampling bias. Intercomparisons were conducted during Project MOHAVE for sulfate versus three times elemental sulfur, for organic carbon versus carbon estimated from concentrations of H and S (OMH), for gravimetric versus calculated mass (CALMAH), and for PIXE versus XRF. These intercomparisons and their findings are summarized below.

Sulfate: The sulfate collected on the nylon filter and analyzed by ion chromatography should be 3.0 times the sulfur collected on the Teflon filter and analyzed by PIXE, based on the stoichiometric ratio. This assumes that all particulate sulfur is in the form of sulfate. Figure 4-1 compares these two values for data from the sites with multiple IMPROVE modules in winter and summer. Because the B module includes a carbonate denuder, which is intended to remove SO_2, the close agreement suggests that any effects such as interaction of SO_2 with soil particles already on the filter are negligible.

Organic Mass: The total organic carbon (OMC) collected on the quartz filter is the sum of the two measured organic carbon concentrations (OCLT and OCHT). They are included in the sum as determined, even if negative. The total organic concentration is obtained by multiplying the sum by 1.4 to include the noncarbon components of the organic particle.

The organic mass can also be calculated from the concentrations of H and S measured on the Teflon filter (Cahill et al., 1989). The total hydrogen on a sample comes from organics, sulfate, nitrate and water. Assuming that all the sulfur is present as fully neutralized ammonium sulfate, that the Teflon filter has negligible hydrogen from nitrate compared to that from sulfate, and that any water volatilizes from the filter during the exposure to vacuum, then the difference between the measured hydrogen and the hydrogen in sulfate is organic hydrogen. The mass of organic material, OMH, can be estimated by multiplying the organic hydrogen by 11 which is consistent with a hydrogen/carbon molar ratio of 1.53.
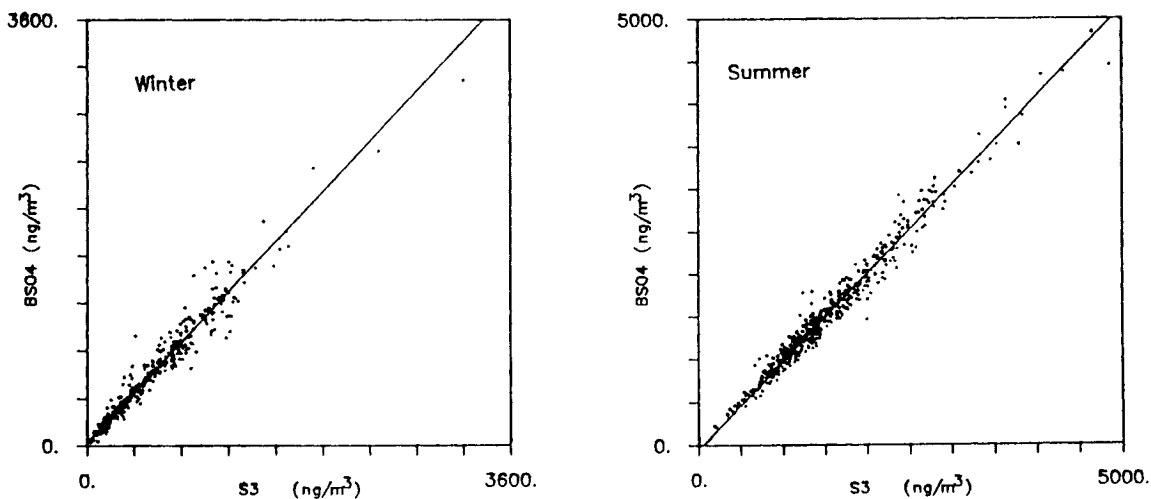
Figure 4-1 Comparison of sulfur collected on Teflon A and measured by PIXE with sulfate collected on nylon B and measured by ion chromatography for 12-hour and 24-hour samples at the IMPROVE sites during both intensives. The sulfur is multiplied by 3.0 to account for the oxide. The left plot is for winter and the right plot is for summer. The slopes are 1.06 (winter) and 1.04 (summer). The correlation coefficients (r^2) are 0.95 (winter) and 0.97 (summer). The number of data pairs are 342 (winter) and 289 (summer).

Figure 4-2 illustrates comparisons of OMC and OMH at the IMPROVE sites within the Project MOHAVE network. The spread of the points and the deviations of the slopes from unity reflect the imprecision and sampling biases inherent in both methods.

In general, the precision for organic mass by either method is not as good as for the other major species, such as sulfate, soil, and nitrate. The precision for OMC is associated primarily with the variation of the afterfilters. The mean relative precision for OMC was 23% for the 24-hour winter samples, 12% for 24-hour summer samples, 39% for 12-hour winter samples and 44% for 12-hour summer samples.

The form of the precision for OMH is somewhat more complicated. Both S and H separately have good precision (5% for S, 7% for H in winter and 12% for H in summer), but when the difference of H-S/4 is small relative to S, then the precision can become large. The key variable to the precision is the ratio of sulfur to organic material. Whenever the ammonium sulfate is greater than 4.5 times OMH, then the precision will exceed 50%. During winter, the mean

ammonium sulfate was only slightly larger than OMH (840 vs. 600 ng/m^3), and the mean precision for OMH was 13% for both 12-hour and 24-hour data. Less than 1% of the samples had a relative precision exceeding 50%. During summer, however, the mean ammonium sulfate was 3 times the organic mass. As a result the overall precision for summer rose to 38%, which is higher than the OMC precision at 24-hour IMPROVE sites. Figure 4-3 gives the ratio of the mean ammonium sulfate to the mean OMH at each site. Note that at any given site, the ratio of sulfate to organic will vary widely from sample to sample, so that the mean ratio does not indicate the precision for each sample.
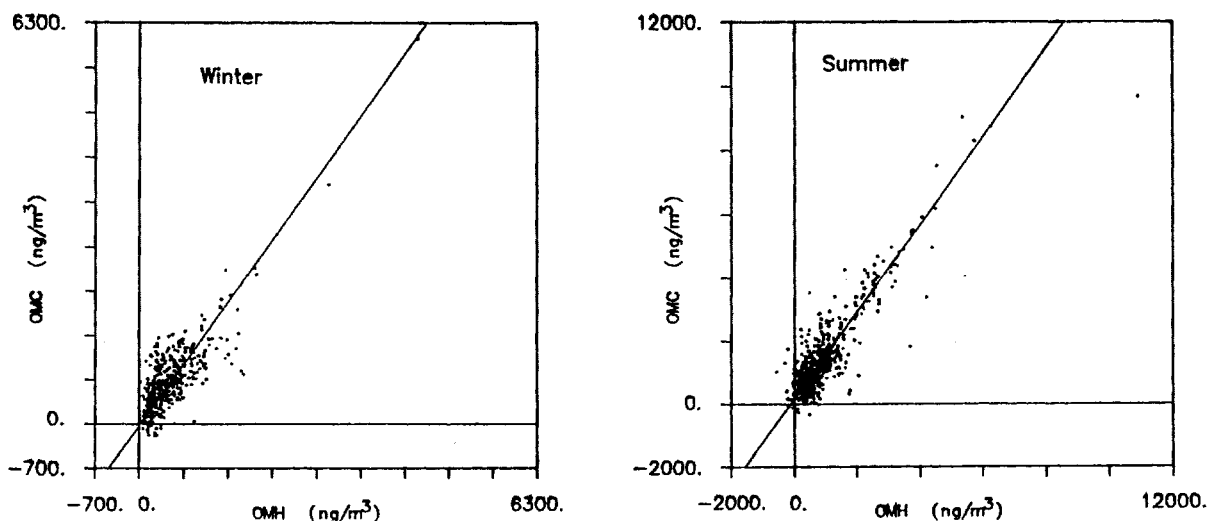
Figure 4-2 Comparison of two organic measurements, OMC and OMH, collected at the nine IMPROVE sites. The left plot is for winter and the right plot is for summer. The slopes are 1.39 (winter) and 1.38 (summer). The correlation coefficients (r^2) are 0.64 (winter) and 0.78 (summer). The r^2 during winter is improved to 0.80 by excluding the 12 hour data. The number of data pairs are 351 (winter) and 286 (summer).

Two possible corrections to the assumptions underlying OMH are (1) for ammonium nitrate on the Teflon filter, and (2) for partially acidic sulfate. If a nitrate correction were applied, it would decrease OMH. The nitrate concentration on the Teflon filter is known only at one site, Meadview, where the simultaneous measurement of NO$_3$ on nylon and Teflon provides a rough estimate of the nitrate levels on the Teflon filter. The ratio of Teflon mean / nylon mean was 0.25 in winter and 0.50 in summer. Thus, 75% of the nitrates in winter were volatilized during sampling. Because OMH and NO$_3$ are uncorrelated the effect is to decrease OMH by a constant value of 20 to 70 ng/m^3, based on the ratios of 0.25 and 0.50.

If some of the sulfate were present as sulfuric acid, OMH would be underestimated, with the amount depending on the concentration of sulfuric acid. For example, if 5% of the sulfur were present as sulfuric acid, then OMH would be underestimated by 10 to 30 ng/m^3 in winter and 40 to 80 ng/m^3 in summer at most sites.

Gravimetric and Calculated Mass: Two forms of the calculated mass can be determined from the measured data. The first is based only on the variables measured on the Teflon filter, and will be labeled CALMAH. This form can be used for samples from the background sites as well

as from the IMPROVE sites. The second form uses the carbon concentrations from the quartz C filter, and will be labeled CALMAC. This can be used only for data from the nine IMPROVE sites.
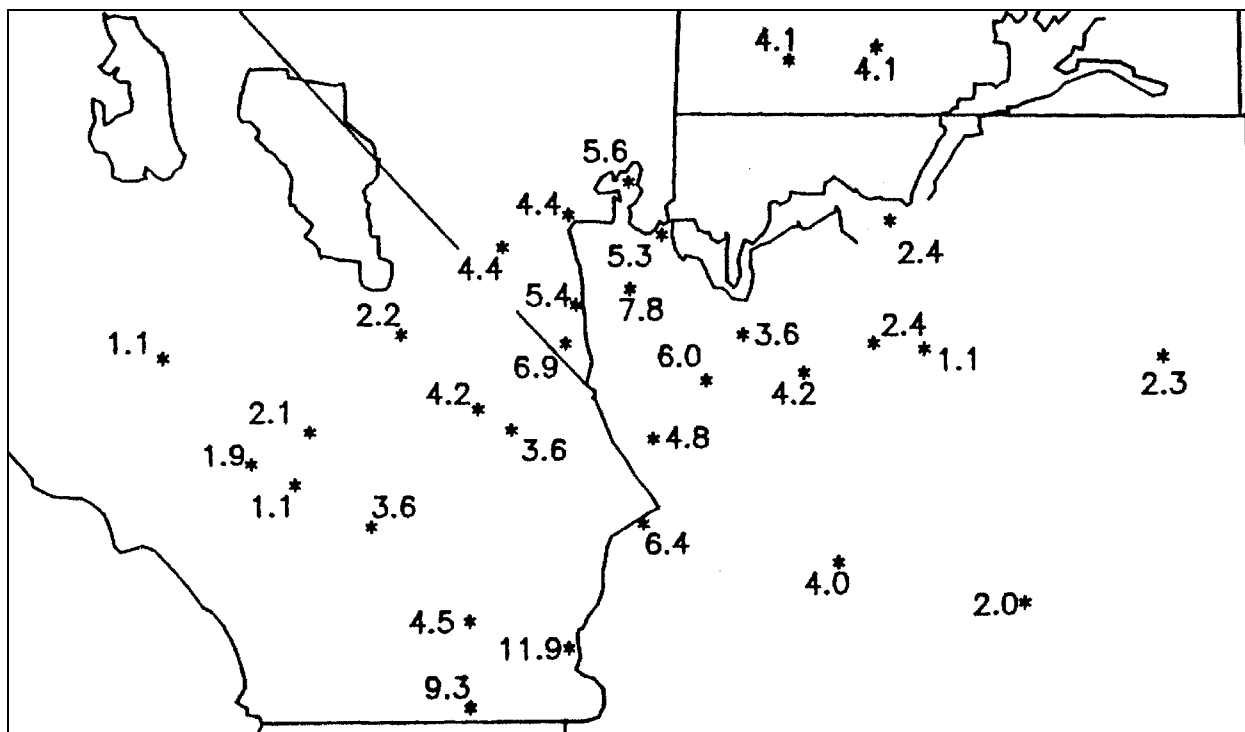
Figure 4-3 Map of ratio of mean ammonium sulfate to mean organic by hydrogen for the summer intensive based on data from the IMPROVE samplers. The ratio for a given sample will vary widely from the overall site ratio.

The calculated mass from the Teflon filter (CALMAH), is the sum of ammonium sulfate, soil, nonsulfate potassium, salt, elemental carbon, and organic carbon. The ammonium sulfate is calculated from the sulfur measured by PIXE. The soil component consists of the sum of the predominantly soil elements measured by PIXE, plus oxygen for the normal oxides, plus a factor of 1.16 for unmeasured compounds. Potassium is treated separately because fine potassium can be derived from both soil and smoke. Salt is calculated from the sodium concentration, as 2.5*Na. Elemental carbon (soot) is estimated from b_{abs}, and organic carbonis represented by OMH. The only components not included in calculated mass are water and nitrate.

Comparison of CALMAH and gravimetric mass at all sites for both intensives are shown in Figure 4-4. Part of the difference between gravimetric and calculated mass is the ammonium nitrate on the Teflon filter, estimated to constitute between 1% and 3% of the calculated mass at most sites. At San Gorgonio, the site with the most nitrate, the ratio rises to 6%. The conclusion is that nitrate generally does not constitute the major part of the missing mass. Since the samples were weighed at a relative humidity of 41 ± 6%, considerable water should be present.

The second form of calculated mass, CALMAC, uses the carbon components from the quartz filter and the other components from the Teflon filter. As in CALMAH, the sum does not include water and nitrates. Comparisons of CALMAC and gravimetric mass for the IMPROVE

sites are shown in Figure 4-5. As with CALMAH, approximately 25% of the measured mass was not reconciled.
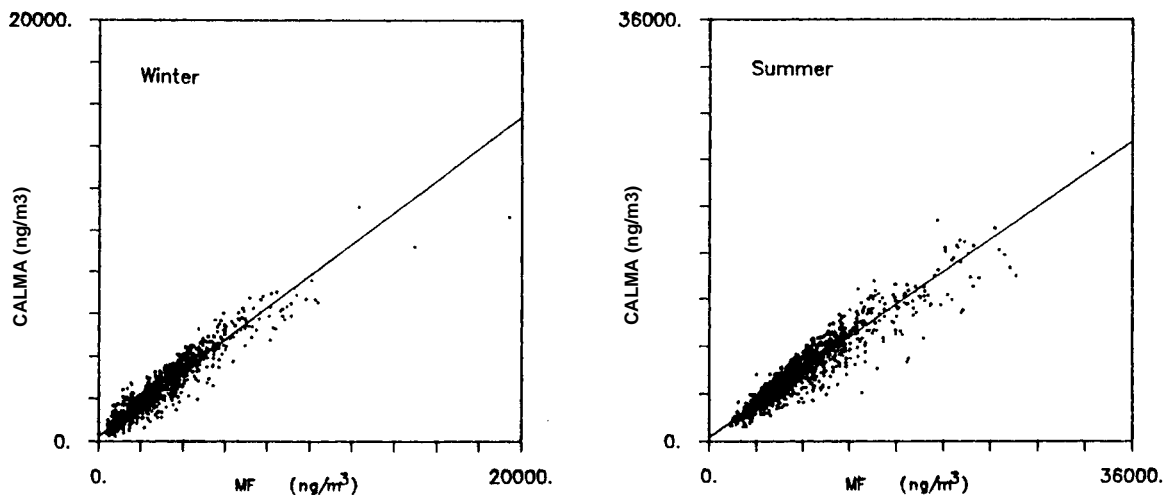
Figure 4-4 Comparison of gravimetric mass (MF) and calculated mass (CALMAH) at all Project MOHAVE IMPROVE sites. The left plot is for winter and the right plot is for summer. The slopes are 0.76 (winter) and 0.70 (summer). The correlation coefficients (r^2) are 0.89 (winter) and 0.89 (summer). The number of data pairs are 1102 (winter) and 1533 (summer).
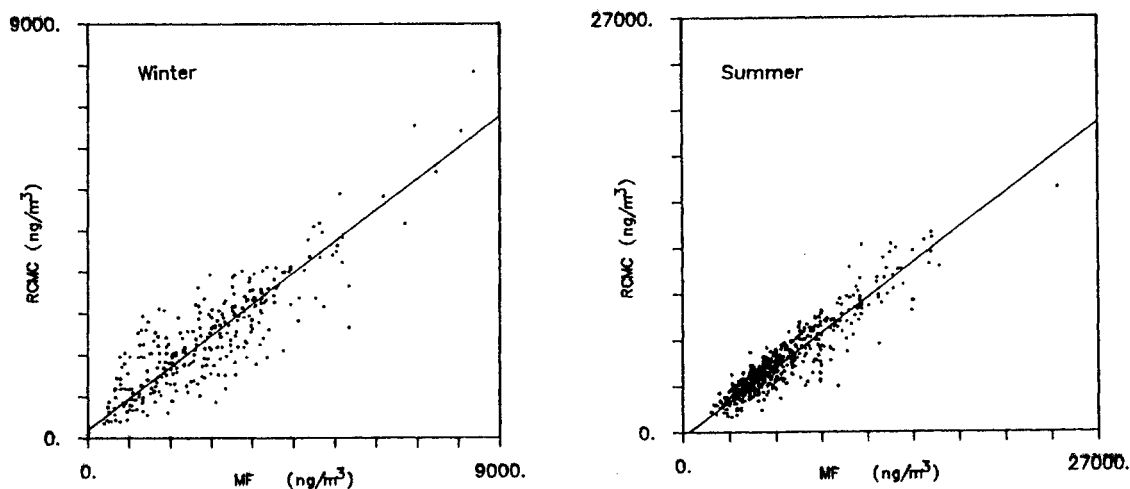
Figure 4-5 Comparison of gravimetric mass (MF) and calculated mass (CALMAC) at all Project MOHAVE IMPROVE sites. The left plot is for winter and the right plot is for summer. The slopes are 0.76 for both intensives. The correlation coefficient (r^2) are 0.75 (winter) and 0.85 (summer). The number of data pairs are 341 (winter) and 285 (summer).

PIXE and XRF: All of the Teflon A filters were analyzed by both XRF and PIXE. The measured concentrations for overlapping elements were compared by scatter plots. Figure 4-6 shows the comparison for the summer intensive for iron and zinc, the two elements with the best overlap. The iron comparison gave a slope of 0.99 ± 0.01 and a regression coefficient (r^2) of

0.99. For the winter intensive the slope was 1.01 ± 0.01 and the regression coefficient was again 0.99.
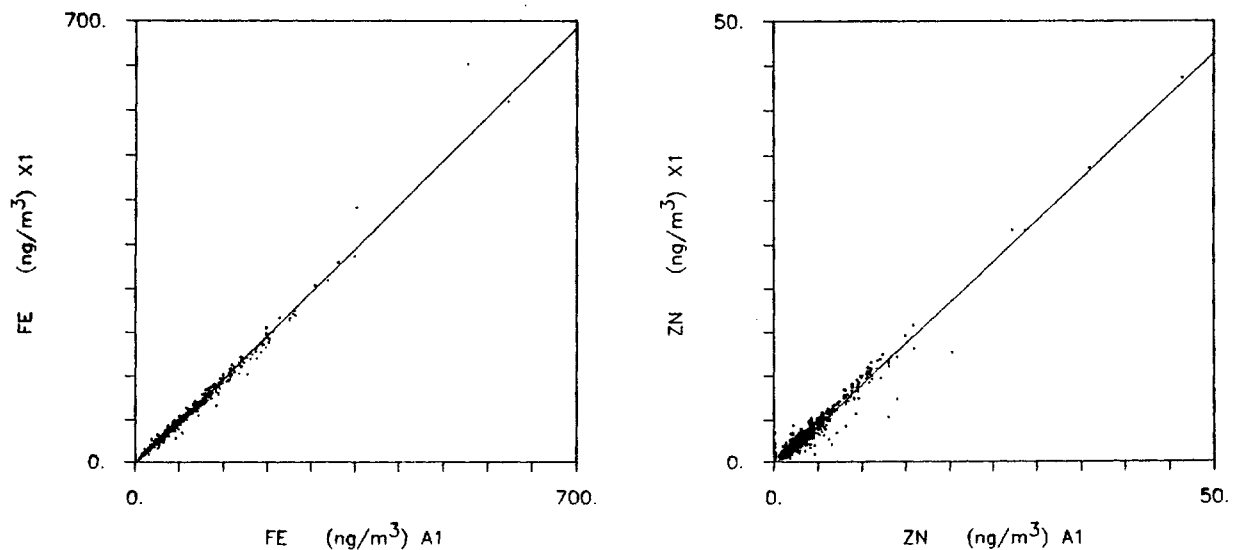
Figure 4-6 Comparison of XRF and PIXE for all Project MOHAVE IMPROVE summer samples for iron and zinc. The PIXE values are on the x-axis and the XRF values are on the y-axis. The slopes are 0.99 (Fe) and 0.93 (Zn). The correlation coefficients (r^2) are 0.99 (Fe) and 0.95 (Zn). The number of data pairs are 1556 for both Fe and Zn.

4.2.2   BYU Aerosol Sampling

The BYU aerosol sampling program during Project MOHAVE used two methods for the collection and determination of $SO_2(g)$, HF(g), spherical aluminosilicate (SAS) particles, and particulate sulfate, nitrate and fluoride during both the winter and summer studies; high-volume cascade impactor and annular diffusion denuder sampling systems. In addition, particulate organic material was determined during the summer at Meadview only using a diffusion denuder sampler. The quality of the BYU aerosol data is summarized below.

4.2.2.1 Completeness

Annular denuder and high volume cascade impactor samples were collected on a twelve-hour basis at Indian Garden, Hopi Point and Meadview from 14 January through 12 February during the Winter Intensive. However, only the 27 January through 9 February time period was selected for the analysis of all components for Chemical Mass Balance (CMB) analysis. Annular denuder and high volume cascade impactor samples were collected on a twelve-hour basis at Hopi Point and Meadview from 12 July through 30 August during the summer intensive sampling period. All available samples were selected for the analysis of all components for CMB analysis. BOSS samples were only collected at Meadview from 15 July through 28 August during the summer intensive sampling period to provide data for attribution of visibility. Table 4-3 lists the completeness of sample collection for the periods during which full analysis was performed.

4.2.2.2 Precision and Lower Quantifiable Limit

The precision of BYU's aerosol measurements was estimated from collocated replicate samples at selected sites during Project MOHAVE and from similar tests using the same instruments during other studies (Eatough, et al., 1997; Cui, et al., 1997). The precision was defined as the standard deviation of the replicate differences:

$$\sigma = \sqrt{\frac{1}{2N}\sum_{i=1}^{N}(C_{1,i} - C_{2,i})^2 - (\overline{C_1} - \overline{C_2})^2} \qquad (4\text{-}7)$$

where N is the total number of replicate pairs, $C_{1,i}$ and $C_{2,i}$ are the concentrations of the chemical species of interest in the two replicate data sets, and $\overline{C_1}$ and $\overline{C_2}$ are the average of each collocated set. The $(\overline{C_1} - \overline{C_2})^2$ term corrects the standard deviation for bias between the two replicate data sets. The collocated standard deviation, σ, is also considered to be the lower quantifiable limit (LQL), or the smallest concentration that can be distinguished in an ambient sample.

Table 4-3 BYU Completeness of sample collection and analysis during project MOHAVE winter and summer intensive studies.

Sampling Site	Winter		Summer		
	Denuder	High Vol	Denuder	High Vol	BOSS
Meadview	100	96	75	83	84
Hopi Point	100	89	94	95	-
Indian Garden	100	82	-	-	-

The percent precision for the replicate sets is calculated as:

$$\sigma_{\%} = \frac{\sigma}{\frac{1}{2}(\overline{C_1} + \overline{C_2})} \times 100 \qquad (4\text{-}8)$$

The results from this statistical analysis of the various collocated data sets are given in Table 4-4. The table provides the number of replicates analyzed, the number rejected, the precision (σ), and the percent precision ($\sigma_{\%}$). For each measured species, statistics are provided for the comparisons performed during Project MOHAVE and for all comparisons performed during all BYU studies, including Project MOHAVE. Collocated low-volume filter packs were not sampled during Project MOHAVE, so the value from other BYU tests is shown. The results listed for particulate organic carbon were obtained exclusively during Project MOHAVE. Detailed statistics for all of the comparisons are provided by Eatough, et al. (1997) for the inorganic species and by Cui, et al. (1997) for organic carbon.

In these calculations, BYU rejected all sample sets on the basis of Taylor's test, which essentially eliminates collocated pairs with a difference greater than three times the standard deviation of the entire data set. Doing so caused them typically to reject about 5 to 10% of the points, which is much higher than one would expect for a Gaussian distribution, for which about 0.3% of points would be expected to lie beyond 3σ. This high rejection rate indicates that the samples fell into two populations: those for which data quality was controlled and quantified

(i.e., those falling within 3σ), and those compromised by measurement errors which could not be explained based on physical evidence (i.e., quality control test data). Thus, the reported precision (σ) represents the variability in the majority of samples that were under control. Because samples were rejected based on statistics and not based on known sampling problems (torn filters, samples dropped in the dirt, etc.), the proportion of rejected sample sets (5 to 10%) represents the probability that any given sample in the data base is highly inaccurate for unknown reasons.

Table 4-4 Summary of BYU Aerosol Measurement Precision

Network/Analyte	No. of Replicate Samples	No. of Replicates Rejected	Sigma (LQL), $\mu g/m^3$	% Precision
ANNULAR DIFFUSION DENUDERS				
Particulate Sulfate				
Project MOHAVE, Hopi Point	56	0	0.28	37.0
Project MOHAVE, Meadview	32	2	0.24	12.4
All BYU Samples	114	2	0.24	40.5
SO_2 (g)				
Project MOHAVE, Hopi Point	52	1	0.12	26.7
Project MOHAVE, Meadview	31	4	0.22	19.4
All BYU Samples	109	12	0.12	17.9
F_{Total}				
Project MOHAVE, Hopi Point	39	3	0.006	54.0
All BYU Samples	48	3	0.006	50.4
LOW-VOLUME FILTER PACKS				
Particulate Sulfate				
All BYU Samples	43	2	0.12	25.2
HIVOL SAMPLERS				
SAS Particles				
Project MOHAVE, Hopi Point	11	0	105 (sphere/m^3)	11.2
All BYU Samples	27	2	170 (sphere/m^3)	17.7
Particulate Sulfate				
Project MOHAVE, Hopi Point	9	0	0.19	16.6
All BYU Samples	29	2	0.20	21.9
SO_2 (g)				
Project MOHAVE, Hopi Point	11	1	0.031	32.3
All BYU Samples	31	8	0.019	32.1
F_{Total}				
Project MOHAVE, Hopi Point	15	1	0.005	78.4
All BYU Samples	19	2	0.003	30.1
BYU ORGANIC SAMPLING SYSTEM (BOSS)				
Particulate Organic Carbon				
BOSS #1: Qtz. filter (denuder)	18	0	0.20 $\mu gC/m^3$	14.4
BOSS #2: Qtz. filter (filter/denuder)	19	0	0.21 $\mu gC/m^3$	18.9
BOSS Charcoal Impregnated Filter	7	0	0.27 $\mu gC/m^3$	37.5

The percent precision of the annular denuder particulate sulfate measurements was poor overall (40.5%), largely because the average sulfate concentration in most of the studies was only about three times the σ value for sulfate. The exception among the collocated sites was Meadview, for which ambient sulfate concentrations were generally higher and the percent precision was lower.

The low volume filter pack sulfate precision was around 25% in all tests performed. The precision of determination of particulate sulfate collected by the high-volume cascade impactor was better than the corresponding precision for the annular denuder. Conversely, the annular denuder provided better precision for SO_2 than did the hivol sampler.

The precision for SAS particles was better in Project MOHAVE than it was overall, but in all cases it was better than 20%. The precision in the annular denuder total fluoride (F_{total}) measurement was poorer for Project MOHAVE than it was overall because concentrations were lower during Project MOHAVE. The precision of the Project MOHAVE hivol F_{Total} measurement was poor due to poor agreement in the replicate HF(g) results. Because the HF(g) data were not reliable, the hivol F_{Total} data were not used in subsequent interpretation of the Project MOHAVE data.

Collocated comparisons were conducted for the BYU organic sampling system (BOSS). The sampling configuration included a charcoal denuder followed by a quartz filter and a charcoal absorbent filter. In addition, collocated data were obtained where a filter pack preceded the denuder to determine the efficiency of the denuder for the removal of gas phase organic material for each sample. The average percent precision (for both configurations) for sampling on the quartz filters was around ±17%. The percent precision on the charcoal impregnated filter was greater, largely due to lower concentrations.

4.2.2.3 Accuracy

As with the IMPROVE sampler data discussed previously, two components of the measurement are critical in assessing the accuracy of aerosol concentrations determined on filters: the accuracy of the flow measurement in the field and the accuracy of the analytical measurement in the laboratory.

Flow measurement accuracy is determined through flow checks using a metering device independent of that used for routine flow measurements. In Project MOHAVE, these checks were conducted during independent performance audits, which were conducted during each of the two intensives. The annular denuder and filter pack samplers were audited during both intensives, the hivol samplers only during the summer intensive.

Flow rates in both the annular denuder and filter pack samplers were found to be significantly compromised during the first part of the winter intensive. For about half of the samplers, the flow readings exceeded the audit values by a factor of two or more. After the audits, BYU discovered that dirt had gotten into many of the mass flow controllers and caused them to malfunction, leading to the erroneously high readings. This problem was corrected in the field by cleaning the flow controllers and adding protective filters. Subsequent audits during the summer intensive found six samplers agreeing with audit values within 10%, another three within 20%. Deviation exceeded 20% for only one filter pack, but water was in that filter pack at the time of the audit.

The high-volume cascade impactors were audited during the summer intensive only. Flows from eight of the nine samplers agreed with the audit values to within 10%, and the ninth fell within 20%.

Annular denuder flow data from the first half of the winter intensive were adjusted by comparing total SO_x (the sum of particulate sulfate and SO_2) measured with the annular denuder to that measured with the high volume sampler, which had demonstrated more reliable flow measurements. SO_x values from the two systems were expected to agree within about ±0.25 $\mu g/m^3$ based on prior studies, so substantial differences could be attributed to flow inaccuracy. The denuder data were adjusted based on the SO_x ratio and the hivol flows, and these adjusted values were reported to the data base.

The BOSS system for organic sampling was not audited during Project MOHAVE. However, a flow audit of the same sampling system was conducted in Azusa, California, in June 1992, just prior to the summer intensive. This audit showed the BOSS flow rates to be within 5% of the audit flow rates.

Analytical accuracy is typically determined through regular instrument checks using independent standards. However, a system audit of the BYU laboratory conducted in April 1992 (between the winter and summer intensives) revealed that rigorous, multi-point calibrations were not being performed, although they were instituted following the audit. To follow up, performance audit samples for sulfate and nitrate were submitted to the BYU laboratory in June 1992. Both aqueous solutions and spiked filters were used in the audit.

BYU's reported values were within 20% of the audit values for all of the aqueous solutions and for spiked $NaHCO_3$-impregnated filters (for sulfate) and spiked nylon filters (for nitrate). The differences for sulfate on two of three spiked quartz filters exceeded 25% of the audit values, with BYU's reported levels below the spiked amounts. Since sulfate results were substantially closer for the other samples, these errors were likely caused by incomplete extraction or by improperly prepared standard filters. Subsequent chamber experiments on the collection of SO_2 by several techniques and studies on consecutive extractions indicated that the BYU single extraction protocol did result in complete extraction of collected SO_2 on BYU prepared carbonate saturated filters. Consequently, the BYU protocols were not changed.

4.2.3   Harvard HEADS Sampler

Harvard University conducted aerosol sampling at Meadview, AZ from July 15 through August 30, 1992. The quality of the HEADS aerosol data is summarized below.

4.2.3.1 Completeness

The number of twice-daily samples possible during the 47-day period was 94. A total of 92 samples (98% of the number possible) was collected and analyzed successfully. However, three of these samples had sampling durations shorter than the 4.5-hour acceptance criterion, and one additional sample had a flow rate reading outside of acceptance criteria. Thus, 88 samples (94% of the number possible) met all acceptance criteria.

4.2.3.2 Precision

The precision of Harvard's aerosol measurements was estimated from 10 collocated replicate samples collected at Meadview on August 24 and on August 27 through August 30. The

precision was defined as the standard deviation of the replicate differences as was done for the BYU aerosol samples as described in Section 4.2.2.2. However, none of the HEADS collocated pairs was excluded from the calculations. Table 4-5 lists the precisions, average measured concentrations, and precisions expressed as percentages of the average measured concentrations for the Harvard measurements. Note that the listed average concentrations include the reported values for concentrations below the lower quantifiable limit. The precisions of all of the species except nitrous acid and ammonia were less than about 15% of the average measured concentrations.

Table 4-5 Precisions and Average Measured Concentrations from Harvard HEADS Measurements

Species	Precision	Average Concentration	Percent Precision
Total strong acidity	1.2 ng/m^3	6.9 ng/m^3	17%
Particulate sulfate	180 ng/m^3	1,704 ng/m^3	11%
Particulate nitrate	18 ng/m^3	131 ng/m^3	14%
Particulate ammonium	46 ng/m^3	419 ng/m^3	11%
Sulfur dioxide	0.023 ppb	0.41 ppb	6%
Nitrous acid	0.14 ppb	0.026 ppb	538%
Nitric acid	0.049 ppb	0.92 ppb	5%
Ammonia	0.35 ppb	0.75 ppb	47%

4.2.3.3 Lower Quantifiable Limit

Harvard estimated the limits of detection (assumed to be the lower quantifiable limits) from previous studies that utilized the HEADS sampler. Alternatively, the lower quantifiable limit can be defined as a multiple of the precision determined from the collocated sampling. Table 4-6 lists the limits of detection estimated by Harvard along with lower quantifiable limits defined as twice the precisions of the measurements. With the exceptions of nitrous acid and ammonia, the lower quantifiable limits estimated from the precisions from the collocated measurements are substantially smaller than the values that Harvard estimated for the limits of detection. This suggests that the precision of the measurements at Meadview was much better than in the previous studies.

4.2.3.4 Accuracy

As with the other aerosol samplers, two components of the measurement are critical in assessing the accuracy of aerosol concentrations determined on filters and denuders: the accuracy of the flow measurement in the field and the accuracy of the analytical measurement in the laboratory.

A performance audit of the flow rate measurement was conducted at Meadview on July 21, 1992, which was the seventh day of sampling. The audit flow rate was 38.0 liters per minute (LPM), which was approximately twice the intended flow rate of 20 LPM. This difference was caused by incorrect instructions to the personnel who operated the sampler. It was corrected, and flow rates for subsequent samples were set correctly. However, additional flow rate audits were not conducted, so the accuracy of the flow rate measurements was not evaluated independently.

Table 4-6 Estimates of Lower Quantifiable Limits of Harvard HEADS Measurements

Species	Limit of Detection Estimated by Harvard	Lower Quantifiable Limit Defined as Two Times the Precision
Total strong acidity	8.2 ng/m^3	2.4 ng/m^3
Particulate sulfate	1,180 ng/m^3	360 ng/m^3
Particulate nitrate	130 ng/m^3	36 ng/m^3
Particulate ammonium	297 ng/m^3	92 ng/m^3
Sulfur dioxide	0.41 ppb	0.046 ppb
Nitrous acid	0.21 ppb	0.28 ppb
Nitric acid	0.41 ppb	0.098 ppb
Ammonia	0.62 ppb	0.70 ppb

These high flow rates for the first seven sampling days reduced the estimated collection efficiencies of the annular denuders for sulfur dioxide, nitrous acid, nitric acid and ammonia from 97.7%, 98.6% 96.6% and 99.8%, respectively, to 86%, 90%, 83%, and 97%. Additionally, the elevated flow rates reduced the cut-point for the impactor from 2.5 µm to 1.8 µm.

Independent audits of the sample analysis were not conducted, so the accuracy of the Harvard measurements can not be evaluated from independent performance audits. However, Turpin et al. (1997) compared data from the Harvard measurements with results from concurrent IMPROVE sampler measurements at Meadview. Since the accuracy of the IMPROVE sampler measurements has been evaluated (see Section 4.2.1.4), these comparisons provide a limited indirect evaluation of the Harvard measurement accuracy. Turpin et al. (1997) report a value of 0.91 for the average sulfate concentration from the IMPROVE nylon filter divided by the average sulfate concentration from the HEADS sampler. The R^2 value for a regression between the two measurements was 0.88 for the 31 sample pairs that were used. These results suggest that the accuracy of the Harvard particulate sulfate measurements is probably within 10%.

4.3 Aerosol Size Distribution Measurements

Aerosol Dynamics Inc. (ADI) measured ambient particle size distributions, and the University of Minnesota (UM) measured particle chemical composition as a function of size. UM also measured particle growth characteristics as a function of relative humidity.

4.3.1   ADI Size Distribution Measurements

ADI developed the Differential Mobility and Optical Particle Size Spectrometer (DMOPSS) to measure ambient particle size distributions in the range from 0.1 to 1.0 µm diameter. This instrument was first used at Meadview from July 14 through August 30, 1992.

Independent standards do not exist to evaluate the accuracy of the instrument, and appropriate data were not available to estimate precision. However, ADI analyzed the results from the measurements to estimate various characteristics of the aerosol that could be compared with other measurements of the same characteristics. These comparisons, described below, suggest that the results of the measurements are reasonable.

Measured total particle volume was strongly correlated with measurements of the light scattering coefficient made by ADI using a nephelometer equipped with a 2.5 µm cut-point inlet (R^2 = 0.79), with a mean scattering-to-volume ratio of 5 m^2/cm^3. ADI also estimated the average particle density to be 1.69 g/cm^3. Dividing the mean scattering-to-volume ratio by this density gives an estimate of 3 m^2/g for the particle light scattering efficiency, which is consistent with other estimates in this report.

The particle scattering coefficient calculated from the size distributions were also well correlated with the nephelometer measurements (r^2 = 0.79), but the mean calculated scattering coefficient was about 20% lower than the mean measured value. ADI suggested that this discrepancy might be accounted for by scattering by particles between 1 and 2.5 µm diameter, which were not measured by the DMOPSS.

ADI also estimated the volume median particle diameter from the DMOPSS data and compared it with the mass median diameter calculated from measurements made concurrently by UM with Micro Orifice Uniform Deposit Impactors (MOUDIs) (see Section 4.3.2). The two diameter estimates were highly correlated and the ratio of the average values was 1.03.

4.3.2 UM MOUDI Measurements

The University of Minnesota measured the size distribution of particulate matter constituents from July 15 through August 30, 1992, at Meadview, AZ, using three Micro Orifice Uniform Deposit Impactors (MOUDIs). Samples were collected once each day from 7:00 am to 7:00 pm MST. The quality of the UM MOUDI data is summarized below.

4.3.2.1 Completeness

Valid data were obtained from all stages and the after filters of all three MOUDIs on 42 of the 47 sampling days (89%). Complete valid sample sets from the individual MOUDIs included 43 days for ions (91%), 44 days for chemical elements (94%) and 43 days for carbon (91%).

4.3.2.2 Precision and Lower Quantifiable Limits

For ion and carbon measurements, UM defines the precision of the MOUDI measurements as the larger of three times the standard deviation of the field blank value divided by the sample volume or the pooled standard deviation of replicate sample analyses, divided by the sample volume. The precisions and LQL's for the MOUDI chemical measurements are summarized in Table 4-7. Replicate ion analyses were performed for 9.5%-12.1% of the samples, and replicate carbon analyses were performed for 13.9% of the stages and 9.1% of the after filters. The precisions of elemental analyses by x-ray fluorescence and PIXE were estimated from counting statistics during sample analyses and results of replicate analyses of archived samples.

The LQLs for ion and carbon analyses were defined as three times the standard deviation of the blank samples, and the LQLs for elemental analyses were defined as 3.3 times the uncertainty in the x-ray counting statistics.

Table 4-7 Precisions and Lower Quantifiable Limits for MOUDI Ion and Carbon Measurements

Species	Precision (ng/m^3)	Lower Quantifiable Limit (ng/m^3)
Chloride	74	24
Nitrite	190	190
Bromide	45	19
Nitrate	56	56
Sulfate	41	22
Ammonium	28	25
Organic Carbon (impactor stage)	79	79
Organic Carbon (after filter)	42	42
Elemental Carbon (impactor stage)	15	15
Elemental Carbon (after filter)	12	12

Sulfate and ammonium were above the LQL in most samples, while the other ions were almost always below the LQL. The precisions of sulfate and ammonium concentrations were typically 10% or less.

The chemical elements that were usually detected on one or more impactor stages in each sample were sulfur, iron, nickel and bromine. For sulfur and iron, the precision was generally 10% or less of the concentration on the stage with the highest average concentration. Precisions for nickel, zinc and bromine were generally less than about 20% of the concentration on the stage with the highest average.

Organic carbon was usually above the LQL on the impactor stages and after filters with precisions typically being about 25-40% of the concentrations. Elemental carbon was usually detected on one to three impactor stages in each sample with precisions of 25-75% of the concentrations.

4.3.2.3 Accuracy

As with the other aerosol samplers, two components of the measurement are critical in assessing the accuracy of aerosol concentrations determined on filters and denuders: the accuracy of the flow measurement in the field and the accuracy of the analytical measurement in the laboratory.

An independent performance audit of the MOUDI flow rates was conducted at Meadview on July 17, 1992. All audit flow rates were within 4% of the nominal 30 LPM sampler flow rate.

The ion and elemental analyses of the MOUDI samples were performed by the same laboratories that performed these analyses on samples from the IMPROVE samplers. The accuracies of those laboratories' analyses were discussed in Section 4.2.1.4.

The accuracy of the carbon analyses was not audited. Turpin, et al. (1997) compared total carbon (sum of organic and elemental carbon) measured concurrently by the IMPROVE and MOUDI samplers at Meadview. The average MOUDI total carbon concentration was 88% higher than the average IMPROVE concentration, and the values were uncorrelated. Turpin et al. (1997) suggested that the poor agreement and the bias may have been caused by the use of an average backup filter organic carbon concentration to correct the IMPROVE front filter organic carbon for adsorption artifacts.

4.3.3 University of Minnesota Particle Growth Measurements

Scientists from the University of Minnesota measured particle growth characteristics as a function of relative humidity at Meadview between July 15 and August 30, 1992. Data were not available to characterize the precision, lower quantifiable limits or accuracy of these non-routine measurements.

4.4 Precision of Tracer Measurements

Several experiments that were performed to quantify the precision of the PFT measurements are described below. The accuracy of these measurements was not characterized.

Use of collocated samplers was a key component of the quality assurance evaluation for Project MOHAVE tracer data. A previous perfluorocarbon tracer study performed by organizations not involved with Project MOHAVE had collocated tracer measurement results showing uncertainties in the tracer measurements larger than the highest concentration at the Grand Canyon receptor sites (Richards, *et al* 1991); thus, demonstration of good precision using collocated samplers was critical for credibility of the Project MOHAVE tracer data. For both the winter and summer intensive periods, two locations (Meadview, at the west edge of Grand Canyon National Park, and Hopi Point, near Grand Canyon Village) were chosen to have 3 tracer samplers each. Not only did this arrangement allow for calculation of collocated precision, it also provided for insurance at these key Grand Canyon monitoring sites in case of sampler failure. In addition to the collocated BATS samplers, the 15 minute real-time sampler at Meadview allows for comparison with the BATS at Meadview for a portion of the summer period. The Environmental Monitoring Laboratory (EML) of the U.S. Department of Energy also made PFT measurements at one site (Dolan Springs); this data allows comparison of the Brookhaven concentrations to a completely independent measurement. The EML study also had duplicate samplers, allowing for calculation of collocated precision for their measurements. Brookhaven National Laboratory was blinded to the locations of samplers, except by site number, as well as to which site number corresponded to collocated measurements.

Some problems were experienced in the collection of samples due to sampler malfunction and, in the summer, incorrect instructions given to site operators. In addition, a small percentage of the samples could not be indisputably assigned sampling times or locations.

Regression statistics (r^2, slope, intercept, standard errors of slope, intercept, and y-estimate) were computed for each pairing of samplers, for each tracer compound, summer and winter. Root-mean-square errors for winter and summer collocated PFT measurements at Meadview and Hopi Point are shown in Table 4-8. Figure 4-7 and Figure 4-8 show regression plots of PMCP and ocPDCH concentrations (above mean background) at the three collocated monitoring sites at Meadview during the winter study. The plots show good agreement (r^2=0.87-0.88 for ocPDCH, 0.97-0.98 for PMCP). Concentrations of ocPDCH at most sites, including the collocated sites were low during the winter study, as winds were predominantly from the north, carrying the MPP emissions and ocPDCH to the south, away from Grand Canyon National Park. Conversely PMCP, which was released to the northeast of the Grand Canyon was frequently observed at elevated concentrations at the Grand Canyon sites during the winter. The spatial concentration patterns for winter and summer will be described in more detail in Section 5.

Figure 4-9 shows scatterplots for collocated summer measurements of released tracers (ocPDCH, PMCP, PMCH, and PTCH) at Meadview. There is good precision for ocPDCH (r^2=0.997); this is especially important because the ocPDCH was used to tag the MPP emissions, the main source of interest for this study. The other tracers concentrations had a higher noise level.

Collocated precision gives a measure of uncertainty in PFT concentrations over the range of concentrations experienced for two or more samplers at a given site. However, there may be additional uncertainty in the concentration of *released* PFTs due to variation in apparent background caused by a combination of actual variation in background and measurement error.
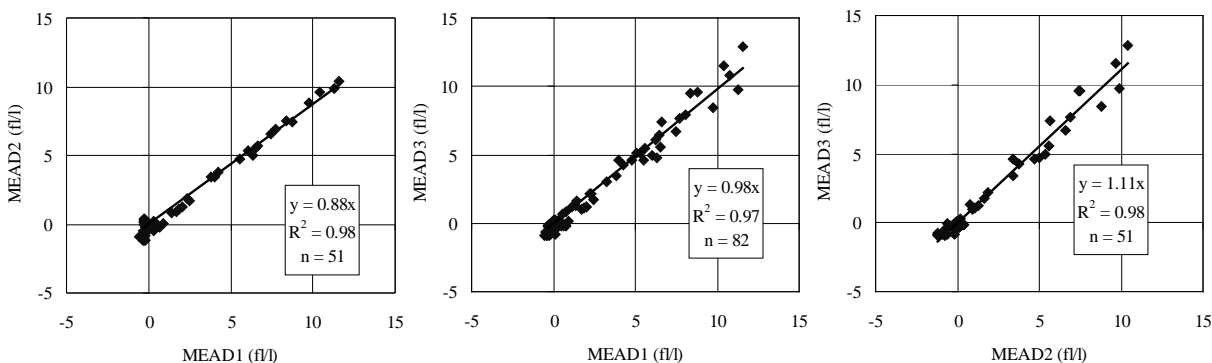
Figure 4-7 Regression of collocated PMCP tracer measurements at Meadview during the winter intensive period.
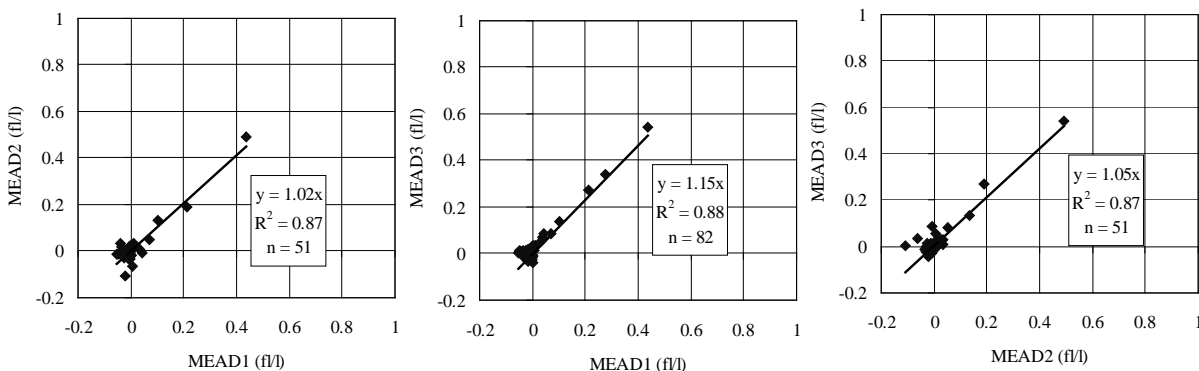
Figure 4-8 Regression of collocated ocPDCH measurements at Meadview during the winter intensive period.

Because the average network-wide background PFT concentration was subtracted for each site, backgrounds that are constant at each site, but varying between sites would result in constant additive biases (systematic error) for each site. Background concentrations varying in time at each site, but averaging the same at all sites would appear as random errors. For determination of PFT concentrations due to the release, the background variation calculation is preferred to collocated precision (especially at near background levels) because it includes both measurement error and actual variation background. At high concentrations of released tracer, collocated

precision measurements more appropriately demonstrate multiplicative errors (e.g. slopes of regression analyses significantly different from one). When considering the amount of SO_2 associated with a given amount of ocPDCH released from MPP, the variation in the SO_2/ocPDCH emission rate must also be considered.
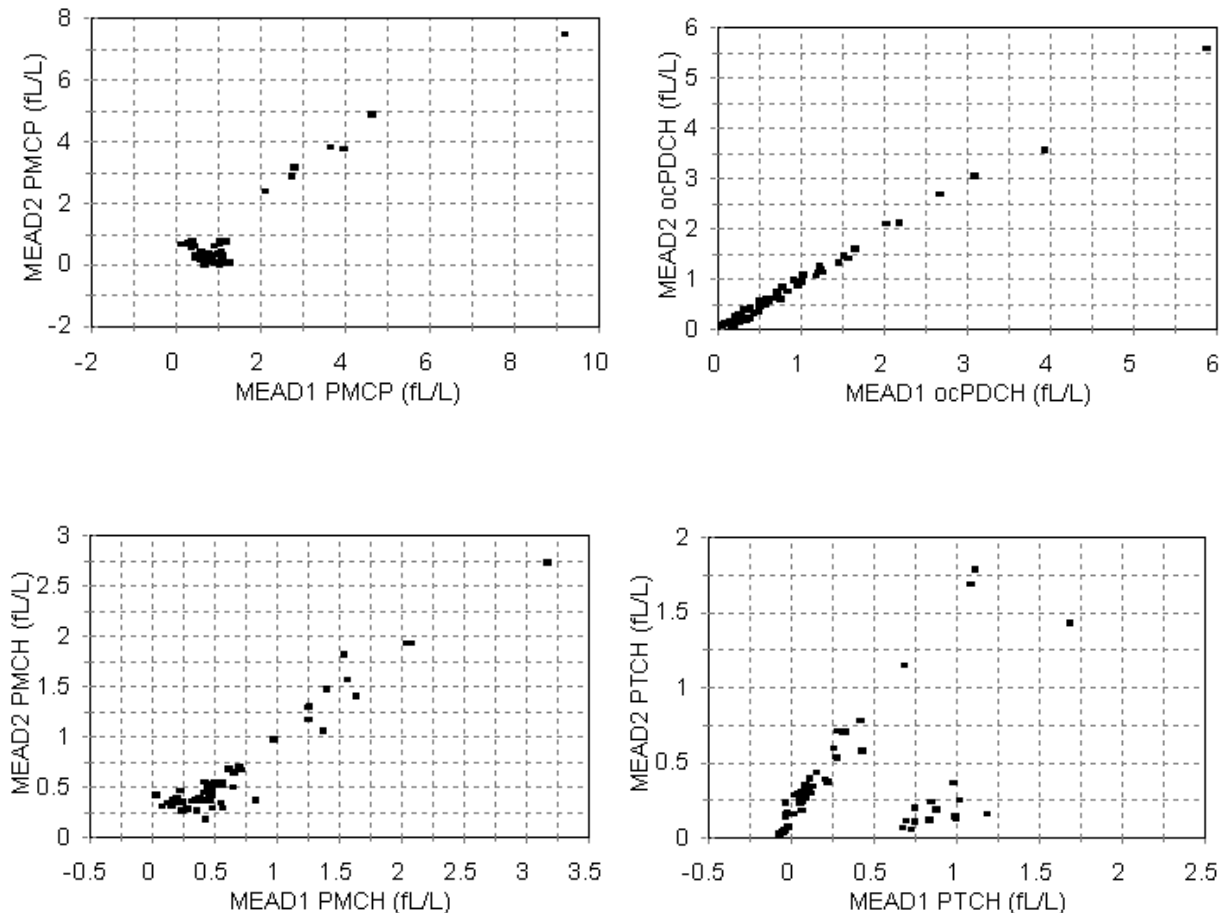
Figure 4-9 Scatter plots of collocated tracer measurements at Meadview, summer intensive period.

Table 4-8 Root-mean-square error (fL/L) for collocated sites.

	Winter		Summer	
	rmse	n	rmse	n
ocPDCH	0.021	(279)	0.059	(246)
PMCP	0.421	(279)	0.43	(246)
PMCH	0.108	(41)	0.28	(246)
PTCH			0.16	(237)

Standard deviations of the PFT compounds (pooled over all sites) during the winter and summer pre-release periods and the interim period between the winter and summer studies are shown in Table 4-9. The ocPDCH background uncertainties of 0.05 fL/L for winter and 0.06 fL/L for

summer are similar to our goal of 0.06 fL/L determined to be the lowest concentration change associated with one estimate of perceptible visibility impact due to MPP. If we consider concentrations of 2 standard deviations above background to be "significantly" above background, then these values of 0.10 fL/L for winter and 0.12 fL/L would exceed this design value. However, because of the conservative nature of the assumptions made in deriving this value, it is unlikely that perceptible visibility impacts would occur unless measured ocPDCH concentrations were greater than 2 standard deviations above mean background.

From July 28, 1992 through August 14, 1992 a gas chromatograph analyzed PFT concentrations for 15 minute sampling periods at Meadview. Although numerous power outages affected the overall data collection, a sufficient number of samples were collected to determine diurnal patterns of tracer concentrations, as well as peak 15 minute to 12 hour average ratios, in particular for ocPDCH emitted from the MPP stack. For each 12-hour averaging period the average of the 15 minute samples from the dual trap analyzer (DTA) were compared to concentrations from the Meadview 12-hour average sample from the BATS. There were usually fewer than 48 valid 15-minute samples for comparison, so the actual sampling periods varied somewhat between the DTA and BATS. The squared correlation coefficient (r^2) between the DTA and BATS (with somewhat different sampling periods) was 0.79 (n=30).

Table 4-9 Standard deviation (fL/L) of pre-release and interim PFT concentrations.

	Winter		Summer		Interim	
	standard deviation	n	standard deviation	n	standard deviation	n
ocPDCH	0.05	(105)	0.061	(155)	0.037	(83)
PMCP	0.84	(105)	0.59	(156)	0.63	(83)
PMCH	0.43	(42)	0.3	(156)	0.48	(46)
PTCH			0.62	(151)		

The Department of Energy's Environmental Monitoring Laboratory (DOE-EML) measured PFTs using the BATS samplers for 2 hour periods at Dolan Springs for the period July 11- July 31, 1992. Dolan Springs is approximately 50 km north-northeast of MPP and was expected to often be in the transport path of MPP emissions during summer late-morning through afternoon periods. Table 4-10 shows collocated RMS error and r^2 for released tracers.

Table 4-10 RMS error and r^2 for DOE-EML collocated tracer measurements at Dolan Springs.

	RMS error (fL/L)	r^2
ocPDCH	0.16	0.98
PMCP	0.28	0.75
PMCH	0.23	0.89
PTCH	0.07	0.99

There were 14 days for which the EML PFT measurements could be compared to the Brookhaven PFT measurements at Dolan Springs. The 2 hour measurements from EML were averaged over 24 hour periods to compare with the BNL measurements. Most days had either 10 or 12 two-hour samples; several days were missing the 1600 and 1800 samples from EML.

Time series plots comparing Brookhaven and DOE-EML concentrations are shown in Figure 4-10. Temporal patterns between Brookhaven and DOE-EML concentrations are similar for all PFTs (r^2=0.99 both ocPDCH and PTCH, 0.90 for PMCP, and 0.77 for PMCH). However, offsets are apparent for ocPDCH and PTCH; for PMCP and PMCH, the values from the two laboratories differ by scaling factors. The offsets indicate differences in apparent background and do not affect concentrations due to the release; thus the ocPDCH from MPP would not be affected by the offsets. The scaling factors would affect concentrations due to the releases at Tehachapi Pass; for this study, this is not important because the tracers from Tehachapi Pass were intended only for use as markers for flow through the pass.
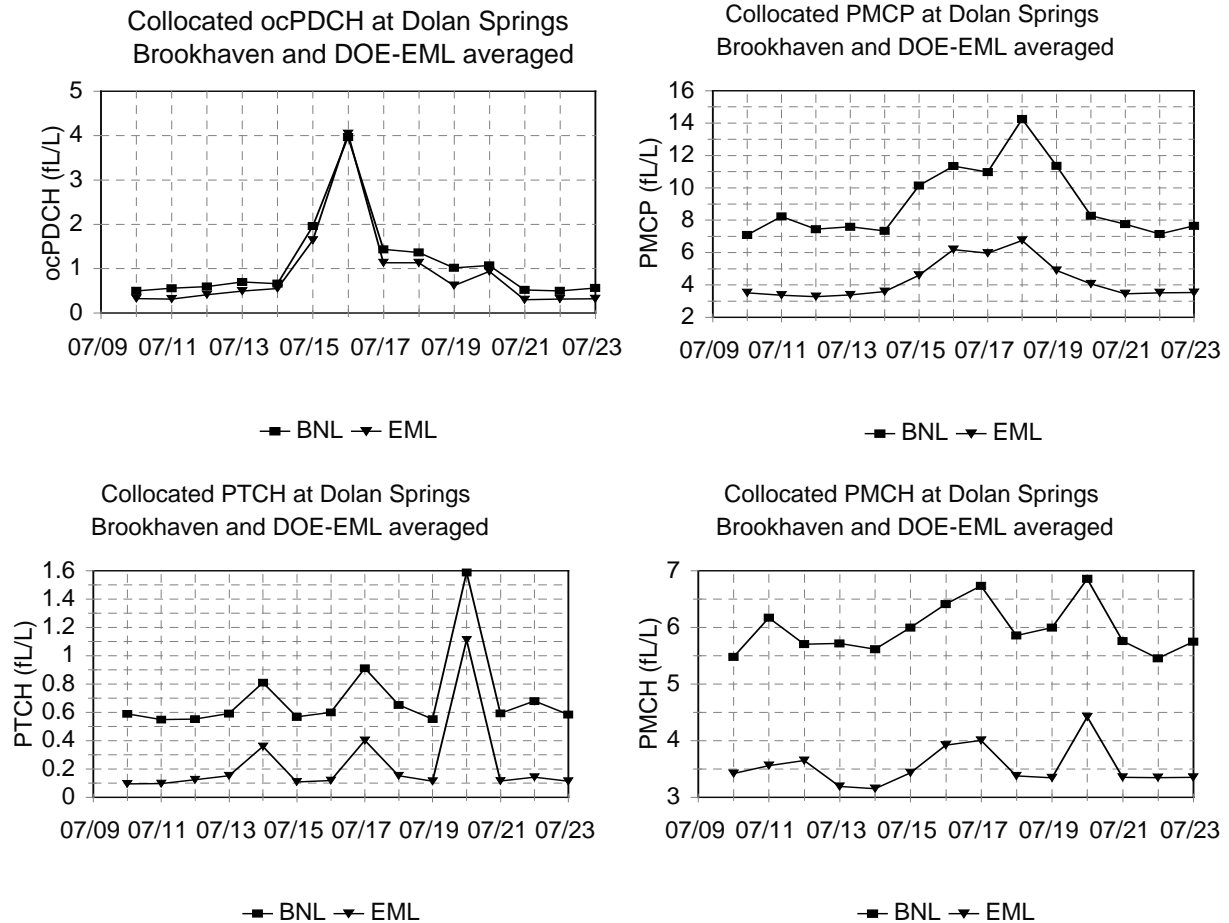
Figure 4-10 Time series of collocated BNL and DOE-EML tracer measurements at Dolan Springs, summer intensive period.

4.5 Meteorological data quality.

This section describes the data quality of the meteorological observations collected during Project MOHAVE.

4.5.1   Upper-Air Wind Speed and Direction

Determination of the accuracy of the wind measurements is problematic because the "true" values are not known. However, comparisons of various measurement methods (e.g. rawinsondes, sodars, tall towers, radar wind profilers) and collocated precision calculations of a given method allow for a general level of uncertainty to be estimated. A review of routine field audits of radar wind profilers using rawinsondes, Doppler sodars, tethered-sonde systems, and pilot balloon tracking showed consistency of wind profiler measurements to within about 1-2 m s^{-1} in speed and 10 to 20 degrees in direction (Neff, 1994). Comparison of radar wind profiler observations to aircraft and tall tower measured winds indicated RMS differences of 1 m s^{-1} and 10 degrees (Angevine & MacPherson, 1996; Angevine et al., 1998). Guidelines for quality assurance of upper air meteorological data prepared for the USEPA give "expected" performance characteristics for radar wind profilers and rawinsondes (Lindsey et al., 1995). These guidelines give expected comparability for radar wind profilers of 2 m s^{-1} in speed and 30 degrees in direction, with systematic differences of 1 m s^{-1} and 10 degrees. The corresponding values for rawinsondes are 5-18 degrees in direction and 3.1 m s^{-1} in speed for comparability, based upon collocated precision, with systematic differences of 0.5-1 m s^{-1} for each component.

During about the first two weeks of the winter intensive study, a radar wind profiler (RWP) was located at MPP and rawinsondes were released nearby in the "Riviera" section of Bullhead City, Arizona, about 4 km southwest of the RWP location. The heights of the MPP RWP site and Bullhead City rawinsonde site were 213 m MSL and 167 m MSL, respectively. Although the instruments were nearby, they were not collocated, the reported measurement heights differed somewhat, and the RWP data were hourly averages while the rawinsonde data were nearly instantaneous. Nonetheless, comparison of the data from the two systems can give an upper limit on the measurement uncertainty of these instruments. Both the RWP and rawinsonde gave wind direction and speed approximately every 100 meters in height. For heights of about 400 m to 2700 m MSL, measurements from both systems were available for comparison. In order to compare values at the same height, the observations were linearly interpolated to the nearest 100 m.

Figure 4-11 and Figure 4-12 compare wind direction and wind speed at the RWP and rawinsonde sites. Because wind directions may vary considerably during light wind speed conditions, the wind direction comparisons are shown only for periods with wind speeds at least 3 m s^{-1}. Table 4-8 shows the percent of wind speed and direction measurements meeting specified criteria. There was a bias of 5 degrees between the Bullhead City rawinsonde resultant wind direction and the MPP radar wind profiler resultant wind direction.
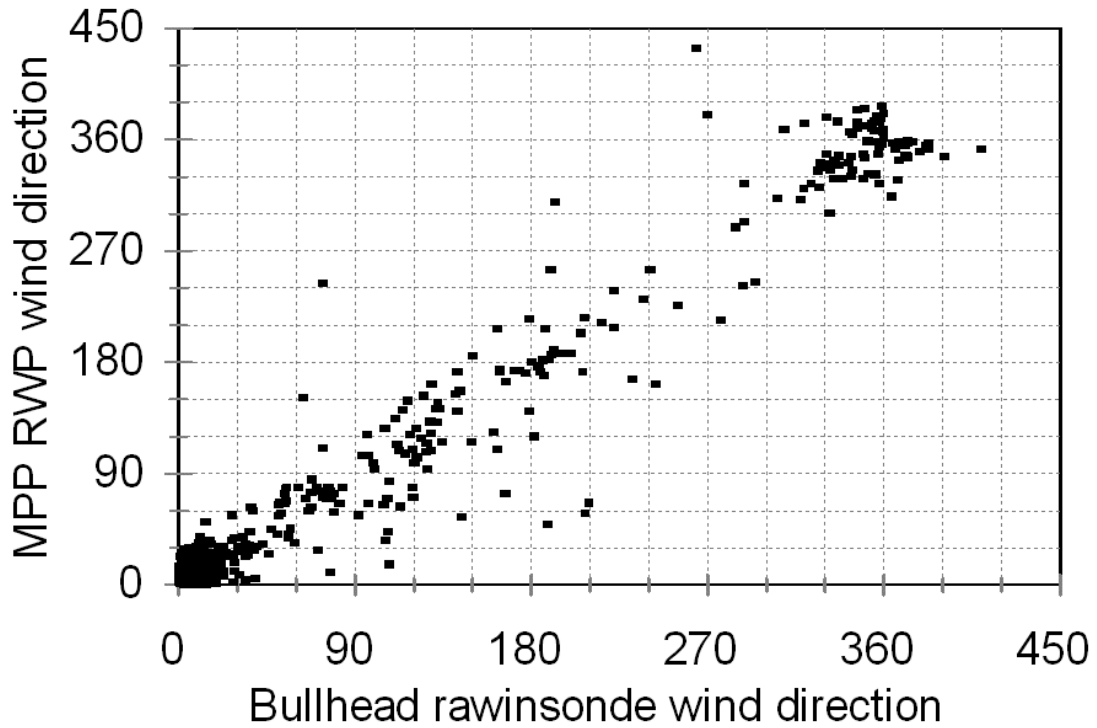
Figure 4-11 Comparison of direction measured by the MPP radar wind profiler and Bullhead City-Riviera rawinsonde during the second half of January 1992.
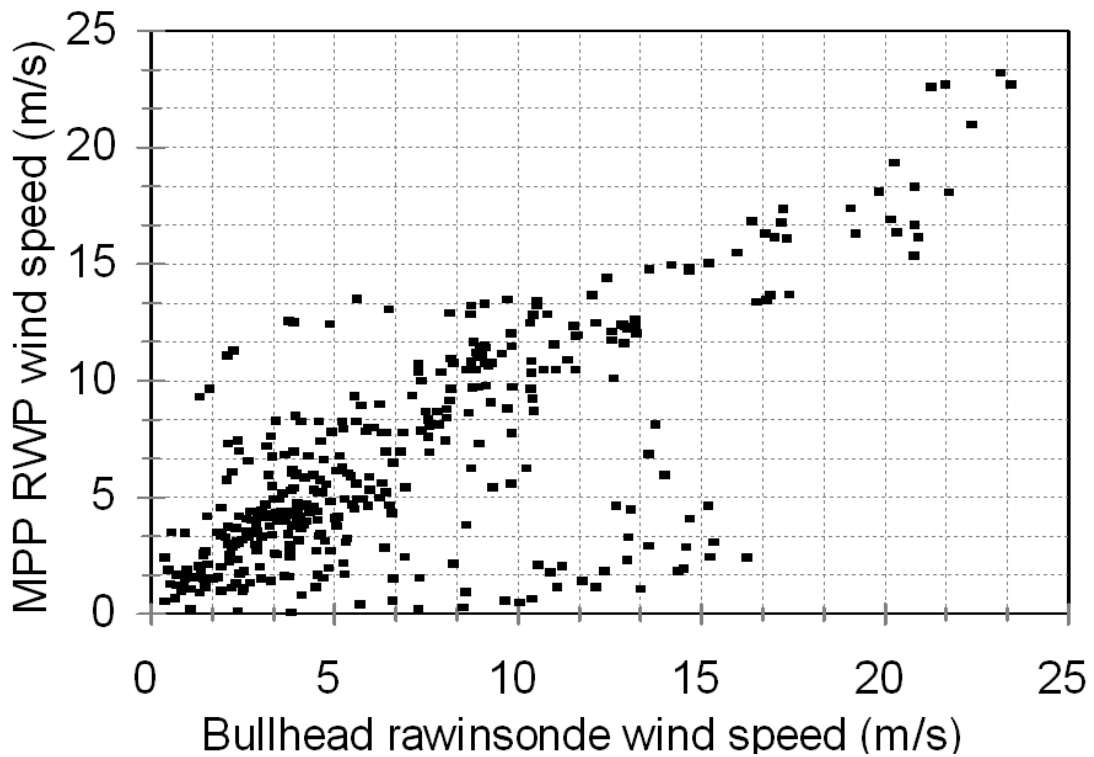
Figure 4-12 Comparison of wind speed measured by the MPP radar wind profiler and Bullhead City-Riviera rawinsonde during the second half of January 1992.

Table 4-11 Comparison of winds from rawinsonde and radar wind profiler.

Wind direction: Percent within given direction difference	
10 degrees	50%
20 degrees	78%
30 degrees	94%
Wind speed: Percent within given speed difference	
1 m s^{-1}	41%
2 m s^{-1}	63%
4 m s^{-1}	84%
Combined wind speed and direction: Percent meeting both speed and direction criteria	
2 ms^{-1} and 20 degrees	52%
4 m s^{-1} and 30 degrees	83%

5. Light Extinction In The Desert Southwest

This chapter describes the spatial and temporal variations of light extinction and its components over the study area.

5.1 Principles of Light Extinction

Perception of haze can be influenced by variables such as angle and intensity of the sun, coloration of landscape features, and the distance to the object being viewed. All of these factors are independent of the chemical composition of the air through which objects are viewed. To control for these interfering perception factors, haze is objectively quantified in terms of the light extinction coefficient (b_{ext}). The extinction coefficient is a measure of the total fraction of light that is attenuated per unit distance and has units of inverse megameters (Mm^{-1}). For example, if the light extinction coefficient of the atmosphere is 30 Mm^{-1}, then ~0.003 % of light ($\lambda = 550$ nm) will not be transmitted through 1 m of air. Light extinction can be measured directly using a tranmissometer.

The extinction coefficient has contributions from both particles and gases. In equation form, this is expressed as:

$$b_{ext} = b_{sg} + b_{ag} + b_{sp} + b_{ap}$$
(5-1)

where the subscripts s, a, g, and p refer to scattering, absorption, gases, and particles, respectively. Each component is described briefly below and typical values in the Grand Canyon region are presented. Light scattering and absorption values represent the attenuation of light with a wavelength of 550 nm.

- b_{sg} (light scattering by gases) is also referred to as Raleigh or natural blue-sky scatter. This term is approximately **11 Mm^{-1}** at Meadview and is a function of air density (depends upon temperature and pressure, which are strongly dependent upon altitude).

- b_{ag} (light absorption by gases) is primarily due to NO_2 in the atmosphere. This can account for a few percent of the total extinction in urban areas, but is generally insignificant in remote regions such as the Grand Canyon where NO_2 levels are substantially lower. This term is assumed to be **0 Mm^{-1}** in this analysis.

- b_{sp} (light scattering by particles) is usually the largest component of the extinction coefficient and is typically dominated by fine particles composed of water, sulfate, nitrate, ammonium, and organic material. Soil and elemental carbon can also scatter light. This is the component in which MPP's sulfur emissions can have the greatest impact. At Meadview from 10/1/91 to 9/30/92, the median DRI nephelometer measurement of b_{sp} was **8.9 Mm^{-1}**. During the period 7/1/92 to 9/3/92, the median Optec nephelometer b_{sp} at Meadview was **11 Mm^{-1}**.

- b_{ap} (light absorption by particles) is due to both light absorbing carbonaceous aerosol and soil. b_{ap} was approximated by measuring the absorption of light through a PM$_{2.5}$ sample filter. This measurement is referred to as b_{abs} while the true light absorption by particles is refered to as b$_{ap}$. The median b_{abs} measurement at Meadview was **7.2 Mm^{-1}** during the winter

intensive study and *6.8 Mm^{-1}* during the summer intensive study. Note: these values may overestimate the true b_{ap} by up to factor of 2 (see Sections 4.1.3 and 4.2.1.4). Because of this uncertainty, most analyses performed in Project MOHAVE used an estimate of b_{ap} calculated from the elemental carbon concentration instead of using the measured b_{ap} (see Section 6.2).

In this section, results will be presented from transmissometers (b_{ext}), nephelometers (b_{sp}), and particle light absorption through filters (b_{abs}).

5.2 Light Extinction in the Southwest

In terms of light extinction, the Grand Canyon is one of the cleanest Class 1 areas in the United States. Figure 5-1 shows the average annual calculated extinction coefficient throughout the IMPROVE network between March 1992 and February 1995 (Sisler *et al.*, 1996). A region of low background extinction exists throughout Nevada, Utah, Colorado, Wyoming, and Arizona. On a national scale, light extinction was generally higher toward the population centers along the west coast, the Ohio River Valley, and the Chesapeake Bay Area. The lowest annual extinction coefficient was observed at Denali National Park in Alaska.
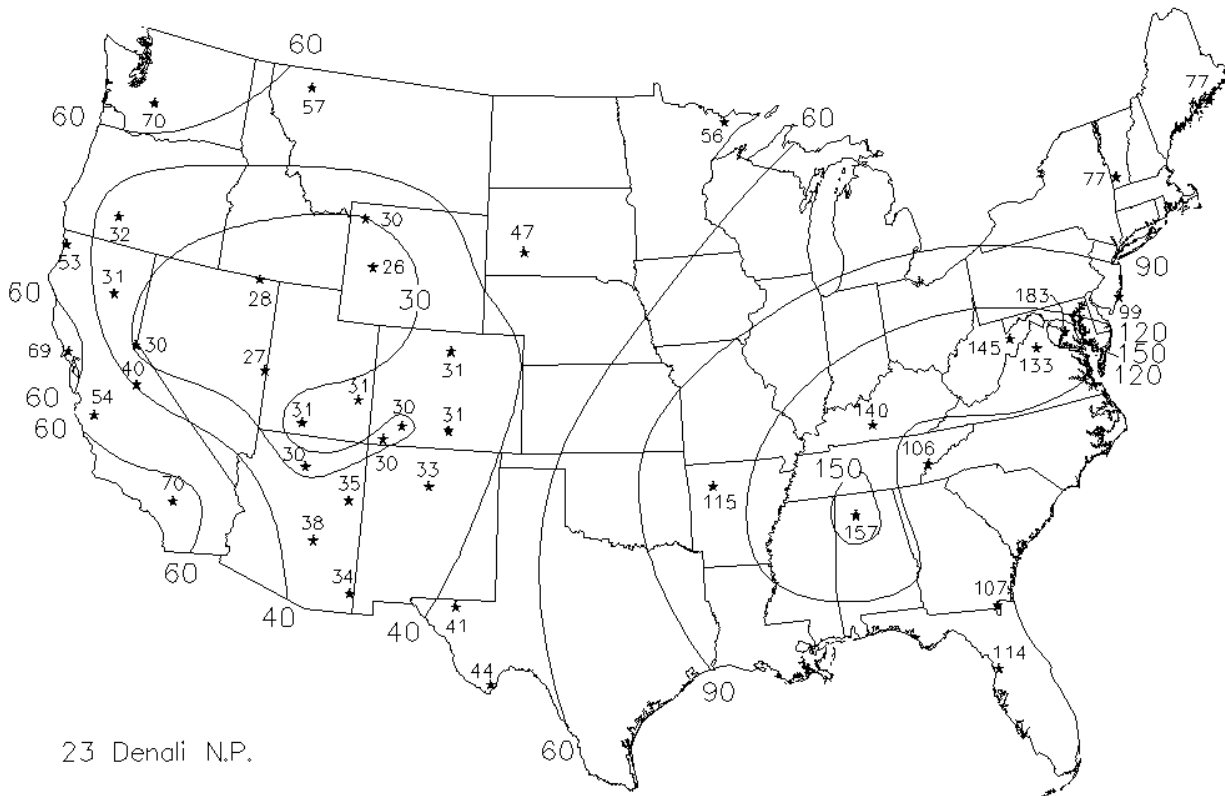
Figure 5-1 Map showing mean annual levels of calculated b_{ext} (in Mm^{-1}) at Class I areas throughout the United States. Data was obtained from the IMPROVE network from particulate matter measurements made between March 1992 and February 1995.

5.3 Haze Levels at the Grand Canyon

Figure 5-2 and Figure 5-3 show the 12-hour average of the transmissometer measured extinction at Meadview (MEAD) and both in (GRCW) and on the rim of (GRCA) the Grand Canyon for the winter and summer intensive study periods. The in-canyon sight path (GRCW) is from Phantom Ranch at the bottom of the Canyon to the South Rim (Grandview Point), with an elevation change of about 1400 m. The South Rim sight path is nearly level (Moran Point to Grandview Point). At least 10 hours of valid data (not influenced by meteorological events such as relative humidity higher than 90%, fog, rain, and blowing dust) were used to calculate each 12-hour averages. The median and maximum b_{ext}, and date of which the maximum b_{ext} occurred are shown in Table 5-1. The values in Table 5-1 were calculated over the intensive sampling periods noted in the table. The episode of high extinction observed in the canyon on 1/10/92 did not occur during this period and was not included at the maximum in the table.

Table 5-1 Summary of 12-hour average Transmissometer Measurements near Grand Canyon National Park.

Site	Winter (1/14/92 – 2/15/92) b_{ext}			Summer (7/12/92 – 9/3/92) b_{ext}		
	Median (Mm^{-1})	Maximum (Mm^{-1})	Maximum Date	Median (Mm^{-1})	Maximum (Mm^{-1})	Maximum Date
MEAD	27.6	42.3	2/2/92 1900	32.5	51.4	8/6/92 1900
GRCA	20.2	31.0	2/4/92 0700	22.7	41.6	8/7/92 0700
GRCW	33.5	39.8	2/2/92 0700	35.5	47.9	7/21/92 0700

Measured extinction was higher within the canyon than at the rim during both winter and summer seasons. The differences between median values at GRCW and GRCA were approximately 13 Mm^{-1} for both seasons. Maximum extinction values at Meadview were higher than either GRCW or GRCA sites. Median and maximum extinction values were higher in summer than in winter at all three sites. Differences in median extinction between winter and summer ranged from 2.0 to 4.9 Mm^{-1}.

It is noteworthy that the maximum extinction periods observed at Meadview and in GCNP are related. During the winter when flows are typically down canyon, the highest measured extinction within the canyon at GRCW was during the day of 2/2/92. The highest 12-hour wintertime extinction at Meadview was measured 12-hours later. Similarly, during the summer intensive study when winds are typically from the south west, the highest 12-hour extinction at Meadview was measured on 8/6/92 in the evening. During the next sampling period, the b_{ext} reached its maximum above the canyon at GRCA. Elevated extinction was also observed within the Grand Canyon at GRCW on 8/7/92. These observations imply that episodes of high extinction are often regional in extent.

There are several reasons why extinction was generally higher within the canyon than at the rim. Sources of pollutants in this region (i.e. population centers and power plants) are generally located at low elevations near water sources. When winds are light, emissions from these areas tend to following natural drainage flows and impact lower elevation monitoring sites. Ventilation of pollutants out of the canyon generally occurs when the lower atmosphere becomes unstable from mid morning to mid afternoon. During the remainder of the day pollutants
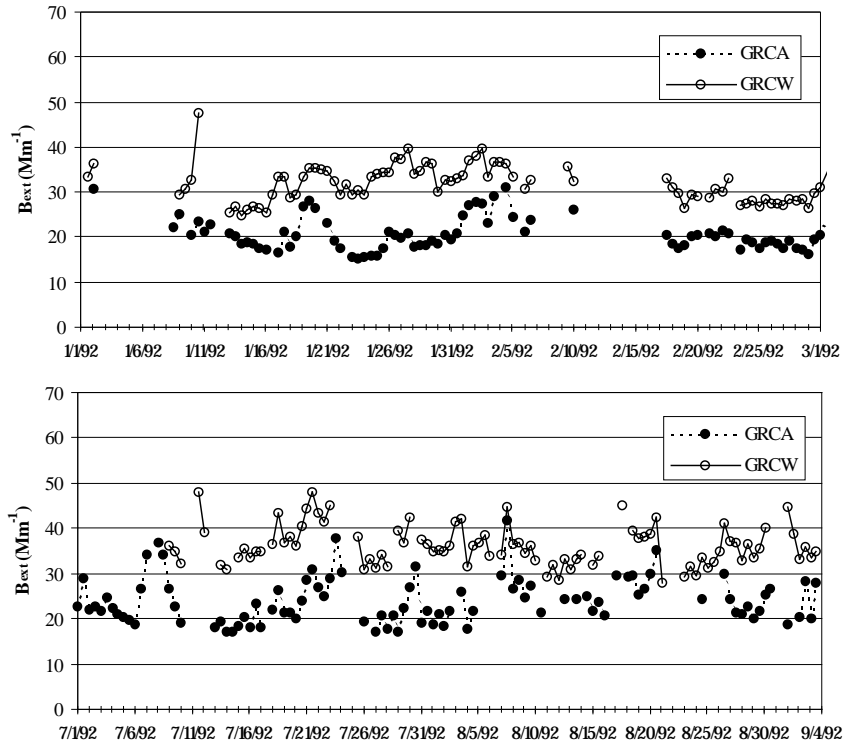
Figure 5-2 Comparison of 12-hour averaged b$_{ext}$ measured in (GRCW) and on the rim of (GRCA) the Grand Canyon.
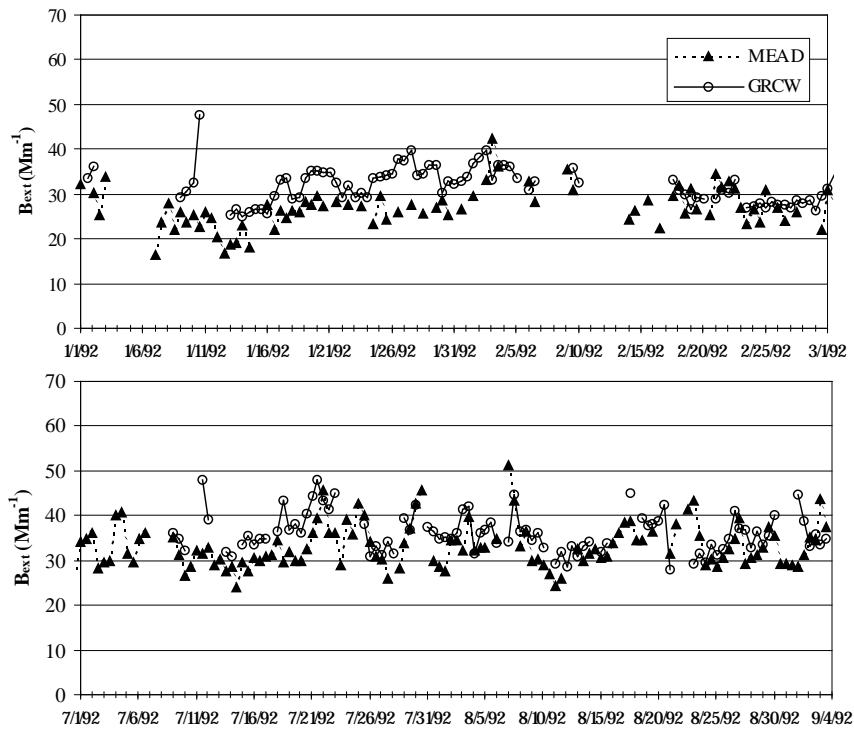
Figure 5-3 Comparison of 12-hour averaged b$_{ext}$ measured at Meadview (MEAD) and within the Grand Canyon (GRCW).

generated at low elevations are frequently confined within the canyon. Consequently, for a large portion of the day, air within the canyon is prevented from mixing with the air above the canyon.

5.4 Diurnal Variation of Light Extinction and Its Components

5.4.1   Light Extinction

The transmissometers measured light extinction at hourly intervals during routine operation. The valid hourly data with weather impacted periods removed are shown in Figure 5-4 and Figure 5-5. With the exception of the transmissometer at Meadview, wintertime light extinction at the Grand Canyon did not exhibit large changes over 12-hour and 24-hour sample durations. (The diurnal variability of the data from Meadview is discussed below.) The summertime extinction signal was more variable at all three sites. There are multiple episodes at each station during the summer in which extinction changes by more than 10 Mm^{-1} over a 3 hour period.

These results suggest that short term impacts to light extinction are frequent during the summer. As a result light extinction attributions to pollution sources averaged over 12 and 24-hour periods may not be representative of the magnitude of the short term impacts.

Figure 5-6 shows hourly averaged light extinction at Meadview measured by transmissometer. Averages were calculated during the intensive studies from valid data measurements collected over periods not influenced by meteorological events such as fog, rain, and blowing dust. The error bars represent the standard error of the hourly measurements.

During the wintertime at Meadview a ~5 Mm^{-1} decrease in measured light extinction was observed during daylight hours between 0900 and 1700. The representativeness of this trend in terms of regional light extinction is questionable since the sight path of the transmissometer was directed through a valley near Meadview. It has been hypothesized that the winter diurnal pattern is due to strong nighttime thermal gradients within the sight path that effectively refract the light from the transmissometer source. This hypothesis is supported by data from a collocated nephelometer at Meadview. Figure 5-7 shows the wintertime diurnal trend of light scattering b_{sp} over the same period as measured by the DRI nephelometer. While a slight reduction (~2 Mm^{-1}) in scattering is observed between 1100 and 1800, the decrease does not seem to be large enough to account for all of the decrease in total light extinction.

Smooth diurnal cycles in light extinction were observed at both GRCW and GRCA. On average, light extinction at the Grand Canyon peaks between 0900 and 1200 during both winter and summer. Diurnal variations typically have a magnitude of ~4 Mm^{-1} at these 2 sites.
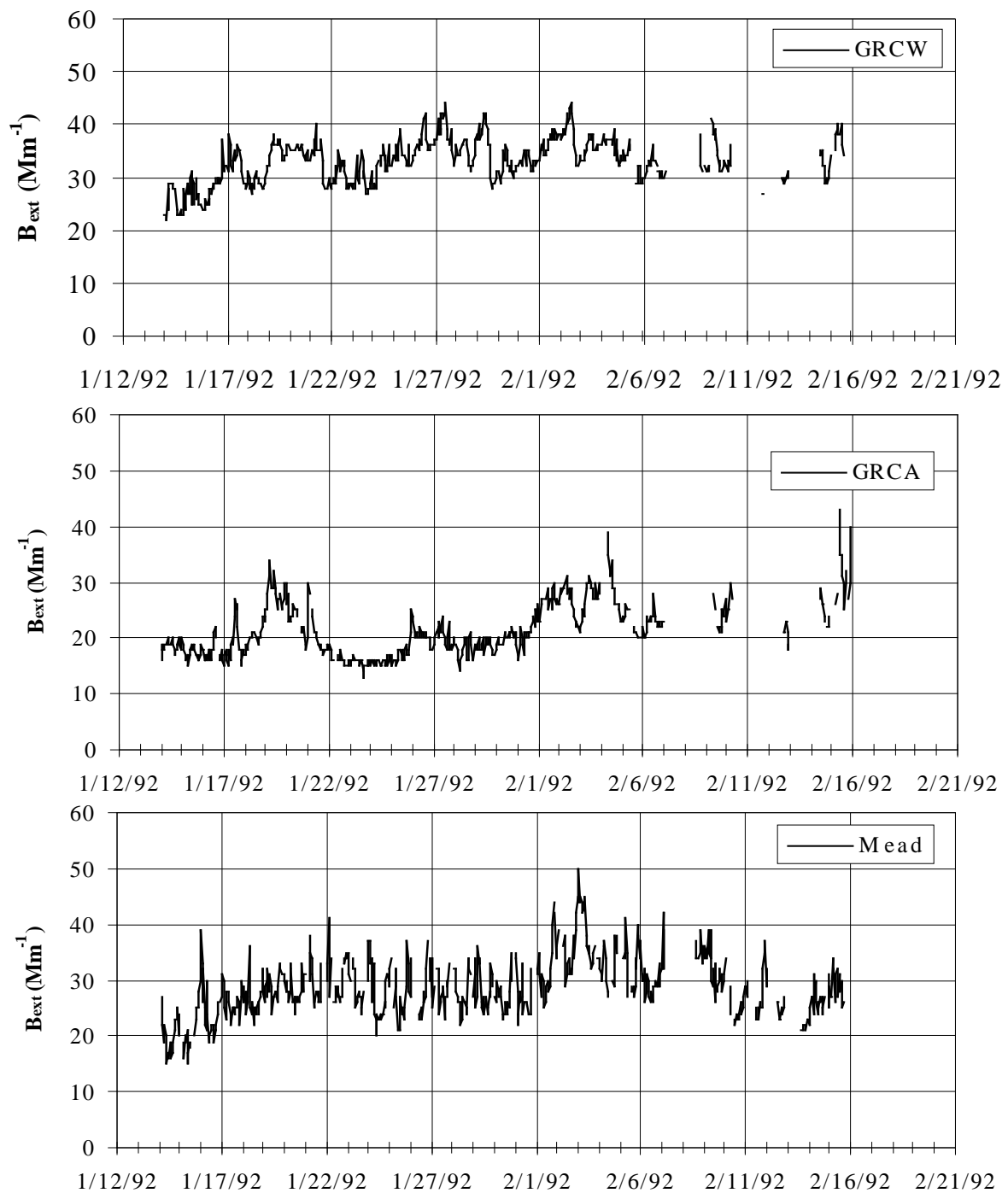
Figure 5-4 Time series of wintertime hourly light extinction at MEAD, GRCA, and GRCW.
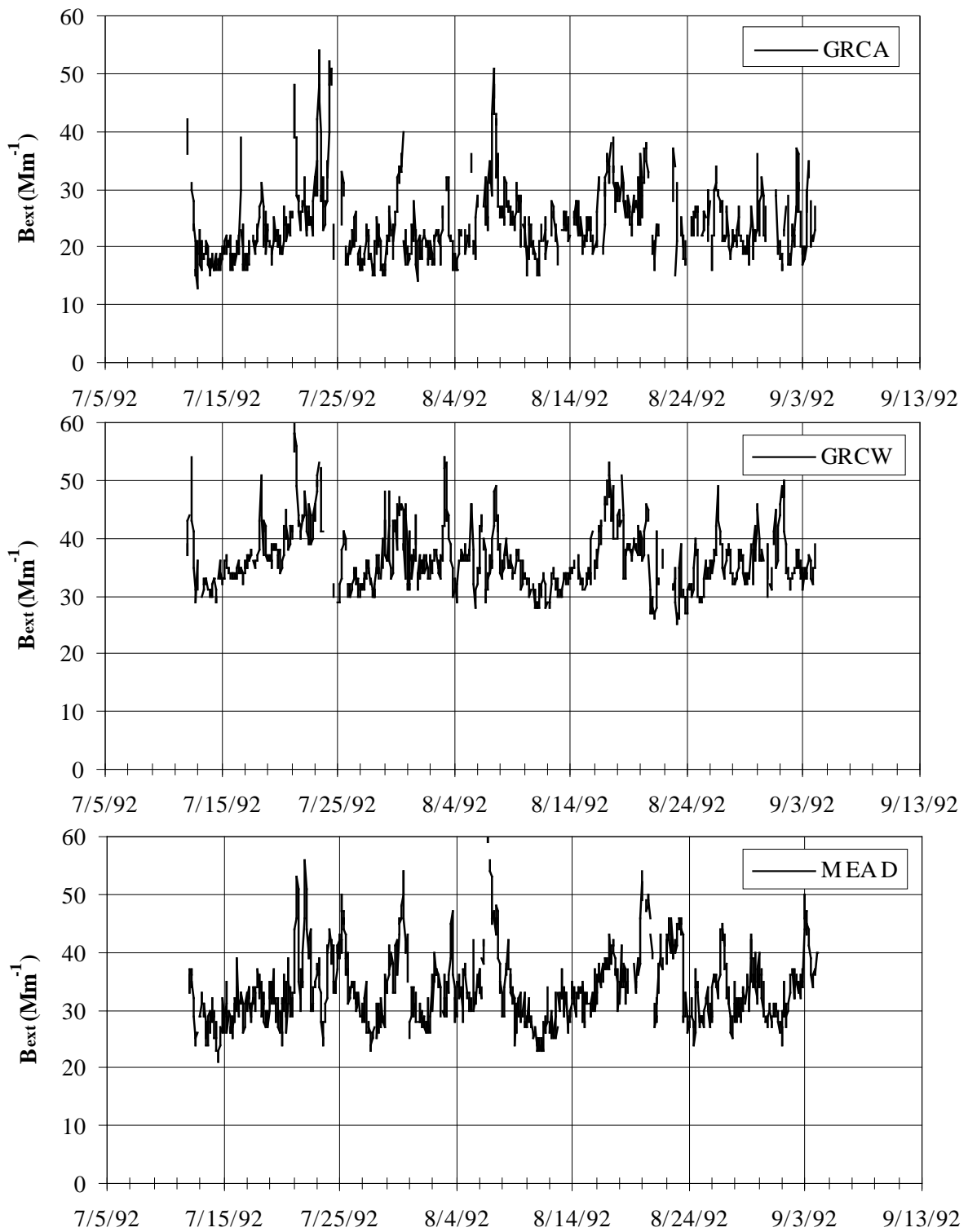
Figure 5-5 Time series of summertime hourly light extinction at MEAD, GRCA, and GRCW.
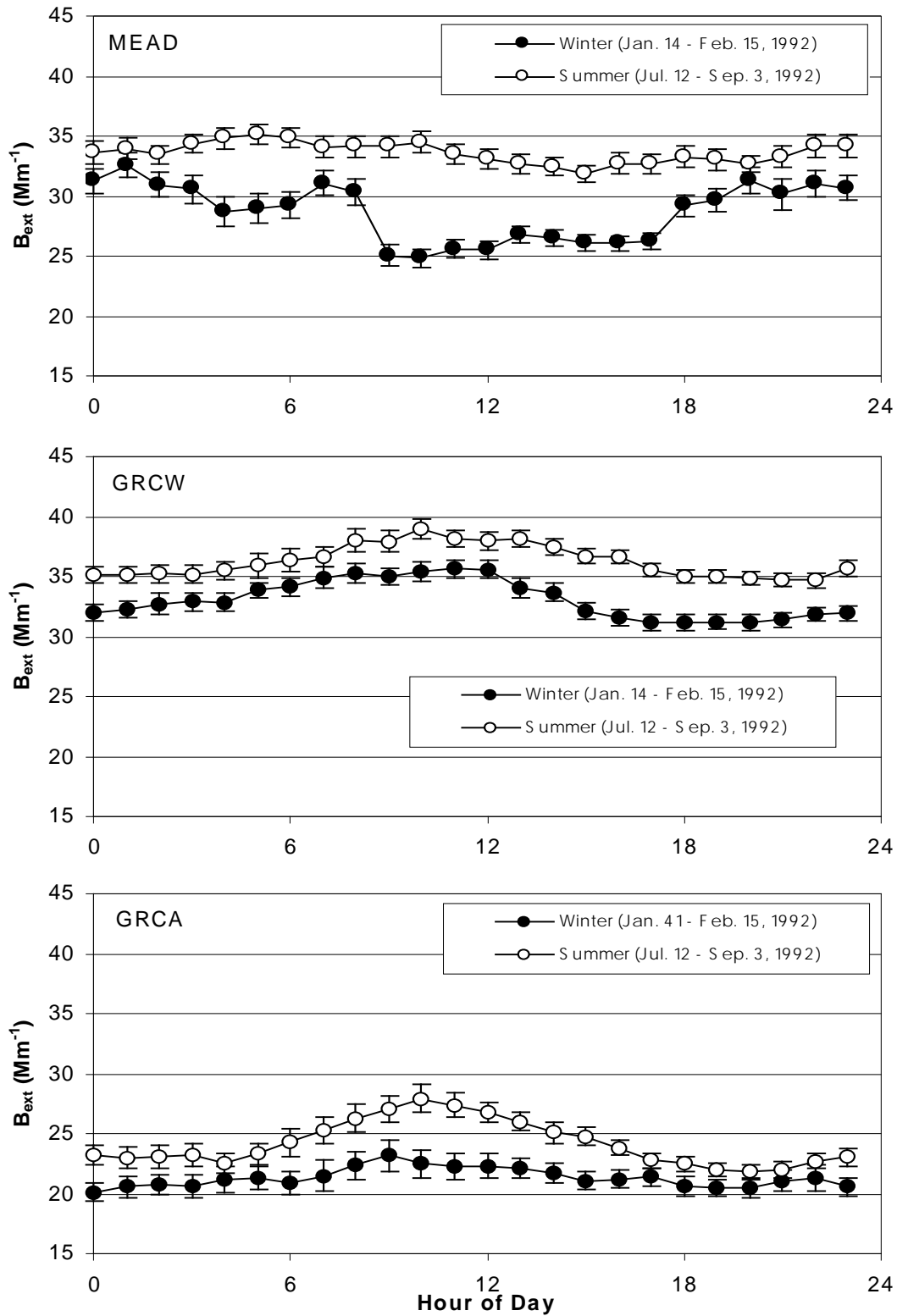
Figure 5-6 Diurnal variation of light extinction on the west side of the Grand Canyon at Meadview (Meadview), within the Grand Canyon (GRCW), and on the south rim of the Grand Canyon (GRCA).
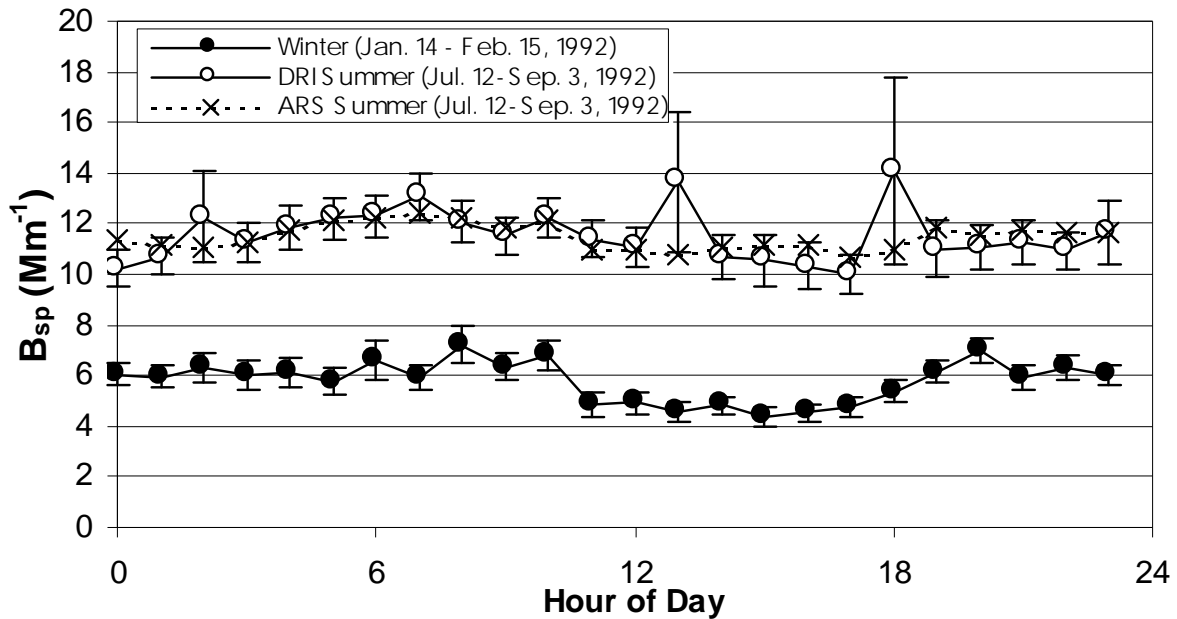
Figure 5-7 Diurnal variation of light scattering by particles measured at Meadview AZ.

5.4.2 Particle Light Scattering

During both the winter and summer intensive studies, DRI operated a nephelometer at Meadview to measure the scattering of light by particles (b_{sp}). ARS also deployed a nephelometer at Meadview during the summer intensive study. Data from the both nephelometers were adjusted to represent only the light scattering due to particles by subtracting the Rayleigh component from the nephelometer signal. (Note that a consistent data validation protocol was not established for the DRI nephelometer measurements so all of the data was labeled as suspect in the MOHAVE database.)

The nephelometer signals in Figure 5-8 behave similarly to the transmissometer signals in that the summertime measurements had greater temporal fluctuations than the wintertime measurements. Occasional high one hour nephelometer readings up to (150 Mm^{-1}) were observed during the summertime with the DRI nephelometer. It is unlikely that these peaks were representative of ambient particle scattering since they were not detected simultaneously with the ARS nephelometer or the transmissometer (Figure 5-5).

Average diurnal patterns were calculated for the nephelometer data in Figure 5-7. High standard errors were observed at 0200, 1300, and 1800 for the DRI summertime diurnal signal. These points coincide with the occurrence of individual high one hour readings and are not representative of the typical diurnal behavior of the particle scattering.
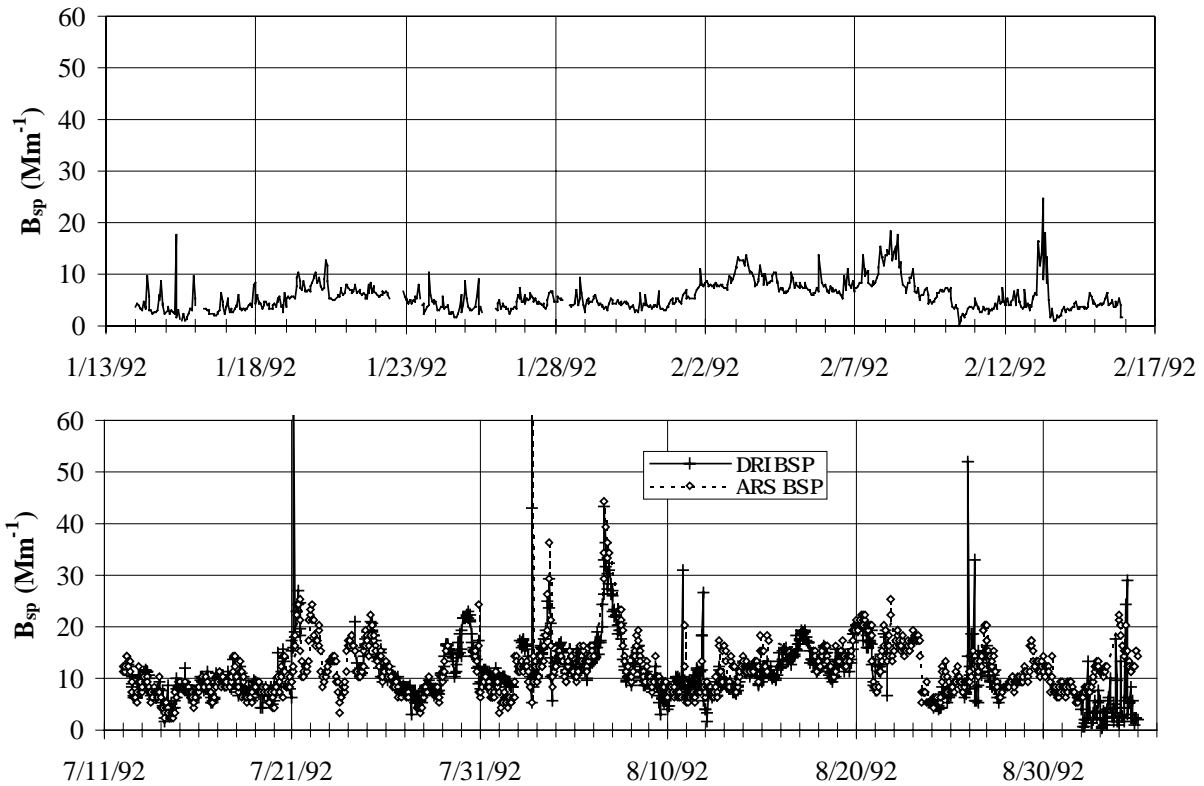
Figure 5-8 Time series of particle light scattering (b_{sp}) at MEAD.

As with the transmissometer measurements at GRCA and GRCW, diurnal patterns in the nephelometer signal peak in the morning between 0500 and 1000 during both the winter and summer intensive studies. The amplitude of the nephelometer diurnal pattern was ~ 2 Mm^{-1} which is less than that observed by the transmissometer.

5.4.3   Particle Light Absorption

Light absorption by particles was measured on aerosol filters collected at 12-hour intervals. While consensus has not been reached on exactly how the b_{ap} measurement relates to the true particle light absorption (see Section 4), the measured b_{ap} signal should have the same relative behavior of the true particle light absorption. Measurements of b_{ap} were conducted at Meadview, Hopi Point on the rim of the Grand Canyon, and Indian Gardens within the canyon. The particle absorption data is shown in Figure 5-9. Particle light absorption was higher in the canyon (INGA) than on the rim (HOPO) for an extended episode between 1/24/92 to 1/30/92. On average, b_{ap} was higher in the summer than in the winter by ~3 Mm^{-1}. Elevated levels of b_{ap} in excess of 15 Mm^{-1} were observed at HOPO for 4 periods during the summer intensive study. Differences between day and night samples of b_{ap} were not significant in either winter or summer at all sites.
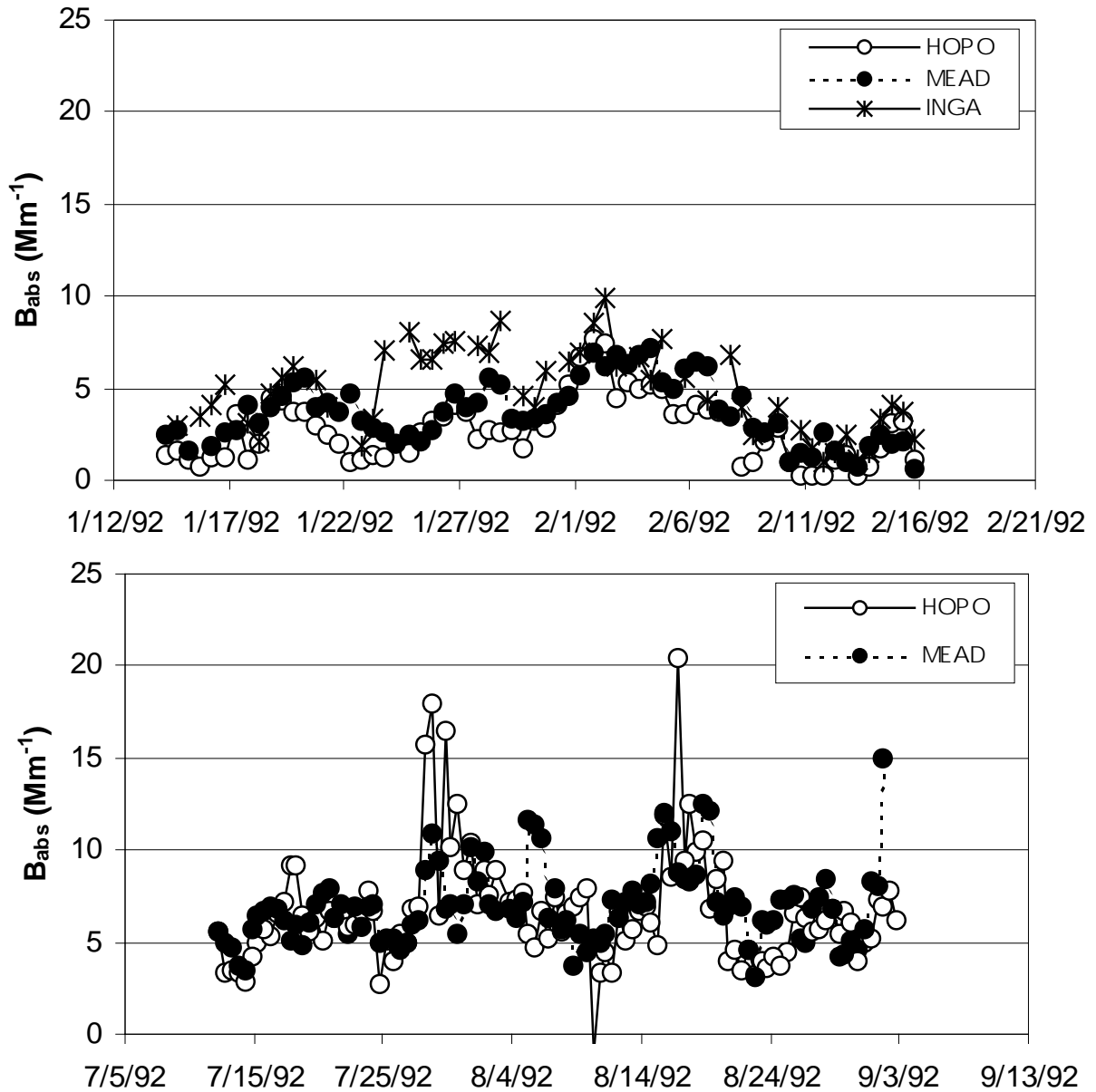
Figure 5-9 Time series of measured b_{abs} from 12-hour duration filters.

5.4.4   Calculating Total Extinction from Components

Sections 5.4.1 – 5.4.3 reviewed measurements of total extinction (b_{ext}), particle scattering (b_{sp}), and particle absorption (b_{abs}). Hasan and Lewis (1983) have carried out theoretical calculations to show that because of the forward angle truncation error of the nephelometer, it underestimates the coarse mass scattering (CMS) by about a factor of 2. White et al., (1994a) were able to show from transmissometer derived total scattering and nephelometer measurements of fine and coarse

particle scattering that the nephelometer underestimates scattering by particles greater than 2.5 μm by about a factor of 2.

Coarse mass (CM), b_{ext}, b_{sp}, and b_{abs} data are available from Meadview during the summer intensive. Since the extinction of light by gases is also known, a balance can be performed between total extinction and its measured components. The coarse mass scattering efficiency of 0.6 m^2/g is taken from a literature review by Trijonis and Pitchford (1987). The coarse mass scattering (CMS in Mm^{-1}) is then calculated as:

$$CMS = 0.6[CM]$$

(5-2)

where [CM] is coarse mass in μg/m^3. Figure 5-10 shows a time series of the sum of b_{sg} (10.6 Mm^{-1} based on air density at Meadview), b_{abs} (IMPROVE sampler), b_{sp} (ARS nepelometer), and CMS/2 (IMPROVE sampler) along with the measured total extinction b_{ext} at Meadview. Note that data for some sampling periods are not shown in the figure.
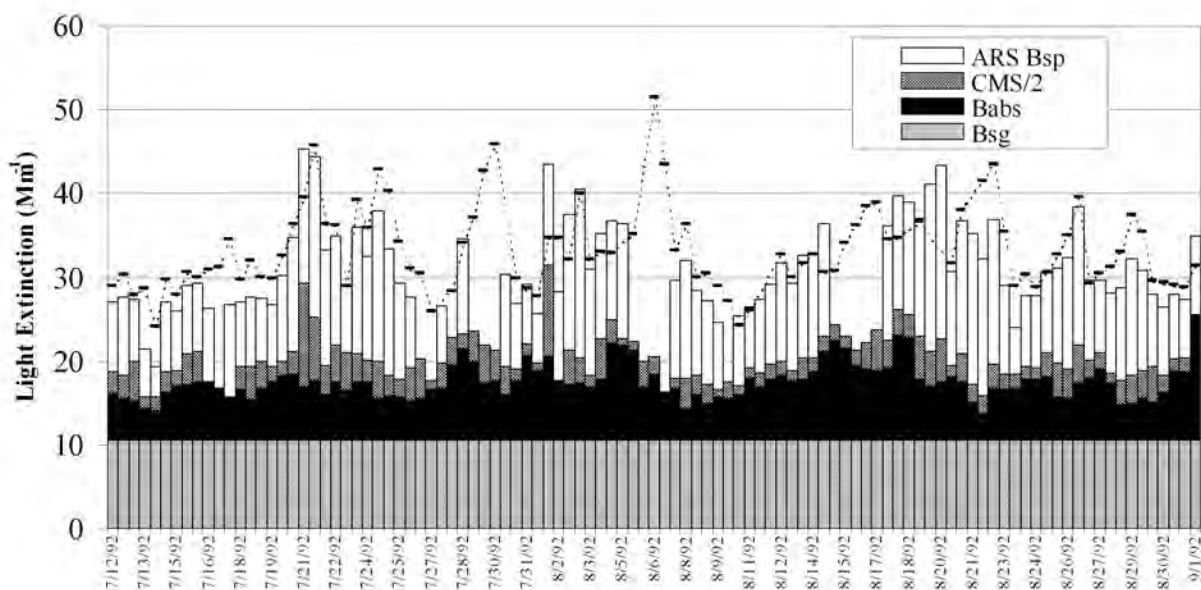
Figure 5-10 Extinction balance comparison of the sum of b_{abs}, b_{sg}, b_{sp}, and CMS/2 with total b_{ext} at MEAD during the summer intensive study.

For sampling periods where all 4 observations are valid, the calculated extinction (b_{sg} + b_{abs} + b_{sp} + CMS/2) was regressed against the observed extinction (Figure 5-11). Light extinction was also calculated using an alternate approximation for b_{ap}. This approximation assumes that elemental carbon is the only light absorbing species, with a mass absorption efficiency of 10 m^2/g (i.e. b_{ap} = 10 [EC]). These calculated extinction values (black circles in Figure 5-11) are lower that the observed values by approximately 5 Mm^{-1}. Malm et al. (1996) and Huffman (1996b) presented evidence that this discrepancy is due to absorption by species associated with high temperature organic carbon (by TOR analysis) as well as soil aerosol.
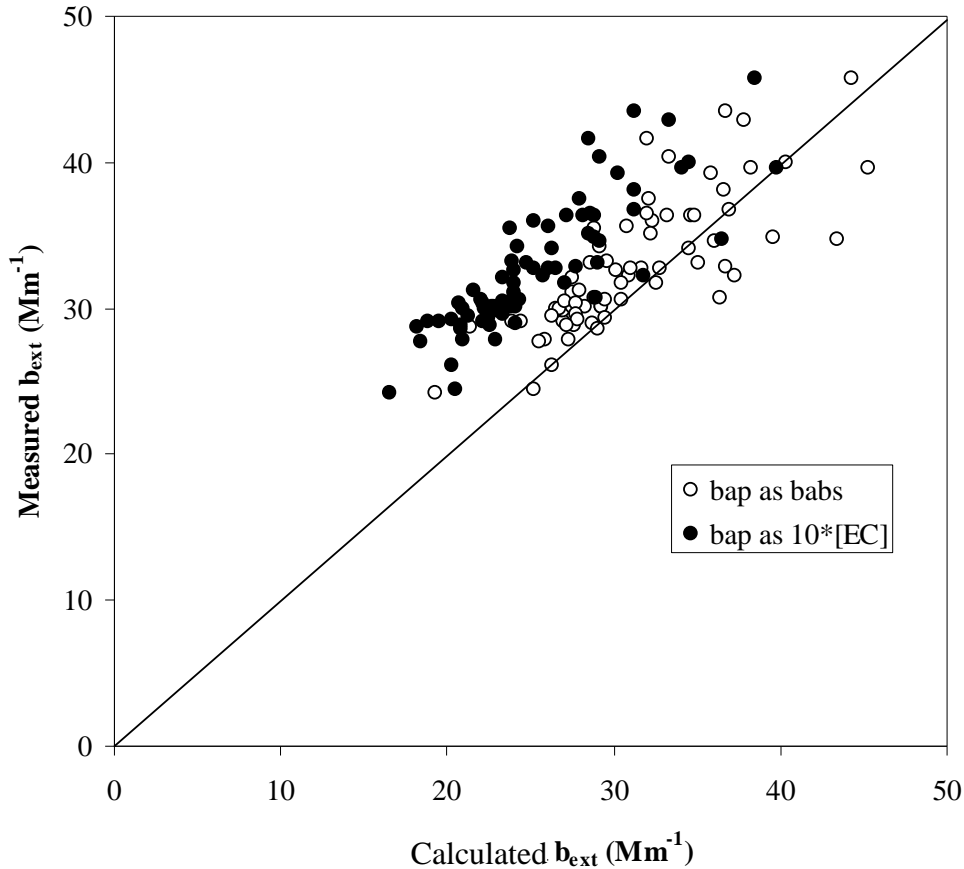
Figure 5-11 Comparison of measured extinction with calculated extinction (b_{sg} + b_{sp} + CMS/2 + b_{ap}). The open circles were calculated using b_{ap} = b_{abs}. The closed circles were calculated using b_{ap} = 10 [EC]. The line is the 1:1 line.

An alternative explanation for the disagreement between the measured extinction and the extinction calculated with the b_{ap} = 10 [EC] formulation is that excess extinction was measured by the transmissometer. This could have resulted from an incorrect value for the effective lamp strength caused by problems with transmissometer alignment or calibration (White, 1993).

This perspective is reinforced by Figure 5-12, which compares two measurements of extinction – b_{ext} by the transmissometer and b_{ap} and b_{sp} by nephelometer and integrating plate, respectively. The two sets of measurements, which are well correlated (r^2 = 0.79 for 77 points), should agree except for the tendency of the nephelometer to underestimate the effect of coarse particle scattering. In fact, they differ by a relatively constant offset of about 5 $^{Mm-1}$ over the entire range. The offset does not correlate with the coarse mass concentration (r^2 = 0.001). This suggests that one of the measurement techniques has a constant error.

Resolution of these discrepancies cannot be definitively achieved using the b_{abs} measurements as the appropriate representation of b_{ap} since these measurements may be too high by a factor of 2 (see Section 4.1.3). Consequently, MPP contributions to total extinction will be estimated using both the transmissometer measured extinction and the chemically calculated extinction using b_{ap} = 10 [EC] (to be discussed in Section 6.2)..
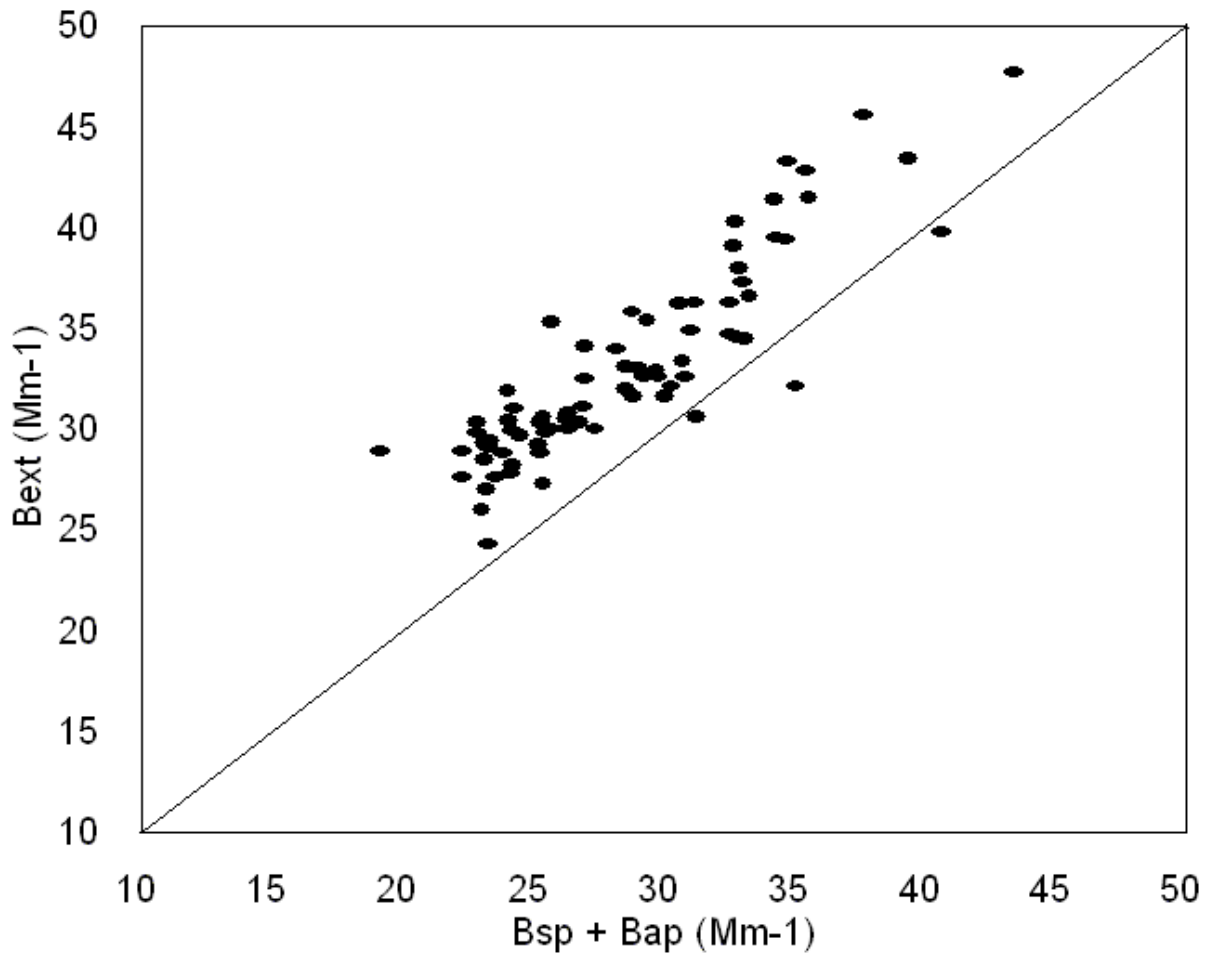
Figure 5-12 Comparison of two measurements of light extinction. The line is the 1:1 line.

5.5 Spatial Variability of Light Extinction and Its Components.

The components of light extinction vary in relative importance over the study region. Figure 5-13 show the summertime spatial distribution of the components of light extinction as measured by nephelometer and integrating plate method on fine aerosol filters. The values plotted in the figure are the median values of b_{sp}, b_{sg} (Rayleigh), and b_{sp} from each location during the summer intensive study. The sizes of the pie charts qualitatively indicate the magnitudes of the median calculated extinction observed at these sites.

The figure shows that near Los Angeles at Tehachapi Pass (TEHA) and Cajon Pass (CAJO), particle scattering (b_{sp}) accounts for more than half the light extinction. The fractional contributions of particle scattering and particle absorption are lower at Meadview (MEAD) than at the remaining sites due to the greater relative effects of Rayleigh scattering at Meadview. Particle absorption (b_{ap}) accounts for between 1/3 to 1/4 of the total extinction across the network. Total extinction decreases from southwest to northeast.
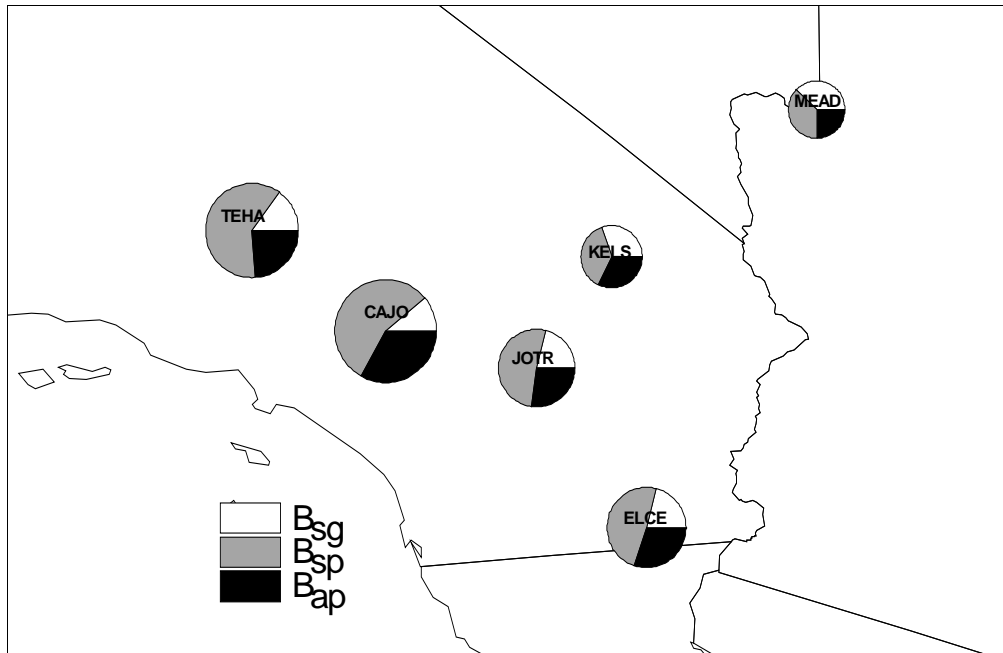
Figure 5-13 Map of summertime calculated light extinction.

6. Chemical Contributions to Extinction

This section estimates the contribution from the major chemical components of light scattering and absorption and examines how these contributions vary from site to site and time to time throughout the Project MOHAVE network.

6.1 Median and Maximum Concentrations of Chemical Components over the Study Region

Table 6-1 through Table 6-4 show the median and maximum aerosol concentrations over the Project MOHAVE network during both the winter and summer intensive sampling periods. The chemical species headings for these tables are defined in Table 6-5. The median concentrations are presented here instead of the average concentrations because median values are insensitive to biases introduced when less than half of the samples are below the lower detectable limit. When median values are shown as 0 in Table 6-1 and Table 6-3, more than 50% of the samples collected were below the lower detectable limit of the analysis.

During the winter months, the highest median levels of fine mass were distributed throughout the network at Cajon Pass (4.7 µg/m^3), Las Vegas Wash (5.9 µg/m^3), and Marble Canyon (4.7 µg/m^3). However, in the summer months, the highest median fine mass concentrations were recorded on the western edge of the network at Cajon Pass (17 µg/m^3), San Gorgonio (11 µg/m^3), and Tehachapi Pass (11 µg/m^3).

Fine particulate trace element concentrations used for chemical mass balance modeling displayed strong spatial gradients over the sampling area. Median wintertime selenium concentrations at Marble Canyon were 4 times greater than the next highest site in the network. The highest median wintertime concentrations of zinc and manganese were observed at Las Vegas Wash. Summertime bromine concentrations were highest on the southwestern edge of the network at Cajon Pass, Barstow, El Centro, and San Gorgonio. Also, median potassium levels were highest at El Centro during the summer.

In addition to the XRF analysis, elemental and organic carbon analysis were performed on samples collected at the Bryce Canyon, Hopi Point, Indian Gardens (wintertime only), Joshua Tree, Meadview, Petrified Forest, San Gorgonio, Sycamore Canyon, and Tonto. For the winter and summer intensive periods at these sites, the average concentrations of the components of the fine mass in the study region were calculated with the equations described by Sisler et al. (1996).

$$[(NH_4)_2 SO_4] = 4.125\,S \qquad (6\text{-}1)$$

$$[NH_4 NO_3] = 1.29 NO_3 \qquad (6\text{-}2)$$

$$[OMC] = 1.4 OC \qquad (6\text{-}3)$$

$$[EC] = EC \qquad (6\text{-}4)$$

$$[Soil] = 2.2 Al + 2.19 Si + 1.63 Ca + 2.42 Fe + 1.94 Ti \qquad (6\text{-}5)$$

Table 6-1 Median aerosol concentrations from the Project MOHAVE wintertime intensive sampling period (1/14/92 – 2/15/92). Concentrations are reported in ng/m³ except for BAP which has units of 10^{-8} m^{-1}.

SITE	AMBO	BAKE	BRCA	CAJO	COCO	DARO	DOSP	HOP5	HOPO	HUMO	ING5	INGA	JALA	JOT2	JOTR	LVWA	MACN	MED5	MED6	MOSP	NEHA	OVBE	PARK	PAUL	PEFR	SAGR	SELI	SPMO	SQMO	SYCA	TEHA	TONT	TRUX	WICK	YUCC
MF	2300	3700	1100	4700	2800	3700	2200	1500	1500	940	2800	2900	1100	3800	3500	5900	4700	1600		1300	1800	3500	4300	3600	3600	1200	2600	1500	1400	2800	2900	3000	3600	2800	3500
BAP	540	1200	200	1200	600	660	420	270	260	160	460	460	160	490	480	1400	880	350		180	360	720	900	730	880	270	510	330	230	640	450	560	560	520	620
M10			2500					6100			7500				11000			3900		7100	2900									6100		6600			
H	72	110	46	130	93	140	78	62	58	43	100	110	44	77	80	190	180	90		45	69	130	130	120	150	48	120	76	61	120	90	140	120	120	110
NA	0	0	0	0	0	13	0	10	0	9	9.6	0	0	0	0	0	11	0		12	0	12	20	15	0	0	0	0	0	0	0	0	0	5.2	0
MG	0	0	0	0	0	0	0	0	0	0	0	0	0	0	0	39	0	0		0	0	0	0	0	0	0	0	0	0	0	0	0	0	0	0
AL	0	67	0	71	0	0	36	0	0	0	0	1.5	0	110	100	0	25	0		0	0	14	49	0	0	0	0	0	0	0	0	0	42	0	37
SI	74	170	21	170	52	50	74	28	30	24	54	45	22	230	230	130	67	37		35	25	130	120	41	53	30	42	38	25	64	54	38	180	39	110
P	0	0	0	0	0	0	0	0	0	0	0	0	0	0	0	0	0	0		0	0	0	0	0	0	0	0	0	0	0	0	0	0	0	0
S	140	160	110	170	190	300	190	150	170	110	250	250	85	130	120	220	440	200		94	140	250	230	180	260	66	190	160	120	140	100	270	170	210	210
CL	0	0	0	0	0	0	0	0	0	0	0	0	0	0	0	0	0	0		0	0	0	0	0	0	0	0	0	0	0	0	0	0	0	0
K	18	33	5.6	37	13	12	15	6.8	7.1	6.2	11	9.3	6	41	45	39	15	11		8.5	9.2	23	35	15	9.2	8.9	11	9.7	5.7	18	13	10	35	14	21
CA	38	64	6.8	44	31	14	30	11	10	7.6	19	18	6.5	41	37	150	22	17		39	11	57	59	21	16	9.2	14	19	8.9	14	16	9.4	220	10	56
TI	6.1	8.6	1.9	6.6	2.7	3.9	5.3	4.3	1.2	1.4	3.3	2.3	2.9	5.5	4.6	5.7	5.7	3.1		4.7	1.2	4.2	4.7	1.7	3.3	0	1.1	0.8	0.5	1.4	0.9	0.47	3.2	0.5	1.7
V	0	0	0	0	0	0	0	0	0	0	0	0	0	0	0	0	0	0		0	0	0	0	0	0	0	0	0	0.34	0	0	0.4	0	0	0
CR	0	0	0.28	0	0	0	0	0	0	0	0	0	0	0	0	0	0	0		0	0	0	0	0	0	0.28	0.14	0.27	0.34	0	0	0	0	0	0
MN	0.75	1.6	0.36	2	1	0.5	0.77	0.36	0.26	0.39	0.49	0.34	0	1.6	1.5	5.4	0.58	0.5		0.58	0.48	0.73	1.3	0.73	0.62	0.46	0.73	0.55	0.44	0.76	0.55	0.61	1.6	0.67	1.2
FE	25	46	3.6	83	17	13	21	7.2	7.2	6.6	9.8	9.2	4.6	41	43	44	17	8.8		9.3	8.5	28	32	15	16	7.9	16	11	8.2	23	14	8.9	48	8.5	32
NI	0	0	0	0	0	0	0	0	0	0	0	0	0	0	0	0	0	0		0	0	0	0	0	0	0	0	0	0	0	0	0	0	0	0
CU	0.54	0.72	0.15	0.97	0.69	3.3	0.34	1.4	1.1	0.4	0.66	0.62	0.13	0.29	0.35	1.8	0.4	1.4		0.38	1.5	0.9	0.64	0.39	0.42	0.44	0.49	2.6	0.29	0.72	0.37	2.5	0.34	1.4	0.78
ZN	2	2.7	0.49	3	1.7	1.8	1.1	0.98	0.8	0.72	0.93	0.93	0.51	1.3	1.5	3.7	1.5	0.75		0.87	1.4	2.2	2.4	1.2	1.3	0.74	1.4	1.2	0.85	1.5	1.5	2.1	1.1	2.2	1.5
AS	0	0	0	0.25	0	0	0	0	0	0	0	0	0	0.12	0	0	0	0		0	0.16	0	0	0	0	0	0	0	0	0	0.15	0.15	0	0	0
PB	0.77	1	0.23	0.79	0.85	0.59	0.62	0.27	0.32	0.29	0.33	0.46	0.27	0.55	0.76	1.9	1.3	0.37		0.43	0.52	0.9	3.8	0.66	0.56	0.34	0.54	0.42	0.36	0.39	0.6	1.4	0.54	1.2	0.76
SE	0.19	0.16	0.09	0.16	0.4	0.47	0.29	0.19	0.18	0.08	0.37	0.42	0.11	0.09	0.035	0.34	2	0.24		0.09	0.26	0.58	0.44	0.28	0.43	0	0.25	0.24	0.14	0.15	0.05	0.32	0.23	0.21	0.31
BR	1.3	1.6	0.56	1.4	1.2	1.2	1.1	0.63	0.69	0.49	0.9	0.94	0.55	0.94	1	1.8	1.6	0.84		0.79	1.2	1.5	2.5	1.1	0.97	0.6	1	0.83	0.68	0.75	0.96	0.73	1	1.1	1.2
RB	0.41	0.85	0	0.42	0.36	0.34	0.42	0	0	0	0	0	0	0.51	0.43	0.65	0	0		0.43	0.34	0.35	0	0.39	0	0	0	0.17	0	0	0	0	0.69	0	0.48
SR	0.45	0.78	0.15	0.59	0.64	0.29	0.45	0.2	0.14	0.15	0.29	0.31	0.18	0.52	0.51	1.7	0.71	0.23		0.35	0	0.8	0.86	0.18	0.24	0.16	0.25	0.26	0.14	0.23	0.26	0.21	0.73	0.18	0.59
ZR	0	0	0	0.19	0	0	0	0	0	0	0	0	0	0.25	0	0	0	0		0	0	0.47	0	0	0	0	0	0	0	0	0	0	0	0	0
MO	0	0	0	0	0	0	0	0	0	0	0	0	0	0	0	0	0	0		0	0	0	0	0	0	0	0	0	0	0	0	0	0	0	0
BSO4			380					550			750				420			640	530	820	220									510		1100			
CLM			7.9					5.8			1.9				30			0	1.5	7.7	14									4.3		10			
NO2M			16					27			20				8.9			20	0	25	1.9									24		18			
NO3M			110					65			96				200			79	9.1	220	230									170		150			
NH4I																			180																
NH3I																			94																
SO2I10			120					670			590				120			110		640	90									270		480			
SO2I25	380	930		760	690			360		310			470			890	5500			200	320	620	1800	130				190	450	330	220		180	490	820
OCLT			0					26			45				34			19		0	29									6.1		0			
OCHT			86					290			490				390			540		670	360									540		570			
ECLT			0					7.2			23				29			6.3		170	43									56		80			
ECHT			19					90			120				85			89		220	75									140		88			

Table 6-2 Maximum aerosol concentrations from the Project MOHAVE wintertime intensive sampling period (1/14/92 – 2/15/92). Concentrations are reported in ng/m^3 except for BAP which has units of 10^{-8} m^{-1}.

SITE	AMBO	BAKE	BRCA	CAJO	COCO	DARO	DOSP	HOP5	HOPO	HUMO	ING5	INGA	JALA	JOT2	JOTR	LVWA	MACN	MED5	MED6	MOSP	NEHA	OVBE	PARK	PAUL	PEFR	SAGR	SELI	SPMO	SQMO	SYCA	TEHA	TONT	TRUX	WICK	YUCC
MF	4900	5700	3400	19000	5500	5400	4800	3900	3400	2600	8200	4800	3600	7300	6500	9400	12000	4300		4200	8700	5000	8400	5700	7200	15000	4900	3800	7300	8400	10000	9800	7000	7300	6300
BAP	1000	2100	630	1800	890	1000	1100	760	710	480	990	840	630	1100	950	2600	1800	720		760	1100	1300	2400	1200	1700	960	1100	670	1200	1500	1400	940	1000	960	1300
M10			10000				35000				24000				30000			13000		17000	17000								13000			14000			
H	180	200	210	750	210	240	170	140	130	130	360	190	190	210	190	340	540	180		170	360	220	280	240	330	700	200	170	160	460	440	430	200	340	260
NA	120	83	22	120	92	64	66	66	89	50	93	63	40	120	130	84	53	140		64	38	59	150	57	53	60	34	50	83	70	180	62	73	63	79
MG	54	26	12	32	32	9.2	13	31	10	15	22	0	25	21	21	120	8	21		21	15	0	9.9	9.4	21	21	15	25	19	15	33	22	34	21	11
AL	150	170	44	310	91	15	100	36	41	21	50	61	46	530	400	130	150	80		95	43	82	200	70	50	68	100	56	23	93	80	34	320	44	110
SI	340	440	89	710	140	140	210	99	90	95	120	95	66	840	760	370	230	160		170	82	200	380	150	140	160	200	120	310	190	350	120	610	110	230
P	45	0	2.6	0	0	0	0	2.5	0	7	0	0	0	0	0	0	0	0		2.8	0	0	0	0	0	3.7	0	2.3	8	0	2.7	0	0	0	0
S	500	380	380	620	420	710	380	420	340	340	1100	590	450	540	550	440	1700	450		370	690	420	660	420	830	560	430	390	310	330	480	640	360	430	430
CL	29	0	1.5	0	0	0	1.2	1.4	1.2	5.2	1.7	0	0	0	1.3	0	1.8	15		2.6	2.1	0	18	4.6	0	1.5	1.7	1.1	3.3	0	79	0	0	0	34
K	51	72	20	120	30	21	43	20	15	16	20	19	17	140	120	71	33	36		38	24	73	110	35	26	39	29	26	31	38	56	52	130	37	99
CA	170	140	20	180	110	31	93	26	41	22	74	60	25	140	130	430	74	40		92	22	150	250	58	22	47	49	44	710	41	91	21	660	27	130
TI	11	15	3.5	16	6.5	5.6	9.5	7	2.3	4.4	8.2	4.4	5.3	16	15	11	11	6.4		6.9	3.4	10	9.5	4.1	7.2	1.9	7.3	2	3.1	5.4	4.7	3.9	7.7	1.3	5.3
V	1.2	1.2	0	2	0.78	0	1.4	1	0.43	1.4	1.9	0.45	1.3	1.3	0.9	1.6	0.76	1.5		1.2	0.74	1.6	0.62	1.1	1.8	1.3	0.71	0.79	0.92	0.95	1.9	0.97	1.1	0.95	0.95
CR	0.68	0.75	0.65	0.85	0.47	0.57	0.94	2.4	1.4	1.3	1	0.36	0.66	0.36	0.92	0.93	1.1	0.84		0.79	0.67	1.3	1	0.93	0.98	0.91	0.86	1.1	1.1	1	0.68	0.83	0.7	0.64	0.65
MN	2.8	4.1	1	6.3	2.3	1.3	2	0.88	0.7	1.1	1.7	1	1.2	5.8	5.1	15	1.4	1.6		2.2	1.2	1.9	4	1.7	1.6	1.7	2.1	1.1	2.3	3	2.6	8.9	4.3	1.5	4.1
FE	97	94	14	180	44	39	57	32	21	22	42	24	17	130	130	95	60	62		44	21	47	79	41	39	34	82	25	68	91	62	75	120	23	74
NI	0.25	0	0	0.34	0.5	0.74	0.36	0.81	1.2	0.49	0.54	0.81	0.1	0.35	0.32	2.3	0.53	0.25		0.16	0.14	0.52	0.22	0.17	0	0.16	0.49	0	0.33	0.15	1.8	0.08	0	0.22	0.17
CU	4.6	25	1.8	2.8	3	54	2.8	25	5.5	1.9	11	4.1	1.7	1.6	1.8	10	2.3	20		6.2	13	6.6	5.4	1.7	1.9	3.4	3.5	6.1	2.4	1.7	13	16	6.7	4.3	5.3
ZN	11	24	3.8	11	3.4	41	4.9	3.8	2.1	3.5	3	1.8	2.7	12	14	6.2	2.7	6		6.6	9	3.9	6.9	4.7	11	7.2	6.4	3.3	5.4	4.4	11	6.4	6.7	5.7	6.8
AS	1	0.5	1.3	1.8	0.51	0.21	0.83	0.49	0.18	0.57	0.7	0.29	0.38	2.5	3	0.7	0.16	1.2		0.9	1.2	0.85	1.1	1.1	2.7	3.2	0.97	0.47	0.77	0.74	0.55	1.1	1	1.6	0.77
PB	1.8	3.6	2	3.3	2.6	2	3.7	1.4	1.2	2.9	1.4	1.2	1.9	2	2.1	4.8	3.8	4		2.3	3.4	7	25	4.1	1.4	1.8	4.3	2.9	4.4	3.2	3.1	4.8	4.6	5.8	3.9
SE	1.1	0.4	0.74	0.36	0.85	2.8	1	1.1	0.67	0.32	2.3	1.9	1.8	0.23	0.27	0.67	15	0.73		1.2	0.91	1.1	1.4	0.68	1.1	0.27	0.83	0.53	0.44	0.38	0.47	0.77	0.66	0.49	0.74
BR	2.2	2.7	1.8	2.4	3.1	1.5	2.7	2.1	1.2	1.4	1.6	1.5	2.3	3.3	2.7	2.6	2.7	4.1		1.9	6.7	3.7	11	2.5	1.5	1.7	1.9	2.5	1.2	1.4	2.2	1.2	2	1.5	2.5
RB	1.7	1.6	0.71	1.6	1.2	0.64	0.79	0.62	0.48	0.73	0.76	0.73	0.88	1.9	2	1.4	1.4	0.41		1	1	0.86	0.97	1.1	0.41	0.57	0.88	1.2	0.83	0.37	0.81	0.44	1.7	0.9	1.5
SR	3.2	2.4	0.31	3.2	2.2	0.85	4.7	1.7	0.35	0.43	0.99	1	0.82	3.9	4	3	2.5	1.9		2.7	0.32	2.3	1.9	0.51	0.53	2.7	0.76	0.56	1.8	0.67	1.4	0.34	1.6	0.43	1.4
ZR	1.2	2.3	0.95	1.2	1.3	1.4	1.3	0.91	0.33	1.3	1.1	0.95	0.91	0.97	0.81	1.8	2.2	1.1		1.9	0.71	1.9	1.1	0.79	1.2	1.3	1	1	1.5	1.1	0.93	0.73	1.7	0.91	1.4
MO	3.5	4.6	2.2	2.3	1.2	0.75	2	1.9	0.31	2.9	2.7	0.55	2.2	0.56	1.5	1.6	3.3	2.1		4.4	1.1	2.1	2.2	1.4	2.6	1.7	1.2	0.84	0	0.98	1.4	0.83	3	0.47	1.3
BSO4			1200				1200				3100				1700			1400	1300						2500	1800			1100			2300			
CLM			36				220				140				140			72	17						35	130			80			62			
NO2M			48				110				46				27			82	160						72	31			44			51			
NO3M			2200				470				570				3100			620	190						820	7500			650			3600			
NH4I																			420																
NH3I																			440																
SO2I10			1100				5400				5700				640			2600							2200	1000			1000			3800			
SO2I25	6100	2300		1300	12000		4000			1200		12000				3400	100000			640	1200	1200	3700	500			2200	7200	2500		650		1200	1900	2900
OCLT			82				270				350				150			120							220	180			520			140			
OCHT			420				930				1200				1000			970							1800	820			3800			1000			
ECLT			41				260				220				110			180							540	280			490			240			
ECHT			130				280				320				220			290							490	190			440			200			

Table 6-3 Median aerosol concentrations from the Project MOHAVE summertime intensive sampling period (7/12/92 – 9/2/92). Concentrations are reported in ng/m^3 except for BAP which has units of $10^{-8} m^{-1}$.

SITE	BAKE	BARS	BRCA	CAJC	CAJO	CIBO	COCO	DECE	DOSP	ELCE	ESSE	HOP5	HOPO	JOTR	KELS	KING	LVWA	MED5	MED6	MOSP	NEHA	OVBE	PARK	PEFR	SAGR	SELI	SPMC	SPMO	SQMO	SYCA	TEHA	TONT	TRUX	WICK	YUCC
MF	9700	10000	4300	17000	17000	6400	7300	8200	5600	10000	7500	4400	4100	9000	7000	5500	7500	5400		5700	4600	6300	7500	4900	11000	4600	5200	5300	4000	6700	11000	6100	6200	5300	5900
BAP	1700	1700	590	3000	3000	920	870	1300	720	1700	1300	650	640	1300	1100	720	1200	680		830	590	790	1100	1000	1600	650	700	700	570	790	1600	810	830	680	820
M10			8100								12000			19000				14000						7700	21000					17000		15000			
H	290	340	130	570	550	170	200	230	150	220	200	140	130	260	210	160	210	170		170	150	170	180	170	420	160	180	160	140	210	380	210	160	160	170
NA	0	0	0	0	0	0	0	0	0	0	0	0	0	0	0	0	0	0		0	0	0	0	0	0	0	0	0	0	0	0	0	0	0	0
MG	0	0	0	0	0	0	0	0	0	0	0	0	0	0	0	0	0	0		0	0	0	0	0	0	0	0	0	0	0	0	0	0	0	0
AL	0	0	0	0	0	0	0	0	0	0	0	0	0	0	0	0	0	0		0	0	0	0	0	0	0	0	0	0	0	0	0	0	0	0
SI	440	250	85	190	210	220	240	200	240	550	280	84	72	200	170	160	270	150		170	140	190	350	120	150	130	140	130	90	160	370	140	320	140	220
P	0	0	0	0	0	0	0	0	0	0	0	0	0	0	0	0	0	0		0	0	0	0	0	0	0	0	0	0	0	0	0	0	0	0
S	660	760	360	1200	1200	640	620	750	550	840	650	380	370	740	640	530	700	520		500	460	580	590	450	720	370	540	550	410	380	620	480	460	490	510
CL	0	0	0	0	0	0	0	0	0	0	0	0	0	0	0	0	0	0		0	0	0	0	0	0	0	0	0	0	0	0	0	0	0	0
K	100	70	21	59	60	76	51	79	51	200	62	21	21	57	50	41	62	35		40	38	47	95	24	41	27	40	40	25	32	110	30	60	42	52
CA	140	74	31	54	55	73	90	60	71	200	76	21	20	47	41	52	140	53		56	44	65	210	26	35	31	40	42	24	28	76	32	290	43	100
TI	11	6.4	1.7	6.7	6.9	4	5.7	4	6.4	7.1	5.5	1.8	1.6	5.1	4.4	2.8	6.2	3.1		3.4	2.4	3.4	5.2	2.5	4.3	3.8	3	2.8	1.7	5.5	9.7	3.2	5.8	2.6	3.3
V	0	0	0	0	1.3	0	0	0	0	1.9	0	0	0	0	0	0	0	0		0	0	0	0	0	0	0	0	0	0	0	0	0	0	0	0
CR	0	0	0	0	0	0	0	0	0	0	0	0	0	0	0	0	0	0		0	0	0	0	0	0	0	0	0	0	0	0	0	0	0	0
MN	0.98	0	0	0	0	0	0	0	0	0	0	0	0	0	0	0	1.1	0		0	0	0	0	0	0	0	0	0	0	0	0	0	0	0	0
FE	110	70	16	95	95	42	55	51	54	100	99	20	16	52	47	33	55	34		36	28	41	68	29	48	43	34	31	21	58	110	31	74	33	48
NI	0	0.2	0	0	0.35	0.17	0	0	0	0.55	0	0	0	0.18	0	0	0	0		0.26	0	0	0	0	0	0	0	0	0	0	0	0	0	0	0
CU	1.4	1.2	0.37	2.1	1.8	0.64	0.96	0.94	0.78	1	0.87	1.2	1.3	0.77	1	0.6	1.2	1.2		0.71	0.6	0.71	0.54	0.74	1.1	0.57	1.1	1.2	0.7	1.4	1.9	3.2	0.6	0.86	0.41
ZN	3.5	3.7	0.83	9.8	9	2	1.9	2.7	1.5	3.6	2.2	0.97	1.1	2.8	2.2	1.3	2.8	1.3		1.6	1.2	1.6	1.9	1.1	4.8	1.2	1.6	1.6	1.1	1.4	2.7	4.4	1.4	1.7	1.3
AS	0	0	0	0	0	0.27	0	0.2	0	0	0	0	0	0	0	0.14	0	0		0	0	0.08	0.26	0	0	0	0	0	0	0	0	0.45	0	0.29	0.18
PB	1.5	1.6	0.39	3.5	3.4	0.88	0.84	1.2	0.64	2.3	0.98	0.64	0.6	1.1	1	0.61	1.2	0.74		0.63	0.48	0.76	1.8	0.47	1.6	0.51	0.64	0.64	0.49	0.58	1.5	1.9	0.64	0.88	0.6
SE	0.48	0.56	0.19	1.7	1.4	0.52	0.5	0.63	0.33	1.3	0.38	0.17	0.16	0.59	0.44	0.27	0.4	0.2		0.3	0.22	0.4	0.44	0.34	0.64	0.25	0.35	0.38	0.22	0.26	0.51	0.34	0.31	0.3	0.28
BR	3.5	4.3	1.4	5.7	5.8	2.9	2.3	3.8	1.9	5.4	2.6	1.6	1.6	3.7	3.2	1.9	2.5	1.8		2.4	1.6	2	2.8	1.4	4.2	1.4	2.2	2.4	1.4	1.4	4.5	1.4	1.9	1.7	1.9
RB	0.32	0	0	0	0	0.13	0.15	0.15	0.14	0.27	0.13	0.1	0.09	0	0.04	0.1	0.19	0.14		0.1	0.11	0.13	0.18	0	0	0	0.09	0	0	0.1	0.25	0.1	0.21	0	0.15
SR	0.8	0.47	0.21	0.57	0.55	0.39	0.81	0.46	0.43	1.1	0.45	0.21	0.19	0.37	0.34	0.3	0.93	0.38		0.34	0.27	0.47	0.95	0.23	0.35	0.19	0.3	0.35	0.2	0.28	0.48	0.22	0.55	0.24	0.4
ZR	0	0	0	0	0	0	0	0.25	0	0	0	0	0	0	0	0	0	0		0	0	0	0.24	0	0	0	0	0	0	0	0	0	0	0	0
MO	0	0	0	0	0	0	0	0	0	0	0	0	0	0	0	0	0	0		0	0	0	0	0	0	0	0	0	0	0	0	0	0	0	0
BSO4			1100								1100			2300				1500	1300					1300	2300					1200		1500			
CLM			7.3								3.9			15				7.3	4.4					0	20					12		8.1			
NO2M			0								0			0				0	0.95					0.2	0					1.7		0			
NO3M			95								100			580				130	53					110	1700					180		110			
NH4I																			450																
NH3I																			110																
SO2I10			310								150			740				610						460	510					270		890			
SO2I25	1500	2000		2300	2200	620	6800	980	1400	1900	1200				1200	890	2100			660	310	1800	500			450	1400	1300	800		2000		800	630	680
OCLT			3.4								0			50				0						21	230					31		16			
OCHT			580								500			1300				430						810	2300					980		930			
ECLT			54								48			300				18						140	490					110		95			
ECHT			56								110			86				83						180	110					210		89			

Table 6-4 Maximum aerosol concentrations from the Project MOHAVE summertime intensive sampling period (7/12/92 – 9/2/92). Concentrations are reported in ng/m³ except for BAP which has units of 10^{-8} m^{-1}.

	BAKE	BARS	BRCA	CAJC	CAJO	CIBO	COCO	DECE	DOSP	ELCE	ESSE	HOP5	HOPO	JOTR	KELS	KING	LVWA	MED5	MED6	MOSP	NEHA	OVBE	PARK	PEFR	SAGR	SELI	SPMC	SPMO	SQMO	SYCA	TEHA	TONT	TRUX	WICK	YUCC
MF	22000	18000	7900	34000	33000	11000	18000	12000	17000	20000	17000	14000	13000	15000	11000	9000	22000	11000		10000	19000	13000	14000	7200	23000	6900	9000	9500	5900	24000	22000	14000	11000	19000	9500
BAP	3400	3500	980	4600	4700	1600	1900	2300	1700	4500	2000	2000	1800	3000	1700	1200	2300	1500		1600	2800	1600	2200	1800	3200	1200	1400	1400	950	3100	2900	1600	1400	2000	1400
M10			16000								36000		39000					48000						32000	52000					50000	48000				
H	920	540	220	1400	1300	330	400	440	640	660	500	680	560	390	440	360	690	380		340	530	340	450	260	710	280	350	380	240	1100	710	300	300	320	320
NA	550	300	75	560	350	650	380	680	510	1000	510	190	100	980	640	330	580	620		390	0	380	690	0	130	0	310	340	0	240	0	0	0	410	430
MG	0	0	54	27	110	130	0	260	170	140	84	77	84	190	120	180	310	230		170	120	140	200	66	99	110	140	48	100	120	310	100	130	230	180
AL	670	430	70	220	210	230	330	380	310	490	370	110	50	220	99	140	140	250		200	50	210	480	160	150	230	99	170	52	900	390	960	600	2000	200
SI	1300	890	190	430	400	470	1000	670	580	1100	690	230	140	480	450	370	850	460		480	330	500	1200	390	280	510	290	300	270	1600	810	1700	1200	3300	500
P	0	0	0	0	0	0	0	0	0	0	0	0	0	0	0	0	0	0		0	0	0	0	0	0	0	0	0	0	0	0	0	0	0	0
S	1400	1500	720	2900	2900	990	1700	1400	1500	1400	1500	790	740	1400	1100	1200	1700	1600		1200	1600	1000	1700	660	1600	680	1500	1500	710	660	1200	1100	960	790	1200
CL	70	0	0	6.1	130	660	250	530	220	730	350	5.3	6	5.9	220	150	160	220		93	82	340	530	3.5	0	2	230	210	0	0	0	6.5	0	0	280
K	230	170	73	150	160	400	150	370	140	530	120	62	39	270	99	100	140	130		94	69	120	320	60	140	67	120	110	90	150	310	240	190	440	150
CA	510	250	67	92	100	130	440	180	160	420	230	83	47	160	140	130	400	180		170	130	210	590	57	67	120	89	92	82	150	190	260	1100	470	310
TI	25	19	3.9	17	14	7.5	22	13	13	17	12	5.7	3.8	13	8.9	6.5	20	14		9.8	7.7	13	19	7.3	56	29	7.2	8.5	5.7	81	30	38	22	56	11
V	3.5	3.2	0.95	7.1	6	2.2	1.8	2.9	1.4	9.2	1.3	1.5	1.3	4.2	1.5	1.8	2.2	2.5		1.7	2.6	1.3	1.6	1.2	2.2	1.3	1.7	2.4	2.3	4.6	2.7	1.6	2.8	1.5	1.9
CR	1.9	0.64	1	0.9	1.5	0.74	0.7	0.47	0.63	2.7	0.87	0.97	0.69	1.2	0.94	0.92	0	0.85		0	0.68	1	1.5	1	1.1	0.69	1.3	0.95	0.71	0.95	1.1	1	0.98	0.71	1.1
MN	6	2.8	0.71	3	2.8	1.9	1.6	2.3	1.6	3.2	3.5	0.97	0.87	1.5	1.6	1.3	6	1.7		1.4	1.2	1.1	5.5	1.1	2.6	3.3	1.2	1.3	1.3	11	4.8	10	3.2	14	2.1
FE	280	190	38	200	190	92	210	150	140	210	210	56	54	96	90	75	160	110		110	64	120	200	78	86	180	63	63	55	630	240	410	230	570	97
NI	0.44	0.6	0.33	1.8	1.4	0.39	0.38	0.85	0.5	3.9	0.5	0.37	0.7	0.47	0.43	0.26	2.3	1.7		0.22	0.36	0.65	0.47	0	0.95	0.32	0.38	0.48	0.3	0.23	0.32	0.57	0.23	0.29	0.59
CU	8	7.7	2.3	6.1	4.2	5.5	19	4.6	2.9	4.6	4.3	17	10	2.6	5.3	2.2	7.5	11		3.4	4.3	3.7	2.4	2	14	7.2	4.6	4.2	5.5	11	7.5	11	1.9	11	3
ZN	7.1	8.1	1.7	17	17	4.5	13	6.6	4.2	21	6.6	3.3	3.1	6.5	4.4	3.8	9.3	5.6		3.3	4.2	4.4	4.3	3.4	9	9.8	3.8	4.2	4.4	3.7	27	44	3.8	7.4	3.6
AS	0.59	0.5	0.33	0	0.55	0.73	0.79	0.77	0.72	2.5	0.73	0.53	0.32	0.62	0.58	0.76	0.63	0.84		0.66	0.52	0.72	1	1.4	0.51	0.74	0.58	0.69	0.68	0.82	0.42	2.1	1	1.8	1
PB	2.4	3.3	1.1	6	5.1	2.2	1.6	1.8	1.7	8.6	2.4	1.2	1.4	1.7	1.8	1.5	4	1.7		1.2	1.7	1.4	31	1.8	2.6	1.7	1.4	1.3	1.5	2.2	4.2	12	1.5	2.5	1.4
SE	0.94	1.1	0.48	2.7	2.4	1	1.3	1.1	0.82	2.2	0.8	0.41	0.31	1.1	0.76	0.53	0.72	0.48		0.55	0.57	0.93	1.6	0.83	1.2	0.49	0.88	0.75	0.5	0.52	0.93	0.67	0.72	0.5	0.47
BR	5.7	9.4	3.6	11	12	6.1	8	8.9	7.3	10	7.1	5.3	4.3	8.5	7.9	6.9	5.7	6.8		4.7	4.5	5.4	6.5	3.3	8.7	3.7	7.9	7.5	4	4	8.2	4	5.2	4.6	5.8
RB	0.83	0.49	0.2	0.45	0.48	0.29	0.58	0.47	0.29	0.65	0.32	0.29	0.36	0.26	0.3	0.29	0.42	0.34		0.29	0.26	0.31	0.37	0.29	0.32	0.29	0.3	0.29	0.25	0.66	0.63	0.96	0.68	1.1	0.26
SR	3.4	1.1	0.49	1.2	0.92	0.84	2.9	1	0.97	2.3	1.1	0.61	0.34	0.81	0.93	0.74	2.6	1.2		0.8	0.69	1.5	2.3	0.44	0.58	0.68	0.99	0.95	0.51	2.2	1.4	1.2	1.5	1.6	0.81
ZR	0.81	0.84	0.68	0.82	0.94	0.38	0.65	0.64	0.49	1.2	0.74	0.33	0.3	0.52	0.54	0.71	0.53	0.2		0.51	1.7	0.58	0.61	0.44	0.47	0.63	0.34	0.39	0.46	1.2	0.75	1	0.87	1.1	0.57
MO	1.5	0.77	1.6	0	1.2	1.4	0	0	0	0	1.1	1.5	1.8	3.2	0	1.7	0	0		2.4	2.8	1.5	1.7	1.5	1.7	0	1.9	0	2	0	0	2.2	0	0	1.4
BSO4			2200								2500		4400					4500	4300					1900	4800					2100	3200				
CLM			150								95		540					320	280					33	140					65	200				
NO2M			21								58		28					56	220					34	34					52	28				
NO3M			420								460		2300					730	520					190	6900					460	420				
NH4I																			1500																
NH3I																			1500																
SO2I10			940								2000		15000					3900						3600	1400					1900	4300				
SO2I25	4100	4500		3800	4500	1300	15000	4500	6200	8200	5200				3500	5200	5700			3900	1200	3800	5500			1600	15000	13000	4000		3100		2600	3300	5500
OCLT			260								1000		490					340						300	770					980	180				
OCHT			1600								5800		2500					1700						1500	4900					5900	1800				
ECLT			170								760		810					250						650	1200					1000	310				
ECHT			120								670		230					300						440	260					770	180				

Equation 6-1 is based on the assumption that the sulfate aerosol is fully neutralized by ammonium. Measurements of S (by XRF) and NH_4^+ (by AC) from the IMPROVE monitors during the summer intensive sampling period at Meadview indicated that the average aerosol molar ratio of $NH_4^+/SO_4^{2-} = 1.8 \pm 0.2$. For the most acidic sample (8/28/92 0700) the ratio $NH_4^+/SO_4^{2-} = 1.4$, and equation 6-1 overestimates the partially ammoniated sulfate mass by ~ 8%. The degree of neutralization of sulfate may have a larger effect on the aerosol's capacity to absorb water. Acidic aerosols absorb more water than neutralized aerosols at the same RH (Malm et al., 1998).

Table 6-5 Row heading definitions for Tables 6-1 through 6-4.

Abbreviation	Description
MF	Fine Mass
BAP	Particle optical absorption
M10	PM_{10} Mass
H	Hydrogen
NA	Sodium
MG	Magnesium
AL	Aluminum
SI	Silicon
P	Phosphorus
S	Sulfur
CL	Chlorine
K	Potassium
CA	Calcium
TI	Titanium
V	Vanadium
CR	Chromium
MN	Manganese
FE	Iron
NI	Nickel
CU	Copper
ZN	Zinc
AS	Arsenic
PB	Lead
SE	Selenium
BR	Bromium
RB	Rubidium
SR	Strontium
ZR	Zirconium
MO	Molybdenum
BSO4	Sulfate (Ion Chromatography)
CLM	Chloride
NO2M	Nitrite
NO3M	Nitrate
NH4I	Ammonium (Teflon)
NH3I	Ammonia from Ammonium (impregnated filter)
SO2I10	Sulfur Dioxide (impregnated filter) PM_{10}
SO2I25	Sulfur Dioxide (impregnated filter) $PM_{2.5}$
OCLT	Organic Carbon (Low Temp)
OCHT	Organic Carbon (High Temp)
ECLT	Elemental Carbon (Low Temp)
ECHT	Elemental Carbon (High Temp)

It should be noted that the IMPROVE sampler does not use an ammonia denuder to protect the acidic particles (collected on the Teflon filter) from acid neutralization. In addition, no precautions were taken to protect the samples during transport and storage. Thus, the

ammonium/sulfate ratio reported above may be positively biased. To date, denuder/filter pack techniques have been used to measure particle acidity and other ionic species (Koutrakis et al., 1992). The samplers consist of 3 components: (1) a $PM_{2.5}$ inertial impactor to remove coarse particles, (2) a diffusion denuder to remove gaseous ammonia from the air sample, and (3) a Teflon filter to collect fine particles.

Differences between the measured fine mass and the sum of the component concentrations above were classified as the unknown fraction. The unknown fractions may be composed of water, salt (NaCl), or other compounds not measured in the suite of chemical analyses. A negative unknown fraction indicates that the sum of the components exceeded the measured mass.

The molecular to carbon mass ratio of 1.4 applied to organic carbon to estimate the total mass of organic compounds may not be appropriate for all types of aerosol. The value was originally derived from measurements collected predominantly in the Los Angeles area. It has been hypothesized that the organic compounds in remote areas are more thoroughly oxidized and that the ratio should be higher than 1.4 (Hegg et al., 1997; Turpin et al., 1997). Better characterization of organic aerosols is needed to resolve this issue, however it is possible that some of the unknown fraction of the aerosol is organic. (Further discussion of these points is provided by Andrews et al., 1999).

The average aerosol chemical component concentrations are summarized in Figure 6-1 and Figure 6-2 for the winter and summer intensive periods. At Hopi Point, Meadview and San Gorgonio in the winter, the negative unknown component indicates that the calculated mass was larger than the measured mass. Component concentrations for each sample were calculated prior to averaging the component concentrations over the intensive sampling period. The figures indicate that summertime fine mass concentrations in the region were between 2 and 3 times greater than the winter concentrations. Ammonium sulfate was a large component of the fine mass aerosol in the region. Organic carbon was the second largest component representing a moderate to large fraction of the fine mass. At most sites, ammonium nitrate, soil, and elemental carbon each contributed a minor fraction to the aerosol mass. San Gorgonio is an exception in that ammonium nitrate accounted for a large fraction of fine mass. The relative contribution of each component did not change substantially from winter to summer across the network however the composition at some individual sites did change. It is notable, that the $PM_{2.5}$ is composed of a variety of components and that the composition at all sites is not dominated by a single component.

Based on IMPROVE data, at Meadview, ammonium sulfate accounted for 47 % and 41 % of the measured fine mass in the winter and summer, respectively. The next largest component was organic compounds which composed 40% of the fine mass in winter but only 11 % of the measured fine mass in the summer. Soil occupied 9 and 11 % of the fine mass at Meadview during the winter and summer. Ammonium nitrate and elemental carbon were minor components. Similar fine aerosol chemical profiles and seasonal patterns were also observed at Hopi Point on the south rim of the Grand Canyon and at Bryce Canyon in southern Utah.

The concentrations of particulate organic material determined using the BOSS denuder were over twice those determined from IMPROVE results. These results indicate that organic material averaged 54 %, ammonium sulfate 29 %, ammonium nitrate 4 %, soil 10 % and soot 2

% of the fine particulate mass at Meadview. The average concentration of fine particulate material, 7.2 $\mu g/m^3$, was comparable to the average coarse (PM_{10} - $PM_{2.5}$) particle concentration of 8.9 $\mu g/m^3$.
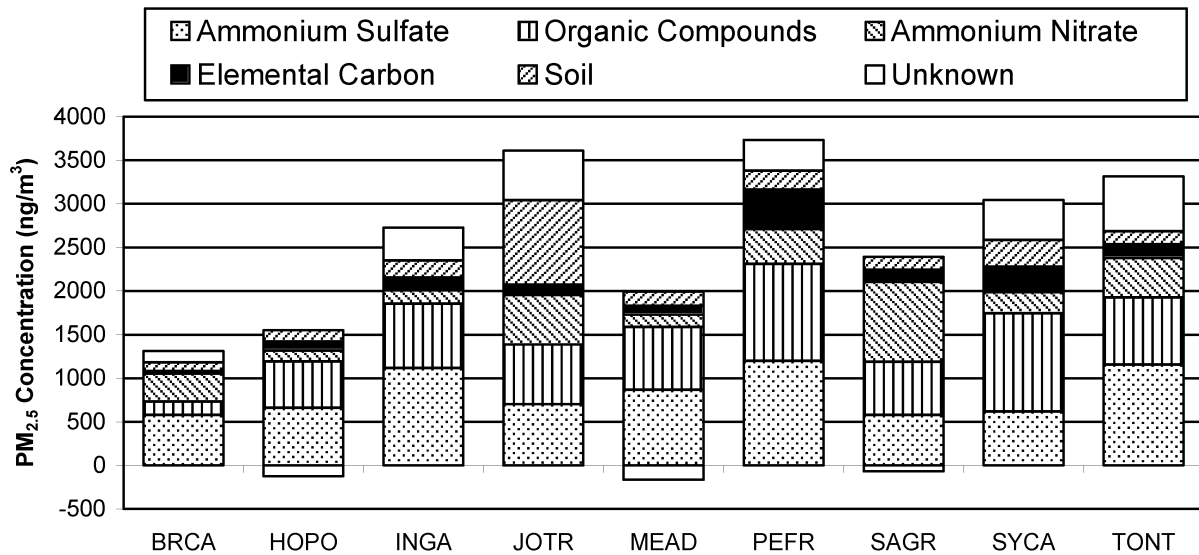
Figure 6-1 Wintertime average PM$_{2.5}$ composition at sampling sites within the Project MOHAVE study area.
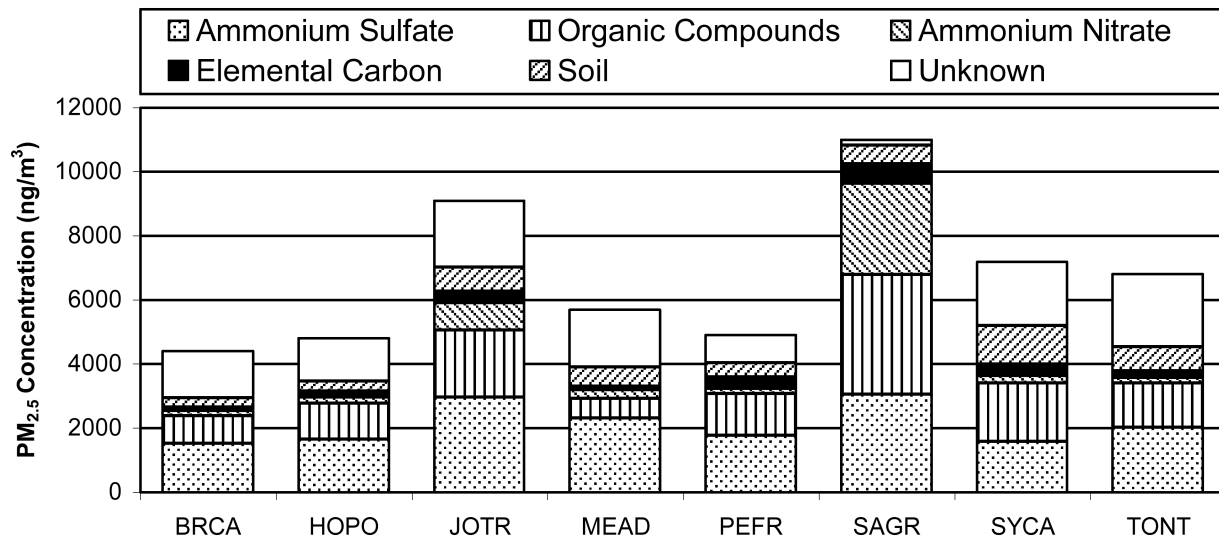
Figure 6-2 Summertime average PM$_{2.5}$ composition at sampling sites within the Project MOHAVE study area.

The two California sites Joshua Tree and San Gorgonio had higher total $PM_{2.5}$ levels than the other sites with carbon measurements. Ammonium nitrate was a substantial component (~20%) of the average $PM_{2.5}$ at San Gorgonio. The proximity of this site to Los Angeles suggests that polluted air from the city frequently impacts this location. At Joshua Tree in the winter time, soil accounts for approximately 27% of the fine mass which is a higher fraction than observed at any

of the other sites in winter or summer. A more detailed analysis of the summer and winter aerosol composition throughout the network is provided by Sisler and Malm (1997) and Gebhart and Malm (1997)

Using the complete speciated data set from the sites where organic and elemental carbon were measured, maps of the average component composition of the $PM_{2.5}$ aerosol were produced. Figure 6-3 and Figure 6-4 show pie charts of the chemical composition of the measured $PM_{2.5}$ during the winter and summer field seasons. The sizes of the pie charts increase with greater average aerosol concentration but are not directly proportional to the concentration. For example Bryce Canyon and Meadview have lower average $PM_{2.5}$ concentrations and smaller pie charts than Petrified Forest and San Gorgonio. The unknown component was not plotted.

The maps show the spatial gradients of the aerosol concentrations for sites with complete speciation. During the winter, higher $PM_{2.5}$ was observed in the southeast and southwest: in the summer, concentrations were highest in the southwest. (Note: Las Vegas Wash had the highest fine mass concentration during the winter intensive study.) In the Grand Canyon region (Meadview, Hopi Point, and Indian Gardens) during both winter and summer, sulfate and organic compounds are the largest components of the fine mass aerosol. This pattern is reflected at all other sites except for Joshua Tree, which had high concentrations of fine soil in the winter.

6.2 Temporal and Spatial Variation of Contributions to Extinction

The preceding section summarized the median, mean and maximum concentrations of chemical components observed throughout the MOHAVE network. The present section examines the daily variability of components at Meadview, the main receptor site.

The apportionment of total extinction into contributions from individual particle fractions raises a number of conceptual subtleties and technical difficulties (White, 1986; Sloane, 1986; White, 1990; Lowenthal et al., 1995; McMurry et al., 1996; Malm and Kreidenweis, 1997; and Malm, 1998). Some attributions are straightforward, like the contribution from scattering by gases. Some attributions are straightforward theoretically but very sensitive to measurement uncertainties, like the contributions from particle absorption, and scattering by large particles. And some attributions are ambiguous conceptually: there is no consensus that it is even meaningful to speak of the contribution from one chemical constituent of a mixed particle. Nonetheless, there is general agreement that some chemical components have more impact on total extinction than others do at similar mass concentrations

An indication of the relative importance of various particle components for visibility can be given by weighting their mass concentrations to approximate their optical effectiveness. The weighting coefficients should in principle vary from sample to sample, reflecting variations in components' distributions with respect to particle size and other factors. Such information is not generally available, although Malm and Kreidenweis (1997) were able to estimate sample-specific ammonium sulfate scattering ranging from 1.5 to 4.0 m^2/g over the summer intensive period. MOHAVE participants accordingly selected the following uniform calculation as illustrative, while recognizing its limitations:

$$b_{ext} = 2 \cdot f(RH) \cdot [(NH_4)_2 SO_4] + 3 \cdot f(RH) \cdot [NH_4 NO_3] + 4 \cdot [OMC] + 10 \cdot [EC] + [Soil] + 0.6 \cdot [CM] + 10.6 \qquad (\ 6\text{-}6\ )$$

In Equation 6-6, total extinction (b_{ext}) and the constant (10.6) Rayleigh contribution from gases have units of Mm^{-1}. Concentrations are in $\mu g/m^3$, and the coefficients have units of m^2/g.
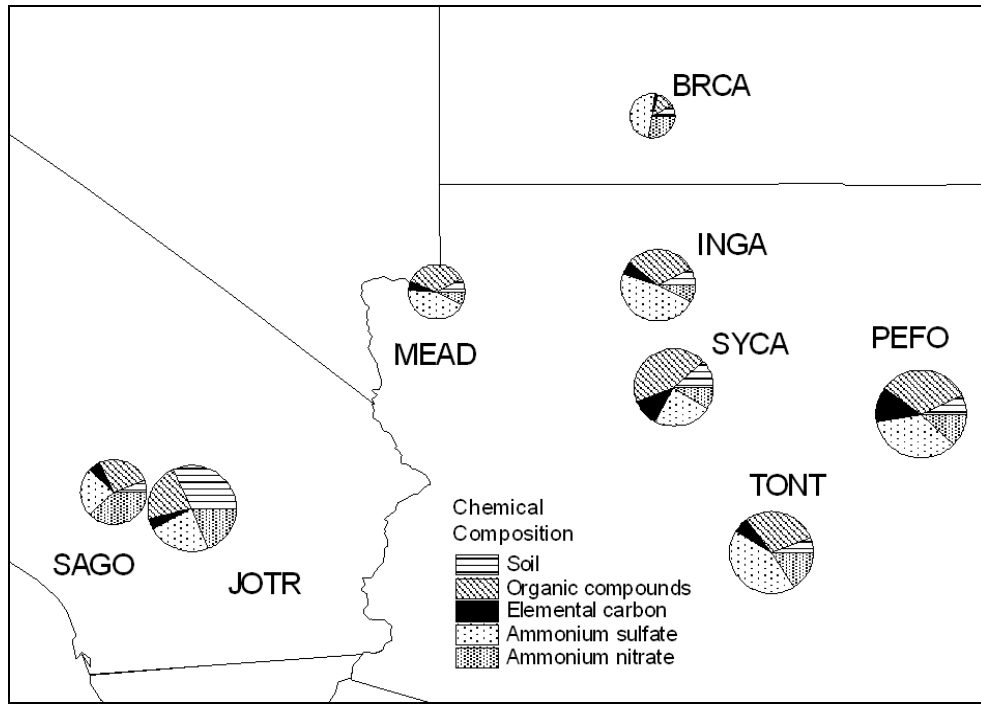
Figure 6-3 Wintertime average spatial distribution of chemical components.
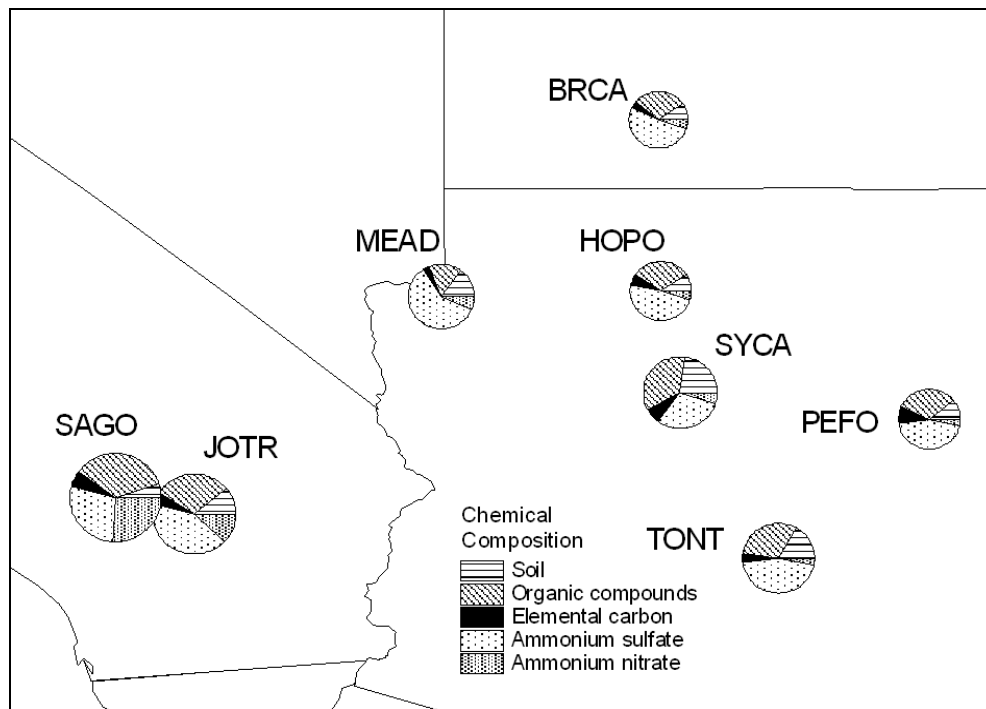
Figure 6-4 Summertime average spatial distribution of chemical components.

Components are as defined in equations 6-1 through 6-5 with the addition of coarse mass, [CM] = PM_{10} - $PM_{2.5}$. The f(RH) term is an empirical factor that accounts for the hygoscopicity of the sulfate and nitrate aerosols. As the humidity increases, the hygroscopic aerosols absorb water vapor and increase in size. Under normal conditions, this increases the aerosol's ability to scatter light in the visible spectrum. The values of $f(RH)$ were derived using a particle growth model coupled with sulfate size distribution data from Meadview (Malm, 1998). The specific scattering of sulfate (2 m^2/g) is a result of Mie calculations using DRUM and MOUDI sulfur size distribution data and external mixing (Malm, 1998). Each of the terms in this equation represents the portion of light extinction due to sulfate, nitrate, organic compounds, elemental carbon, soil, coarse particles, and Rayleigh scattering. Notice that the use of elemental carbon to represent particle absorption may be the cause of the calculated extinction being systematically less than transmissometer extinction (see Section 5.4).

Using the IMPROVE aerosol chemical speciation and relative humidity data from Meadview, the relative components of light extinction ther can be estimated using Equation 6-6. For each 12 hour IMPROVE aerosol sample, the total extinction was calculated using Equation 6-6. The average and standard deviation of the component fraction of total extinction are plotted in Figure 6-5. On average, for both winter and summer, the largest single component of light extinction at Meadview is scattering. The remaining components comprise a larger fraction of the total extinction during the summer than during the winter since total light extinction is higher in the summer. The second largest component based on Equation 6-6 is organic compounds in winter (15%) and coarse mass in summer (16%). Sulfate particles from all sources are estimated to be responsible for 13% and 18% of the total light extinction in the winter and summer, respectively. The combined estimated contributions of fine soil, elemental carbon, and ammonium nitrate account for ~10% of the light extinction in both summer and winter.
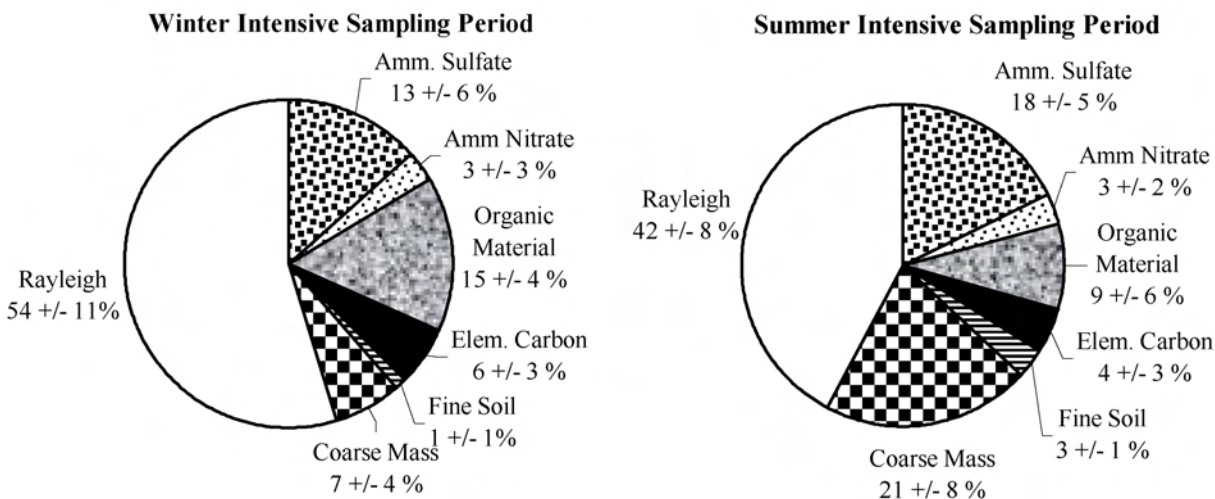
Figure 6-5 Seasonally averaged relative light extinction components at Meadview.

The concentration of fine particulate organic material determined using the BOSS denuder sampler was much smaller than that of the organic material retained on the IMPROVE filter. As a result, if the denuder results were substituted into equation 6-6, the relative fraction of organic

compounds to light extinction would increase by about 50% compared to the results shown in Figure 6-5.

The calculated extinction time series based on IMPROVE data for each sample collected during the intensive periods are shown in Figure 6-6 and Figure 6-7. On the left side of the figures are the relative contribution of each component to light extinction. On the right side of the figures are the absolute contributions to extinction. The total light extinction measured by the transmissometer is also shown in the right panels. Transmissometer data is only shown when there are 10 or more valid measurements within the 12 hour sampling period.

During the winter intensive, the calculated extinction is consistently less than the observed extinction. This is also true in the summer with the exception of the 7/21/92 0700 and 8/1/92 1900 samples. Coarse mass concentrations during these sampling periods were higher than the remaining periods from the summer intensive. It is possible that local sources near Meadview were producing coarse particles that would have impacted visibility on a local scale yet had negligible impact on extinction along the sight path of the transmissometer.

The average measured extinction was larger than the average calculated extinction during the winter and summer intensive periods by 9 ± 5 Mm^{-1} (31%) and 8 ± 6 Mm^{-1} (23%), respectively. Possible explanations for this discrepancy between calculated and measured extinction include any combination of the following:

- Equation 6-6 does not account for light absorption due to organic carbon species evolved at high temperatures by TOR analysis and fine soil particles (Malm et al., 1996 and Huffman, 1996).

- The mass of organic material may be under represented due to an inappropriate choice of the mass to carbon ratio in equation 6-3 (Hegg et al., 1997; Turpin et al., 1997).

- The transmissometer measurements may be larger than the true extinction due to an incorrect value for the effective lamp strength caused by problems with transmissometer alignment or calibration. (White et al., 1993).

6.3 Frequency of Different Atmospheric Constituents' Contribution to Different Levels of Haze

Using the simplified extinction Equation 6-6, the relative component contributions to extinction can be calculated at Meadview during the summer and winter intensive sampling periods. The results are displayed as frequency distributions of extinction budget contributions (Figure 6-8 and Figure 6-9). The frequency distributions indicate the potential for a single component to dominate the light extinction budget.

Highest winter sulfate contributions to extinction were ~30% for the 2/7/92 700 and 2/8/92 700 samples. This was the highest relative contribution to extinction during the winter intensive for all components except Rayleigh scattering.
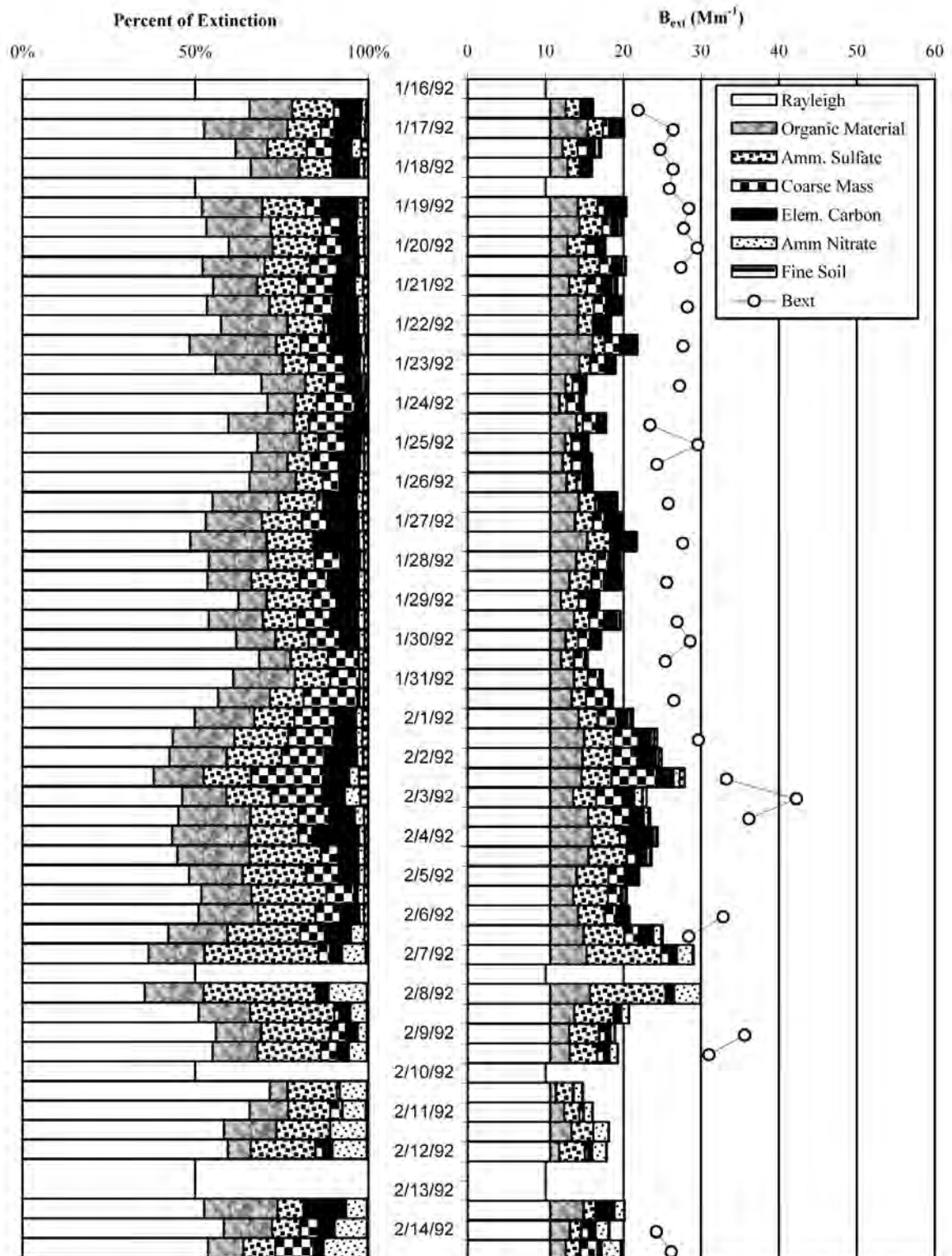
Figure 6-6 Wintertime relative (left panel) and absolute (right panel) calculated extinction at Meadview. The measured extinction from the transmissometer is shown as the open circles on the right panel.
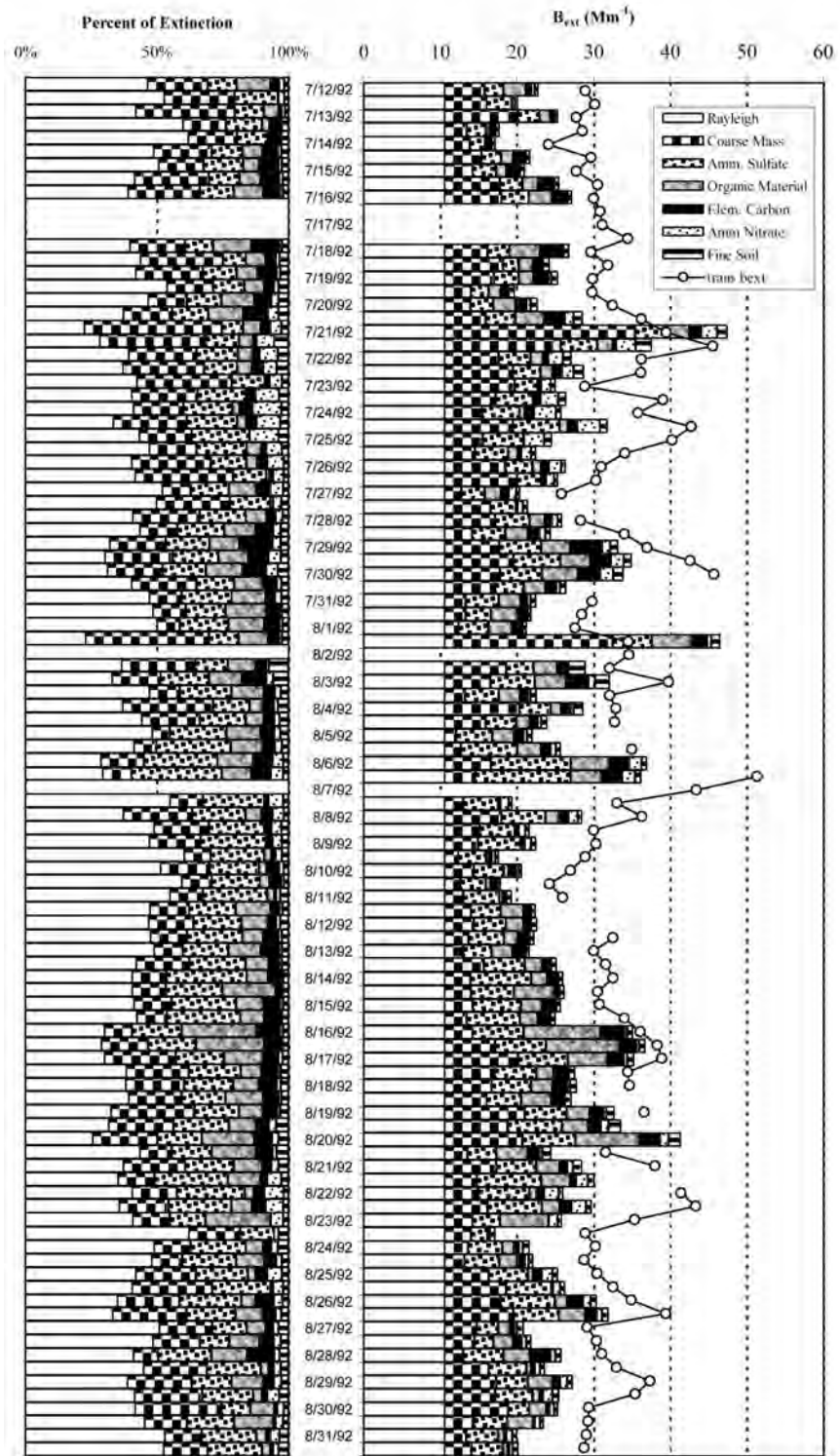
Figure 6-7 Summertime relative (left panel) and absolute (right panel) calculated extinction at Meadview. The measured extinction from the transmissometer is shown as the open circles on the right panel.
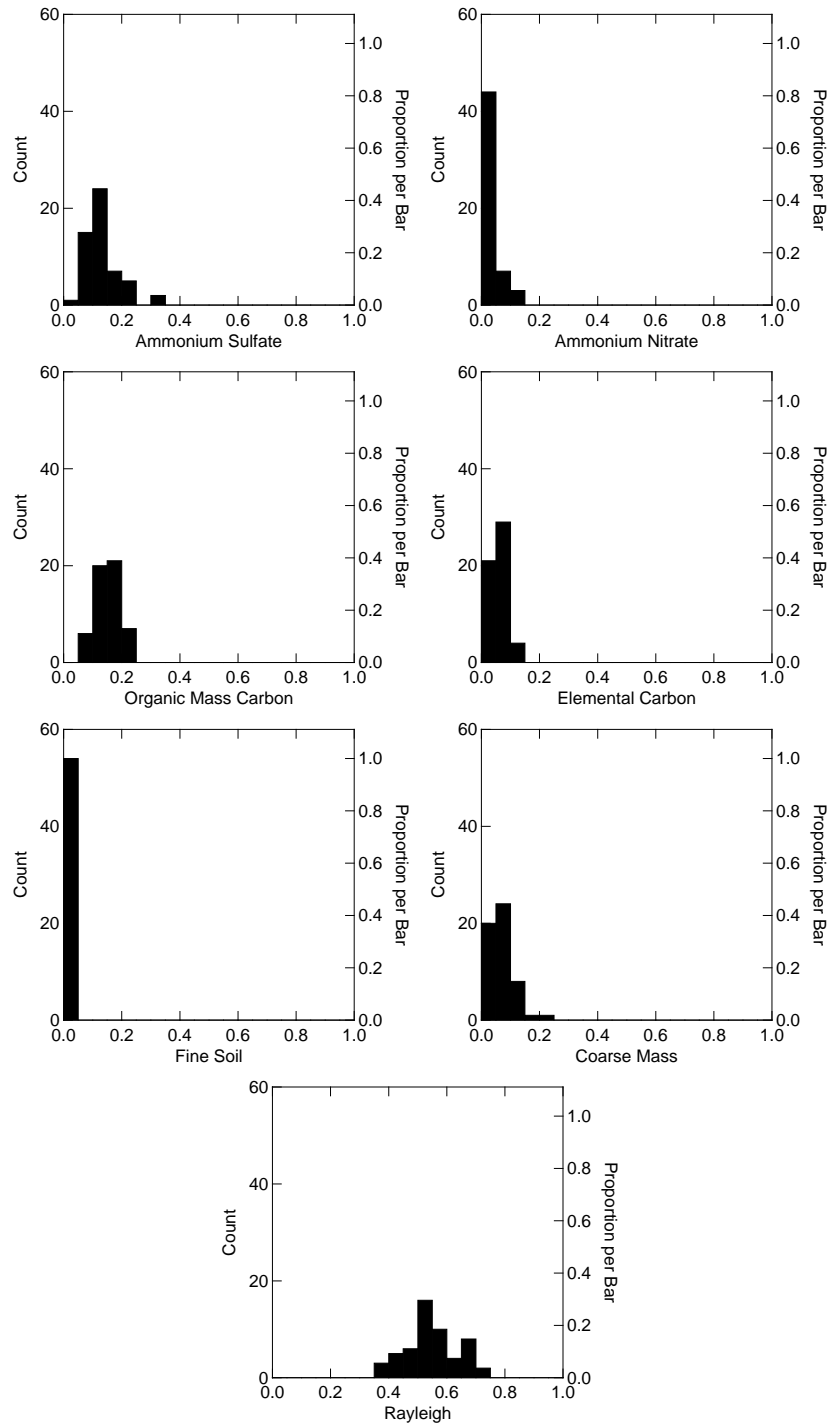
Figure 6-8 Winter relative chemical contribution frequency distribution to light extinction at Meadview based on IMPROVE data. The axis labeled "Count" represents the number of observations and the axis labeled "Proportion per Bar" represents the fraction of all observations within the bin.
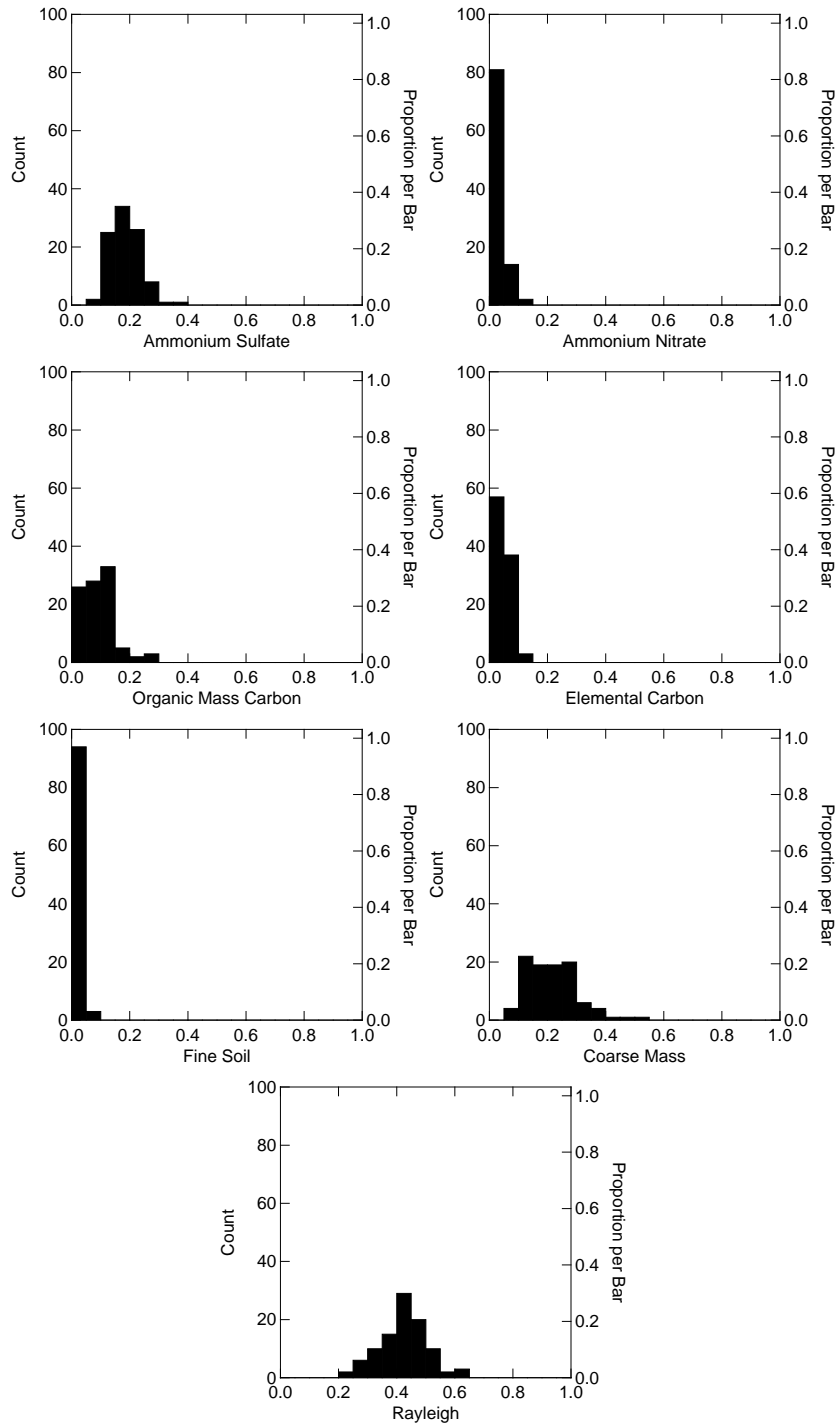
Figure 6-9 Summer relative chemical contribution frequency distribution to light extinction at Meadview based on IMPROVE data. The axis labeled "Count" represents the number of observations and the axis labeled "Proportion per Bar" represents the fraction of all observations within the bin.

During the summer intensive, the maximum estimated sulfate extinction accounted for 35% of the calculated extinction on 8/6/92 1900. Organic compound are estimated to have contributed a

maximum of 28% of the extinction during the 8/16/92 700 sample. On 7/21/92 700, equation 6-6 predicts that coarse mass contributed a maximum of 53% of the light extinction. For these three sampling periods, different components were the largest estimated contributors to extinction. Thus, complete control of the sources of a single extinction component would not have the same impact on light extinction for all days.

The figures also show that during the intensive sampling periods, fine soil never accounted for more than 10% of the light extinction. In addition, ammonium nitrate and elemental carbon never accounted for more than 15% of the light extinction.

7. Temporal Changes in Meteorology, Transport, and Air Quality

This section compares the Project MOHAVE study year to other years in terms of meteorology and air quality and describes seasonal and yearly variations in transport patterns.

7.1 Representativeness of Meteorology and Air Quality

7.1.1   Meteorology

The Grand Canyon Visibility Transport Commission evaluated calendar year 1992 for climatological representativeness for the 15-year period from 1977-1982 and 1984-1992 (Farber, 1995). This 15-year period, which is half the accepted climatological base period of 30 years, was dictated by the availability of visibility and aerosol data in the area. The calendar year was divided into two meteorological seasons: winter, January-April and November-December; and summer, the remaining months (May-October). To determine representativeness of each season, a chi-squared analysis was performed and then each season was comparatively ranked.

This analysis determined that 1992 was a "typical" year and that both winter and summer were "typical" seasons in a mix of "atypical" years and seasons. The 15 years examined had wide inter-annual variability among each season and both winter and summer of 1992 were not out of this wide variability range.

Winters exhibit less inter-annual variability than summers. The chi-squared summation value for the 15 winter seasons was 166 compared to 229 for the 15 summer seasons. This result may seem unexpected. One might expect greater variability during winter because of alternating storm and fair weather patterns compared to essentially fair weather patterns during summer. However, during winter, patterns are more strongly defined, more predictable (dominated by fair weather patterns) and surprisingly, do not reflect too much variation in the interannual variability of the storm pattern. By contrast, summers have less clearly separated patterns and, because of the intrinsic fuzziness of the two dominant patterns, the "thermal low" and "monsoonal", have greater inter-annual seasonal variability.

1992 was a moderate El Niño year in the southwestern United States, which led to above normal precipitation and clouds, particularly during the winter season. The chi-squared value for the winter of 1992 was about 20 compared to a seasonal average of 11. Most of this high value emanated from atypically high "thermal low" patterns (strong westerlies in the desert southwest) which occurred nearly 40% of the winter compared to the climatological average of 25%.

The summer was more climatologically normal than the winter. The 1992 summer season chi-squared value was 15 compared to the climatological average of 20. There are some important caveats. Summer 1992 (May-Oct) had the lowest number of troughs and the fourth highest number of monsoonal patterns for the 15 years examined. The heart of the summer was characterized by a strong and persistent high with above normal precipitation and accompanying clouds. This is typical of an El Niño year because there is more than the usual amount of sub-tropical moisture flowing into the region.

7.1.2 Light Extinction

Transmissometer-measured light extinction in 1992 at the south rim of the Grand Canyon and in the canyon were compared to the years 1987-1994. Generally, the 1992 year and summer and winter seasons were representative of the observed range of extinction. The annual median extinction at Grand Canyon ranged from 21 to 23 Mm^{-1} with 1992 recording a representative 22 Mm^{-1}. The summer seasonal median extinction on the rim ranged from 21 to 27 Mm^{-1} with 1992 recording 24 Mm^{-1}. Within the Canyon, summer median extinction ranged from 30-36 Mm^{-1} with 1992 recording 32 Mm^{-1}. The winter seasonal median ranged from 17 to 20 Mm^{-1} on the rim with 1992 recording 19 Mm^{-1}. Within the canyon the median ranged from 25 to 33 Mm^{-1} with 1992 being at the high end, 33 Mm^{-1}.

The entire frequency distribution (Figure 7-1 through Figure 7-4) from 10th through 90th percentile was also examined. For the summer, both on the rim and in-canyon 1992 was typical of the longer term average through the 50th percentile. However, from the 60th through 90th percentile, 1992 was nearly the clearest summer year. For example, at the 90th percentile, extinction in the Canyon ranged from 40 to 46 Mm^{-1} with 1992 being 40 Mm^{-1}.

On the rim, winter was slightly hazier than average until the 90th percentile, where it was average. In the canyon, the 1992 winter was hazier than average throughout the distribution. As expected, winter experiences the lowest extinction on the rim. This should not be surprising given that, more than 80% of the time, winter trajectories have a relatively clear northerly origin. In surprising contrast to the clear plateaus during winter, winter extinction in the canyon is actually higher than summer extinction on the rim throughout all percentiles. This is due to winter mesoscale drainage flows throughout the Colorado Plateau. These large scale drainage flows dominate for 18 hours daily during fair weather periods. A variety of anthropogenic sources from eastern Utah, western Colorado, northern Arizona and northwestern New Mexico feed into this extensive drainage system. Somewhat surprisingly, even during summer, when the atmosphere is well-mixed, there is still appreciably higher extinction in the canyon compared to the rim.   Nocturnal drainage flows still occur most summer nights (see Section 5.3).

7.1.3 Sulfate

Particulate sulfate concentrations at both Meadview and Hopi Point were examined. The concentrations were representative at both locations compared to other years.

At Meadview, SCENES data collected from 1984 through 1989 were compared to the Project MOHAVE data. All values are expressed in particulate S. For the entire year, the SCENES 50th percentile was 0.37 ug/m^3 compared to the Project MOHAVE year of 0.36 ug/m^3. Between the 10th and 90th percentiles, the two studies are quite comparable with not more than 0.03 ug/m^3 separating the two studies at any percentile.
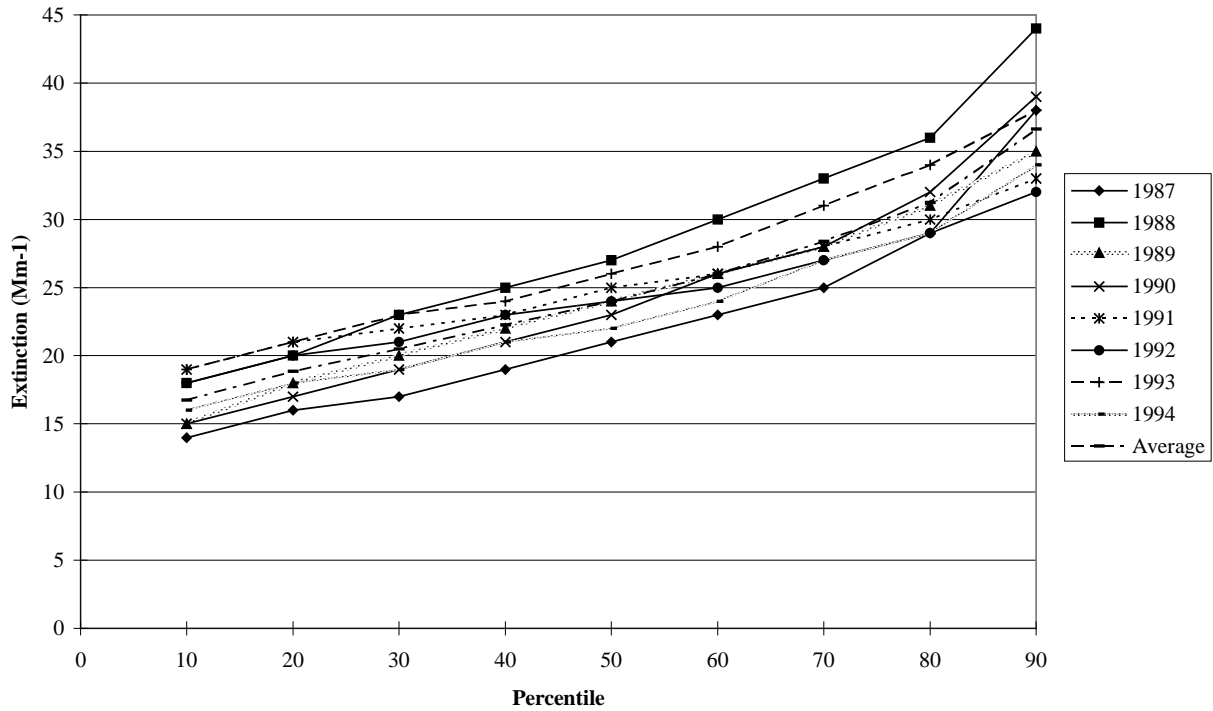
Figure 7-1 Frequency distribution of light extinction at Grand Canyon by season and year: south rim, summer (May – October).
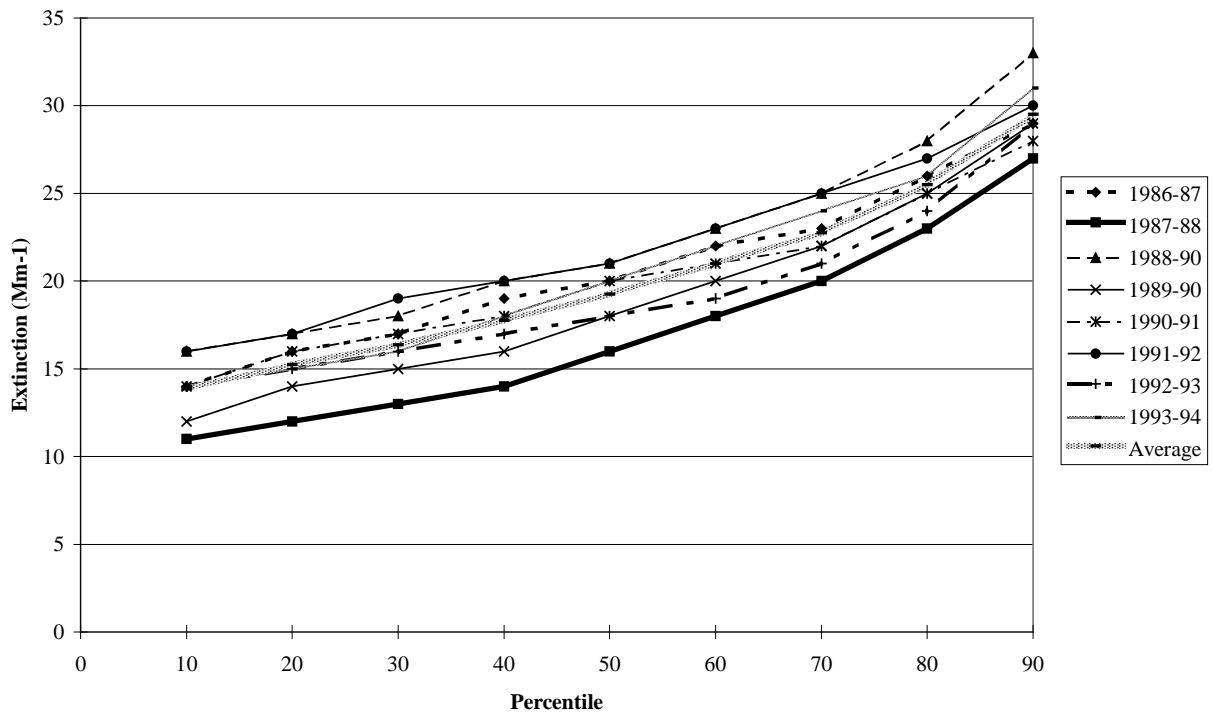
Figure 7-2 Frequency distribution of light extinction at Grand Canyon by season and year: south rim, winter (November – April).
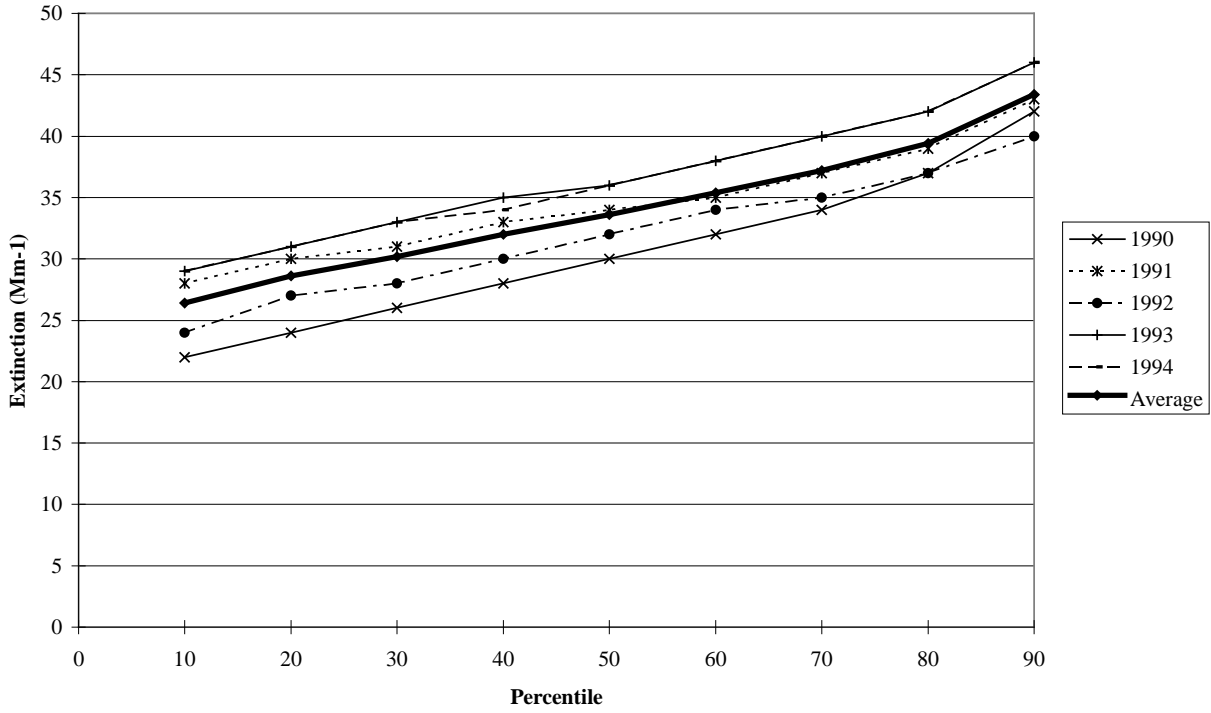
Figure 7-3 Frequency distribution of light extinction at Grand Canyon by season and year: in-canyon, summer (May – October).
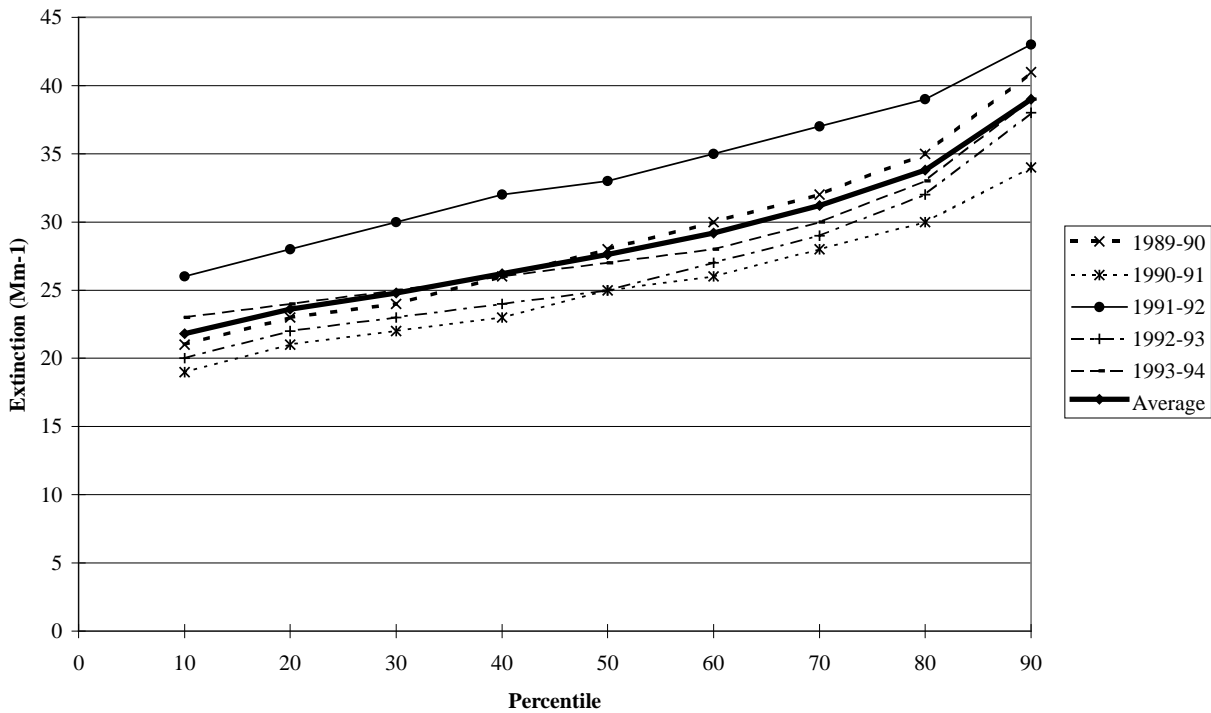
Figure 7-4 Frequency distribution of light extinction at Grand Canyon by season and year: in-canyon, winter (November – April).

For the summer, (May-September), the 50th percentile at Meadview during SCENES was 0.44 μg/m^3 compared to 0.51 μg/m^3 during the 1992 Project MOHAVE summer (see Figure 7-5 and Figure 7-6). Below the 50th percentile, the Project MOHAVE summer was approximately 0.06 μg/m^3 higher, perhaps a result of the absence of "cleaner" troughs and more monsoonal periods and high pressure periods during 1992. Above the 50th percentile, the concentrations between the two studies were very similar. For the summer intensive monitoring period (July 12 through August 31), the SCENES 50th percentile was 0.50 μg/m^3 compared to 0.53 μg/m^3 for Project MOHAVE. Below the 50th percentile, the Project MOHAVE summer intensive period was approximately 0.03 to 0.05 μg/m^3 higher than the SCENES period. Above the 50th percentile, the SCENES period was higher by about 0.03 μg/m^3. (It should be noted that SCENES and Project MOHAVE used different sampling techniques, which may result in some systematic differences.)

For the period corresponding to the winter intensive monitoring period (January 14-February 13), the SCENES 50th percentile was 0.22 μg/m^3 compared to Project MOHAVE 0.19 μg/m^3. The SCENES winter intensive period had consistently higher S concentrations from the 10th through the 90th percentile by as much as 0.1 μg/m^3 at the higher end.

At Hopi Point, the data record is longer than at Meadview and contains data from even before the 1984 start of SCENES through the present. Here the Project MOHAVE period is compared to SCENES (1984-1989) and IMPROVE (1987 through Sept 1997). Particulate S concentrations showed a downward trend in the higher percentiles from 1984 through Sept 1997. For the entire Project MOHAVE year, the 50th percentile was 0.29 μg/m^3 compared to SCENES 50th percentile of 0.27 μg/m^3 and IMPROVE 50th percentile of 0.22 μg/m^3. SCENES is higher than IMPROVE for all percentiles by approximately 0.02 μg/m^3 at the low end to 0.11 μg/m^3 at the high end. Project MOHAVE is between these two sets of data. The Project MOHAVE and SCENES summer medians were identical at 0.34 μg/m^3 compared to IMPROVE 0.30 μg/m^3. The Project MOHAVE summer intensive study median was 0.38 μg/m^3 compared to SCENES 0.40 μg/m^3 and IMPROVE 0.30 μg/m^3 (see Figure 7-6).

7.2 Transport Patterns

An overview of synoptic scale and mesoscale meteorology affecting the study area was given in section 2.2. In this section, trajectory analyses and other information are presented to describe how the seasonal and year-to-year variations in meteorology affect transport to the Grand Canyon.

7.2.1   Seasonal synoptic scale transport patterns

Typical synoptic-scale patterns can be seen by back-trajectory analyses. ATAD (Atmospheric Transport and Dispersion) back-trajectories were run for Hopi Point for the period 1979-1992, 4 trajectories per day. In brief, the ATAD model is a Lagrangian particle model with a single variable depth transport layer, the depth of which is determined by atmospheric stability using interpolation of measured vertical temperature profiles. Average transport layer winds are interpolated spatially and temporallyfrom nearby radiosonde stations (Heffter, 1980). These trajectories were grouped by ½ month periods. The annual cycle of transport patterns can be
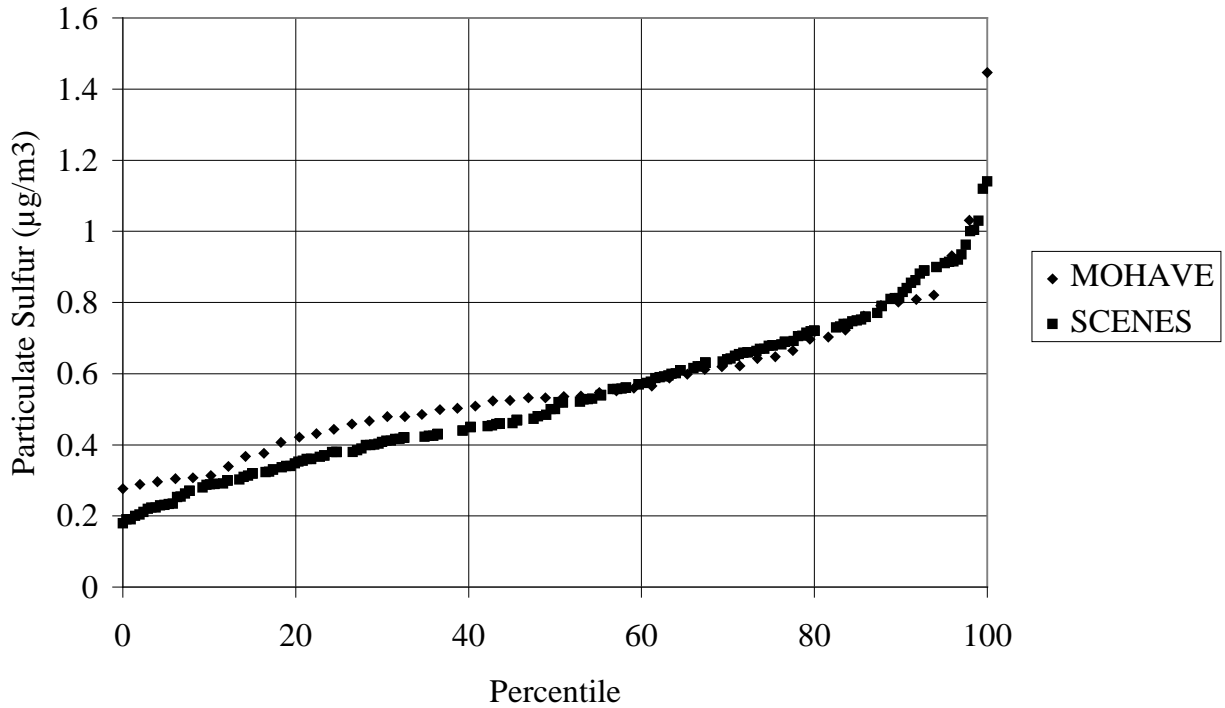
Figure 7-5 Frequency distribution of particulate sulfur at Meadview for the MOHAVE summer intensive period (July 13 – September 2) compared to the same period for SCENES.
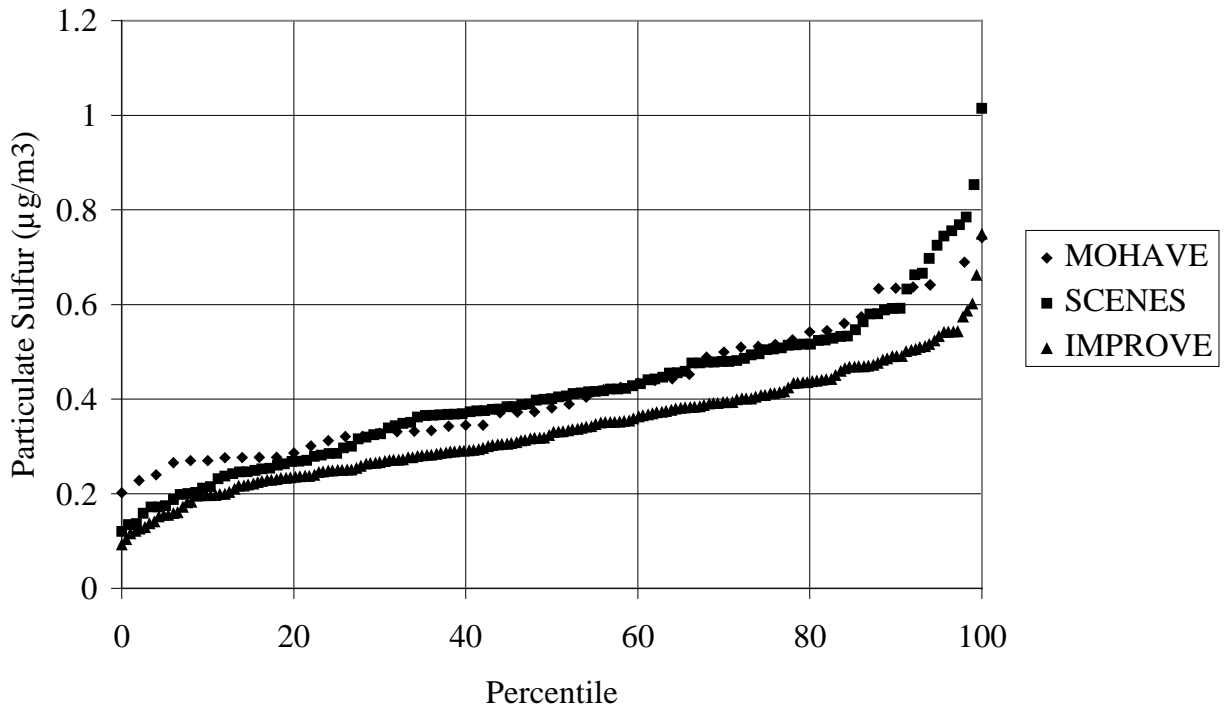
Figure 7-6 Frequency distribution of particulate sulfur at Hopi Point for the MOHAVE summer intensive period (July 13 – September 2) compared to the same period for SCENES (1984-1989) and IMPROVE (1987-1997).

discerned by looking at 6 specific half-month periods. Figure 7-7 shows the fraction of back-trajectories passing over grid cells of 2 degrees latitude by 2 degrees longitude for these 6 half-month periods. Northwesterly flow is common in late-fall and winter and the frequency peaks in late November (Figure 7-7). In mid-winter no direction dominates the synoptic scale transport pattern (Figure 7-7b). During this time low-pressure systems frequently pass through the region, resulting in a variety of wind directions as the pressure gradient direction and hence wind direction changes as the systems approach and pass through the area. In spring a transition period occurs between the northwesterly flow common in winter to the dominant southwesterly flow in the summer. In late April (Figure 7-7c), a bi-modal distribution of southwesterlies and northwesterlies is observed. Late June marks the peak of the frequency of transport from the southwest (Figure 7-7d). By mid-late summer, flows from the southeast (accompanied by considerable moisture) are more frequent (Figure 7-7e). Finally, in late September, transition to northwesterlies is beginning, although southwesterly and southeasterly patterns are still significant (Figure 7-7f).

7.2.2   Effect of transport patterns upon haze levels

Several analyses (e.g. Kahl *et al.*, 1997, Green and Gebhart, 1997, Vascancelos, 1997, Gebhart and Green, 1995, White *et al.*, 1994a, Gebhart and Malm, 1994) have been performed in the last few years that consider the relationship between transport patterns and air quality at Grand Canyon National Park. These analyses used aerosol and optical data from either the SCENES network (1984-1989) or the IMPROVE network (late 1980's to early 1990's). The conclusions are consistent among the different analyses and include:

- Clear (low b_{ext}) air most commonly arrives during winter and from the northwest.

- Hazy (high b_{ext}) air most commonly arrives during summer and from the southwest; air arriving from the southeast, mainly in summer is also dirty, but less frequent.

- Most particulate sulfur transported to the Grand Canyon is from the southwest; however, average concentrations of fine sulfur are highest with transport from the southeast.

- Transport from the northwest has the lowest average particulate sulfur concentrations.

Figure 7-8 (Green and Gebhart, 1997) shows the probability that air arriving at Grand Canyon with trajectories passing over each grid cell had light extinction coefficients at Grand Canyon in the lowest 20 percentile for the period 1988-1992. Trajectories from the north were likely to be associated with low b_{ext}, while trajectories from the south were unlikely to be associated with low b_{ext}.
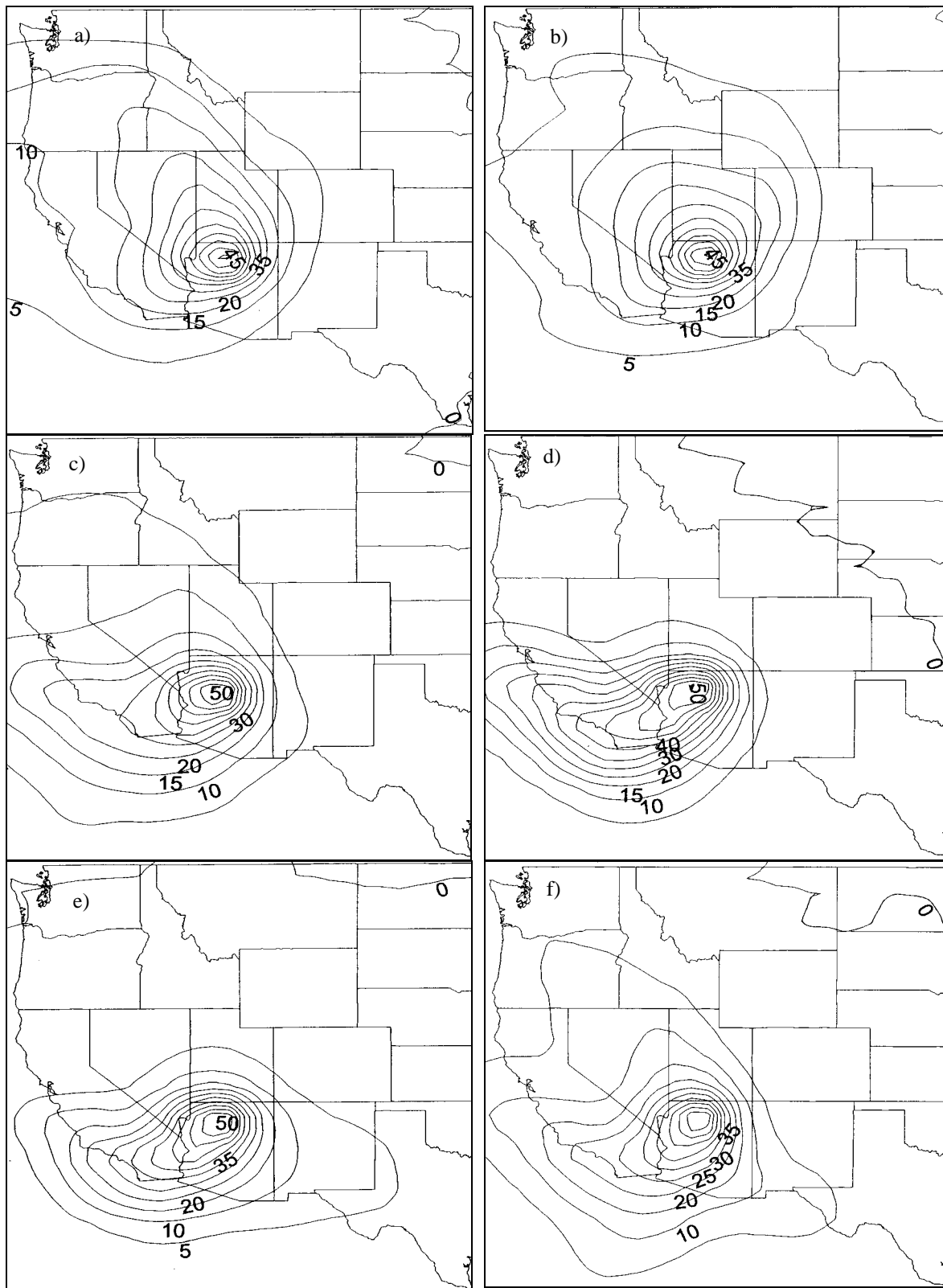
Figure 7-7 Percent of trajectories passing over 2 degree longitude by 2 degree latitude grid cells en route to Grand Canyon, 1979-1992. a) Nov. 16-30; b) Jan. 1-15; c) Apr. 15-30; d) June 15-30; e) August 1-15; f) Sep. 15-30.
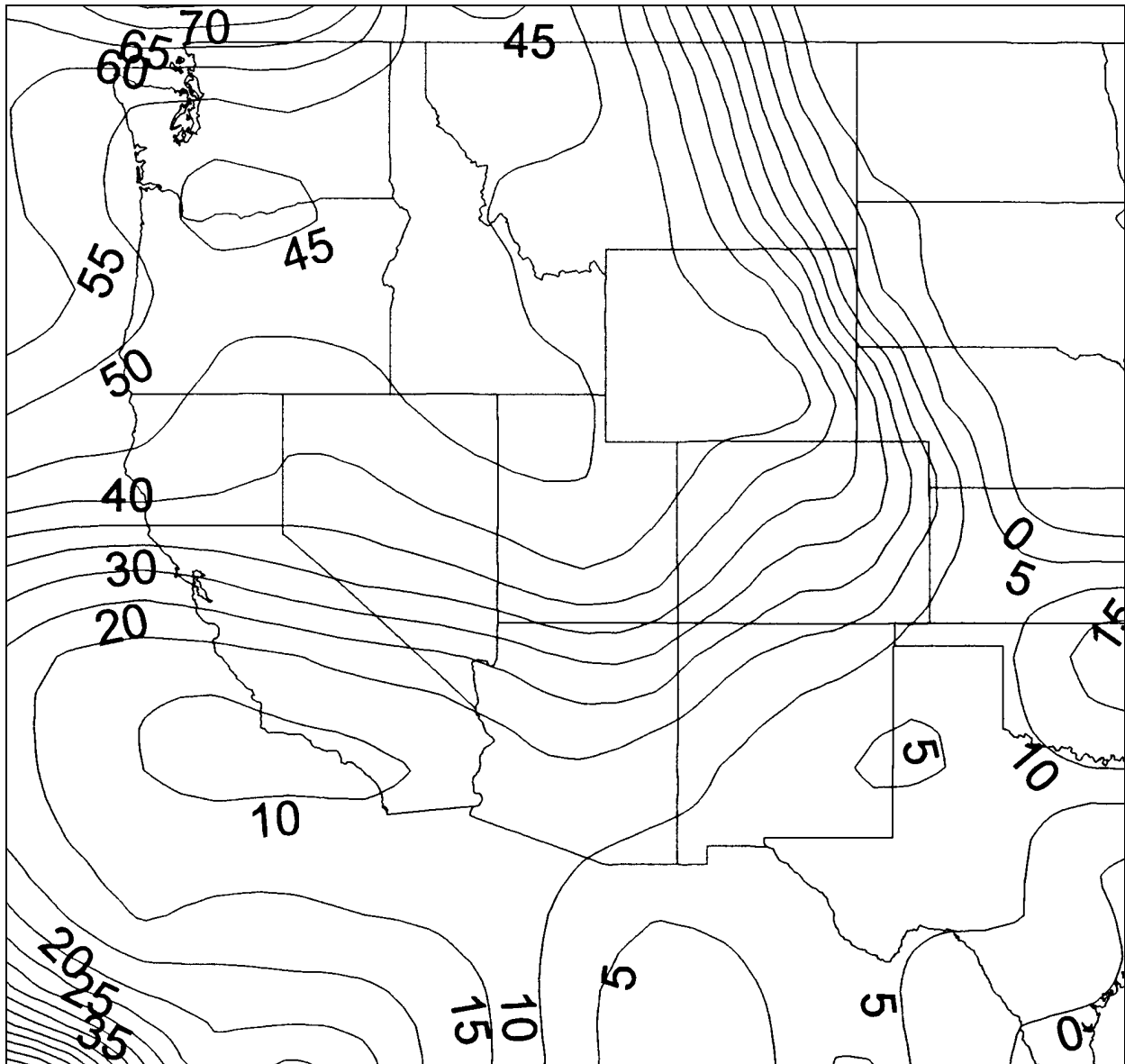
Figure 7-8 Probability that air arrived at Grand Canyon with low light extinction (lowest 20th percentile) after passing over each area, according to ATAD trajectories, 1988-1992.

7.2.3 Mesoscale transport patterns

Project MOHAVE tracer data provides quantitative and qualitative information about transport and dispersion in the study area. While the tracer data showed some variation from day to day within the summer and winter periods, typical patterns did emerge. Figure 7-9 shows the frequency of samples significantly above background concentrations during the PFT release periods for sites in the winter intensive that collected at least 20 days of samples, and for sites in the summer intensive period that collected at least 30 days of samples. A sample is considered to be significantly above background if its concentration is greater than the background plus 3 standard deviations of the measured background concentration. Shaded contour patterns are

included to guide the viewers to sites of similar frequency and should not be literally interpreted as spatial patterns.

Figure 7-9c shows Dangling Rope tracer in winter was most often transported to sites to the southwest, with even higher frequency for sites in or near the Colorado River Canyon. MPP tracer in winter was transported most frequently to sites to the south (Figure 7-9a). The Dangling Rope PFT data are above background concentrations in greater than 40% of the samples along the Colorado River through the entire length of the Grand Canyon and in more than 20% of the samples as far down river as MPP. Unfortunately, there were only a few sites south of MPP with sufficient data to track the MPP tracer flow very far. However winter flow is not exclusively downslope as shown by small, but non-zero, frequency for PFT above background concentrations to the north of MPP for its PFT and to the northwest of Dangling Rope for its PFT.

In the summer, the MPP PFT is above background levels most of the time at sites north of MPP, which indicates a northerly predominant direction of flow (Figure 7-9b). At San Gorgonio, 66% of the samples were determined to be above background for the MPP PFT: most of these samples were from one lid and many were only marginally above background. This suggests a possible analytical problem, for example variation in response of the gas chromatograph, rather than actual elevated concentrations of ocPDCH. Alternatively it is possible that a small source of ocPDCH or compounds that are analyzed as ocPDCH (interferences) are present in the greater Los Angeles area.

PFT from El Centro in summer is also seen most frequently at sites to the north (Figure 7-9e). From the Tehachapi location the flow tends to be toward sites to the east (Figure 7-9d). Lack of monitoring sites to the north of the Tehachapi Pass PFT release site prevents conclusions concerning travel in that direction, though it is clear that flow does not frequently carry that tracer to sites to the southeast.

7.2.4   Influence Functions

Figure 7-10 shows maps displaying mean influence functions for the PFT tracers. Influence functions are the emission rate normalized PFT concentrations (i.e. tracer concentration divided by emission rate) and have units of seconds/cubic meter. This convention readily permits the estimation of the contribution of a particular source to the atmospheric concentration (in $\mu g/m^3$) at a receptor by multiplication of the influence function by the emission rate (in $\mu g/s$) of the source. Values shown in Figure 7-10 have been multiplied by 10^{-9} and contour intervals are in logarithmically distributed intervals. In order to reduce the uncertainty of the influence functions, periods of constant tracer emission were selected such that the average daily emission rate did not differ by more than 20% from the mean daily emission rate for the period. Since Dangling Rope, El Centro, and Tehachapi were located at the perimeter of the sampling network, influence functions were not calculated for the first two days of a constant emission period. This was assumed to be a sufficient time for the tracer to reach all of the sites within the network. Since the Mohave Power Project was centrally located in the network, influence functions were not calculated on the first day of each period. At least 20 days of influence functions at each site were required for the average to be plotted on the maps.
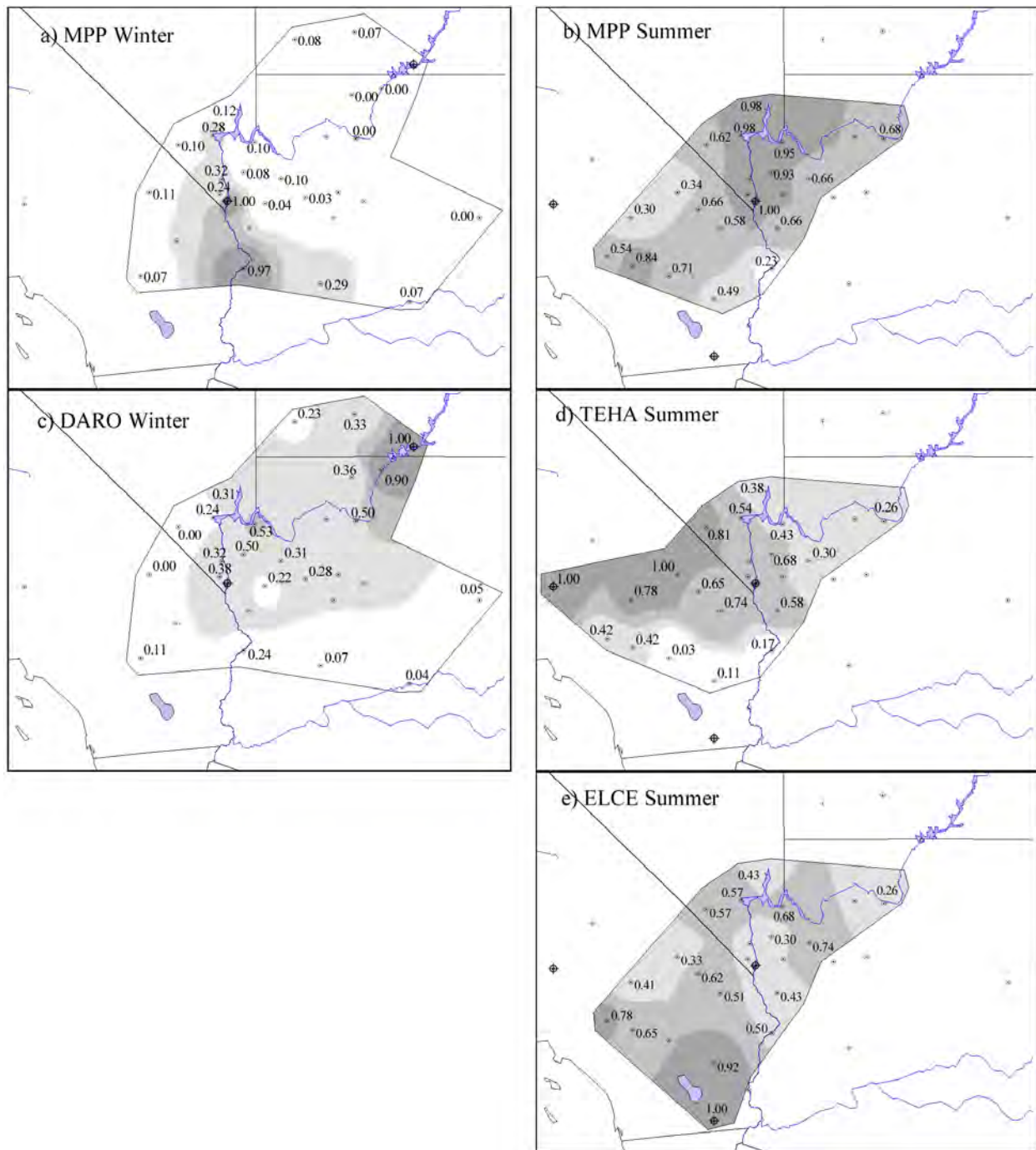
Figure 7-9 Maps of the frequency that tracer was detected above background for each of the four PFT release locations. Only data meeting completeness criteria were used to generate the contours. The polygons surround the sites meeting the completeness criteria.
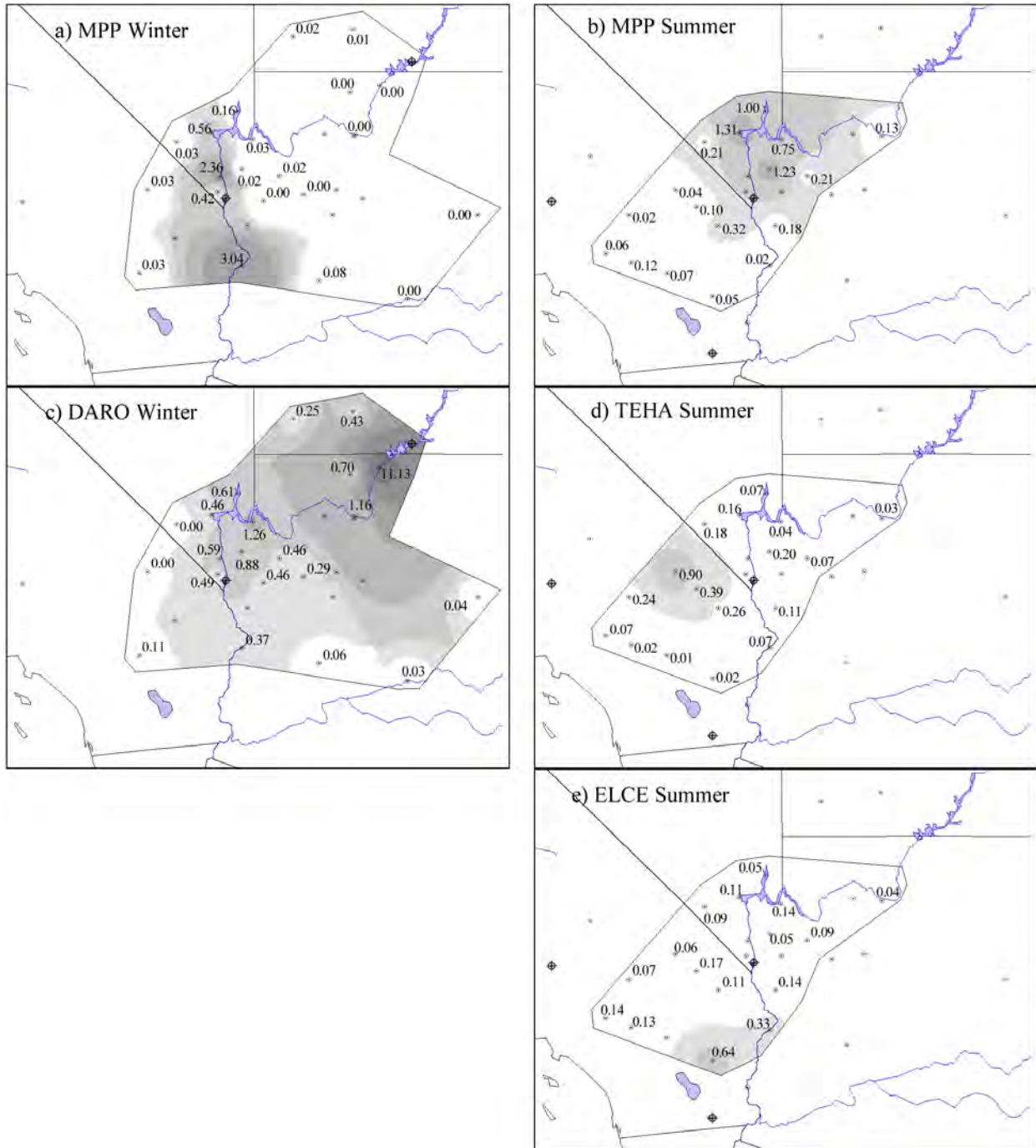
Figure 7-10 Map of average PFT influence functions (10^{-9} s/m^3) measured at receptor sites.

Influence functions are a direct measure of the average dispersion between the emission and monitoring locations. The spatial patterns of the mean influence functions illustrate the typical tracer distribution observed throughout each season. As might be expected, the largest values on the maps in Figure 7-10 are during the winter intensive period, and these tend to be at sites along the Colorado River canyon which acts as a natural conduit for airflow in the winter. The effect in winter of monitoring site height above local terrain can be seen in the Dangling Rope average influence functions for Hopi Point (situated on high local terrain) and Meadview (at mid-level

with respect to local terrain). The influence function is somewhat higher at Meadview than at Hopi Point in spite of the former being more than twice the distance from Dangling Rope than the latter. Winter flow for MPP also follows the Colorado River with the greatest influence function values to the south at Parker. Summer MPP average influence function values are highest at sites to the north with the largest average value at Las Vegas Wash. Tehachapi Pass average influence functions are largest in the northeastern Mojave Desert, while for El Centro the sites to the north (Desert Center and Parker) and northwest (Joshua Tree) of the release site have the largest average values. A predominant feature of winter flow shown by the PFT data is drainage down the Colorado River. Under these circumstances the dispersion is retarded by confinement within the terrain as can be seen with the high average influence functions at large distances downwind. Sources on the Colorado River east of the Grand Canyon, as represented by the Dangling Rope PFT, can have significant influence throughout the entire length of the Grand Canyon and beyond. MPP emissions are transported primarily to the south along the river and are soon beyond the few sites in the Project MOHAVE network to the south of MPP. While the direction of the flow was expected, the magnitude of the influence functions for the Dangling Rope release were surprisingly large at the more distant sites on the lower Colorado River. Neither of the two earlier winter studies that released tracer from near that location (WHITEX and the NGS Visibility Study) had tracer monitoring sites as far downriver as in Project MOHAVE.

Summer flow is generally from the south along the Colorado River (El Centro and MPP) and from the west (or possible southwest) from the western edge of the Mojave Desert (Figure 7-10 b and e). However, from the joint El Centro - Tehachapi frequency plots (not shown here) there appears to be a convergence zone over much of the Mojave Desert. PFTs from both of the two California release locations are above background in 20% to 30% of the 24-hour periods at all of the eastern Mojave Desert sites. Given that the flows from the greater Los Angeles and San Diego urban areas are likely to be located between the paths taken by the two PFTs, emissions from these areas must be at least as frequently transported through this region. This is consistent with predominate summer surface wind flow patterns for California, which have transport from the California Central Valley south-southeast over Tehachapi Pass, transport from the California South Coast Air Basin to the east into the Mojave Desert and flow to the north over the eastern half of the California - Mexico border. Convergence over the Mojave Desert can be explained by the thermally induced low pressure often centered over that area in summer which draws cooler air in from the California Central Valley, Pacific Coast and the Gulf of California. From this it is reasonable to conclude that the eastern Mojave Desert is a major transport route for emissions from much of the State of California during the summer.

The average summer MPP influence function values at Las Vegas Wash and Overton Beach are comparable to the average value at Dolan Springs in spite of the former being more than twice the distance from MPP. This suggests that MPP emissions are consistently over most of Lake Mead (north of MPP along the Colorado River) with relatively little dilution. An examination of the spatial MPP PFT influence function patterns for sample periods that have the highest influence functions at Meadview (where Lake Mead meets Grand Canyon) show that they are associated with flow passing over the Dolan Springs site to the east of MPP and not in the Colorado River canyon. This would seem to imply the need for a more westerly component to the wind to produce the largest MPP PFT concentrations in the western Grand Canyon.

7.3 Effect of Sulfur Dioxide Emissions Reductions on Sulfate Concentrations in the Western U.S. since 1979

Sulfur dioxide emissions in the Southwest have declined substantially in the past two and a half decades. As Figure 7-11 shows, SO_2 emissions in 5 southwestern states (AZ, CA, NM, NV, and UT) decreased from about two million tons per year in 1980 to about one million tons per year in 1991, a change of about 50% (DOE, 1995). Because of prevailing meteorology, emissions in these states are those most likely to influence Grand Canyon visibility.

Analysis of the effects of past changes in emissions on air quality illustrates what previous emissions reductions have accomplished and can provide a yardstick for evaluating the potential effects of future changes. To this end, this section evaluates the particulate sulfur concentration trends at Class I areas on the Colorado Plateau and at other locations in the Southwest and
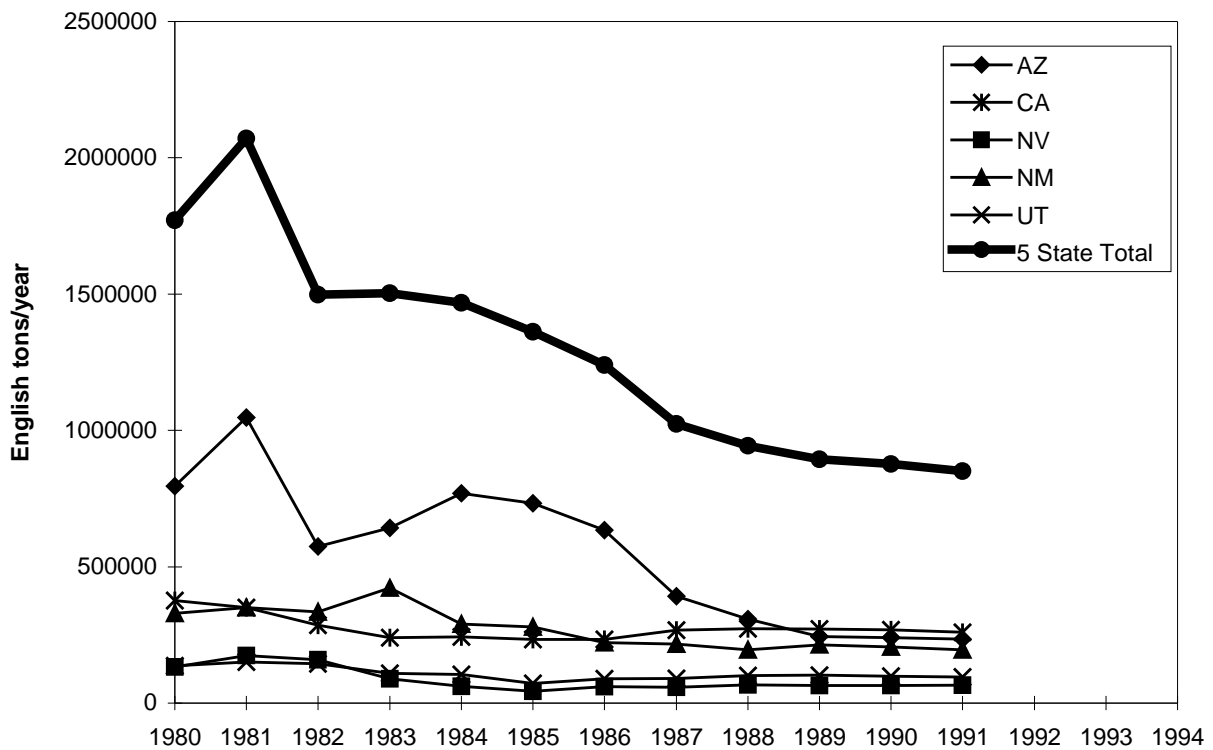
Figure 7-11 Trends in SO_2 emissions in 5 southwestern states.

compares them with the trends in SO_2 emissions in the area. According to Malm *et al.* (1994), sulfate-containing particles accounted for 32% of the average mass of fine particulate matter ($PM_{2.5}$) at Hopi Point in Grand Canyon National Park during the three years 1988-90, and they attributed 35% of the average light extinction due to particles to these same sulfate-containing particles. One might expect that the large decrease in sulfur emissions between 1980 and 1991 would be reflected in ambient particulate sulfur concentration measurements.

7.3.1 SO$_2$ Emissions Trends

The five states whose emissions are plotted on Figure 7-11 are the ones whose emissions are most likely to affect visibility on the Colorado Plateau. In 1991 they accounted for about 60% of the SO$_2$ emissions in the 11 states of the West. Mexican emissions of SO$_2$ from sources relatively near the border with the U.S., especially from smelters, grew during this period, but reliable emission trend data are not available.

The emissions trends shown in Figure 7-11 are dominated by the variability in Arizona emissions, which were largely due to smelter operations there. In fact, the large year-to-year variability between 1980 and 1982 reflects a smelter industry strike in 1980 and a very wet El Niño year with low production in 1982. Subsequent decreases during the decade are largely the consequence of shutdowns of several smelters and the installation of emissions control equipment on others. Therefore, the main trend since 1980 has been a strong decline in overall SO$_2$ emissions in the Southwest, especially in southern Arizona because of smelter emission reductions. Not reflected in this graph is an unquantified increase in Mexican emissions.

7.3.2 Particulate Sulfur Trends

Atmospheric concentrations of sulfate or particulate sulfur have been measured since 1979 by the National Park Service (NPS), using two different methods. From 1979 to 1987 the measurements were made in the Western Fine Particle Network (WFPN) with a Stacked Filter Unit (SFU) at a flow rate of 10 l/min for 72 hours (Flocchini *et al.*, 1981). The substrate on which the sample was collected and the area over which it was deposited varied over the years, as indicated in Table 7-1. Since 1987 the aerosol measurements have been performed as part of the IMPROVE program, using multi-unit IMPROVE samplers, at a flow rate of 22.8 l/min for 24 hours (Malm *et a.l*, 1994).

Table 7-1. Chronology of Class I Area Particulate Matter Measurements

Period	Sampler	Sample Duration	Filter and Sampling Area
7/79 - 5/82	Stacked Filter Unit (SFU)	72 hr	Nuclepore (14 cm^2)
6/82 - 5/86	Stacked Filter Unit (SFU)	72 hr	Teflon (3.5 cm^2)
6/86 - 11/87	Stacked Filter Unit (SFU)	24 hr	Teflon (1.1 cm^2)
3-88 - present	IMPROVE Sampler	24 hr	Teflon (2.2 cm^2)

Throughout all of the periods listed in Table 7-1, the analysis technique for sulfur in the samples has been the Particle Induced X-ray Emission (PIXE) method, performed by the Crocker Nuclear Laboratory at the University of California at Davis. The PIXE procedure was changed in 1988, when a second detector was added to improve the sensitivity for elements heavier than iron (Eldred & Cahill, 1994). This change improved the precision and minimum detection limits for sulfur, from 8% and 1.9 ng/m^3 in 1982-86 to 5% and 1.4 ng/m^3 from 1988 onward.

Looking at the particulate sulfur measurements, Figure 7-12 shows the behavior of annual average particulate sulfur concentrations at Hopi Point in Grand Canyon National Park and at

three other Colorado Plateau locations for the 15 years from 1980 to 1994. The annual average concentration trend shows a small increase over the 15 years.

When analyzing trends in measured concentrations over periods that include changes in sampling techniques, the possibility that the method changes could have affected the measured concentrations has to be taken into account to assure that a perceived trend does not just reflect a change in the sampling and analysis techniques. The consistency in the annual averages over the 1987 sampler transition seems to suggest that the transition did not cause any significant change in the reported values, but this observation has to be viewed cautiously because the 1987 average does not include the winter season during which the samplers were replaced.

We also confirmed independently that the sulfur concentration trend reflected in Figure 7-12 is not biased greatly by the sampling technique change in 1987 nor by the absence of winter data for 1987, during the transition. We reviewed the sulfur concentrations measured at Hopi Point between 1985 and 1988 by the SCENES cooperative study. SCENES used a different sampler (SCISAS) and the SCENES concentrations during this period were consistently about 10-15% higher than those from the SFU and the IMPROVE sampler. Except for this bias, however, the annual mean sulfur concentrations measured by SCENES closely follow the year-to-year trend
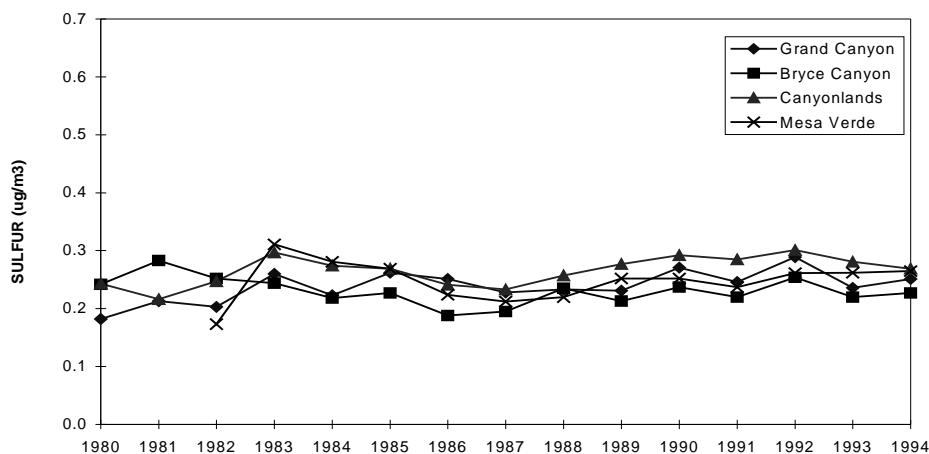
Figure 7-12 Annual average particulate sulfur concentrations measured by the WFPN and IMPROVE at Hopi Point in Grand Canyon National Park and at three other nearby locations.

for 1985 to 1989 shown in Figure 7-12 and suggest no introduction of a noticeable change due to the transition.

(One should note that White (1997a) has suggested that the SFU-IMPROVE transition at Shenandoah National Park may have introduced uncertainty into the long-term particulate sulfur trend there. Patterson, *et al.* (1998) argue, however, that such a systematic effect was not observed over the 20 IMPROVE sites they analyzed.)

Thus, despite substantial decreases in SO_2 emissions in the Southwest, we find that a concomitant decrease in particulate sulfur concentrations has not been observed at Hopi Point and at other locations on the Colorado Plateau. In fact, no decrease has been observed at all there.

To explore the reason for this counterintuitive behavior, we analyzed sulfur concentration trends at Class I areas located away from the Colorado Plateau. Figure 7-13 shows the WFPN/IMPROVE annual particulate sulfur concentrations at Big Bend National Park, in southwestern Texas, and at Chiricahua National Monument and Tonto National Forest, both in southern Arizona. The average particulate sulfur concentrations at all three locations are higher than those found at the Colorado Plateau samplers.

Figure 7-13 shows that sulfate concentrations at Big Bend have been increasing since their lowest level in 1984. On the other hand, sulfate concentrations at Tonto and Chiricahua in the 1990's are lower than they were in the early 1980's. (Large year-to-year variability during the WFPN sampling and a 4-year gap in Tonto data introduce some uncertainty to this conclusion, however.)

Eldred and Cahill (1994), also analyzed the same data. They concluded that sulfur concentrations from mid-1982 to mid-1992 decreased at an average rate of 2.7% per year at Mesa Verde and 3.5% per year at Chiricahua. Trends of less than 0.6% per year (either increase or decrease), which is less than the standard error of the estimates, were found at Big Bend, Bryce Canyon, Canyonlands, and Grand Canyon. Their statistical findings are consistent with the results presented here.

We can conjecture about the reasons for the observed behavior. The largest SO_2 emissions reductions took place at the smelters in southern Arizona, a region from which transport infrequently reaches the Colorado Plateau except during late summer monsoons. Therefore, these emission reductions had little effect on annual average sulfate concentrations on the Colorado Plateau. At locations in southern Arizona (Tonto and Chiricahua), however, the effects of the more nearby smelter emission changes were noticed, including effects of the strike in 1980, the wet year in 1982, and permanent shutdowns of two smelters in 1985.

During this same period (mid 1980's), the Nacozari smelter entered service in Mexico. This smelter location is far enough south and east of the Tonto and Chiricahua Class I areas that its emissions don't affect the air quality at those locations frequently. Rather, the generally westerly flow carries its emissions toward Big Bend National Park, where the sulfate concentrations shown in Figure 7-13 appear to reflect both the U.S. smelter emissions reductions in the early 1980's and subsequent increases in Mexican emissions since then, from smelters and other sources.

The above analyses have addressed trends in particulate sulfur concentrations. A similar attempt to discern a trend in total $PM_{2.5}$ mass concentrations was not successful, however, because it was found that the IMPROVE determinations of gravimetric mass concentrations are larger than those measured by the SFU.

The analyses above have demonstrated that trends in particulate sulfur concentrations on the Colorado Plateau from 1980 to 1994 have been weak despite substantial decreases in regional SO_2 emissions. Receptors to the south, in the vicinity of the smelters that have produced most of the emission reductions, have shown some decrease in sulfate particle concentrations, although the average change has been less than the reduction in emissions. Thus, it appears that the averageColorado Plateau air quality has been relatively detached from the SO_2 emissions

changes. This does not mean, though, that emissions changes in southern Arizona and northern Mexico will not affect Colorado Plateau air quality occaisionally.
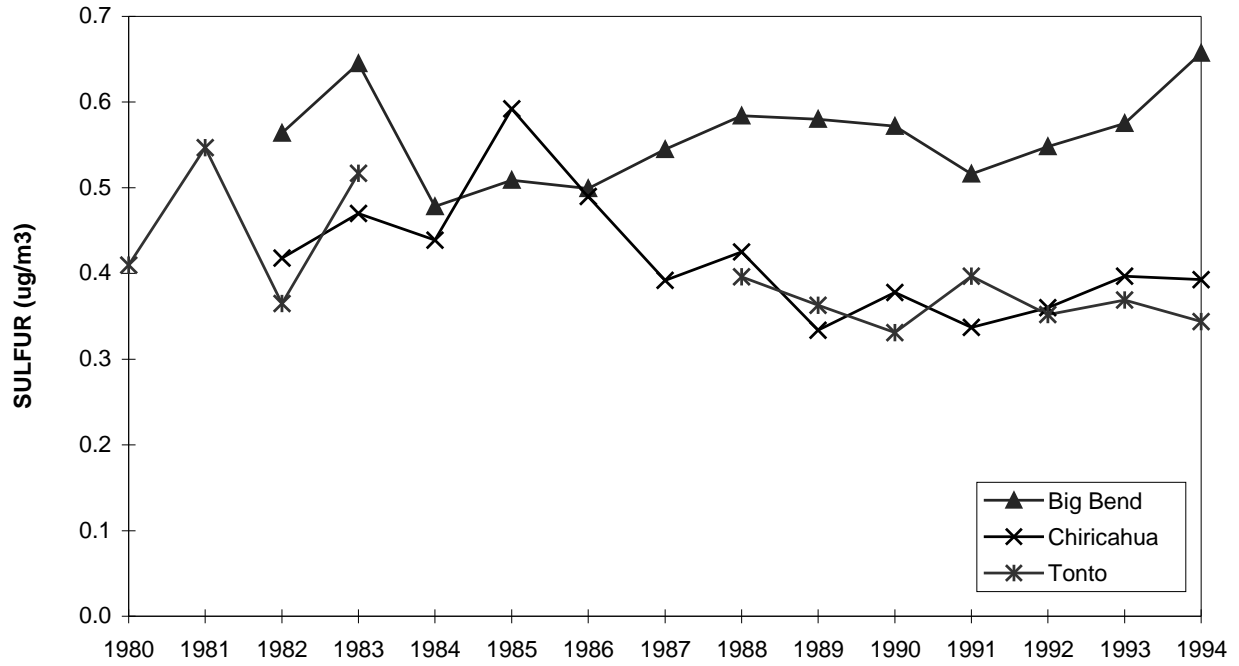
Figure 7-13 Annual average particulate sulfur concentrations measured by the WFPN and IMPROVE at three locations away from the Colorado Plateau.

8. Source Contribution Assessment Methodology

This section addresses the methodology that was used to estimate the contribution of the Mohave Power Project to ambient sulfate concentrations and light extinction at Grand Canyon National Park. Because of the topographic and meteorological complexity of the study environment, no single attribution model was expected to be usable under all circumstances. Rather, the overall attribution approach consisted of the use of several techniques in concert to strive to obtain a credible range of attribution estimates.

An initial effort at estimating attribution used several receptor analysis techniques and simulation models, which were applied without knowledge of the results of the perfluorocarbon tracer (PFT) experiments that took place during the two intensive study periods. The modeling results were then tested against the measured PFT concentrations and it was found that the models generally performed poorly, as we describe below in Section 8.2. To provide improved predictions, the information from the PFT experiments was incorporated into new or revised models, either as input or as a basis for setting parameters. The approaches that resulted, described in Section 8.3, were then used to develop the final attribution estimates of the study, as presented in Section 9.

8.1 Overview of Attribution Approach

The process of identifying and quantifying the estimated impact of MPP's emissions on Grand Canyon sulfate concentrations and light extinction was accomplished using two types of assessment tools.

The first type – receptor data analysis or receptor modeling – is an analysis of concentration and chemical composition data collected at one or more receptor locations, sometimes in combination with meteorological information, and comparison of the receptor data with the composition of emissions from sources of interest. Receptor modeling is a diagnostic approach that analyzes measurements to derive a plausible accounting of the emissions that produced measured concentrations and compositions. Although conceptually straightforward, receptor modeling depends on accurate measurements of ambient concentrations and, in many cases, on accurate characterization of the compositions of emissions from major source categories. In practice, some receptor analysis methods can be statistically complex. Receptor analysis can only be used to analyze conditions at the times and locations for which measurements exist; it has no predictive capability for other times and locations.

The fundamental assumption for many of the receptor-oriented methods is that the concentration of the tracer is in the same ratio to the concentration of the species of interest (e.g., total sulfur from the MPP) at both the source and receptor. This means that the tracer emissions are assumed to accurately follow the SO_2 emissions rate from the MPP stack and that the tracer and the target species all undergo diffusion, deposition, and conversion at the same rates. In practice this limits such methods to inert gaseous or fine particle species with minimal deposition. Hybrid models, that add a parametric representation of chemical conversion and/or deposition to the basic receptor model, are used to overcome this limitation. Several of the receptor models used for Project MOHAVE are of this hybrid form.

The second method – source emissions simulations or simulation modeling –uses mathematical models of the transport, diffusion, deposition, and chemical conversion of the emitted air pollutants to predict ambient concentrations resulting from emissions. Such models, which rely on our understanding of the physics and chemistry of the atmosphere, are conceptually able to predict air quality impacts at all locations and times. Because of limitations in our knowledge of atmospheric behavior, our ability to portray that knowledge mathematically, and the ability of computers to carry out the needed calculations in a reasonable amount of time, all models require some input data on meteorology and air quality, in addition to the obvious requirement of emissions information.

It needs to be recognized that it is an extremely difficult task to predict with reasonable accuracy the tracer concentrations at Meadview and Hopi Point which are located approximately 110 km and 280 km away from the MPP point source, respectively. Rugged terrain, lakes and rivers exist between the source and receptors. In this setting, the atmospheric system is complex, and therefore models that attempt to portray its behavior faithfully tend to be complex and are very sensitive to small errors in assumptions about processes. Models that use more measured information or simplify the mathematical representations of processes tend to be simpler, but, in turn, may suffer from errors due to that simplification. Furthermore, as was noted in Section 1.1, the outage study concluded that the average MPP contribution to sulfate at Meadview was less than 15%. Therefore, it was essential that the reasonableness or accuracy of simulation modeling be tested against measurements, as they were in Project MOHAVE.

The concentrations that are calculated at specific receptor points by emission simulation models are very sensitive to the input wind field description, particularly the wind direction. A small error in wind direction can change plume impact at a distant receptor from a "direct hit" to a complete miss, or vice versa. (For example, the straight-line distance from MPP to Meadview is 110 km, so a 5° difference in mean wind direction will shift the centerline of the MPP plume by 10 km in the crosswind direction.) Because a dense grid of wind field measurements was not available, interpolation of measurements in space and time was necessary to construct a complete wind field for modeling. Modelers used several different schemes to construct representations of complete wind fields.

8.2 Evaluation of Initial Attribution Methods

Initial efforts to determine the contribution of the Mohave Power Project to ambient air quality were unsuccessful. Four dispersion modeling techniques and two receptor modeling approaches were applied, using meteorological and air quality measurements made during the two Project MOHAVE intensive study periods. The predictions were tested against 12- and 24-hour measurements of concentrations of the perfluorocarbon tracer (PFT) that was released from the MPP at the same time. (The PFT data were not available to the modelers when they prepared their predictions.)

The models tested are listed below. (The references given here describe the models, not their application for this evaluation.)

- HAZEPUFF, a Lagrangian puff model (Latimer, 1993)

- DRI/CSU Lagrangian Particle Model. The Colorado State University Lagrangian particle dispersion model (Uliasz and Pielke, 1993), with wind fields from the Desert Research Institute three-dimensional second order closure mesocale meteorological model (Enger, *et al*; 1993; Enger and Koracin, 1994)

- DRI semi-Gaussian trajectory-type dispersion model (Enger, 1990), using the same wind fields as used for the DRI/CSU Lagrangian Particle Model

- VISHWA. Use of source-receptor transfer coefficients from VISHWA, an Eulerian grid-based regional air quality model that was applied by the Grand Canyon Visibility Transport Commission using meteorological fields produced by the RAMS meteorological model (Tombach *et al.*, 1996)

- NPS Chemical Mass Balance (CMB). A simplified chemical mass balance approach that apportioned secondary sulfate, applied by the National Park Service

- BYU CMB. An application of the CMB approach using regional source profiles, by Brigham Young University

- RMAPS. A spatial pattern correlation model (Henry, 1997a and 1997b).

Table 8-1 presents the results of the evaluations, from Green and Tombach (1998), for all methods but RMAPS. The PFT used for those evaluations was the ocPDCH (ortho-cis-perfluorodimethylcyclohexane) isomer portion of the oPDCH tracer injected into the MPP stack effluent. It was assumed for the purposes of this evaluation that the measured PFT concentrations were free of error. In reality, as shown in Section 4.4, the ocPDCH precision was about 6% of the mean measured concentration listed for Meadview in Table 8-1. That same precision represents about one-third of the Hopi Point average concentration, however, so some of the performance evaluations reflect measurement uncertainty. The accuracy of the PFT measurements has not been characterized.

None of these techniques was successful at predicting the ambient 12- and 24-hour average PFT concentrations reliably. The best correlation between the predicted and measured concentrations was $r^2 = 0.17$, for HAZEPUFF model predictions of 12-hour concentrations at Hopi Point (where the measurements are more uncertain); this means that the model was able to account for 17% of the variation in the ocPDCH observations at Hopi Point. The concentrations predicted by HAZEPUFF averaged more than twice those measured, however. Furthermore, the same model only achieved an insignificant r^2 of 0.02 for predictions at the Meadview receptor, where the observed concentrations were higher and more precise than at Hopi Point.

Values of r^2 for all other methods were less than 0.1, both for predictions at Hopi Point and Meadview. This performance was not acceptable for meeting the Project MOHAVE objectives, particularly since the ability to predict secondary sulfate concentrations can be expected to be even poorer than it was for predicting the inert PFT tracer concentrations.

In addition to the models described in Table 8-1, predictions by a spatial pattern correlation receptor model, RMAPS (Henry, 1997a) were also evaluated. RMAPS apportions the average

concentration of a species, as measured at many sites, among several spatially distinct sources and can be applied to primary or secondary species; no assumptions concerning transformation or deposition rates are required.

RMAPS has been applied to predict the impacts of emissions from several source regions, including a "Colorado Valley Source" located in the vicinity of MPP and the Las Vegas area (Henry, 1997b). Green and Tombach (1999) describe tests of the RMAPS concentration predictions for the Colorado Valley Source against the maximum particulate sulfur that could be attributed to MPP based on measured PFT concentrations and assuming 100% conversion of SO_2. This comparison was done at 21 receptor locations, with concentrations averaged over the summer intensive.

Table 8-1 Summary of Evaluations of Initial Attribution Methods against PFT Measurements

Model	Mean conc., fl/l	Standard deviation, fl/l	Coeff. of variation	Bias (pred./ meas.)	Correl. coeff., r	RMS error, fl/l	RMS error/ mean meas. conc.
Meadview, 12 hour averages							
Observed ocPDCH[1]	0.91	0.93	1.02				
DRI/CSU[1]	0.55	0.93	1.71	0.60	-0.04	1.39	1.53
HAZEPUFF[1]	1.88	1.60	0.85	2.07	0.14	1.99	2.18
NPS CMB[1]	3.64	1.57	0.43	3.98	0.18	3.20	3.50
Observed ocPDCH[2]	1.15	1.11	0.97				
BYU CMB[2]	0.15	0.14	0.94	0.13	0.11	1.51	1.32
Meadview, 24 hour averages							
Observed ocPDCH[3]	0.95	0.68	0.72				
DRI Semi-Gaussian[3]	0.77	1.40	1.81	0.81	0.00	1.56	1.65
Hopi Point, 12 hour averages							
Observed ocPDCH[4]	0.20	0.17	0.83				
VISHWA[4]	0.24	0.41	1.74	1.19	0.30	0.40	1.97
HAZEPUFF[4]	0.57	0.68	1.21	2.83	0.43	0.73	3.62
Observed ocPDCH[5]	0.24	0.16	0.69				
BYU CMB[5]	0.12	0.22	1.94	0.49	0.03	0.31	1.32

[1] For those 12-hour periods with DRI/CSU, HAZEPUFF, and NPS ocPDCH predictions at Meadview (n=81).
[2] For those 12-hour periods with BYU ocPDCH predictions at Meadview (n=41).
[3] For those 24-hour periods with DRI/semi-Gaussian ocPDCH predictions at Meadview (n=38).
[4] For those 12-hour periods with VISHWA and HAZEPUFF ocPDCH predictions at Hopi Point (n=99).
[5] For those 12-hour periods with BYU ocPDCH predictions at Hopi Point (n=53).

The RMAPS-predicted spatial patterns for emissions from the Colorado Valley Source showed significant impact south of MPP, while such impact was not observed in the tracer data.

Specifically, for 13 of these receptors, mostly located in the 180-degree sector to the south of MPP, the RMAPS predictions exceeded the maximum amount of particulate sulfur that could be created from MPP emissions. The excess was sometimes more than a factor of two and in all cases was well beyond the uncertainty bounds assigned to the RMAPS and PFT tracer calculations. Based on these observations, Green and Tombach (1999) concluded that the RMAPS predictions of the impacts of the Colorado Valley Source are not a valid representation of the impacts of MPP. The reasons for this discrepancy have not been analyzed.

8.3 Descriptions of Final Attribution Methods

Since the initial modeling approaches lacked skill in transporting emissions to the correct locations, it was decided to use the PFT information on the transport and diffusion of the MPP plume and of emissions from the other tracer sources to endeavor to produce more credible attributions of sulfate. As a result, all of the methods that were ultimately used to attribute air quality and light extinction impacts to the Mohave Power Project and other sources relied to some degree on the PFT measurements. These methods, which are described in this section and summarized in Table 8-2, provide the basis for the conclusions presented in Section 9. Full descriptions of their applications in Project MOHAVE are provided in the documents referenced in Table 8-2; copies of those documents that not generally available are included in Appendix C. Two of the methods (Modified CMB and Modified HAZEPUFF) are revisions of methods used in the initial evaluation (BYU CMB and HAZEPUFF, respectively).

It should be noted that those techniques that explicitly used the PFT information in their calculations are no longer general purpose models, but rather ones that have been "tailored" for Project MOHAVE and more specifically to the conditions during the tracer releases. These models cannot be assumed to have the same predictive ability in the absence of tracer data as they do when tracer data are available, especially when conditions differ from those that prevailed during the tracer releases. In that sense the source simulation models under these conditions are as limited in their forecast ability as are all receptor models.

Because of the limitations and uncertainties of the modeling methods, the results of any single method were not used in isolation to arrive at a source attribution. Rather, many different methods were used to reach consensus source attributions. As we describe below, mechanisms by which MPP and other sources could impact Grand Canyon National Park were conceptualized and then the modeling approaches were used to make the concepts more quantitative. The approaches used fall into two broad classes. Some of the approaches were quite rigorous but contained extreme assumptions, such as the assumption in the Tracer Max approach that 100% of MPP SO_2 is converted to sulfate, to make them tractable. Such approaches were useful for helping set the broad physical upper and lower bounds within which the actual attributions had to lie. Other approaches, that were typically theoretically more complex and used more realistic assumptions, were used to attempt to narrow the range within which the actual attribution might occur.

Brief descriptions of each method are provided below. Each technique has inherent in it some assumptions about atmospheric behavior. The key assumptions are discussed below and are summarized in Table 8-3.

Table 8-2 Methods Used to Estimate Source Contributions

Method	Description	Inputs	Outputs	Reference
RECEPTOR DATA ANALYSES				
Tracer Max (Tracer Scaling)	Estimation of total sulfur impacts by scaling PFT measurements; provides upper bound for potential sulfate impacts	PFT and particulate S concentrations at receptors; emission ratio of S/PFT;	Contribution of PFT source to ambient S; upper bound estimate of contribution to particulate S	Green and Tombach (1999)
Exploratory Data Analysis	Statistical analysis of SO_2, particulate sulfur, and PFT measurements	PFT, SO_2, and particulate sulfur concentrations and b_{sp} at receptors; meteorological classes	Spatial correlations of particulate sulfur, temporal correlations of PFT, SO_2, and particulate sulfur at specific sites	Mirabella and Farber (1999)
Tracer Regression	Regression of b_{ext} against PFT, industrial halocarbons, and water vapor mixing ratio	PFT, halocarbon, and mixing ratio measurements at receptors	Contributions to b_{ext} from emissions in source regions of the chosen tracers	White *et al.* (1999)
TAGIT	Estimation of sulfate impact by identifying unimpacted sites from PFT measurements	PFT and particulate S concentrations at multiple receptors	SO_2 and particulate S concentrations attributable to sources/source regions where PFT was emitted	Kuhns *et al.* (1999)
Modified CMB (MCMB)	Chemical mass balance receptor modeling, modified to account for conversion and deposition of SO_2 and sulfate	Source/source-regions and receptor concentrations of SO_2, sulfate, and markers -- elements, spherical aluminosilicate, b_{abs}; relative times of travel; ROME estimates of relative conversion rates for emissions from different sources/source-regions.	SO_x and sulfate attributable to sources/source- regions	Eatough, Farber and Watson (1999)
TMBR	Tracer mass balance regression; regressions of SO_2 against PFT and of particulate sulfur against PFT	Concentrations at receptors of PFT, SO_2, and particulate sulfur	SO_2 and particulate S concentrations attributable to MPP	Ames and Malm (1999)
DMBR	Differential mass balance regression; hybrid of tracer-based dilution calculation with parameterized deposition and conversion	Concentrations at receptors of PFT and SO_2; times of travel from source to receptors; estimates of conversion rates; index of cloud cover	SO_2 and particulate S concentrations attributable to MPP	Ames and Malm (1999)

Method	Description	Inputs	Outputs	Reference
SOURCE EMISSIONS SIMULATIONS				
Modified HAZEPUFF	Lagrangian puff model; interpolated wind field; first order sulfate chemistry	Wind profiler soundings, PFT and SO_2 emissions from MPP, relative humidity	Distribution of concentrations of PFT, SO_2, sulfate, and light scattering attributable to MPP	Latimer (1993); Mirabella (1996a; 1996b)
CALMET/ CALPUFF	Multi-layer Gaussian puff model with parameterized first order chemical conversion; diagnostic meteorological model	Surface and upper air meteorological data, topography, PFT and SO_2 emissions from MPP, solar radiation, ambient O_3	Distribution of concentrations of PFT, SO_2 and sulfate attributable to MPP	Vimont (1997)
RAPTAD/ HOTMAC/ ROME	Three-dimensional Lagrangian random puff model; primitive equation meteorological model; Lagrangian plume model with explicit reaction chemistry for gaseous and aqueous conversion of SO_2 and other species	Meteorological soundings, topography and land use, solar radiation; MPP emissions of PFT, SO_2, NO_x, and trace metals; background chemical concentrations; PFT concentrations at receptors	Complete meteorological field; distribution of concentrations of PFT, SO_2 and sulfate in MPP plume, at surface and aloft	Yamada (1997, 1999); Lu and Yamada (1998); Seigneur *et al.* (1997); Karamchandani, *et al.*, (1998);

Table 8-3 Principal Assumptions of the Apportionment Methods

Method	Emissions	Meteorology	Ambient AQ	Sulfur Chemistry	Deposition
RECEPTOR DATA ANALYSES					
Tracer Scaling (Tracer Max)	Constant ratio of MPP SO_2 to PFT emissions	N/A	N/A	100% conversion of SO_2 to particulate S, but not greater than measured value	No deposition
Tracer Regression	Halocarbon represents So. Calif. Source region and mixing ratio represent source region to south; all source regions accounted for by PFT, halocarbon and mixing ratio	N/A	N/A	N/A	No deposition
TAGIT	MPP is only cause for elevated S at tracer-impacted sites	N/A	Background particulate S spatially uniform	N/A	N/A
Modified CMB (MCMB)	Constant ratio of SO_2 plus particulate sulfur to marker species in emissions from all sources except MPP; incoming air mass composition represents profiles for other sources than MPP; halocarbon marks So. Calif. source region	Time of travel deduced from modeled wind field	None	Linear conversion; conversion rate for MPP emissions lower than regional rate; conversion rate for Las Vegas emissions higher than regional rate.	Linear; different rates for SO_2 and sulfate
TMBR	Constant ratio of MPP SO_2 emissions to PFT emissions	N/A	N/A	N/A	N/A
DMBR	Hourly emissions for SO_2 and PFT	Time of travel deduced from modeled wind field; index of cloud cover estimated from photographs	MPP emissions explain some of the observed variability in receptor SO_2	Linear conversion, with rate dependent on cloud cover index; rate "optimized" for best fit with SO_2 measurements	Linear; different rates for SO_2 and sulfate

Method	Emissions	Meteorology	Ambient AQ	Sulfur Chemistry	Deposition
SOURCE EMISSIONS SIMULATIONS					
Modified HAZEPUFF	None	$1/r^2$ interpolation of 3 wind profilers	None	Linear conversion rate based on solar radiation; aqueous conversion assumed to take place when RH > 80% at additional rate of 2%/hr	No deposition
CALMET/ CALPUFF	None	For Meadview impacts, wind field generally derived from MPP profiler sounding using 5-km grid CALMET diagnostic model; for regional impacts used 3 Project MOHAVE profiles with terrain blocking in model; calendar solar radiation, modified by cloud cover; modified PGT diffusion	Measured surface O_3 representative of conditions aloft	Conversion rate based on measured O_3 and RH; daytime "dry" conversion rate set at 2%/hr, "wet" daytime rate at 20%/hr for 3 hours per day, and nocturnal conversion rate at 0.2 %/hr,	Based on micrometeoro-logical parameter estimates for dry deposition and on measured rainfall for wet deposition
RAPTAD/ HOTMAC	None	Wind, temperature, humidity, and clouds derived by 4-km grid HOTMAC prognostic model nudged by data from 3 soundings and 3 radar wind profilers	N/A	None; modeled inert PFT tracer only	None
ROME	None	Used HOTMAC 4-km grid wind field	Assumed background chemical concentrations	Explicit chemical mechanisms for both gas phase and aqueous pahse	Linear; different rates for day and night, vary with species.
N/A _ parameter or calculation not applicable for this method None = No significant assumptions were made					

8.3.1 Tracer Max (Tracer Scaling)

The ambient PFT data, scaled by the tracer/SO_2 stack emission ratio, were used to deduce the maximum possible MPP contribution to particulate sulfur at Meadview and Hopi Point if all SO_2 were to be converted to particulate sulfur and there were no deposition losses (Green and Tombach, 1999). Whenever the maximum possible particulate sulfur that was calculated in this way exceeded the measured value, then the measured value was set as the maximum possible value (i.e., it was assumed that MPP contributed 100% of the measured particulate sulfate concentration).

Key assumptions of the Tracer Max method included the following: (1) The ocPDCH tracer and MPP sulfur (emitted as SO_2) were transported and dispersed identically together to the receptor; (2) There was no deposition of tracer or either MPP SO_2 or particulate sulfur enroute; and (3) The tracer/SO_2 emission ratio was constant (i.e., the PFT emissions rate tracked the variations in the SO_2 emissions rate). In actuality, SO_2 and sulfate will undergo some deposition enroute, while the tracer is essentially non-depositing; therefore the ratio of sulfur to PFT decreases in time. The assumption of a constant ratio means that more particulate sulfur is apportioned to the source than is correct.

The fundamental assumption of the Tracer Max tracer scaling approach is that all of the SO_2 is assumed to convert to particulate sulfate or at least enough of it is converted to match the sulfate concentration measured at the receptor. This assumption produces an upper-bound impact of the MPP source -- it is impossible to have a higher contribution. A lower contribution is certainly possible and is likely, especially in the cloud-free conditions under which sulfate formation proceeds slowly.

The confidence in the validity of these upper bound estimates of MPP sulfur contributions is high. It needs to be re-emphasized, however, that the Tracer Max estimates do not indicate what a realistic contribution might be.

8.3.2 Exploratory Data Analyses

Statistical, temporal, and spatial relationships between the ambient concentrations of the PFT released from MPP, SO_2, and particulate sulfur, and of light scattering, measured during the summer intensive were analyzed by Mirabella (1997). This analysis provided qualitative insight into the contributions of MPP to SO_2 and particulate sulfur in various regions and compared the behaviors of these four variables.

Specifically, Mirabella (1997) compared the 24-hour average MPP tracer, sulfur dioxide, and particulate sulfur concentrations across the network and analyzed the spatial and temporal correspondence between these three parameters in addition to light scattering at various individual sites. In addition, the authors examined the correspondence between MPP tracer and light scattering at Meadview for 12-hour and 1-hour averaging time periods. Using a previously-developed meteorological classification scheme (Farber et al., 1997), Mirabella (1997) also evaluated whether their conclusions differed under various meteorological regimes.

8.3.3   Tracer Regression.

The tracer regression method (White *et al.*, 1999) attempts to explain light extinction at Meadview based on contributions from three sources – MPP, Southern California, and southern Arizona/northern Mexico. The light extinction is related to these source contributions through multiple linear regression, in which assumed markers for each of the three sources are the independent variables and b_{ext} at Meadview is the dependent variable. Methylchloroform (an industrial solvent) is taken to represent urbanized Southern California, the mixing ratio of water vapor to air is taken to represent the contribution of air from more humid regions to the south, and the PFT to represent MPP emissions. In each case, the tracer is assumed to be a conservative indicator, as required by the receptor-oriented regression procedure

The principal assumptions of the tracer regression method have to do with the source regions represented by each tracer. Except for the use of PFT as an MPP indicator, these assumptions involve approximation. It is possible that methylchloroform is emitted from industries in other locations besides Southern California. Moist air does not come only from the south of Meadview, although that locale is probably the predominant source region in the summer period for which the method was applied. In either case, if the tracer is not unique to the region or source to which it is assigned, then emissions will be attributed erroneously to that region or source.

It should also be noted that any regression analysis of this kind will underestimate attribution if the "signal" is noisy, as would be the case if the light extinction were to vary because of unaccounted for background effects. (This limitation also applies to other regression based methods such as TMBR below).

8.3.4   TAGIT

The Tracer-Aerosol Gradient Interpretive Technique (TAGIT) (Kuhns *et al.*, 1999) uses PFT data to identify sites which are not significantly impacted by MPP during specific sampling periods and can be considered to represent the regional background concentration. The MPP-attributable particulate sulfur at a receptor is calculated as the measured excess concentration of sulfur over that at nearby sites with background levels of tracer. Sites with tracer levels below 3 sigma of the background concentration were considered to be representative of regional background sulfur concentrations.

The accuracy of TAGIT depends on the assumption that the only cause for increased sulfur above the regional background at locations where PFT is found is emissions from MPP. Under certain conditions, such as when another source is along a trajectory that intercepts the MPP, it is possible that this assumption will be violated, but there is no way to quantify when this occurs. Under those conditions TAGIT will erroneously apportion to MPP the sulfur from the non-MPP source. Because the difference in sulfur particle concentrations in PFT impacted and unimpacted areas is sometimes small, it is possible for TAGIT to attribute a negative concentration impact to MPP. The precision of the TAGIT attribution can be estimated when there are several nearby sites reporting background tracer concentrations near the impacted receptor. For many instances, the variability of these multiple estimates were larger than the particulate sulfur attributed to

MPP by TAGIT. While individual attibutions by TAGIT are noisy, the method is likely to provide credible results of average attribution over the study period.

8.3.5   Modified CMB (MCMB)

The CMB technique involves correlation of the composition of the aerosol at receptors with "profiles" of the composition of emissions from various classes of sources. The product of the analysis is an apportionment of the receptor SO_x (the sum of SO_2 and particulate sulfate) to the selected classes of sources. In its basic form the technique is only usable for conserved species, i.e., ones that do not undergo chemical conversion.

The basic BYU CMB method that was used initially, as described in Section 8.2, was modified into a hybrid technique that includes a representation of chemical conversion of SO_2 to sulfate particles (Eatough, *et al.*, 1999). Slightly different variants of the technique were used for the summer and winter intensive periods. We focus here on the approach that was used for apportionment of sulfur oxides and sulfate at Meadview and Hopi Point during the summer intensive.

The Modified CMB (MCMB) method uses several elemental and chemical tracers of opportunity as marker species for MPP and major source regions (the Las Vegas area, urban Southern California, the San Joaquin Valley, Baja California, southern Arizona and northern Mexico). The source profile for each source region was determined by measuring the elemental and chemical composition of ambient aerosol approaching the study area from the direction of the source of interest. The chemical conversion of SO_2 to sulfate is addressed using reactivities derived from the ROME modeling (see below) and from optimization of assumed linear conversion rates. The transport routes and times of travel are defined by several wind field models and the potential for clouds to affect the chemistry during the transport of MPP emissions is addressed through the Cloud Interaction Potential (CIP) of the DMBR model (see below). It is important to note that the PFT concentration data were used in the evaluation and modification of the model, but are not used as input data.

Fundamental assumptions of the MCMB method are the equal conservation of the tracer and target species and that all significant contributors to SO_2 and sulfate at Meadview and Hopi Point are identified in the CMB profiles. A further assumption in the MCMB approach is that the ratio of SO_x (sum of SO_2 and sulfate) to the marker species in the source profiles is constant from day to day. Profiles and the profile uncertainty for regional sources, such as Southern California, were developed from ambient measurements at substantial downwind distances during a few days. If the ratios vary outside the determined uncertainty or represent mixes of materials from different source regions the method will apportion SO_2 and sulfate incorrectly among sources. Furthermore, regional profiles tend to be more collinear and less orthogonal than profiles for discrete source types.

The MCMB application also assumes that SO_2-to-sulfate conversion rates at any given time are the same throughout the modeling domain for emissions from all sources except Las Vegas and MPP. Las Vegas and MPP conversion rates can be higher and lower, respectively than the conversion rates from other sources. Results of the ROME model calculations were used to parameterize the relative reactivities of emission from MPP and Las Vegas as compared to other

sources. Sensitivity tests have shown that the apportionment of sulfate to sources is sensitive to the relative values that are used.

The MCMB analysis was not able to apportion all of the sulfur oxide present at Meadview for some samples. It was assumed the underattribution of sulfur oxide was due to separation of particles and gases in the nighttime stable MPP plume and the unattributed SO_2 was therefore assumed to have originated from MPP.

8.3.6 TMBR

Tracer Mass Balance Regression (Malm *et al.*, 1989; Ames and Malm, 1999) compares the covariance of SO_2 or particulate sulfur measurements with those of the PFT through an ordinary least-squares regression. The regression coefficients are interpreted as indicators of the attribution of the sulfur constituent to MPP.

The merit of the TMBR is the significance of the regression coefficient (P=.03) which allows us to state that there is a highly significant statistical relationship between PFT concentration and ambient sulfate concentration at Meadview. That only a small fraction of the ambient SO_4 variability is explained by PFT ($r^2 = 0.06$) is not surprising, and TMBR neither makes nor does it rely on any assumptions about what this covariability should be. A low correlation coefficient is not counterintuitive given the non-linearity of secondary sulfate production.

8.3.7 DMBR

Differential Mass Balance Regression (Latimer *et al.*, 1989, Ames and Malm, 1999) expands on the TMBR approach by explicitly considering the conversion of SO_2 to particulate sulfur. In this hybrid approach, information about transport time from source to receptor and cloud cover is used with linear conversion and deposition rates to estimate the particulate sulfur concentration at the receptor. The rate constants for the conversion of SO_2 and for SO_2 deposition were chosen by statistical optimization of the correlation between the predicted MPP contribution to SO_2 at Meadview and the measured SO_2. This optimization procedure makes no *a priori* assumption about the amount of variability explained by the MPP contribution to ambient SO_2.

In addition to the usual constraint on equivalent behavior of tracer and sulfur emissions, the DMBR method estimates the amount of conversion of SO_2 to particulate sulfur based on a linear conversion rate. The time of travel is estimated from a wind field model and an hourly conversion rate was derived empirically based on a Cloud Interaction Potential (CIP) and the measured concentrations of SO_2. The CIP, derived from observations of clouds in photographs, attempts to reflect the presence of cloud water in the conversion process. But, since the height of the clouds cannot be readily deduced from the photographs, the CIP is a crude indicator of the effect of cloud water on chemical reactions at the MPP plume height.

8.3.8 Modified HAZEPUFF

HAZEPUFF (Latimer, 1993) is a puff model that simulates the transport, diffusion, and deposition of puffs emitted hourly from a source. The puffs are advected by an externally prescribed wind field and diffuse at rates based on the common Pasquill-Gifford stability classes.

Conversion of SO_2 to sulfate takes place linearly in dry air at rates computed by the model based on solar radiation. Whenever the ambient relative humidity is above 80% it is assumed that clouds are present and an additional aqueous conversion rate of 2%/hr is added to the dry rate. Dry deposition is treated linearly with deposition velocities of 0.91 and 0.14 cm/s for SO_2 and sulfate, respectively. HAZEPUFF does not consider wet deposition.

Since HAZEPUFF had limited skill in predicting MPP impacts during the initial model evaluation (See Section 8.2), it was modified for the final attribution assessment. The principal change was an adjustment in stability classes, which reduced the tendency of the model to overestimate concentrations. Also, the puff cross sections were made Gaussian, which is more realistic than the "top-hat" profiles used initially. The wind field used was derived from the three Project MOHAVE wind profilers. These changes improved the performance of the model, when tested against the PFT measurements, giving a bias of 0.84 and $r^2 = 0.24$ at Meadview for 24-hr averages of the PFT concentrations. The correlations for 12- and 1-hr averages were lower than the 24-hr correlations.

8.3.9 CALMET/CALPUFF

CALMET/CALPUFF is a combination of a diagnostic meteorological model (CALMET) and a Lagrangian puff air quality model (CALPUFF). Hourly radar profiler wind data taken during the summer intensive period provide the input data for CALMET. This modeling system was applied only after the PFT data had been made available, and the PFT information was used for making the choice of input wind data.

The CALPUFF/CALMET system was used to simulate two types of conditions, both of which may be considered as bounds to the range in which actual impacts of MPP might lie. One type of conditions, which was simulated for most of the 1992 calendar year (see Section 9.6), is based on the assumption that all sulfate formation took place in cloud-free air. This can be considered to produce a lower bound to the extend of actual sulfate formation. The other type of conditions, which was simulated only for the summer, is based on the assumption that the MPP plume interacted with clouds for a specified period of time each day. Because clouds were not present every day and the assumed period of interaction was long, this condition was taken to approximate an upper bound to potential MPP impacts.

For the first type of conditions, the internal chemistry algorithm of the model was used to calculate the conversion of SO_2 to sulfate. This algorithm is based on homogeneous, "dry" chemistry. For the second type of conditions, where the Mohave Power Plant plume interacts with clouds, aqueous phase chemistry is likely to occur, which would result in much higher conversion rates than the internal algorithm of the model would predict. Therefore, as a bounding exercise, for the the second analysis it was assumed that all the plume material interacted with clouds for three hours every day and the SO_2 was converted to particulate sulfate at a rate of 20% per hour during those three hours. These two analyses, labeled "CALPUFF Dry" and "CALPUFF Wet," respectively, can be considered as estimates of lower and upper bounds to the impacts of MPP emissions

The initial settings and choices of input meteorological data were selected to improve comparisons between predicted and measured PFT concentrations (Vimont, 1997). The wind

fields generated by the CALMET diagnostic meteorological model were derived from three Project MOHAVE radar profilers. The final calculations, which were done for most of the year, were made using only the MPP profiler because it was the only one that operated for nine months. The ability of CALPUFF to predict PFT tracer concentrations was degraded slightly when only the MPP profiler was used for input data. The grid scale of the wind field was 5 km, which is sufficient to represent major topographic features but will smooth over many smaller ridges, peaks, and valleys. The Pasquill-Gifford-Turner (PGT) diffusion algorithm, with transitioning to time-dependent dispersion curves at longer distances, was used to represent the plume diffusion.

CALPUFF simulates daytime SO_2 conversion to particulate sulfur using a linear mechanism with a conversion rate that is based on solar radiation, PGT class, ambient ozone concentration, and relative humidity. The algorithm produces a maximum conversion rate of about 4%/hr at 100% RH, which is lower than generally-accepted peak aqueous conversion rates. On the other hand, the algorithm does not attempt to quantify the time spent in clouds, which could produce a lower hourly-average rate than the peak that occurs whenever the plume is in a cloud. Both of these factors were addressed in the "CALPUFF Wet" upper-bound aqueous conversion calculations by selection of a 20%/hr conversion rate for three hours per day in clouds.

The CALMET/CALPUFF system, with SO_2 conversion turned off, was tested against the PFT data. Two different comparison tests were performed. In the first test, the concentration predicted to occur at the receptor located at the coordinates of the monitor, or at one of the 8 adjacent receptors, was compared with the PFT measurement. The one value of these 9 that best matched each measurement was used in a statistical evaluation of model performance. This test, therefore, assesses how well the measurement was approximated by the model prediction, even though meteorological uncertainty may have cause the prediction to slightly miss the correct receptor location. For Meadview, using only the MPP wind profiler data, the correlation in this best-of-nine comparison was $r^2 = 0.47$. The correlations were even higher at Las Vegas Wash (LVWA; $r^2 = 0.81$) and Dolan Springs (DOSP; $r^2 = 0.80$). These values suggest that the model's transport and diffusion mechanisms are fundamentally sound.

As one might expect, the prediction at the exact receptor cell correlated less well with the PFT measurement there. These correlations were $r^2 = 0.00$ at Meadview and Las Vegas Wash and $r^2 = 0.08$ at Dolan Springs. Such values are similar to those tabulated in Table 8-1 and indicate that the CALMET/CALPUFF system was no better at predicting impact at a specific point than were the methods evaluated initially. Since the CALMET/CALPUFF calculations did not explicitly use the PFT data, such a conclusion is not surprising.

Nevertheless, because of its credible performance in the best-of-nine cell comparison and its computational efficiency, the CALMET/CALPUFF modeling system was used to develop a general estimate of the magnitudes of impacts that might be expected under specific conditions. The conditions chosen were the bounding conditions of, first, a totally cloud-free atmosphere and, second, one with an arbitrary degree of in-cloud conversion. Neither the CALPUFF Dry nor CALPUFF Wet simulation should be considered a realistic representation of impacts under the varying meteorological conditions that actually occur.

8.3.10 HOTMAC/RAPTAD/ROME

The most explicit simulations of the project involved three atmospheric models applied for the period August 6 through 16, 1992. The three-dimensional mesoscale prognostic meteorological model HOTMAC was used for simulating airflows. The three-dimensional Lagrangian transport and diffusion model RAPTAD was used for simulations of transport and diffusion of an inert species (e.g., tracer gas). The result was a 3-dimensional field of winds, turbulence, temperature, and clouds with a horizontal resolution of 4 km. The ROME reactive plume model was then used to simulate chemical reactions and particle formation in the plume.

The turbulence parameterization in HOTMAC is treated in a more rigorous manner than the PGT classification used in CALMET. The combination of HOTMAC and RAPTAD is designated as an "alternative guideline model" in Appendix B of the U.S. EPA's Guideline on Air Quality Models. The application of HOTMAC and RAPTAD here is described in Yamada (1999).

Rawinsonde data on wind, potential temperature, and water vapor mixing ratio at Cottonwood Cove, Dolan Springs, and Page, and radar wind profiler data from Mohave Power Plant, Truxton, and Meadview were used to provide initial and boundary conditions to HOTMAC simulations. The HOTMAC meteorological predictions above 374 m AGL were also "nudged" by these measurements.

RAPTAD used the wind and turbulence distributions modeled by HOTMAC and simulated ocPDCH tracer concentrations from MPP at sampling sites in the study area. Also, hypothetical releases from Reid Gardner Power Plant and the Las Vegas area were simulated.

The RAPTAD-modeled tracer concentrations were compared with the 12-hour or 24- hour averaged concentrations measured at sampling sites in the study area. The overall performance of the model over 8 sites for 11 days gave a bias of 1.54 (i.e. the model values averaged 1.54 times the measurements) and $r^2 = 0.61$. The best performance occurred at Dolan Springs ($r^2 = 0.93$) and Kingman, ($r^2 = 0.83$), based on 11 data points for each. At Meadview alone, however, the 24-hr r^2 was 0.11 and the bias was 2.01, based again on only 11 data points. At Hopi Point, the r^2 was 0.03, with a bias of 0.63.

Using the HOTMAC/RAPTAD plume trajectories and diffusion, the reactive plume model, ROME (Reactive and Optics Model of Emissions) was used to estimate the contribution of the MPP to sulfate concentrations in the Grand Canyon region for portions of the same summer period of August 6 to 16, 1992 (Karamdanchani *et al.*, 1998). ROME uses a Lagrangian approach to describe the transport and dispersion of a plume emitted from a stack, and simulates the gas- and aqueous-phase chemical reactions that occur as the plume mixes with the background air. The model includes state-of-the-science formulations of the governing atmospheric processes as described in Seigneur et al. (1997). The model has been tested for a number of applications similar to the Project MOHAVE exercise (e.g., Seigneur et al., 1999; Gabruk et al., 1997).

Selected HOTMAC/RAPTAD plume trajectories originating at MPP and arriving at Meadview or Hopi Point were simulated, taking the plume height to be the initial value calculated by the model. Measured tracer concentrations at these two locations were used to scale modeled sulfate concentrations attributable to MPP emissions of SO_2. Particulate sulfate measurements at

Meadview and Hopi Point were used to estimate MPP sulfate contribution relative to measured values. Trajectories were selected based on their potential for interaction with clouds, their proximity to the two receptor locations, and their plume dimensions to provide a comprehensive representation of the range of MPP plume settings that impact the two receptors.

Ambient (background) concentrations were inferred from limited surface and aircraft measurements of VOC, CO, ozone, NO_x, H_2O_2, SO_2, NH_3, Fe and Mn concentrations from the Project MOHAVE database. Literature review and consultation with experts were used to obtain background concentrations for species that were not measured, such as formaldehyde, other aldehydes, and PAN.

Plume conditions, including plume trajectory data (location, width, and vertical mixing) and meteorological data (temperature, relative humidity, pressure, and cloud liquid water content) were based on the HOTMAC and RAPTAD output. Emissions of SO_2, NO_x and PFT from MPP and the measured ratios of MPP Fe and Mn emissions to SO_2 emissions were other inputs.

Wherever information needed to conduct the simulations was not available or was available in the form of a range, the conditions chosen were those that would provide an estimate of the largest reasonable MPP contribution to the sulfate concentration at the receptor. In addition, sensitivity studies were conducted by varying several input parameters over their plausible range of values.

Clouds were assumed to exist whenever the estimated cloud water content (from HOTMAC output) was higher than 0.01 g/m^3. All such cases during the 11-day period were simulated. Net updraft velocities in clouds were assumed to be zero.

The MPP puffs were assumed to be non-overlapping to maximize the SO_2 oxidation rates under oxidant limited conditions in the plume. Realistic, but lower than expected dry deposition velocities for SO_2 and sulfate were used. This would contribute to a slight overestimation of atmospheric SO_2 and sulfate concentrations.

8.3.11 Evaluation of Windfields

An important component of the numerical models used to apportion MPP SO_2 and sulfate is the accuracy of the windfields. Koracin *et al.* (1998) developed a method that utilizes tracer measurements to compare and evaluate wind fields as predicted by different atmospheric models or obtained from interpolation and extrapolation of measurements. The technique evaluates only the windfields prior to the incorporation of dispersion calculations. Windfields that transport tracer close to the receptors with high measured tracer concentration score highest using this method. Details of the method are provided in the Koracin *et al.* paper, which is included in Appendix C. The main objective of the method is to quantitatively describe and indicate which wind fields are best able to reproduce the main transport of tracers. The method has been applied to MPP tracer (ocPDCH) measurements conducted in summer 1992. Wind fields obtained from four atmospheric models CALMET (Vimont 1997), HOTMAC (Yamada and Bunker 1988), MM5 (Grell et al. 1995), EK (Enger et al. 1993, Koracin and Enger 1994) were tested. For the limited period in which windfield data were available from all four models (8/6/92 – 8/13/92), the analysis indicated that the performance of the CALMET, EK, and MM5 and wind fields were

comparable, while HOTMAC scored slightly higher for the 10 day it was employed(i.e. was more accurate) than the other models.

8.4 Computer Simulation of Visual Air Quality

In order to assist in interpreting the quantitative data on the MPP impact on the light extinction coefficient, b_{ext}, that was developed using the models described above, various levels of visibility degradation in typical Grand Canyon National Park views have been displayed in images that can be viewed on a computer screen. Two views in GCNP, one at Tuweep, at the western end of the park, and the other at Desert View, located east of Hopi Point, were used for this purpose. In each case, mathematical models of radiative transfer were used to calculate the changes in the appearances of these views due to various levels of light extinction. The approach used to generate these simulated views is described here. The actual views are contained in a CD-ROM that accompanies this report and are described in Section 9.8.

8.4.1   Radiative Transfer Concepts

Radiant energy, as it passes through the atmosphere, is altered by the scattering and absorption by gases and particles. Image-forming information is lost by scattering of radiant energy out of the sight path and absorption within the sight path. Further, ambient light from direct, diffuse, and reflected radiance is scattered into the sight path. This adds radiant energy called "path radiance" to the observed radiation field, so that

$$N_r = N_o T_r + N^*$$
(8-1)

where:

N_r = observed image radiance at distance $= r$
N_o = inherent image radiance at distance $= 0$
T_r = transmittance of sight path of length $= r$
N^* = path radiance of sight path

The transmittance of the sight path is calculated from measured extinction or the distribution of particles and gases along the sight path. The path radiance is more difficult to estimate. A reasonable assumption under uniform illumination (cloud free sky or uniform overcast) is to estimate the path radiance with an equilibrium radiance model:

$$N^* = N_s(1 - T_r)$$
(8-2)

where N_s = sky radiance at horizon above sight path

These equations can be applied to each pixel of a photographic image, to represent the effect of the atmosphere on that image.

The bulk atmospheric optical properties such as extinction, scattering, and absorption coefficients, single scattering albedo, and the scattering phase matrix are required to apply the above equations to each element of a scenic view. They are calculated by an aerosol model. The Mie theory model assumes spherical particles for externally-mixed, homogeneous or internally-mixed, coated aerosols.

A backward photon trajectory, multiple scattering, Monte Carlo, radiation-transfer model was used to calculate sky radiances. The inherent radiance of each terrain pixel was estimated with the equilibrium radiance model, sky radiance model, and distance to the target for each pixel.

The modeled image radiance field for a selected level of extinction was then calculated by first using the new extinction value and distance to each terrain pixel to calculate a new path transmittance. Second, the new path radiance was calculated using this transmittance and modeled sky radiance in Equation 8-2. Third, the new apparent image radiance field was calculated by using these values in Equation 8-1. These new image radiance files were then used in the image processing modules to generate the final images, as described below.

8.4.2   Image Processing Techniques

The original images that started the process described above were two 35 mm color slides taken at Tuweep and Desert View. The slides necessarily represent cloudless skies under the cleanest visual air quality conditions possible. Aerosol and optical data associated with the day the picture was taken were also used.

Color film may be regarded as a measurement tool that creates a map of an incident image spectral radiance field. The film's red, green and blue emulsion layers collect the radiation and convert it through chemical changes to exhibit varying density values related to the initial scene element radiances. The time interval that the film views the scene multiplied by the radiance of the scene element is known as the exposure of the film. Since every pixel of a slide is exposed for the same time interval, the varying densities are directly related to the initial scene element radiance (N_r).

The slide image was digitized through three wide band filters at different colors. The typical spectral function results in nearly Gaussian filters with peaks centered near 650 nm (red), 550 nm (green), and 450 nm (blue), with little overlap of the effective filter responses. Each terrain pixel in the image was then assigned a specific distance, elevation angle and azimuth angle with respect to the observer position, using detailed topographic maps of the area.

To produce the new image, which displays the scene appearance at a chosen level of extinction, the above information was used in the calculation of a new radiance field. That modeled radiance field describes the appearance of every pixel on the photograph, each of which has been altered by the scattering and absorption that were artificially added to the initial image. The results, when viewed as a photograph or on a color computer monitor, then portray the original digitized photograph under the different atmospheric conditions. The two views are portrayed under 13 different extinction levels in the CD-ROM enclosed with this report.

8.4.2   Human Perception of Visibility Change

In order to better understand the perception of the changed visibilities in the images on the CD-ROM, it is useful to briefly discuss some aspects of the human perception of visibility changes.

Human perception of changes in visual air quality is a complex function of atmospheric properties such as lighting conditions, cloud cover, and ambient extinction; scene characteristics

such as size, shape, color, texture and distance to features; and observer characteristics. A robust complete model of human perception of visual air quality has yet to be developed. Nevertheless, reasonably valid concepts can be developed from a simple analysis of apparent target contrast:

$$C_r = 1 - \left(\frac{t N_r}{s N_r} \right)$$

(8-3)

where:

$$
\begin{array}{lll}
C_r & = & \text{apparent target contrast at distance r} \\
{}_t N_t & = & \text{background sky radiance at distance r} \\
{}_s N_r & = & \text{target radiance at distance r}
\end{array}
$$

Apparent target contrast can be further defined as:

$$C_r = C_0 \exp(-b_{ext} r) \left(\frac{s N_0}{s N_r} \right)$$

(8-4)

where:

$$
\begin{array}{lll}
C_r & = & \text{apparent target contrast at distance r} \\
C_0 & = & \text{inherent target contrast at distance } r = 0 \\
b_{ext} & = & \text{average extinction coefficient of sight path} \\
r & = & \text{distance to observer} \\
{}_s N_0 & = & \text{sky radiance at target } r = 0 \\
{}_s N_r & = & \text{sky radiance at distance r}
\end{array}
$$

Apparent target contrast is a good indicator of visibility. As the extinction goes up, C_r decreases, (i.e. the target becomes less noticeable). As extinction decreases, the target becomes more noticeable (i.e. darker against the background). Apparent target contrast can be used to determine whether the target can be perceived and, when perceived, the apparent contrast can also be used to evaluate the visual quality of its appearance.

With the assumption of equal sky radiances at the target and observer (uniform illumination of the scene), equation 8-4 reduces to:

$$C_r = C_0 \exp(-b_{ext} r)$$

(8-5)

Equation 8-5 can now be used to determine the change in C_r for various targets as a function of changes in extinction. For example, Figure 8-1 plots the calculated changes in contrast (delta contrast) of targets from 1 to 100 km distant as a function of percent changes in extinction at Grand Canyon National Park during a condition representative of the MOHAVE summer intensive. An inherent contrast of -0.80 was assumed for all targets, which approximates the appearance of a dark scenic element against the horizon sky.

As extinction is decreased, at some level of delta C_r, changes in visual air quality become perceptible. There is uncertainty as to the actual size of delta C_r that is detectable, and the value differs from individual to individual and varies with viewing condition. A value of 2% contrast change (delta C_r = 0.02) is sometimes used as an approximation, and that value is marked on Figure 8-1. With an assumed perceptible threshold of 0.02 in delta C_r and the assumed target

contrast of –0.80, Figure 8-1 indicates that all targets past 15 km distant will experience perceptible changes in apparent contrast (i.e., delta $C_r > 0.02$) with a 10% decrease in the light extinction coefficient. If the target has less contrast or the human perception threshold is larger, then a larger change in extinction will be required to produce a perceptible change. For example, if the contrast change threshold is 0.05 (another values that is sometimes used), then the decrease in light extinction would be imperceptible on Figure 8-1.

The simplified model illustrates some of the general concepts of detection of visibility change. Real scenes have elements of varying contrasts and color at different distances, and so their response to a change in extinction is not easily shown quantitatively. The images on the CD-ROM provide a qualitative representation.

We should note here that the fractional change in extinction is generally considered to he proportional to the human response, e.g.., a 20% change in extinction is perceived similarly whether the change in visibility is from 100 km to 80 km or from 10 km to 8 km. This is the basis for the deciview scale for representing extinction (Pitchford and Malm, 1994).

The simulation of human perception of actual scenes by using photographs or computer images is not perfect, however. Based on color matching experiments performed at the Grand Canyon, Henry (1999) points out that such images are less colorful and more blue than the true scenic view that is observed on site. These conditions appear to derive from the limitations of the photographic film that is the basis for the initial images that were digitized. A consequence of these limitations is that the artificial images overstate the visual effects of increasing haziness.

Consequently, one should not rely on the computer images to provide quantification of thresholds of human perception of visibility change in terms of extinction changes. Rather, these images should be considered approximations that portray the essential effects of extinction change, albeit only semi-quantitatively.

8.5 Discussion of Assessment Results

Each of the assessment methods except Tracer Regression and the exploratory data analysis produced estimates of the MPP-contributed sulfate at Meadview during the summer intensive monitoring period. Several methods also provided results at Hopi Point and/or for the winter intensive monitoring period.

Time plots of the 12-hour estimated MPP-contributed sulfate at Meadview and Hopi Point for all of the assessment methods are shown in Figure 8-2 through Figure 8-7. TAGIT results, which are limited to 24-hour duration estimates, are displayed as double 12-hour points at the same level for each day. Note that TAGIT occasionally produces negative contribution estimates. These occur when the particulate sulfur concentrations at nearby monitoring sites with little or no tracer were, on average, somewhat higher than that at the receptor site. These negative values should be interpreted as zero contribution by MPP.

All methods agree on the relative importances of the four site - season combinations (compare vertical scales), with Meadview having greater impact in either season than Hopi Point and summer showing greater impacts than winter. Meadview summer measured particulate sulfate and a method labeled Tracer Potential are also shown in Figure 8-4. Tracer Potential is Tracer
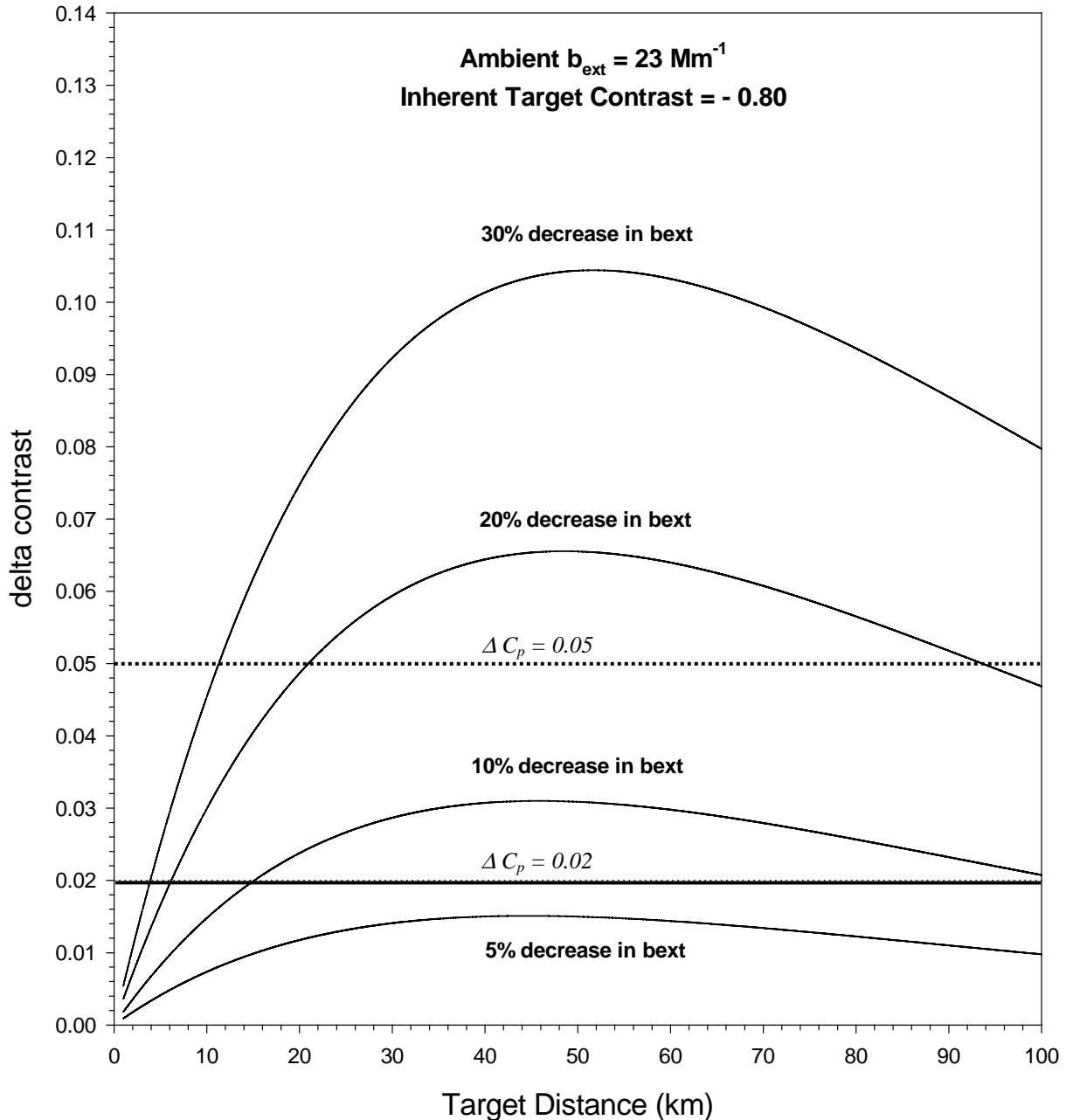
Figure 8-1 Change in apparent target contrast for % change in ambient extinction.

Max without the constraint of substituting the measured sulfate from the tracer scaled SO_2 when the tracer scaled SO_2 exceeds the measured sulfate. Thus, Tracer Max (not plotted) is either equal to measured sulfate or Tracer Potential, whichever is lower. It was included in this plot to show the effects of that constraint, which is important for about half of the summer intensive monitoring periods at Meadview. This was done to show that there are many periods where the tracer data provide a considerably more restrictive upper bound than the measured sulfate.

The Meadview summertime plot is the most useful for the comparison of the various methods' estimates. Many, but not all, methods agree on which time periods have relatively high estimates
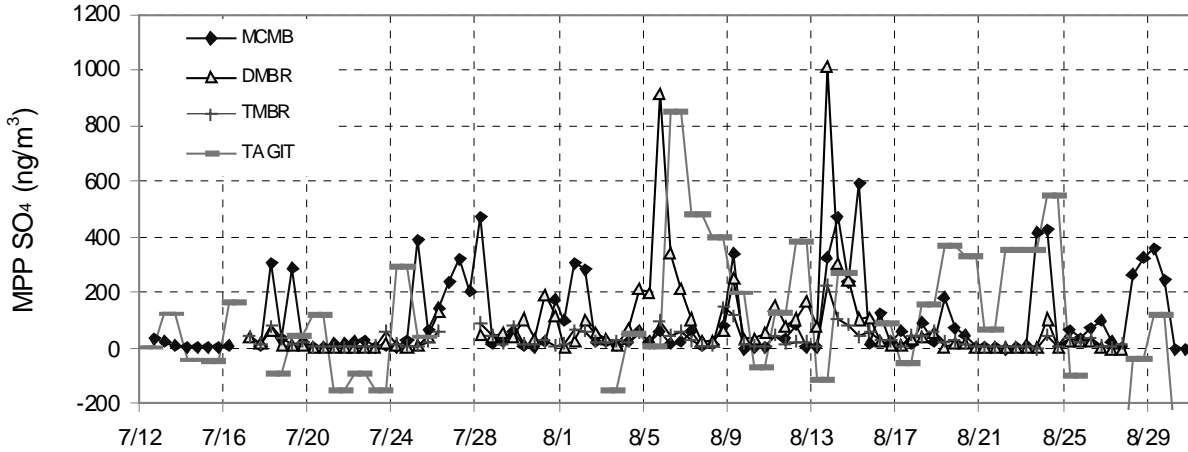
Figure 8-2 Source attribution sulfate time series from receptor models for MPP at Meadview during the summer intensive.
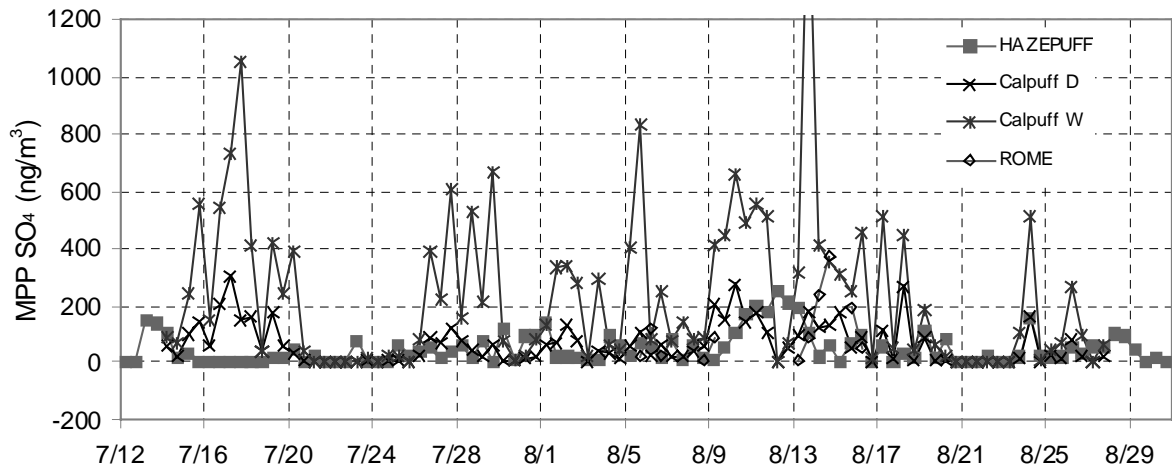
Figure 8-3 Source attribution sulfate time series from simulation models for MPP at Meadview during the summer intensive.
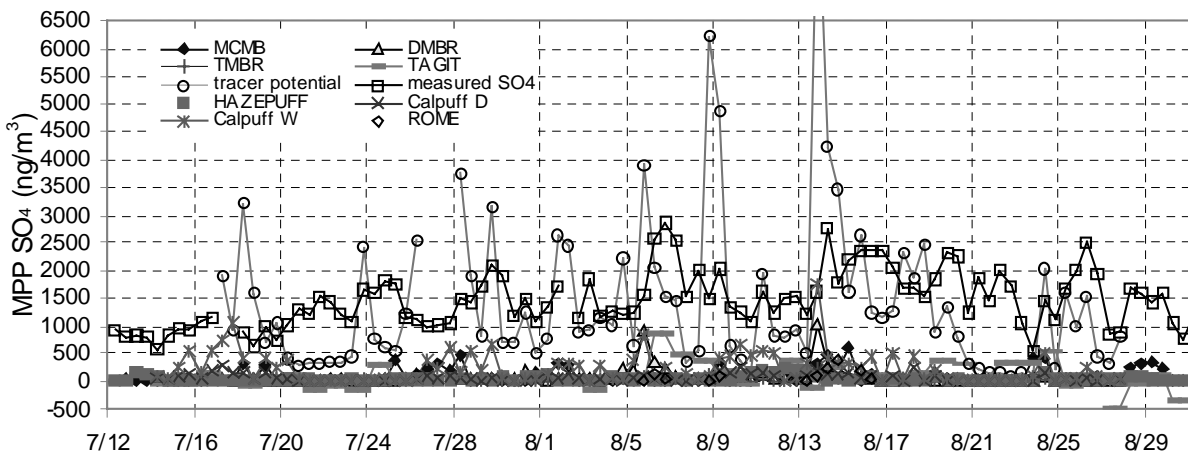
Figure 8-4 Source attribution sulfate time series from all models for MPP at Meadview during the summer intensive. Measured sulfate and tracer potential are also included for comparison.
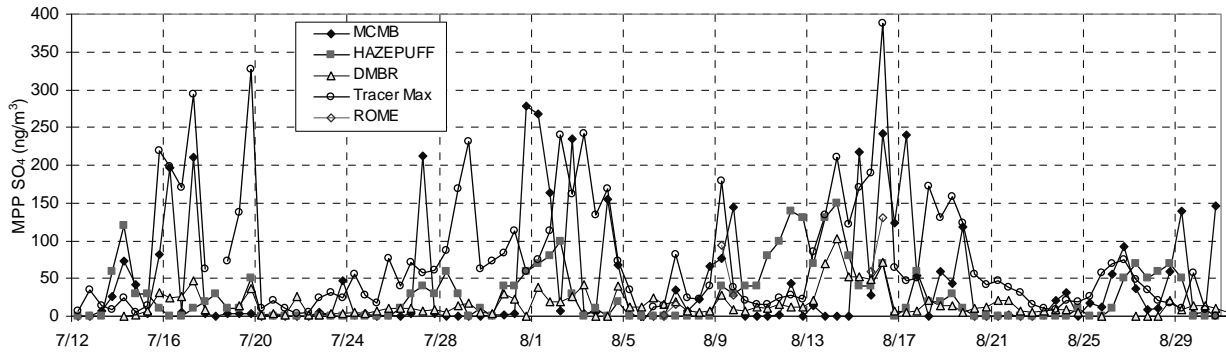
Figure 8-5 Source attribution sulfate time series for MPP at Hopi Point during the summer intensive.
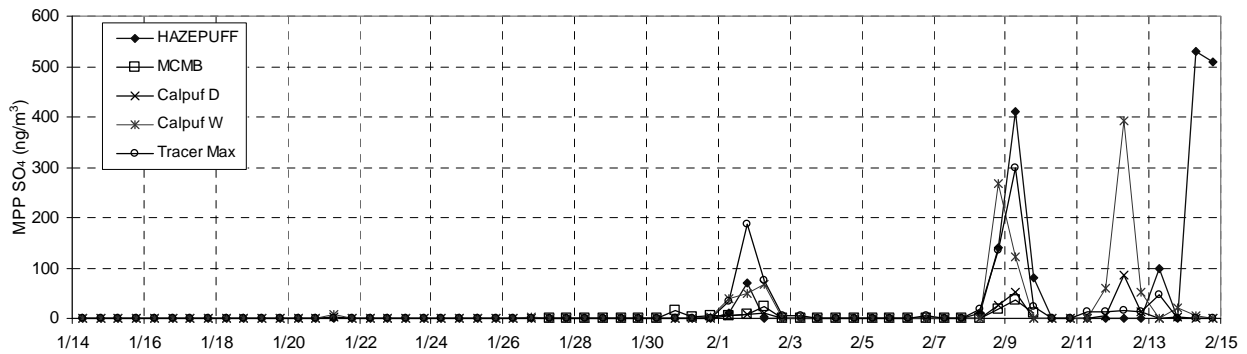
Figure 8-6 Source attribution sulfate time series for MPP at Meadview during the winter intensive.
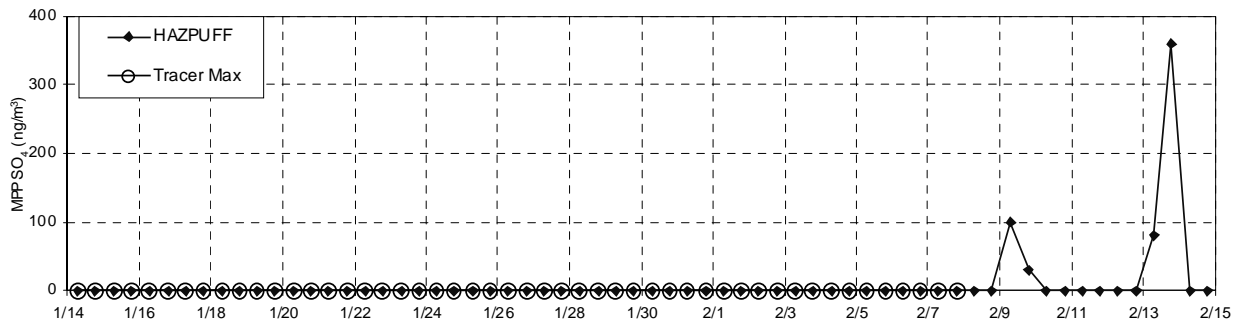
Figure 8-7 Source attribution sulfate time series for MPP at Hopi Point during the winter intensive.

of MPP sulfate contributions. Much of the agreement can be explained as due to the common use of tracer concentration or the skill of some methods to estimate it (all methods except TAGIT and HAZEPUFF). For these methods that tend to agree on high impact periods, only high tracer concentration periods are candidates for high estimated MPP contribution to particulate sulfate. Variations in the peaks among these methods are probably mostly due to differences in the approaches used to represent the process of SO_2 to particulate sulfate conversion. For example, CALPUFF Wet assumes some wet conversion for every time period and so it estimates peaks

from July 15 to July 20 where the other methods, by assumption or by incorporation of data, knew that only dry chemistry occurred on those cloud-free days.

Among the methods that used tracer data, TAGIT is unique in that the PFT concentration was not used to determine the primary emission impact of MPP at the receptor site. It was only used to classify sites as MPP-impacted or background sites, so that the average particulate sulfate concentration at the background sites could be subtracted from the receptor site concentration. TAGIT peaks are not well correlated with tracer peaks or with the peaks of most of the other methods. In fact there are a number of time periods where TAGIT produces very small estimates when the other methods produce peaks and TAGIT peaks when other methods have rather small estimates.

This substantial temporal discrepancy between TAGIT estimates and those of the other methods was the cause of considerable technical debate among the project analysts. For any of the periods with substantial disagreement, if TAGIT is correct then the other methods are incorrect or if the other methods are correct then TAGIT is incorrect. A number of difficult questions were examined. How can MPP contribute a substantial amount of sulfate (estimated by non-TAGIT methods), if the concentrations of sulfate outside of the MPP impact area are as high as inside the impact area (TAGIT)? Can the higher sulfate concentrations at a receptor site compared to those at a tracer-free background site be just a coincidence and not imply an MPP contribution? The conclusions from these discussions are that both the TAGIT and non-TAGIT methods can be incorrect for any specific time period. TAGIT can be fooled by background gradients caused by pollution fronts as they traverse the region. The non-TAGIT approaches require information about the oxidation of SO_2 to particulate sulfate and the rate of SO_x deposition. Small errors in these representations can have a major effect on the sulfate concentration predictions.

Unfortunately, for the periods of disagreement, no procedure was discovered to determine which of the methods is more likely to be incorrect. TAGIT is unique among the methods in not requiring the highly uncertain use of some approach to account for SO_2 conversion. Had estimates from TAGIT agreed fairly well with those from any of the other methods on a day-by-day basis it would have strengthened the confidence in those results substantially. However, this is not the case.

Decisions on managing MPP emissions will likely turn on the frequency distribution of MPP's sulfur contributions rather than its contributions to any specific sampling period. In section 9.4 the results from the various methods are accordingly displayed as cumulative frequency distributions. Some project analysts are uncomfortable with this form of presentation, however. The principal concerns are that (i) the format conceals the lack of agreement between models evident in the time series in Figure 8-2, Figure 8-3, and Figure 8-5, and (ii) the inclusion of bounding estimates (from Tracer Max and CALPUFF Wet and Dry) in a percentile plot invites misinterpretation. These concerns are discussed in the following paragraphs.

The lack of agreement among models as to when MPP impacts were most likely to have occurred undercuts our confidence that any of the models reliably represent the essential atmospheric processes involved. The cumulative frequency plots in section 9.4 appear to show better agreement between the various models; in particular, all of the non-bounding estimates

yield similarly small impacts during at least 50% of the sampling periods. The viewer of these plots must bear in mind, however, that the sampling periods contributing to the upper percentiles of one model may be those contributing to the lower percentiles of another. Consequently, the conclusions about relative MPP contributions drawn from the frequency distributions must be deemed to be less rigorous than those conclusions that are derived directly from the model outputs.

In particular, it should be recognized that every point in the cumulative frequency distributions for bounding estimates (CALPUFF Dry at the lower bound and CALPUFF Wet and Tracer Max as upper bounds) meets specific bounding assumptions. Therefore, such bounding distributions do not approximate any real distribution in which conditions range from those at the lower bound to those at an upper bound. Furthermore, it cannot be assumed that actual dry conditions are represented by the lower percentile values of CALPUFF Dry and cloudy conditions are bounded by the upper percentile values of CALPUFF Wet. Depending on the extent of ventilation during dry and wet conditions, it could very well be that cloudy conditions are bounded by the lower percentile values of CALPUFF Wet, or by a selection of points from throughout the distribution. Also, for example, if a 90th percentile CALPUFF Wet concentration corresponds to an actual condition, that condition may be at the 97th percentile (or, conversely, at the 85th percentile) in the actual distribution resulting from both dry and wet conditions

The reality is that we don't know the frequency of cloud interaction, nor do we trust that any of the models consistently provides the true impact under dry or wet chemistry conditions. The result is that we are unable to indicate the amount of distortion in what are in fact only estimates of bounding curves. However, the bounding estimates are displayed in the next section despite these problems because some of the analysts thought it useful to identify the bounds of a range of results that is likely to include the true distribution of MPP contributions.

The only truly indisputable bounds are zero impact for a lower bound and the Tracer Max curve for an upper bound. However, these represent highly unlikely conditions of 0% and 100% conversion of MPPs SO_2 to particulate sulfate (or for some periods Tracer Max is 100% of the measured sulfate, which is also highly unlikely). Though the range of results between these two bounding conditions is certain to include the true distribution, it is unrealistically large and is not recommended as the basis for judging the range of MPP impacts.

9. Source Contributions Assessment

This section addresses the principal goal of Project MOHAVE, to estimate the contribution of the Mohave Power Project (MPP) to visibility impairment in Grand Canyon National Park (GCNP). To a lesser extent this section addresses the contributions of other sources.   While most of the discussion is concerned with the new data and assessments generated as a part of Project MOHAVE, historic and climatological assessments are used to provide a context from which to the evaluate the merits of the newer information.

9.1 What is the *a priori* basis for believing that MPP could be an important source of haze at GCNP?

A few simple elements in a logical argument provide the basis for suspecting that MPP may be contributing to visibility impairment at GCNP. As indicated in Section 6, particulate sulfate is one of the important components responsible for visibility impairment (14-18% of the light extinction). MPP and the Navajo Generating Station (NGS), located on the Colorado River to the southwest and east of GCNP respectively, are responsible for most of the SO_2 emissions in the region. At 40,325 tons/year and 76,219 tons/year respectively their emissions have corresponded to about 40% of the total point source SO_2 emissions within California, Arizona, and Nevada (Grand Canyon Visibility Transport Commission, 1996). SO_2 converted to sulfate particles in the atmosphere is responsible for the vast majority of ambient particulate sulfate.

Previous studies (Malm et al., 1989b; Richards et al., 1991) demonstrated that NGS was responsible for some of the haze in GCNP under certain meteorological conditions that occur in the winter. These involve drainage flow from NGS toward GCNP, usually with low clouds in the canyons. The clouds are thought to be responsible for more rapid conversion of SO_2 to particulate sulfate, which can produce occasionally dense hazes in the canyons.

Conditions that could result in MPP contributions to visibility impairment at GCNP involve flow from the southwest and either slow net transport speed or clouds to increase amount of particulate sulfate produced by conversion of the MPP emitted SO_2. As shown in Figure 7-7, we know that MPP emissions are usually transported towards the western end of GCNP by wind flow from the south in the summer (April through September) and away from GCNP by flow from the north in the winter (November through February). Though infrequent and short-lived, winter storm systems occasionally result in flow to the north or northeast with clouds present. While the early summer period is typically characterized by few clouds, from about mid-July through mid-September monsoon conditions bring moisture from the Gulf of California and Gulf of Mexico that results in frequent cumulus cloud formation during the daylight hours.

Project MOHAVE summer and winter intensive periods were chosen to coincide with periods that include the summer monsoon and winter storm conditions in order to investigate the wind pattern and cloud conditions that are thought to have the greatest chance for MPP contributions to haze at GCNP. Wind data and model results using CALPUFF indicate that for other seasons, MPP emissions are transported toward Meadview at a frequency between that observed for the summer and winter study periods.

These meteorological patterns also cause flow of emissions towards GCNP from source areas to the southwest in the summer, such as Southern California, northern Mexico, and the San Joaquin Valley and from sources such as NGS to the northeast during typical winter conditions. During the summer, the persistent flow from the south and southwest may result in MPP emissions becoming embedded in the emission plumes from the substantial upwind source areas, confounding the separate assessment of MPP impacts.

9.2 What do pre-Project MOHAVE assessments indicate about source contributions to visibility impairment at GCNP?

The 1979 VISTTA study provided early indications of transport to the Grand Canyon area from Southern California. Macias et al. (1981) analyzed a late June haze episode by collating information from intensive aerosol measurements at the eastern end of the Grand Canyon with routine monitoring at locations upwind and with calculated back-trajectories. They found that emissions had been rapidly transported into the desert after several days of stagnation and buildup over Southern California. An interesting feature of this smog front was a marked increase in the size (and hence scattering efficiency) of sulfate-containing particles.

The VISTTA case study was given a climatological context in studies by the National Park Service. Iyer et al. (1987) calculated daily back-trajectories for Hopi Point, in order to study routinely monitored sulfate concentrations there as a function of the arriving air's history. Statistical analyses associated from 14% to 26% of the observed sulfate in the individual years 1979-1984 with Southern California, from 7% to 24% with copper smelters in Ely Nevada and southeastern Arizona, and from 0% to 20% with MPP. (Note that the SO_2 emission rates have changed considerably since this period.) In a subsequent reanalysis of aerosol and meteorological data from the 1980's, Malm (1992) associates 27% of the observed sulfate to Southern California and Baja California, 14% to Arizona copper smelters, and 17% to MPP.

Soon after the VISTTA study, exploratory measurements had provided a chemical fingerprint for anthropogenic influence, showing an episode of increased ozone and light scattering at Spirit Mountain to coincide with a pulse of methyl chloroform and Freon-11 (Hoffer et al., 1981). Routine monitoring of halocarbons was initiated at Spirit Mountain and Meadview in the mid-1980's, along with other air quality measurements. Intensive sampling in and around Los Angeles (Bastable et al., 1990), and the Toxic Release Inventory of methylchloroform (Sheiman et al., 1990), showed the Los Angeles basin to be the main identifiable source area for regional halocarbons.

The urban California origin of the methylchloroform arriving at the Grand Canyon was confirmed by time series and trajectory analyses. These showed a clear weekday-weekend cycle in ambient concentrations, lagging the pattern of industrial emissions by the day or two needed to traverse the intervening desert (White et al., 1990). Nearly all above-background concentrations came in air that had passed near Los Angeles (Vasconcelos et al., 1996; Vasconcelos, 1998).

Hourly ozone concentrations, which were monitored only at Spirit Mountain, were observed to track concurrent methylchloroform concentrations and foregoing Los Angeles Basin ozone concentrations (White et al., 1991). On this empirical basis, most of the above-background ozone at Spirit Mountain was related to transport from urban Southern California. Hourly

scattering coefficients tracked hourly methylchloroform concentrations (Miller et al., 1990), but haze/methylchloroform ratios varied significantly from day to day, precluding a quantitative apportionment.

MPP is almost exactly on a line from the Los Angeles Basin to the Grand Canyon, so the same winds that carry MPP's emissions toward GCNP also bring air from Southern California. Air arriving at the canyon from MPP can thus be expected to have higher than average background sulfate concentrations, due to the apparent prominence of Southern California as a regional source. Conversely, air arriving at the GCNP from most other directions can be expected to have lower than average backgrounds. Consequently, receptor analyses based on natural atmospheric variability have great difficulty resolving the two sources' contributions. It appears likely, for example, that the large year-to-year variability (from 0% to 20%) in the Iyer et al. (1987) MPP attributions reflects instabilities in their apportionment of southwestern emissions between MPP and upwind industry.

The geographically induced collinearity between Southern California's and MPP's contributions can be sidestepped by focusing on emissions rather than transport as the source of the signal sought at Grand Canyon. Unscheduled hiatuses in MPP's operation sometimes cause emissions reductions that are unrelated to atmospheric transport, dispersion, and transformation. Outages can thus be viewed as unplanned experiments to test the actual ambient effect of reducing emissions.

In particular, MPP was inoperable for the seven-month period June through December, 1985. The effect of this outage was examined by Murray et al. (1990), using 1984-1987 SCENES data from Spirit Mountain, Meadview, and Hopi Point. The authors found interannual variabilities of 15%-25% in ambient sulfate levels, with data from the 1985 shutdown falling in the range for normal operation. No effect of the shutdown on the distribution of 24-hour sulfate concentrations was found, even after adjusting for meteorological variations with multiple regression analyses. The 95% confidence bounds for average MPP summer impact were from less than 11.6% to less than 21% at Meadview and less than 3.3% to 7.8% at Hopi Point during favorable transport conditions.

Switzer et al. (1996) revisited the 1985-1987 SCENES data from the perspective of daily plant operating levels, accounting in their analysis for numerous shorter outages in one or the other of MPP's two units. Like Murray et al. (1990), they could find no discernible change in the frequency distribution of Meadview particle sulfur levels during periods of partial or complete MPP shutdowns.

The empirical studies of ambient concentration as a function of plant load provide a kind of "ground truth" on the effect of reduced MPP emissions. Even their truths rest on assumptions, however. Murray et al. (1990) assume that MPP's emissions were the major relevant variable that changed during the 7-month plant shutdown, that emissions from other sources were the same as in surrounding years, and they only accounted for some aspects of meteorological variability. Switzer et al. (1996) assume that atmospheric transport is independent of plant operation, neglecting any possible effect of reduced loads on plume rise. They further assume that the Spirit Mountain observatory receives negligible MPP sulfate, an assumption that is

consistent with the findings of Murray et al., but that operational difficulties prevented Project MOHAVE from checking.

An instrumented aircraft was employed during several summers to map the emissions plume as far downwind of MPP as it could be followed (Hegg et al., 1985). These efforts focused on the morning hours, before the plume was entrained and diluted by the deepening surface mixing layer. The elevated plume was sufficiently coherent at this time to be detectable, by instrumentation, out to ranges in excess of 100 km. At extreme range, the plume was generally situated west of Lake Mead. In the afternoons, when winds were expected to carry emissions toward GCNP, extended tracking beyond a few kilometers proved impossible. Under these conditions MPP emissions were diluted to the point where they could not be distinguished in real time from the varying ambient background.

The Winter Haze Winter Haze Intensive Tracer Experiment (WHITEX) was designed to evaluate the feasibility of attributing single point source emissions to visibility impairment in selected geographical regions. WHITEX measurements were conducted during a six week period in January and February 1987. During this time, an artificial tracer, deuterated methane (CD_4), was released from the NGS at Page, AZ near the eastern end of the Grand Canyon. Aerosol, optical, tracer, and other properties were measured at Hopi Point, which is in GCNP, and other locations. Synoptic weather maps indicated a high frequency of high pressure over the area, which resulted in transport of the NGS plume from the northeast toward GCNP. Trajectory analysis and deterministic modeling indicated transport from the area of NGS to Hopi Point during the period with highest sulfate concentrations there.

The extinction budget at Hopi Point on the south rim of the Grand Canyon indicated that sulfate aerosol (and associated water) contributed two-thirds of the non-Rayleigh light extinction during WHITEX. Attribution analysis used the Tracer Mass Balance Regression (TMBR) receptor model and the Differential Mass Balance (DMB) hybrid model. The separate analyses estimated that NGS was responsible for 70% to 80% of the sulfates measured at Hopi Point during WHITEX (Malm et al., 1989b and Latimer et al., 1989). Based on these results, the NPS concluded that NGS contributed substantially to sulfate and light extinction at Hopi Point.

The WHITEX data analysis methodology, results, and use of the results were cause for considerable controversy. The National Academy of Sciences Committee on Haze in National Parks and Wilderness Areas evaluated WHITEX (National Research Council, 1990). The Committee neither fully supported or discredited the WHITEX report. Based on evaluations of meteorological, photographic, chemical, and other physical evidence, the Committee concluded "at some times during the study period, NGS contributed significantly to haze in CGNP." However, the committee also concluded that "WHITEX did not quantitatively determine the fraction of sulfate aerosol and resultant haze in GCNP that is attributable to NGS emissions."

A key uncertainty identified by the Committee is the use of TMBR and DMB to apportion secondary species such as sulfate. Limitations of the regression analysis noted by the committee are: "(1) satisfactory tracers were not available for all major sources; (2) the interpretation did not adequately account for the possible covariance between NGS contributions and those from other coal fired power plants in the region; and (3) both models employ an inadequate treatment of sulfur conversion, which is an important controlling factor in the formation of haze at GCNP."

Another limitation noted by the committee was the lack of measurements within the canyon (beneath the rim).

The NGS Visibility Study was conducted by the Salt River Project (SRP), the operators of NGS, with measurements from January 10 through March 31, 1990. Its purpose was to address visibility impairment in GCNP during the winter months and the levels of improvement that might be achieved if SO_2 emissions from NGS were reduced. The study was performed to provide input to the rulemaking process of the EPA regarding NGS SO_2 controls (Richards et al., 1991).

Perfluorocarbon tracers (PFT) were released from each of the three stacks of NGS. Surface and upper air meteorology, particle and gaseous components, and tracer were measured at many sites. Deterministic modeling was done to estimate the contribution of NGS and other sources to sulfate levels for two 6 day periods with poor visibility. Various data analysis techniques were used to examine the relationships among NGS emissions, meteorology, air quality, and visibility during both episode and non-episode conditions.

The SRP study concluded that NGS emissions were absent from the vicinity of Hopi Point most of the time. The study estimated that the average contribution of NGS to fine sulfur at Hopi Point was small, although NGS sulfur dominated during one 4-hour period. However, it was noted that the frequency of wind directions transporting the plume toward GCNP was lower than normal during this time period.

The contribution of soil dust to haze was the focus of intensive measurements in the final year of the SCENES program (White et al., 1994). Intercomparisons of the collocated and size resolved optical and aerosol measurements indicated that predominantly coarse-particle dusts contributed almost half of the total particle scattering at Meadview on spring and summer afternoons. Subsequent analyses of back-trajectories associated elevated dust concentrations with air from Southern California (Vasconcelos et al., 1996).

9.3 What can we learn about source contributions directly from the Project MOHAVE data?

Insight into the relative contributions to Grand Canyon sulfate by various source regions and categories has been provided by two analyses of spatial patterns of sulfate concentrations, modified CMB receptor modeling, and by analysis of the behavior of the PFT tracers released during Project MOHAVE and of other air mass tracers, such as methylchloroform. The findings of these analyses are discussed here.

9.3.1 Spatial Pattern Analyses

Gebhart and Malm (1997) and Henry (1997b) analyzed spatial patterns of sulfate in the Project MOHAVE region. Gebhart and Malm used empirical orthogonal function (EOF) analysis, a form of spatial factor analysis. They deduced four spatial patterns that together explained 82% of the particulate sulfur variance during the summer intensive. In order of decreasing importance, these EOF patterns encompassed sources along (1) the lower Colorado River Valley, including MPP and Las Vegas urban area; (2) the southern California urban area stretching toward northern Arizona and southern Nevada; (3) areas to the south of the study region, including northern Mexico; and (4) a California EOF addressing such areas as the San Joaquin Valley.

Henry (1997b), using the RMAPS technique described in Section 8.2, similarly identified summertime spatial patterns that included a southern California urban area gradient; a lower Colorado River Valley source including the MPP and the Las Vegas urban area; and a southeast area including southern Arizona and northern Mexico. Henry attributed about half of the sulfate observed at the western end of the GCNP to the lower Colorado River Valley area while at the central portion of the Canyon, the majority of the sulfate emanated from sources to the southeast. (Section 8.2 discusses how these findings compare with the observed patterns of the PFT tracer.)

White (1997b) critiqued the work of Henry and concluded that the lower Colorado River Valley spatial pattern might be merely an extension of the southern California urban area region. Nevertheless, both these investigators agree that summer GCNP sulfate and resulting haze emanates from several source regions probably stretching from southern California eastward through Arizona and northern Mexico.

9.3.2 Modified CMB Attributions

As part of Project MOHAVE, the CMB hybrid model, MCMB (described in Section 8.3.5) was used to identify the important area and point sources impacting the GCNP (Eatough *et al.*, 1999 – enclosed in Appendix C). Some eight area sources and four point sources were characterized by emissions profiles. Attributions of both SO_2 and sulfate due to each source were produced for both Meadview and the central portion of the GCNP.

According to this model, at Meadview, the MPP is responsible on average during the summer for about 40% of the SO_2, but only about 5% of the sulfate. Although MPP is the dominant SO_2 source in the region, a generally low conversion rate of SO_2 to sulfate means that it contributes a much smaller fraction of the sulfate. The most important sulfate contributor at Meadview was found to be the Las Vegas urban area. Other important contributors to sulfate at Meadview are sources to the west and southwest.

At the heart of the GCNP, the dominant source of sulfate was found to be emissions from Baja California, a conclusion that is similar to the modeled findings of the Grand Canyon Visibility Transport Commission (Grand Canyon Visibility Transport Commission, 1996). Las Vegas is still an important source, along with the San Joaquin Valley. There is also some suggestion that sources to the south and southeast are more important here than they were at the western end of the GCNP at Meadview.

9.3.3 Perfluorocarbon and Halocarbon Tracer Analyses

The perfluorocarbon tracers (PFTs) released from MPP and several other locations and measured at about 30 receptors provide a direct ability to identify flow patterns and the extent of dispersion during the intensives. Details of the releases and sampling are given in Section 7.2.3 and 7.2.4. Based on analysis of these measurements, the following description of the flow patterns emerges.

During the winter, the predominant flow feature is drainage down the Colorado River along lower terrain. Under these circumstances the dispersion is retarded by confinement within the terrain as reflected in relatively high average tracer concentrations at large downwind distances.

Sources on the Colorado River east of GCNP (e.g., NGS), as represented by the Dangling Rope tracer, can have significant influence throughout the entire length of the Grand Canyon and beyond. The MPP emissions in the winter were transported primarily to the south along the Colorado River and were soon beyond the few tracer monitoring sites to the south of MPP. The MPP tracer was above background levels for about 6% of 24-hour sample periods at Meadview and was never measured above background levels at Hopi Point during the winter intensive monitoring period.

Large site-maximum concentrations for the MPP tracer at the Las Vegas Wash and Overton Beach sites during winter demonstrate that dispersion during occasional transport in a direction opposite to the predominant flow is comparable to that in flow in the predominant direction. This is somewhat surprising since the principal mechanism for such contrary flow is the passage of synoptic weather systems that generally entail mixing through a much greater depth, implying significantly increased dispersion.

Summer flow is generally from the south along the Colorado River (El Centro and MPP tracers) and from the west or possibly the southwest from the western edge of the Mojave Desert (Tehachapi Pass tracer). The MPP tracer was found to be above background levels for more than 90% of the summer intensive monitoring days for the sites around Lake Mead (Meadview, Overton Beach, and Las Vegas Wash), north and northeast of MPP. At Hopi Point, the MPP tracer concentrations were measured above background levels for about half of the days during the summer.

There appears to be a convergence zone over much of the Mojave Desert because tracers from both of the California release locations (Tehachapi and El Centro) were above background in 20% to 30% of the 24-hour sample periods at all of the eastern Mojave Desert sites. Given that flows from the greater Los Angeles and San Diego/Tijuana urban areas are likely to be located between the paths taken by the tracers from these California release locations, emissions from these areas must be at least as frequently transported through this region. From this it is reasonable to conclude that the eastern Mojave Desert is a major transport route for emissions from much of the State of California during the summer.

Transient haze events near the mouth of the Grand Canyon might potentially be attributed to patches of effluent from MPP. However, project analysts found no pattern of association between measured MPP tracer concentrations and light scattering at Meadview for 12-hour averaging periods during the entire summer intensive monitoring period, or for 1-hour averaging periods during the time with continuous tracer measurements at Meadview. This finding is demonstrated in the scatter plots provided below in Figure 9-1 and Figure 9-2. Correlation coefficients for these data are virtually zero indicating an absence of overall stable proportionality between light scattering and tracer concentrations at Meadview. The absence of any obvious relationship cannot rule out MPP contributions to haze in the GCNP, but strongly suggests that other sources were primarily responsible for the haze.

Although hourly extinction was not associated with MPP tracer, it did track concentrations of methylchloroform and water vapor (tracers of opportunity for air from Southern California and southern Arizona/northern Mexico) at times during the summer intensive study, according to the Tracer Regression method of White et al. (1998) (see Section 8.3.3). Multiple linear regression

of extinction on MPP tracer, methylchloroform, and water vapor during a 14 day period accounted for 74% of the observed variance, with methylchloroform and water vapor the significant explanatory variables. From methylchloroform ans water vapor alone, one can predict the observed extinction within 10% (one deciview) almost two thirds of the time, 250 of 398 hours (see Figure 9-3). From the data in that figure, one can determine that observed extinction was within one deciview (dv) of the prediction from methylchloroform and water vapor almost two-thirds of the time, 250 of 398 hours. The residual, representing extinction decoupled from the regional methylchloroform and water vapor tracers, exhibited no evident relationship with the MPP tracer.
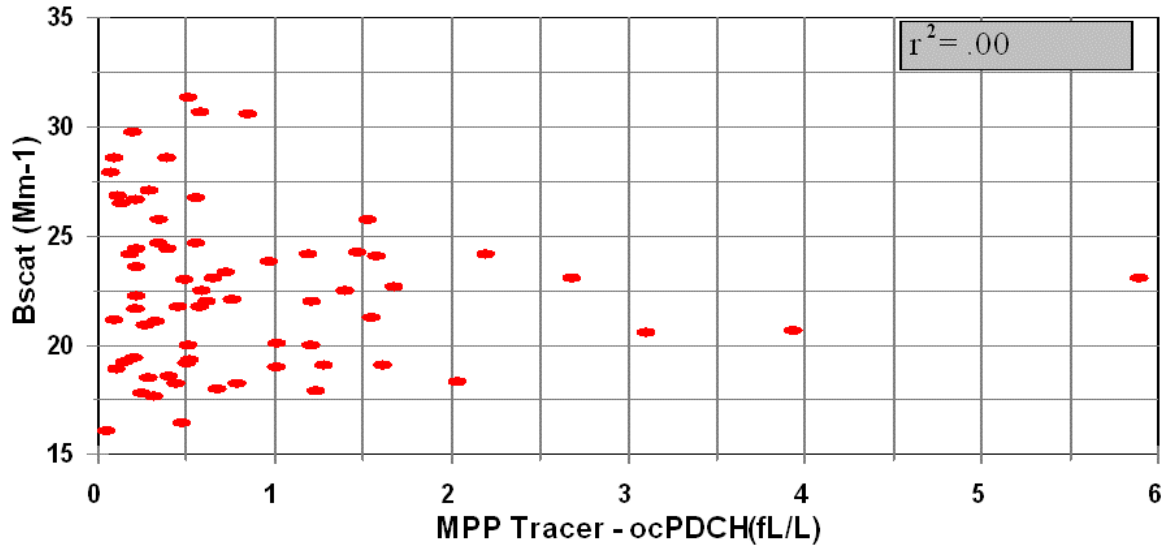
Figure 9-1 Scatter plot of light scattering and MPP tracer at Meadview - 12 hour averaging time.
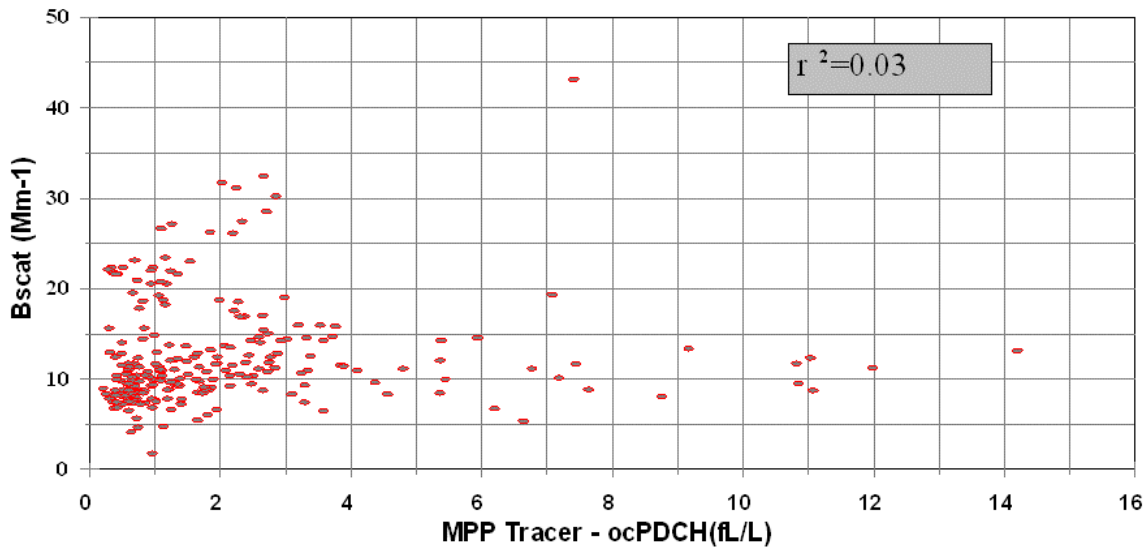
Figure 9-2 Scatter plot of light scattering and MPP tracer at Meadview - 1 hour averaging time.
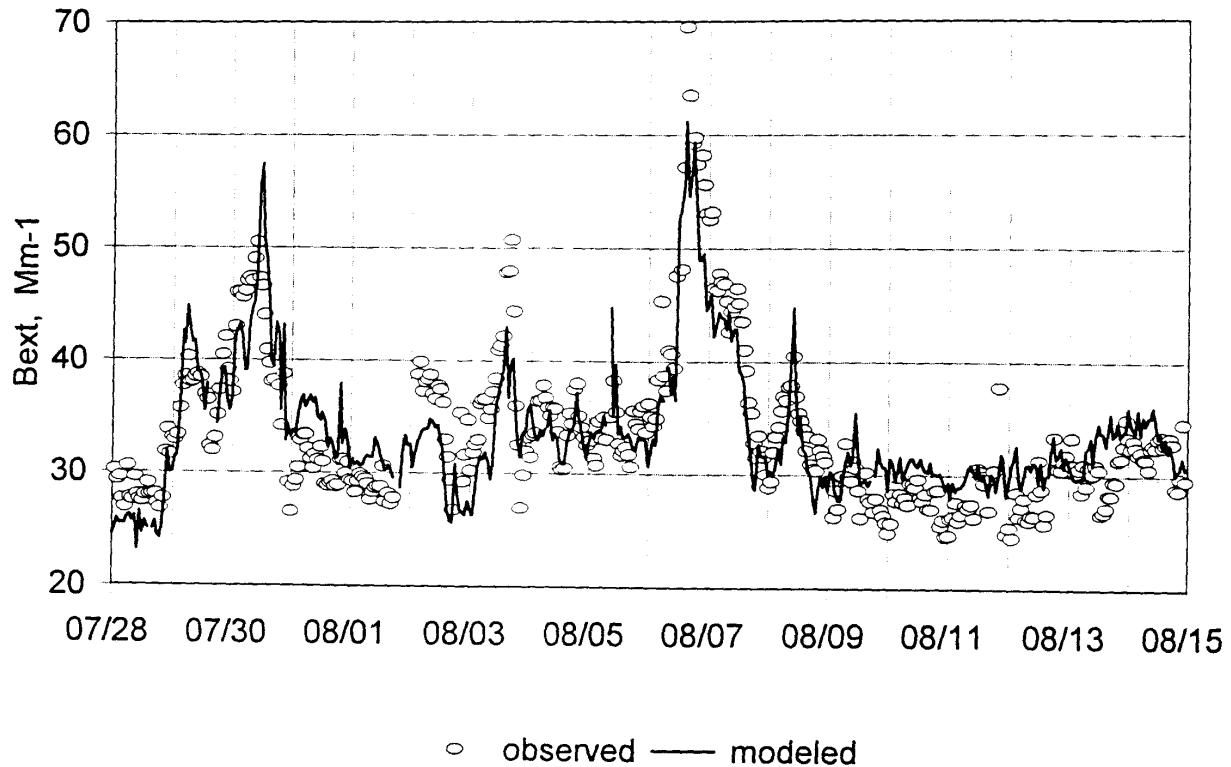
Figure 9-3 Time series of measured light extinction and modeled light extinction as a linear function of methylchloroform and water vapor concentration.

Two conclusions emerge fairly directly from these observations of PFT and halocarbons.

- Regional haze near the Grand Canyon can exhibit strong spatio-temporal gradients. Abrupt changes in species concentrations arise where distinct airmasses meet, whether as vertical layers or horizontal fronts. The factors that generate and shift the airmass boundaries implied by the hourly data have yet to be determined.

- Some of the worst haze near the Grand Canyon is associated with transport from Southern California and the regions to the south of Grand Canyon. The results of these analyses do not support a more quantitative apportionment of source contributions, although the modified CMB analyses (see Section 8.5.3) do address this issue. Hourly tags are unavailable for some potentially significant haze sources, such as nearby Las Vegas, California's San Joaquin Valley, and northern Mexico. Moreover, some of the observed association with distant emissions could reflect enhanced conversion of local emissions in a more reactive background.

The MPP emissions impact at a receptor will be as both primary and secondary particles. With very few assumptions, the MPP tracer data can be used to make reliable estimates of the MPP contribution of primary fine particulate matter at any of the tracer monitoring sites. This is accomplished by multiplying the measured ambient MPP tracer concentrations by the ratio of primary particulate to tracer emission rates for MPP. Assumptions include (1) a constant fine particulate matter to tracer ratio, which is approximately correct except when the electrostatic

precipitators are not functioning normally, and (2) no depositional loss of the fine particulate matter during transport from MPP to the monitoring sites, which is reasonable except under precipitation conditions. The ratio of tracer to fine particulate matter emission rates is determined from in-stack measurements of fine particulate matter and SO_x concentrations (Eatough, 1993) combined with the ratio of tracer to SO_x emission rates that was kept nearly constant as part of the study design. Using this method, the maximum 12-hour duration primary particulate mass concentration contributed by MPP at Meadview is about 190 ng/m^3. This corresponds to a maximum fraction of measured fine mass concentration of about 4% and a maximum fraction of measured light extinction of about 1.8%, where the light extinction is calculated using 3 m^2/g as the extinction efficiency. Corresponding maximum 12-hour duration values at Hopi Point are much smaller.

An alternative means of estimating the primary particle impact is from measurements of spherical aluminosilicate (SAS) particle concentration measurements at Meadview. Assuming that all SAS particles measured at Meadview originated from MPP (which makes this estimate higher than actual), primary particle mass from MPP was less than or equal to 30 ng/m^3 for all 12-hour sampling periods during the summer intensive. This corresponds to an extinction impact at Meadview due to primary MPP emissions of less than 0.1 Mm^{-1}, or less than 0.4% of the total extinction. These values are even smaller than those estimated from the tracer scaling.

The duration of MPP plume impacts is also of interest. A limited amount of high-time resolution tracer monitoring data is available at the Meadview monitoring site for several weeks during the summer intensive period (from July 28 to Aug. 14). Data gaps nearly every day caused by short-term periodic power outages make the data record far from ideal, however it is sufficient to provide some insights into the duration and timing of MPP plume impacts at Meadview in late summer. Figure 9-4, a time plot of the 20th, 50th, and 80th percentile of hourly tracer data shows that the MPP tracer tends to be greatest at Meadview in the mid-afternoon and evening hours during the summer intensive. That is not to say that the MPP plume exclusively reached Meadview during these hours. For example the 80th percentile points indicate that peaks can occur in the early and mid-morning hours.

Appendix B contains a brief description of the method used to estimate the duration of the MPP emissions impacts at Meadview during the summer. Determining the typical duration of the presence of MPP emissions at Meadview is complicated by the inability of the high-time resolution tracer monitor to reliably differentiate background tracer levels from those just above background and by the data gaps on many of the days. The range of impact duration estimates is from about 4 hours to 16 hours depending primarily on the day and to a lesser extent on the assumptions used in the estimation method. For the 14 days with sufficient high-time resolution tracer data, a mean and standard deviation of 8.2 ± 3.4 hours results from using the assumption that the impact duration is estimated to be twice the minimum time required to accumulate half of the day's cumulative dose.
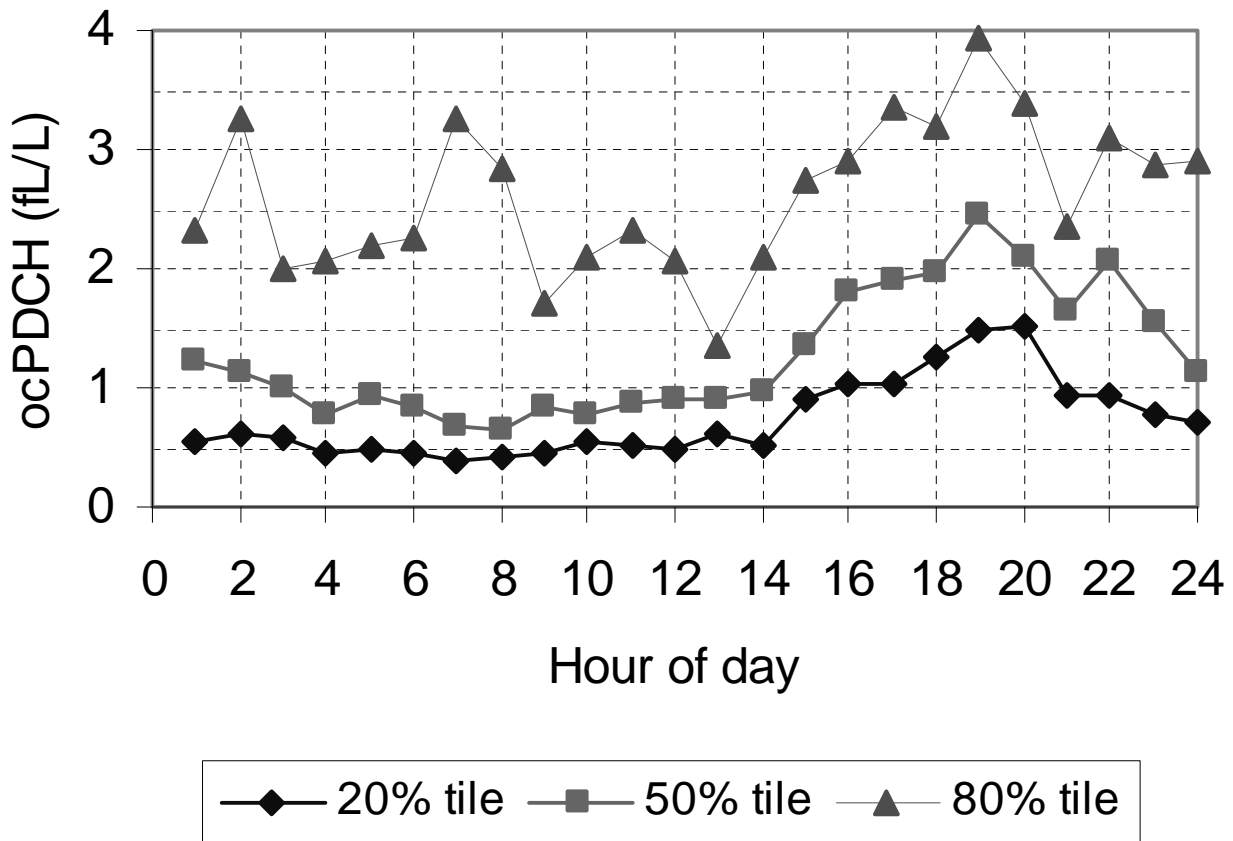
Figure 9-4 20th, 50th, and 80th percentile ocPDCH tracer concentration at Meadview by hour of day, July 28- August 14, 1992. Concentration includes a background of about 0.5 fl/l.

9.4 What is a likely range of 12-hour MPP contributions to GCNP sulfate during the intensive monitoring periods?

Methods described in Section 8.3 were used to estimate the sulfate contribution of MPP at Meadview and Hopi Point monitoring sites. As indicated in Section 8.4 (and also in Table 9-2 later in this section) the results of the various methods do not agree well on a sample period by sample period basis. Though it would be useful to identify one or more methods as providing the best estimates for some or all sample periods or conversely to identify methods that are thought to make poor estimates, no approach for making such determinations was agreed upon and no effort was made to rank the credibility of the methods. Therefore we present here the findings of all methods.

Because decisions on managing MPP emissions will likely turn on the frequency distribution of MPP's sulfur contributions rather than its contributions to any specific sampling period, the attribution results are presented as cumulative frequency distributions. A discussion of issues concerning this form of presentation appeared in Section 8.5. Most important, it needs to be recognized that the cumulative frequency distributions hide the fact that there are discrepancies in the sample period predictions between the various methods. Therefore, the cumulative frequency distribution presentations below should be viewed as interpretations of the modeled attribution results that were presented in Section 8.5, and should be considered less rigorous

presentations of the relative MPP contribution than the direct presentations of impacts given there.

Figure 9-5 through Figure 9-7 contain cumulative frequency distributions (CFDs) of the 12-hour estimated MPP contributions to particulate sulfate concentration by the various methods for the summer and winter intensive monitoring periods at Meadview and the summer intensive period at Hopi Point. No impact was estimated for the winter at Hopi Point.

The information on these plots portrays the basic findings of the attribution methods and of several efforts to estimate upper and lower bounds. Predictions of MPP contributions to ambient sulfate by various models are indicated with solid black points. Potential upper and lower bounds, which are not intended to represent estimates of actual MPP contributions, were determined by several methods and are indicated by open points. The methods used for attribution and for the bounding estimates are all described in section 8.3. Figure 9-5 also shows the cumulative frequency distribution of sulfate measurements at Meadview.

As might be expected, the lower-bound method that assumes only dry SO_2 to particulate sulfate conversion (CALPUFF Dry) generally estimates lower MPP contributions than those models that attempt to incorporate wet conversion (MCMB, DMBR, and ROME). HAZEPUFF, which has a simple algorithm for aqueous conversion sometimes predicts less sulfate than CALPUFF Dry. At the upper end of the range, the upper bound method that mandates daily wet conversion (CALPUFF Wet) produces estimates greater than those of all four of the models. Tracer Max results are shown as an ultimate upper bound but should not be considered estimates of actual conditions because the assumption of 100% of SO_2 to particulate sulfate conversion is extremely unlikely to be realized. However, the Tracer Max curve is useful to show how much lower the other estimates are compared to this firm upper bound result.

Not surprisingly, results of the various modeling methods tend to agree more closely for the lower percentile MPP impact estimates, which are ultimately bounded by zero impact, and they depart most in their estimates at the upper extreme of impact. One cause for this expansion of the range among methods at higher estimated MPP impact values is the variation between the methods' approaches to estimate the fraction of SO_2 converted to particulate sulfate. While some methods have very simplistic approaches to estimate conversion and others are more complex, there is no simple way to determine which yield the better result. Just as the range among results expands at the higher impact extreme, it is reasonable to expect that the uncertainty limits increase for any of the estimates as the predictions approach the upper level extreme values for that method. With this in mind, most of the material presented below will focus on the range of MPP estimated impacts for the 50th and 90th percentiles cumulative frequencies.

Shown in Table 9-1 are the ranges of 50th and 90th percentile values of particulate sulfate estimated by the various methods. Bounding estimates, excluding Tracer Max, are also given in parentheses. Estimated sulfate contributions by MPP are greatest at Meadview in both seasons and greatest in the summer at both sites. As pointed out above, the high end of the range for Meadview for summer is established by CALPUFF Wet bounding results. This method's assumption of wet conversion for each 12-hour estimate is less likely to be correct for conditions below about the mid-point of the cumulative frequency distribution (50th percentile) than above it
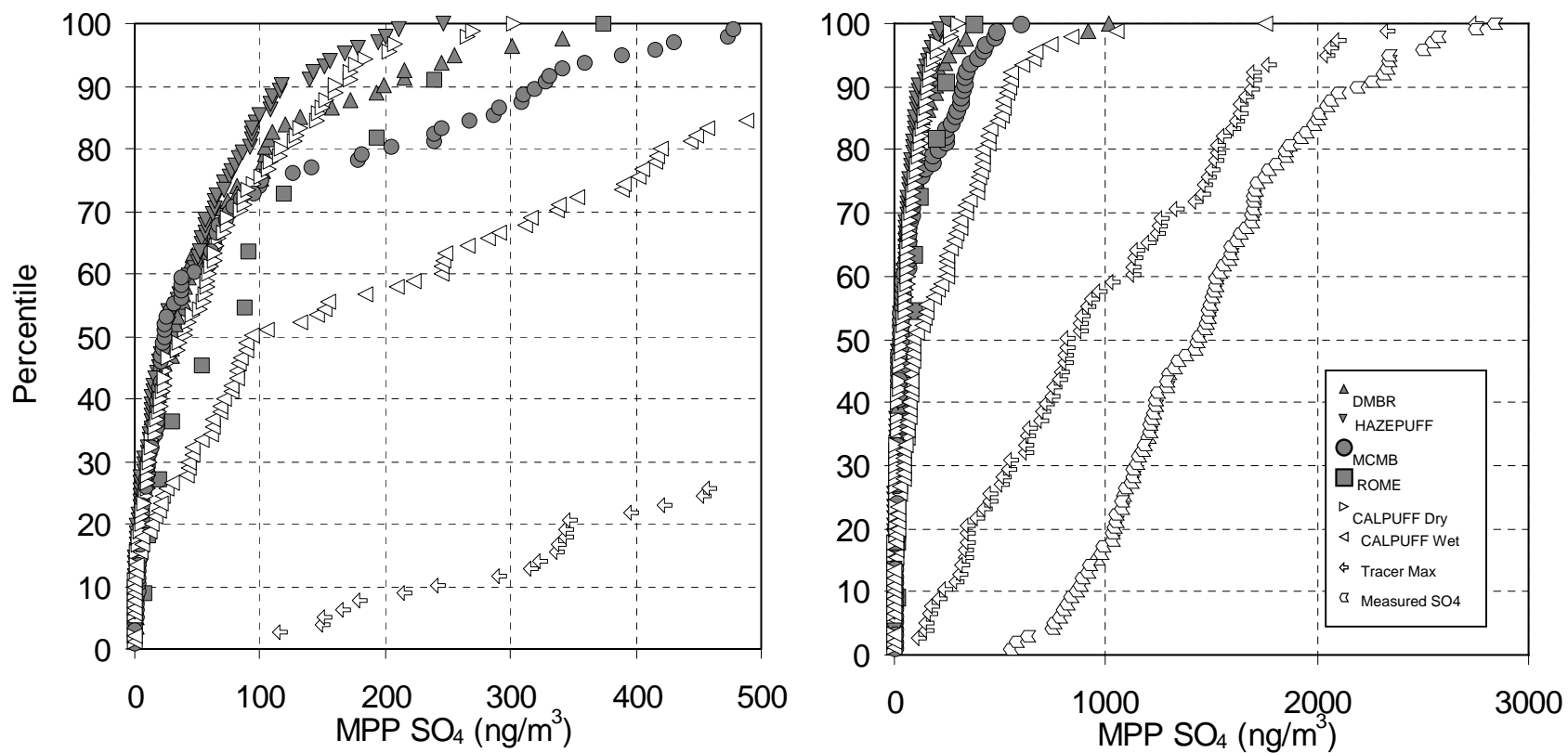
Figure 9-5 Cumulative frequency plots of 12 hour sulfate attribution to MPP at Meadview during the summer intensive. Filled symbols represent estimates of MPP attribution; open symbols indicate bounding calculations and physical upper bounds. Note: Inconsistent modeling results can yield similar frequency distributions.
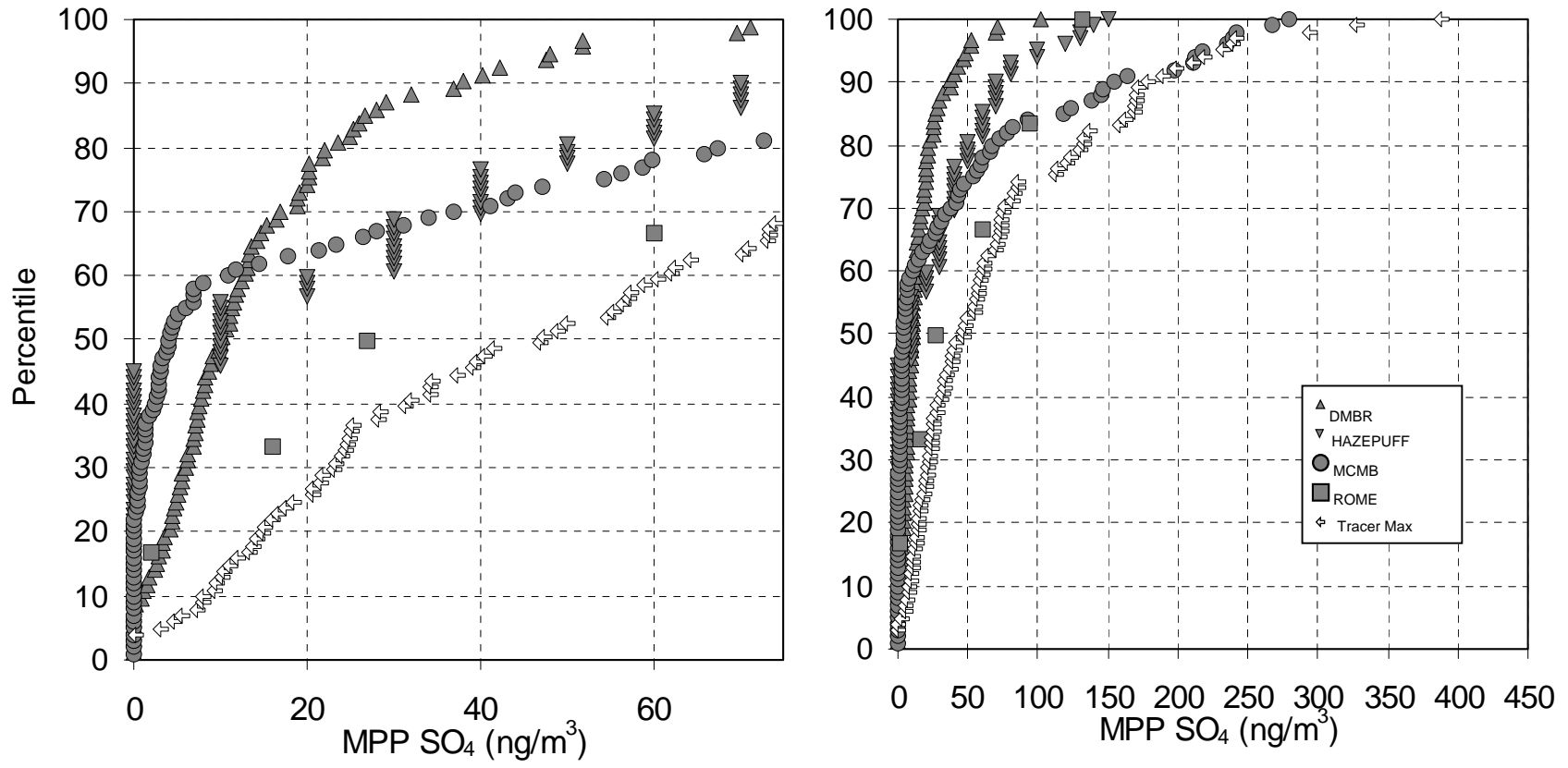
Figure 9-6 Cumulative frequency plots of 12 hour sulfate attribution to MPP at Hopi Point during the summer intensive. Filled symbols represent estimates of MPP attribution; open symbols indicate bounding calculations. Note: Inconsistent modeling results can yield similar frequency distributions.
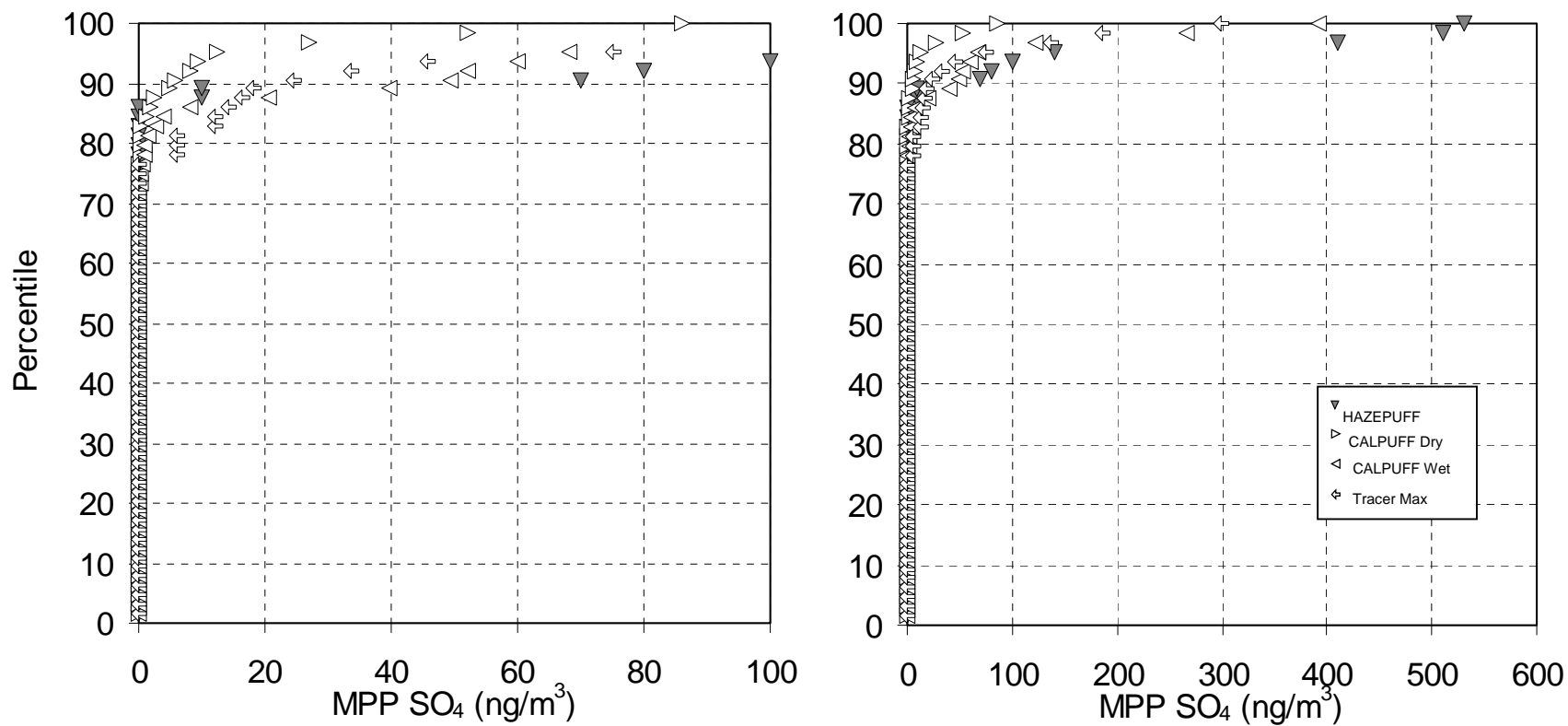
Figure 9-7 Cumulative frequency plots of 12 hour sulfate attribution to MPP at Meadview during the winter intensive. Filled symbols represent estimates of MPP attribution; open symbols indicate bounding calculations. Note: Inconsistent modeling results can yield similar frequency distributions.

because clouds were few or not present as often as half of the time (Ames et al., 1998). Surprisingly, the high end of the 90th percentile range for Meadview during the winter intensive was established by the MCMB method, which slightly exceeded the CALPUFF Wet bounding estimates. If the MCMB results are credible then the SO_2 to particulate sulfate conversion during the winter must occasionally exceed that assumed by CALPUFF Wet.

Table 9-1 Range of estimated 12-hour MPP sulfate (ng/m^{3}) for the 50th and 90th percentile conditions. Model attribution results excluding the bounding estimates of CALPUFF Wet and Dry are shown in bold. Values in parentheses represent the ranges of all attribution results.

	Winter		Summer	
	50th	90th	50th	90th
Meadview	(0.0 to 0.0)	40 (5 to 50)	**23** to **71** (23 to 93)	**120** to **320** (120 to 540)
Hopi Point	(0.0 to 0.0)	(0.0 to 0.0)	**4** to **27**	**38** to **160**

In order to estimate the relative importance of MPP compared to all other sources of particulate sulfate, each estimate of MPP-contributed particulate sulfate was divided by the measured sulfate concentration for the corresponding sample period. Cumulative frequency distribution plots of the estimated relative contribution of particulate sulfate by MPP are shown in Figure 9-8 through Figure 9-10. These curves look similar to those in the Figure 9-5 through Figure 9-7, with the ordering from highest to lowest estimates of the various methods being the same over most of the percentile values. It should be recognized, however, that the various points on a single frequency distribution curve may have been reordered, since a given concentration can represent a small fraction of a large measured value or a large fraction of a small measured value.

The qualitative similarity of the curves for absolute and relative concentrations suggests that there are no systematic relationships between the MPP impact estimates by the various methods and the ambient sulfate concentrations which are the denominators of the relative concentrations. This is confirmed by the correlation coefficients between predictions by the various methods and measured particulate sulfate at Meadview during the summer shown in Table 9-2.

One point exceeds 100% in Figure 9-8, a CALPUFF Wet bounding estimate of about 1700 ng/m^{3} on a day with measured sulfate of about 1600 ng/m^{3}. All other estimates are well below Tracer Max.

As expected from the previous discussion of meteorology, Meadview in either season has larger estimated fractional MPP contributions at the 50th and 90th percentile than at Hopi Point, and the summer intensive period ranges exceed those of the winter intensive for both sites (see

Table 9-3). Notice that the high end of the 50th percentile range for the estimated MPP fraction of particulate sulfate at Meadview during the summer intensive monitoring period is roughly half of the upper limit of possible average MPP impact determined in the "outage study" (8% compared to 15%) reported by Murray et al. (1990) and discussed in Section 9.2.

Table 9-2 Cross-correlation coefficients (r) for predicted MPP sulfate by the various methods and the tracer concentrations, measured sulfate and transmissometer extinction coefficients for summer at Meadview. Numbers of data pairs are shown in the second table below.

	MCMB	HAZE PUFF	DMBR	CALPUFF Dry	CALPUFF Wet	TMBR	TAGIT	ROME	SO4	Tracer Max	ocPDCH	b_{ext}
MCMB	1.00											
HAZEPUFF	0.03	1.00										
DMBR	0.24	0.22	1.00									
CALPUFF Dry	0.43	0.14	0.28	1.00								
CALPUFF Wet	0.29	0.15	0.60	0.75	1.00							
TMBR	0.45	0.00	0.70	0.40	0.56	1.00						
TAGIT	0.18	0.11	0.07	-0.04	-0.13	0.06	1.00					
ROME	0.46	-0.18	-0.08	0.16	-0.08	0.02	-0.04	1.00				
SO4	0.14	0.00	0.16	-0.01	0.02	0.24	0.56	0.25	1.00			
tracer max	0.37	0.03	0.42	0.38	0.37	0.71	0.16	0.58	0.56	1.00		
ocPDCH	0.45	-0.01	0.69	0.39	0.56	1.00	0.02	0.04	0.23	0.71	1.00	
b_{ext}	-0.18	-0.27	-0.04	-0.38	-0.24	-0.11	0.44	-0.18	0.67	0.06	-0.12	1.00

	MCMB	HAZE PUFF	DMBR	CALPUFF Dry	CALPUFF Wet	TMBR	TAGIT	ROME	SO4	Tracer Max	OcPDCH	b_{ext}
MCMB	96											
HAZEPUFF	96	102										
DMBR	79	81	81									
CALPUFF Dry	87	90	81	90								
CALPUFF Wet	87	90	81	90	90							
TMBR	79	81	81	81	81	81						
TAGIT	36	39	31	34	34	30	39					
ROME	11	11	11	11	11	11	3	11				
SO4	94	99	78	87	87	78	37	11	99			
tracer max	77	78	78	78	78	78	32	11	78	78		
ocPDCH	79	81	81	81	81	81	32	11	78	78	81	
b_{ext}	96	102	81	90	90	81	39	11	99	78	81	102

Table 9-3 Range of estimated 12-hour MPP fraction of measured sulfate (%) for the 50th and 90th percentile conditions. Model attribution results excluding the bounding estimates of CALPUFF Wet and Dry are shown in bold. Values in parentheses represent the ranges of all attribution results.

	Winter		Summer	
	50th	90th	50th	90th
Meadview	(0.0 to 0.0)	**3.5** (0.7 to 4.8)	**1.7** to **3.3** (1.7 to 8.0)	**8.7** to **21** (8.7 to 42)
Hopi Point	(0.0 to 0.0)	(0.0 to 0.0)	**0.4** to **1.6**	**3.1** to **13**

Figure 9-8 Cumulative frequency distributions of 12-hour estimated MPP percentage contributions to particulate sulfate concentration at Meadview during the summer intensive. Filled symbols represent estimates of MPP attribution; open symbols indicate bounding calculations. Note: Inconsistent modeling results can yield similar frequency distributions.
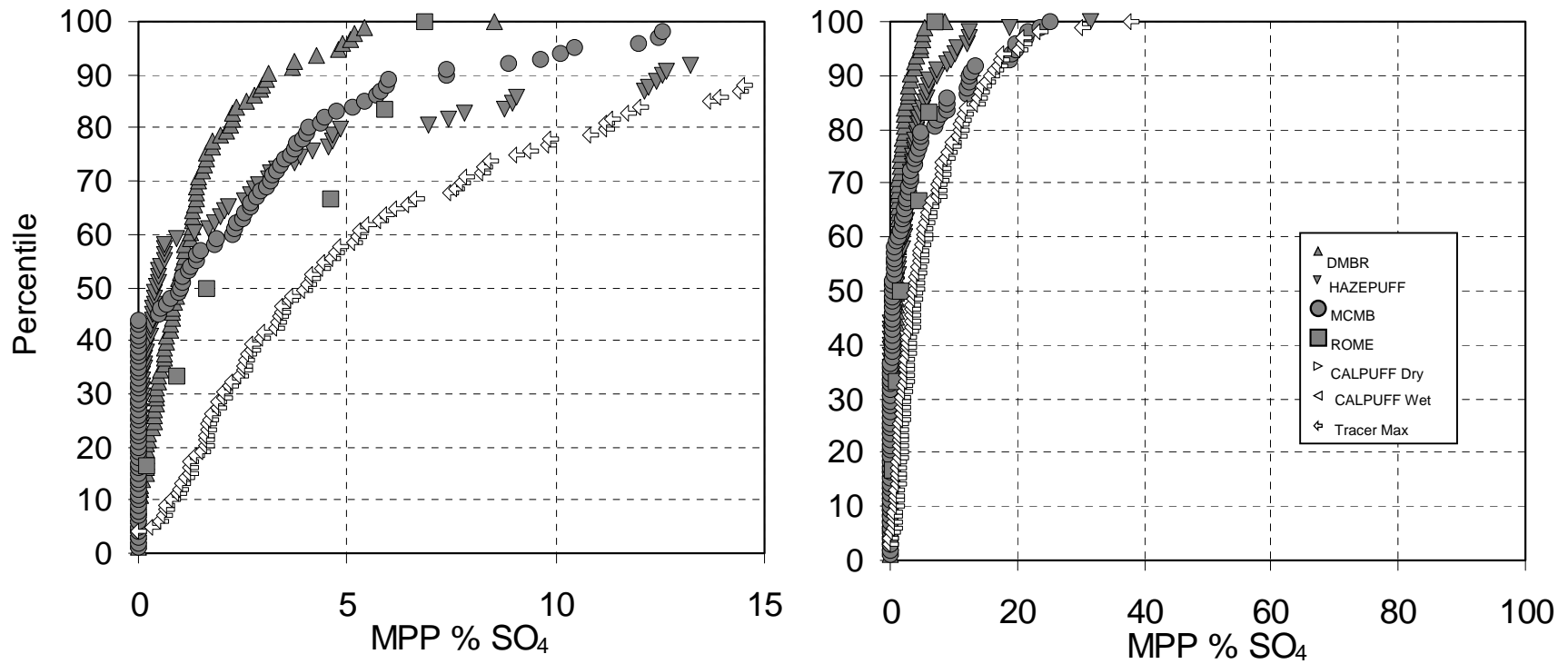
Figure 9-9 Cumulative frequency distributions of 12-hour estimated MPP percentage contributions to particulate sulfate concentration at Hopi Point during the summer intensive. Filled symbols represent estimates of MPP attribution; open symbols indicate bounding calculations. Note: Inconsistent modeling results can yield similar frequency distributions.
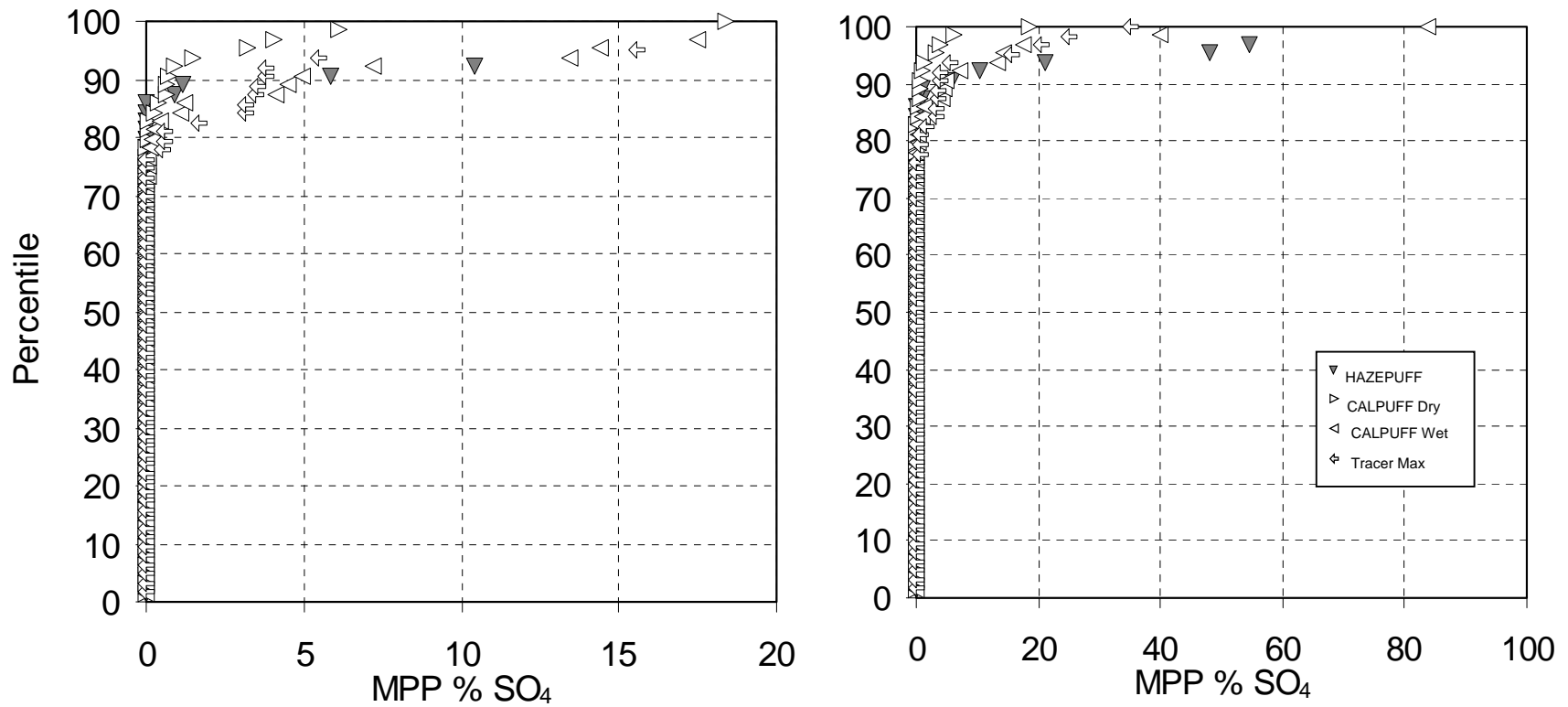
Figure 9-10 Cumulative frequency distributions of 12-hour estimated MPP percentage contributions to particulate sulfate concentration at Meadview during the winter intensive. Filled symbols represent estimates of MPP attribution; open symbols indicate bounding calculations. Note: Inconsistent modeling results can yield similar frequency distributions.

9.5 What is a likely range of 12-hour and 24-hour MPP contributions to GCNP light extinction during the intensive monitoring periods?

As described in Equation (6-6) in Section 6.2, the amount of light extinction coefficient contributed by particulate sulfate can be estimated by multiplying the ammonium sulfate concentration expressed in micrograms per cubic meter by 2 times an appropriate water growth function of relative humidity. This method was used to convert estimates of MPP-contributed particulate sulfate to estimates of MPP-contributed light extinction coefficient for both monitoring sites and intensive monitoring seasons.   As was pointed out in Section 8.4.3, the perceptibility of a change in haze depends on many factors, but for many situations a fractional change in light extinction coefficient is a reasonably linear index for haziness.   Accordingly, estimates of MPP-contributed haze were divided by the corresponding light extinction coefficient values to produce estimates of fractional changes in light extinction coefficient due to MPP.

Cumulative frequency distributions of the estimates of 12-hour MPP-contributed fractional light extinction coefficient are shown in Figure 9-11 through Figure 9-13, where transmissometer measurements were the source of the total light extinction coefficient. The shapes and relative positions of the various curves are not much changed from the corresponding particulate sulfate cumulative distribution curves. Again this is probably due to a lack of a strong correlation between the 12-hour estimated MPP contributions and the measured extinction coefficient, as reflected in Table 9-1.

The ranges of estimated MPP fractional contribution at the 50th and 90th percentile frequencies corresponding to the methods shown in Figure 9-11 through Figure 9-13 are summarized in Table 9-4. To gain appreciation for the perceptibility of changes corresponding to the fractional change in light extinction coefficient shown in the table, view the set of computer generated photos in the back of the report and described in Section 9.8.

Table 9-4 Range of estimated 12-hour MPP fraction (%) of measured light extinction coefficient for the 50th and 90th percentile conditions. Model attribution results excluding the bounding estimates of CALPUFF Wet and Dry are shown in bold. Values in parentheses represent the ranges of all attribution results.

	Winter		Summer	
	50th	90th	50th	90th
Meadview	(0.0 to 0.0)	**0.1** (0.1 to 0.4)	**0.2** to **0.6** (0.2 to 1.0)	**1.3** to **2.8** (1.3 to 5.0)
Hopi Point	(0.0 to 0.0)	(0.0 to 0.0)	**0.1** to **0.4**	**0.5** to **2.6**

As was mentioned in Section 5.4.4 and Section 6.2, there is a concern that the Meadview transmissometer-measured light extinction coefficient may be systematically too large. To explore how much this would affect the results shown in Figure 9-11 through Figure 9-13 and summarized in Table 9-4, the MPP fractional contributions to light extinction coefficient values for each method were recalculated using calculated extinction instead of the transmissometer measurements. The calculated extinction should generally slightly underestimate the true light extinction coefficient (See Section 5.4.4). The results of this are displayed in Figure 9-14 through Figure 9-16 and summarized in Table 9-5. The most substantial change resulting from the use of calculated in place of transmissometer-measured light extinction coefficient is at
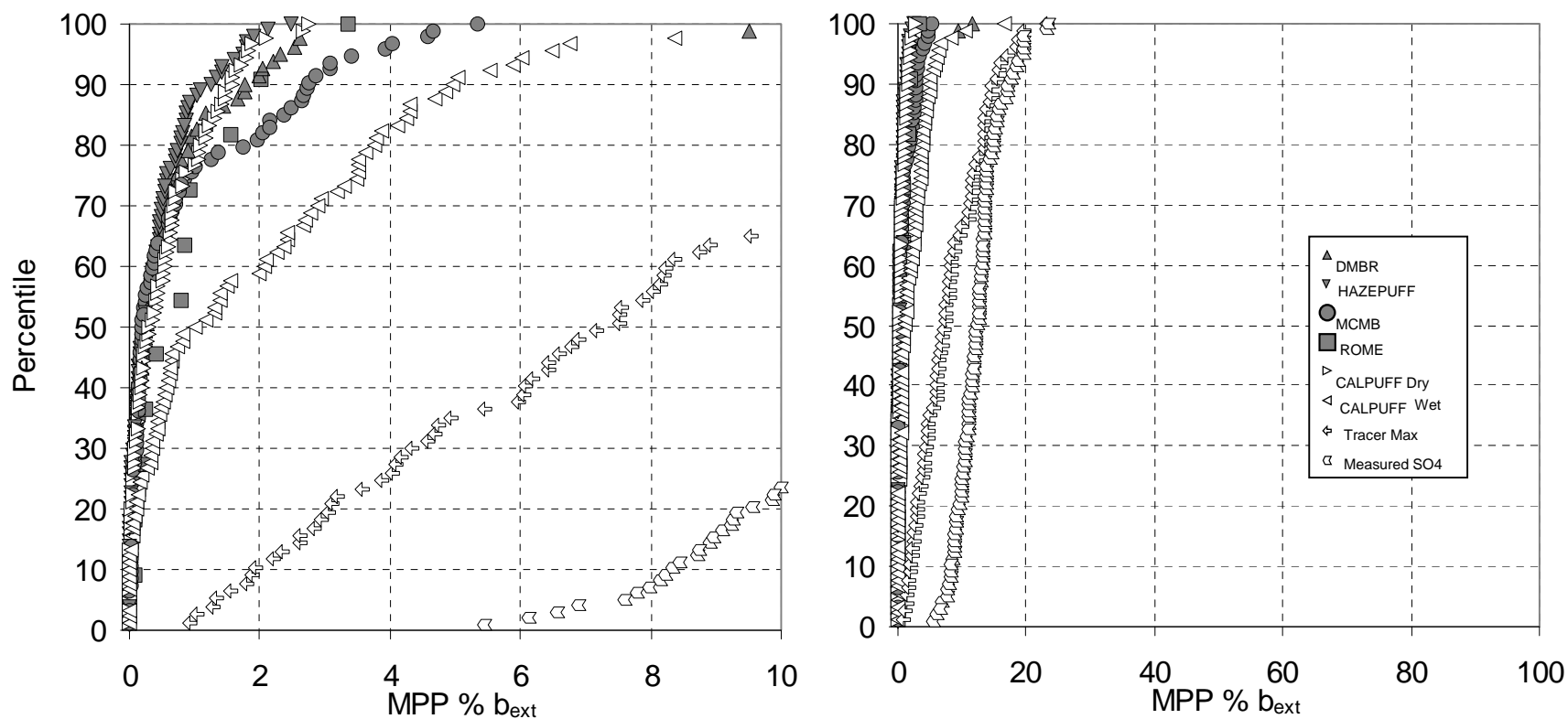
Figure 9-11 Cumulative frequency distributions of 12-hour estimated MPP percentage contributions to measured light extinction at Meadview during the summer intensive. Filled symbols represent estimates of MPP attribution; open symbols indicate bounding calculations and physical upper bounds. Note: Inconsistent modeling results can yield similar frequency distributions.
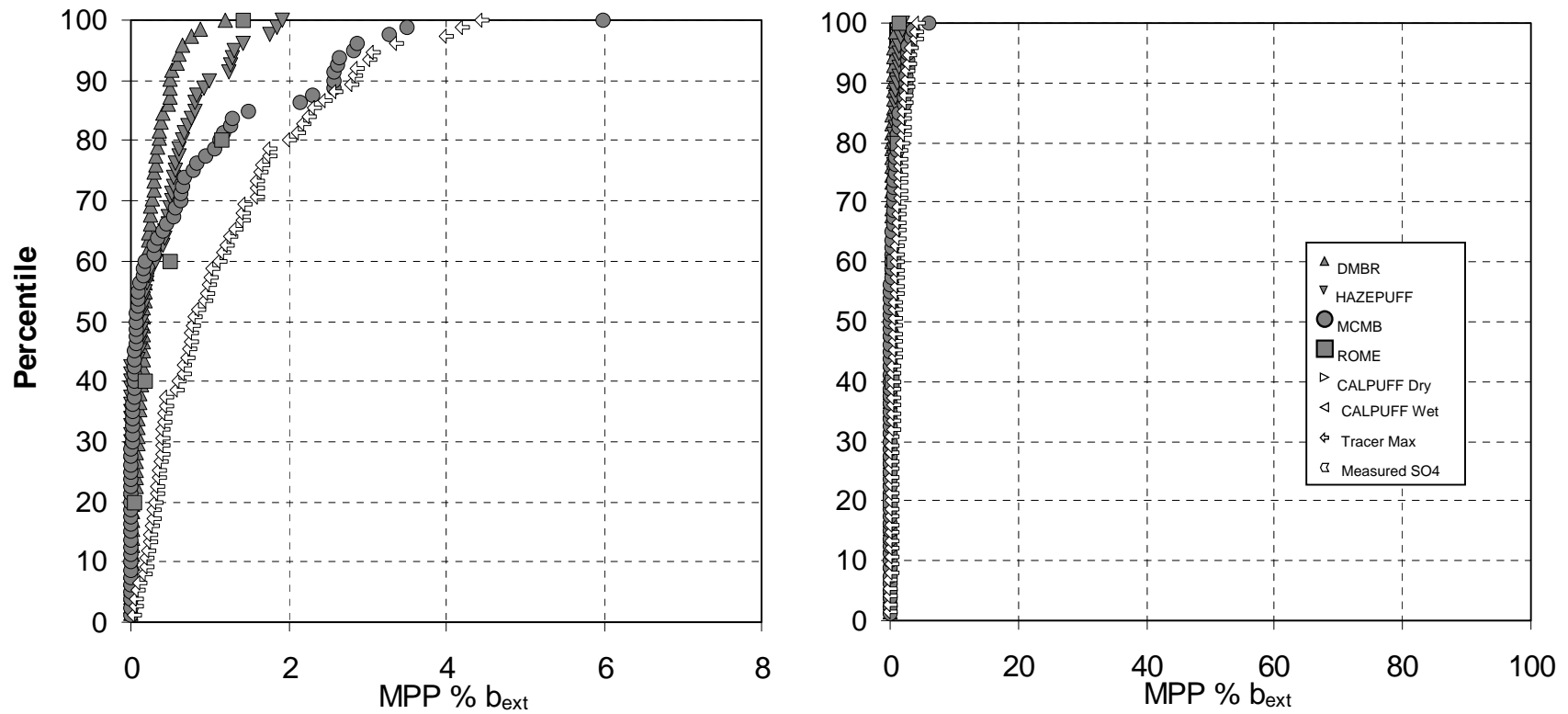
Figure 9-12 Cumulative frequency distributions of 12-hour estimated MPP percentage contributions to measured light extinction at Hopi Point during the summer intensive. Filled symbols represent estimates of MPP attribution; open symbols indicate bounding calculations. Note: Inconsistent modeling results can yield similar frequency distributions.
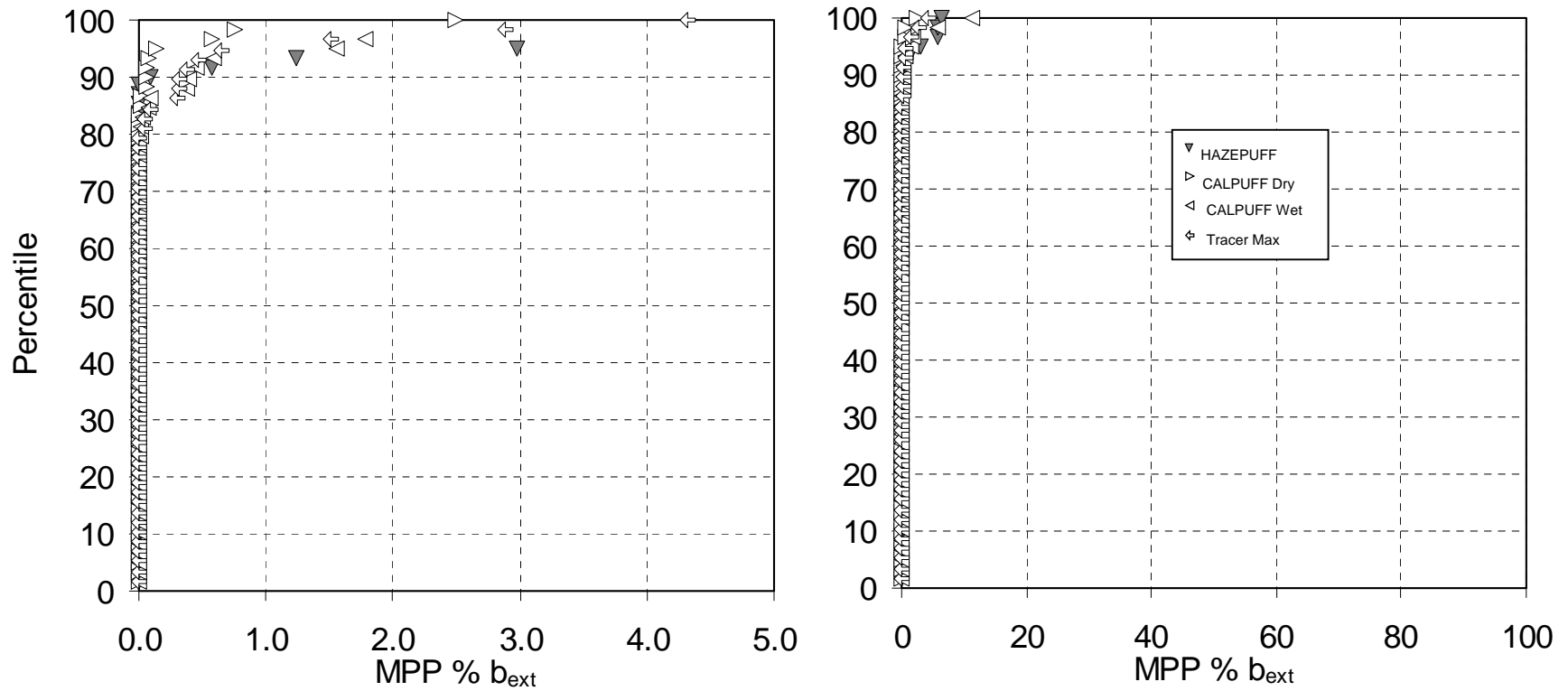
Figure 9-13 Cumulative frequency distributions of 12-hour estimated MPP percentage contributions to measured light extinction at Meadview during the winter intensive. Filled symbols represent estimates of MPP attribution; open symbols indicate bounding calculations. Note: Inconsistent modeling results can yield similar frequency distributions.

Meadview during the summer where the range is larger by about one third to one half using the calculated values.

Table 9-5 Range of estimated 12-hour MPP fraction (%) of calculated light extinction coefficient for the 50th and 90th percentile conditions. Model attribution results excluding the bounding estimates of CALPUFF Wet and Dry are shown in bold. Values in parentheses represent the ranges of all attribution results.

	Winter		Summer	
	50th	90th	50th	90th
Meadview	(0.0 to 0.0)	**0.2** (0.1 to 0.4)	**0.3** to **0.8** (0.3 to 1.2)	**1.9** to **4.0** (1.9 to 6.7)
Hopi Point	(0.0 to 0.0)	(0.0 to 0.0)	**0.1** to **0.3**	**0.6** to **2.3**

TAGIT results have not been shown in the figures and tables thus far, because TAGIT is only able to provide 24-hour estimates while all other methods can provide 12-hour estimates. The 12-hour results for all methods can be combined to produce 24-hour results so that they can be compared with those from TAGIT. Cumulative frequency distribution curves of the estimated fraction of MPP contribution to 24-hour transmissometer-measured light extinction coefficient are shown in Figure 9-17 through Figure 9-19 and summarized in Table 9-6.

Table 9-6 Range of estimated 24-hour MPP fraction (%) of measured light extinction coefficient for the 50th and 90th percentile conditions. Model attribution results excluding the bounding estimates of CALPUFF Wet and Dry are shown in bold. Values in parentheses represent the ranges of all attribution results..

	Winter		Summer	
	50th	90th	50th	90th
Meadview	(0.0 to 0.0)	**0.0** to **0.4**	**0.3** to **0.6** (0.3 to 1.5)	**0.9** to **3.5** (0.9 to 4.8)
Hopi Point	(0.0 to 0.0)	(0.0 to 0.0)	**0.0** to **0.4**	**1.1** to **5.3**[1]

Comparing corresponding curves in Figure 9-11 through Figure 9-13 and Figure 9-17 through Figure 9-19 shows that, at the high end of the distribution, the 12-hour estimated values will generally be greater than their counterpart 24-hour estimated values because the highest 12-hour values are not necessarily in the same 24-hour period. Except for reducing the highest values somewhat the corresponding curves in the two figures are very similar.

The addition of TAGIT provides a feature not seen in the results of the other methods, negative estimates of contribution by MPP. These values indicate that nearby monitoring sites with little or no MPP tracer had somewhat higher particulate sulfate on average than at the receptor site for some days. They should be interpreted as near-zero contribution by MPP. For Hopi Point summer, the uncertainty of TAGIT results is sufficiently large over the entire range that the results should all be considered below detection limits. TAGIT estimates for Meadview are not thought to be below detection limits of the method, however. The reader is referred to the description of TAGIT in Section 8.3.3 for a more complete explanation of the method.

As previously mentioned, extreme value estimates by any of the methods are believed to have the greatest uncertainty and should not be trusted as a true reflection of greatest MPP impacts.

---

[1] The TAGIT method that produced this result has substantial uncertainty as applied to MPP impacts at Hopi Point. The value associated with the next highest method for the 90th percentile is 2.5%, which seems to be a more reasonable upper limit.

However, some idea of the potential for extreme impacts can be obtained by examining the range of the greatest individual-day MPP attributions generated over the entire tracer period. The predictions of study-maximum (100th percentile) MPP contribution to Meadview light extinction during an individual 12-hour monitoring period was from about 2.5% to 11%, as seen in Figure 9-11. (The CALPUFF Wet bounding estimate takes this range up to 16%.) This wide range of estimates underscores the fact that the disagreement among estimates was greatest when estimating the highest 12-hour MPP contribution. Notice that even the upper end of this range is less than the Tracer Max upper bound result for the highest 12-hour estimate of about 23%. As explained in Section 8.3.1, Tracer Max yields an absolute upper bound obtained, in part, from the measured tracer concentrations. It makes the assumption that all emitted MPP sulfur is converted to sulfate without depositional loss during transport to Meadview, which eliminates any possibility of underestimation. Careful inspection of scatter plots of high time resolution optical and tracer data (e.g., Figure 9-2) was unable to detect any patterns of association that directly corroborate the higher MPP contributions at Meadview calculated by the models.
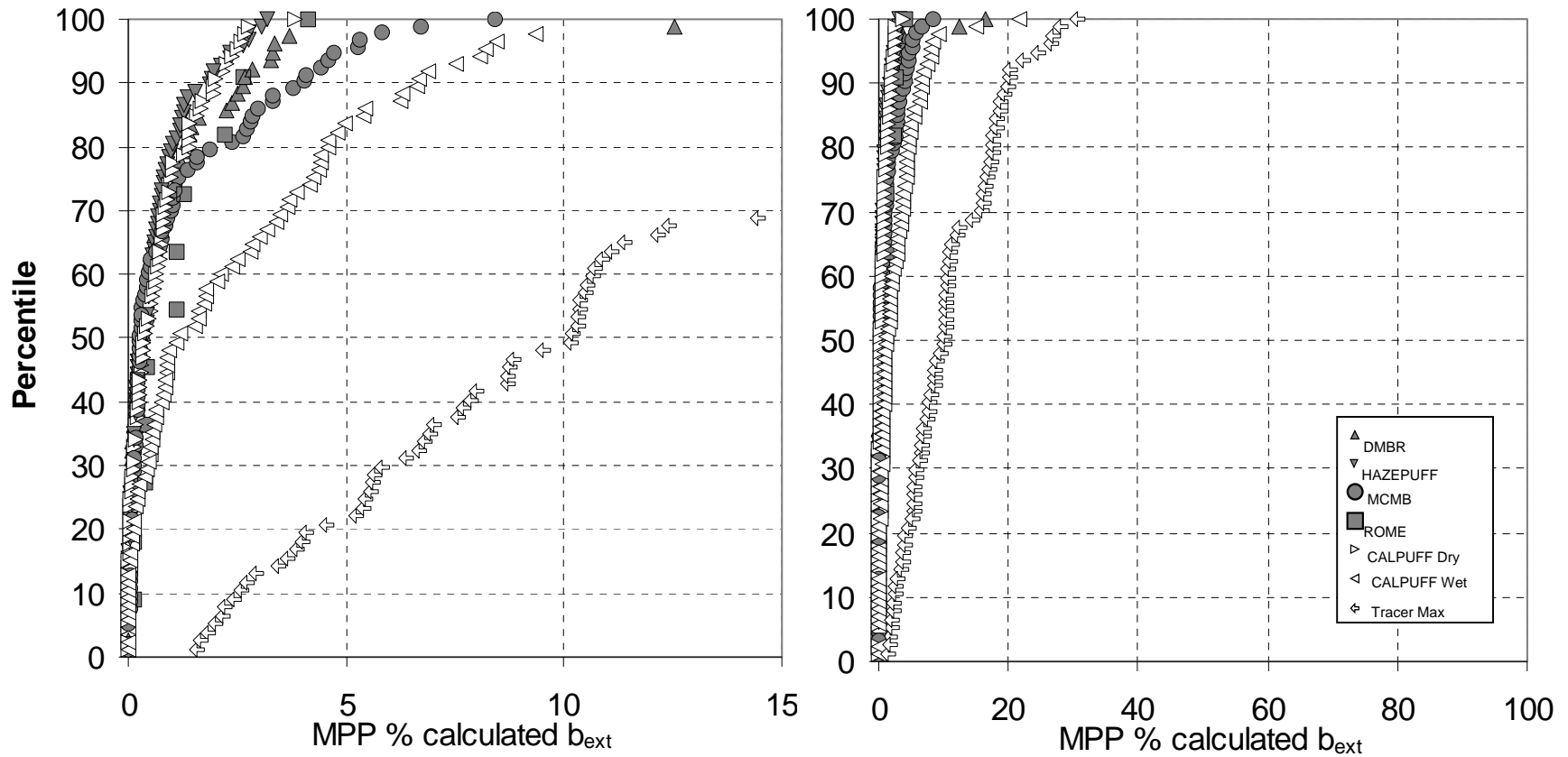
Figure 9-14 Cumulative frequency distributions of 12-hour estimated MPP percentage contributions to calculated light extinction at Meadview during the summer intensive. Filled symbols represent estimates of MPP attribution; open symbols indicate bounding calculations. Note: Inconsistent modeling results can yield similar frequency distributions.
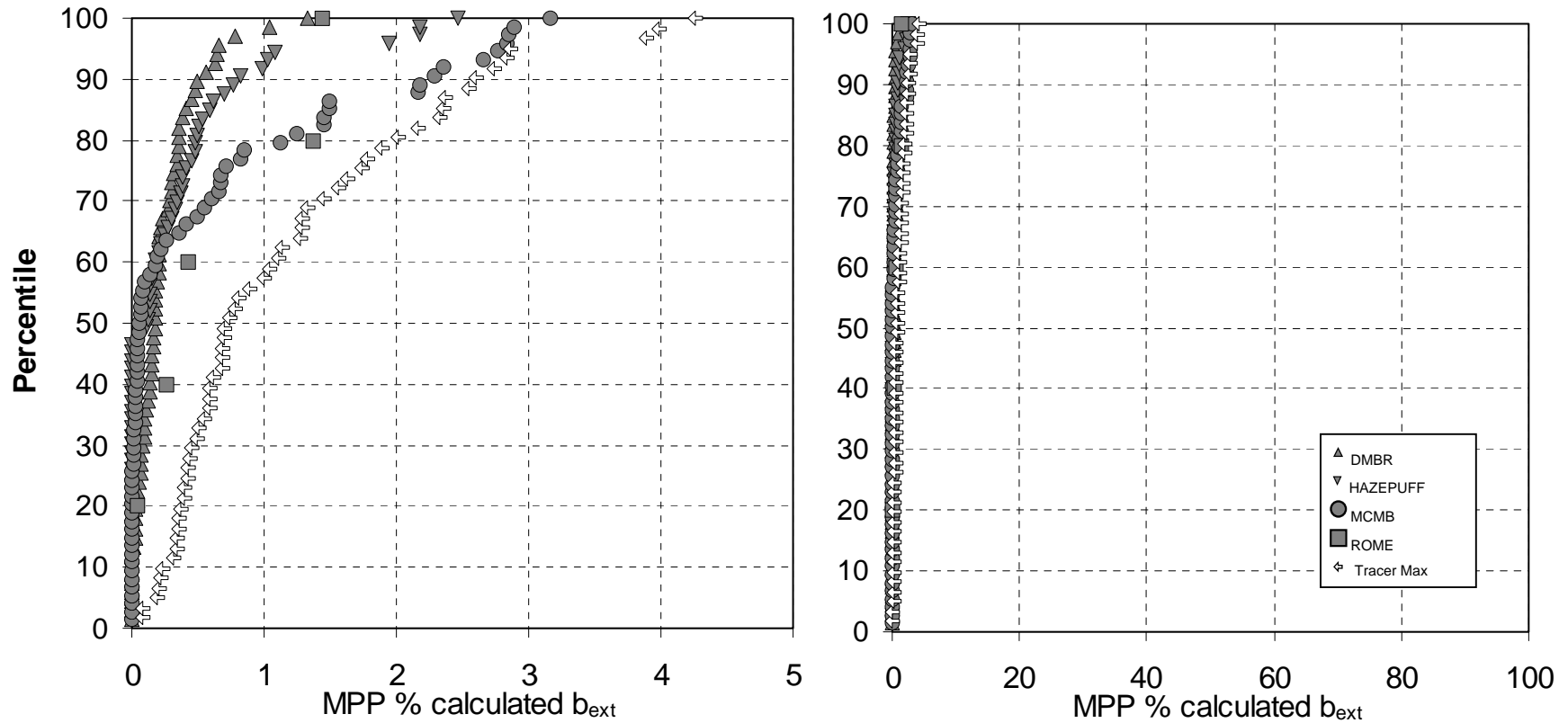
Figure 9-15 Cumulative frequency distributions of 12-hour estimated MPP percentage contributions to calculated light extinction at Hopi Point during the summer intensive. Filled symbols represent estimates of MPP attribution; open symbols indicate bounding calculations. Note: Inconsistent modeling results can yield similar frequency distributions.
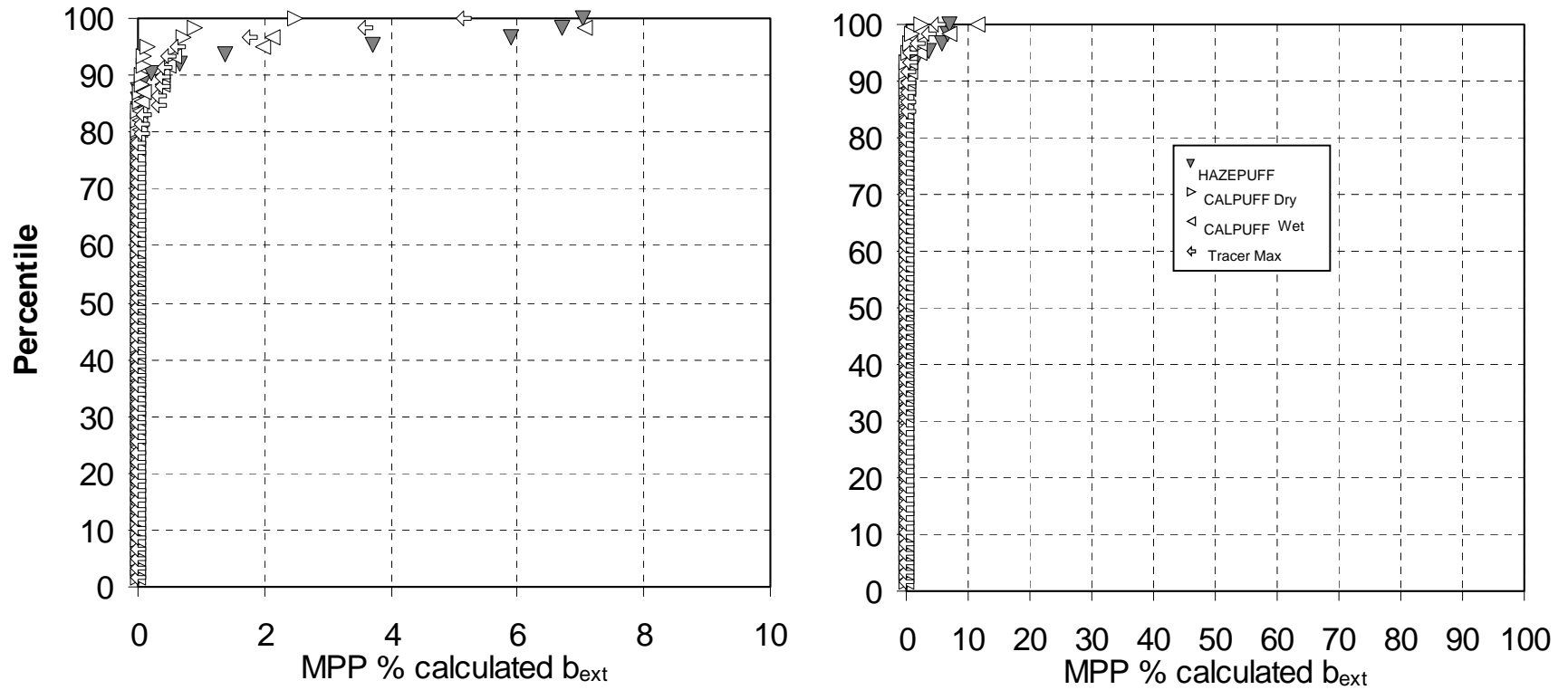
Figure 9-16 Cumulative frequency distributions of 12-hour estimated MPP percentage contributions to calculated light extinction at Meadview during the winter intensive. Filled symbols represent estimates of MPP attribution; open symbols indicate bounding calculations. Note: Inconsistent modeling results can yield similar frequency distributions.
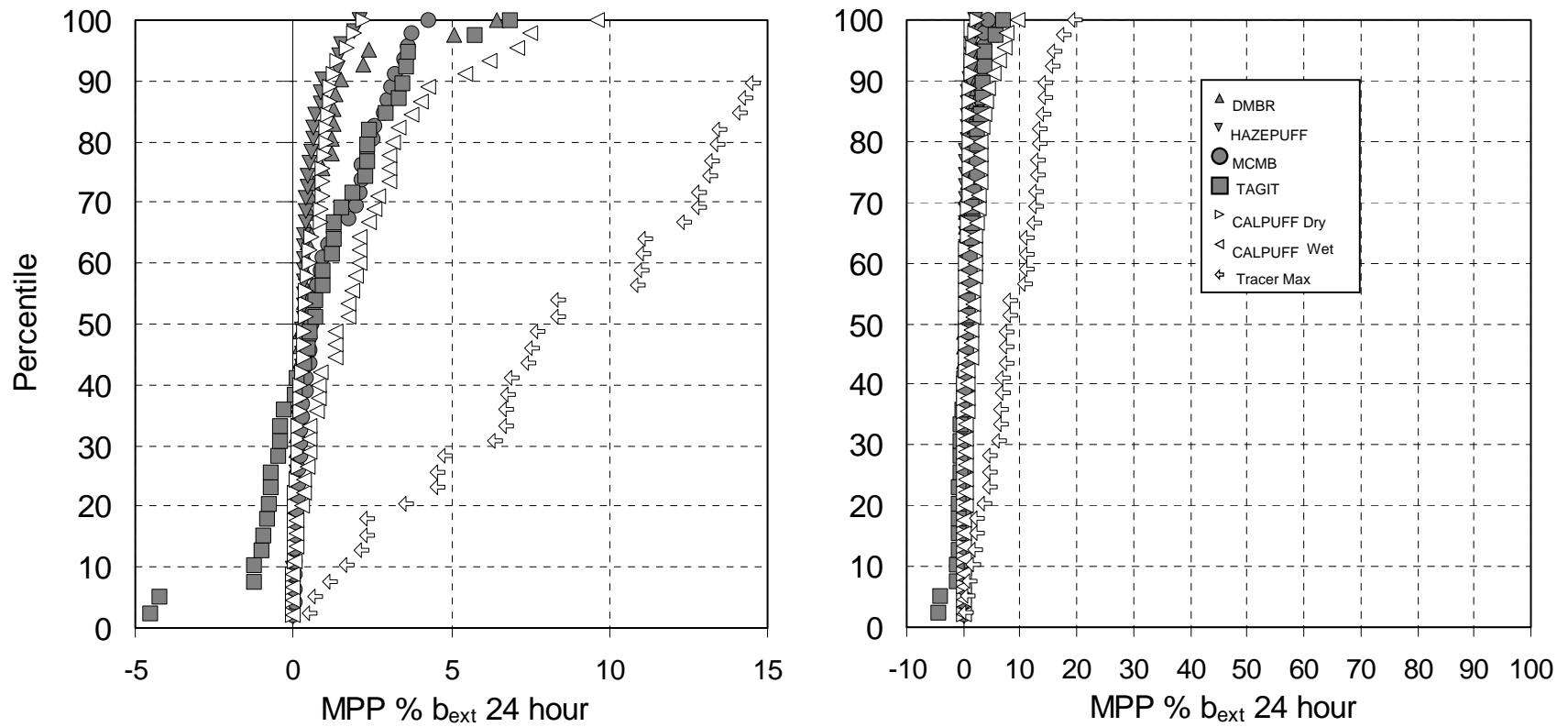
Figure 9-17 Cumulative frequency distributions of 24-hour estimated MPP percentage contributions to measured light extinction at Meadview during the summer intensive. Filled symbols represent estimates of MPP attribution; open symbols indicate bounding calculations. Note: Inconsistent modeling results can yield similar frequency distributions.
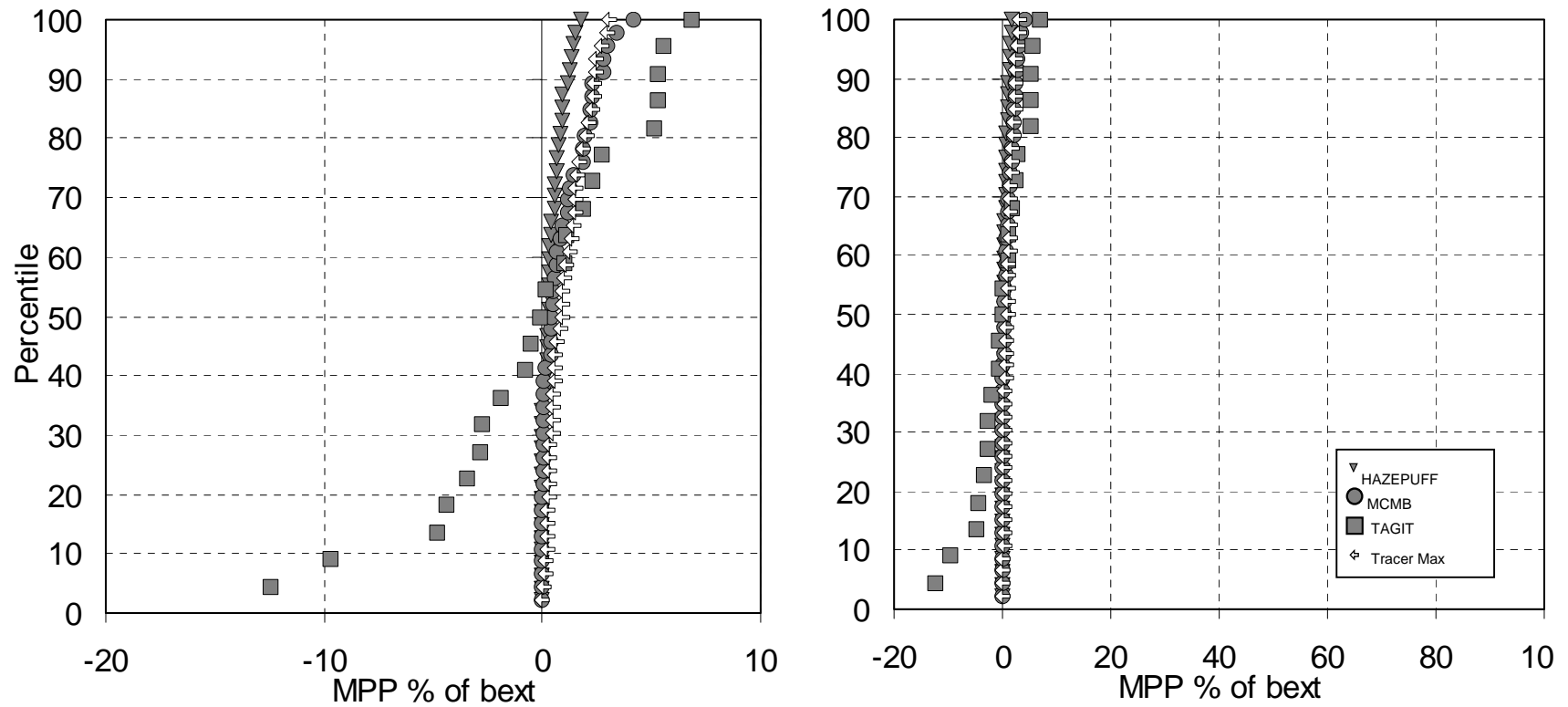
Figure 9-18 Cumulative frequency distributions of 24-hour estimated MPP percentage contributions to measured light extinction at Hopi Point during the summer intensive. The TAGIT results for Hopi Point are highly uncertain. Filled symbols represent estimates of MPP attribution; open symbols indicate bounding calculations. Note: Inconsistent modeling results can yield similar frequency distributions.
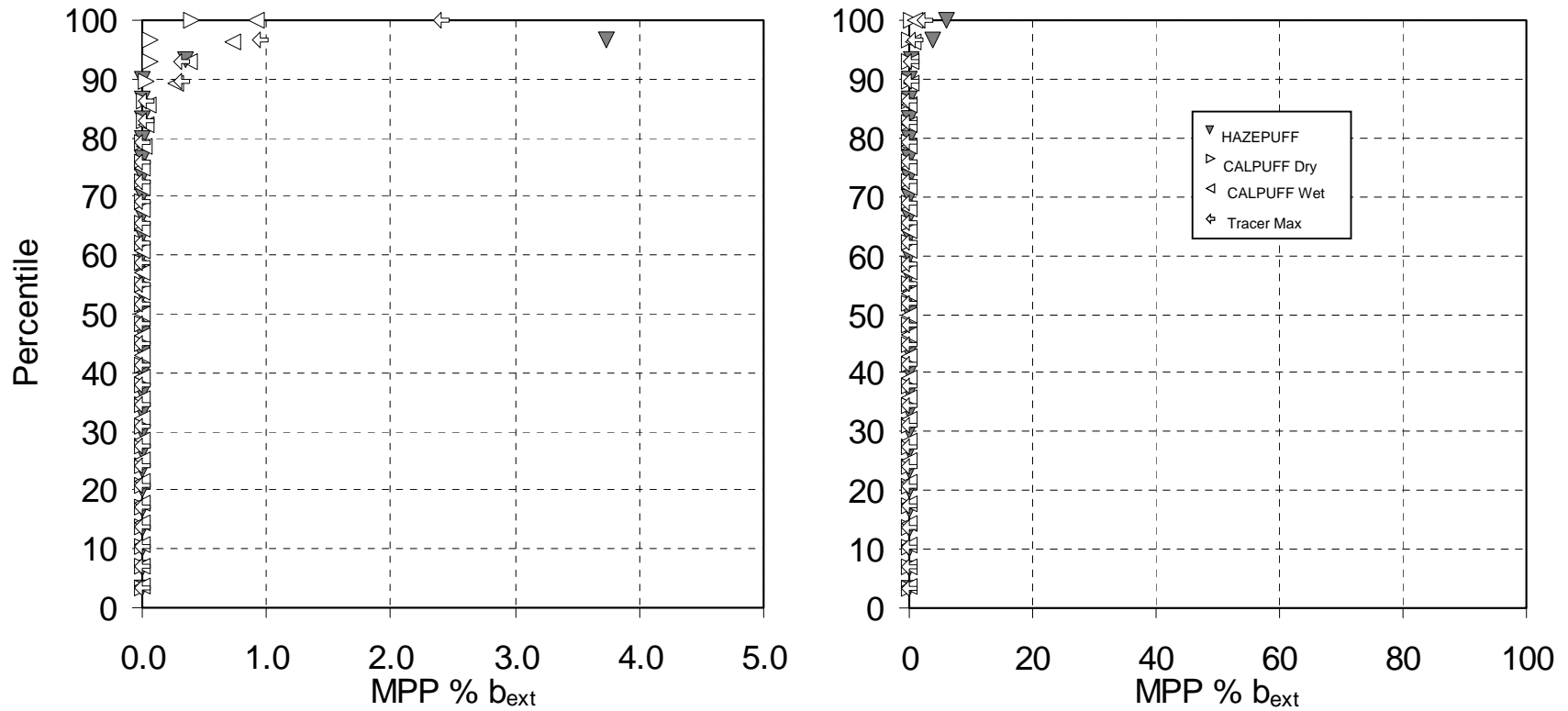
Figure 9-19 Cumulative frequency distributions of 24-hour estimated MPP percentage contributions to measured light extinction at Meadview during the winter intensive. Filled symbols represent estimates of MPP attribution; open symbols indicate bounding calculations. Note: Inconsistent modeling results can yield similar frequency distributions.

9.6 What can we say about MPP impacts on haze at GCNP during periods without tracer data?

For those periods of the year without tracer measurements, it cannot be reliably known whether MPP emissions are reaching Grand Canyon National Park. The model CALPUFF Dry was run to estimate transport and lower bound impacts during the approximately 9-month period for which radar wind profiler data was available at MPP. This data counted heavily in the calculation of the transport of emissions from MPP in the CALPUFF analysis, and thus CALPUFF was not run for periods during which wind profiler data from MPP was not available.

CALPUFF did not rely explicitly on the PFT data, but only used it for selecting the best wind field representation for the summer. For the rest of the year, when PFT data were absent, this selection was not possible and therefore the predictions may be poorer than those for the summer.

Figure 9-20 shows the frequency distribution of CALPUFF Dry predicted MPP sulfate at Meadview for the January-February, March-April, May-June, July-August, and September 1-20 periods of 1992. Predicted MPP sulfate is highest for the July-August and September periods and lowest in January-February with March-April and May-June intermediate.

Frequency distribution curves of percent of measured light extinction due to predicted MPP sulfate can be generated by applying assumed extinction efficiencies of ammonium sulfate of $2*f(RH)$ m^{2}g^{-1}, as was done for the intensive study periods. These curves for the January-February, March-April, May-June, and July-August periods of 1992 are shown in Figure 9-21. A curve is not shown for the September period because ambient total light extinction data were not available for most of that period. Below about the 90th percentile, the July-August period has the greatest predicted percent contribution of MPP sulfate to light extinction; however from about the 90th percentile and up, the March-April period has higher predicted percent light extinction than July-August. This is a result of the higher relative humidity during the March-April period than the July-August period, causing greater predicted extinction from a given amount of sulfate.

The ratios of CALPUFF dry estimated MPP 12-hour sulfate values at Meadview for the 50th and 90th percentile conditions for the bi-monthly periods January-February, March-April, and May-June to the July-August period are given in Table 9-7. Corresponding light extinction ratios are given in Table 9-8.

One of the most interesting periods during the summer of 1992 was the two days following the discontinuation of tracer release from MPP at 0700 on August 31. Although visibility levels were not unusual, the first two days in September had the highest sulfate measurements recorded throughout the area that summer and represent some of the highest measurements ever made in the area. Because of the lack of tracer data, only a few methods could be used to estimate the contribution of MPP. The results of these are considered to have greater uncertainty than for periods with tracer data and are not included in the specific findings presented in this report. Some of the results of these showed relatively high MPP contribution to sulfate (Ames and Malm, 1999 – in Appendix C). However, there are alternative explanations that would indicate other sources are responsible for much of the measured sulfate (Eatough and Farber, 1999).
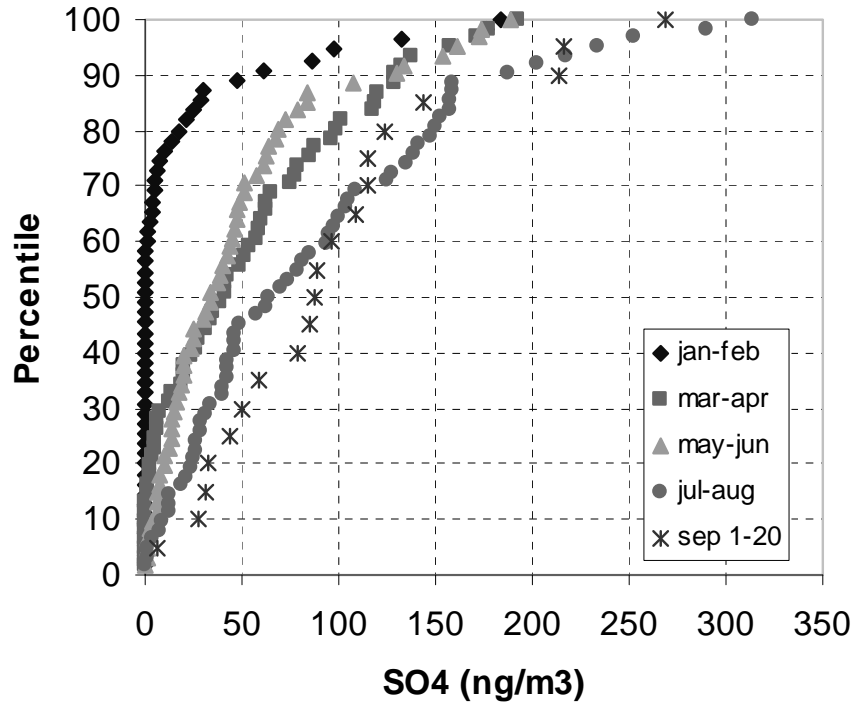
Figure 9-20 Frequency distribution of CALPUFF Dry predicted MPP particulate sulfate at Meadview by 2 month period, 1992.
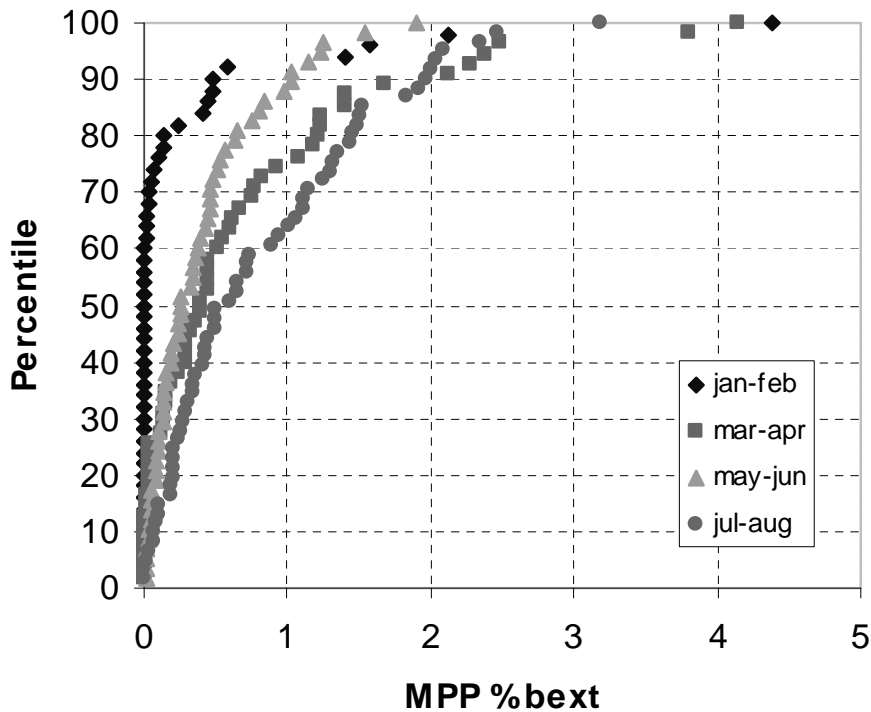
Figure 9-21 Frequency distribution of predicted percent MPP-caused light extinction at Meadview using CALPUFF Dry, by 2 month period, 1992.

Table 9-7 Ratio of CALPUFF Dry estimated MPP 12-hour sulfate values for 50th and 90th percentile conditions for months not during the intensive monitoring period to corresponding values estimated for July and August.

January-February		March-April		May-June	
50th percentile	90th percentile	50th percentile	90th percentile	50th percentile	90th percentile
0.0	0.2	0.5	0.8	0.4	0.6

Table 9-8 Ratio of CALPUFF Dry estimated 12-hour MPP fraction of the light extinction coefficient values for 50th and 90th percentile conditions for months not during the intensive monitoring period to corresponding values estimated for July and August.

January-February		March-April		May-June	
50th percentile	90th percentile	50th percentile	90th percentile	50th percentile	90th percentile
0.0	0.5	0.7	0.9	0.4	0.7

9.7 What can we infer about short-term (e.g., 3-hour) impacts on haze at GCNP?

Visibility impairment, as an instantaneous effect of air pollution, can manifest itself in much less than 12 hours. It seems unreasonable to assume that the MPP impact is uniform throughout any 12-hour sample period. Therefore the 12-and 24-hour average impact assessment results underestimate the magnitude of the peak short-term visibility impacts in any of those periods by the simple process of averaging peak impacts with low impacts. Due to inadequate information it may not be possible to properly determine the highest reasonable short-term impacts from MPP, but it should be possible to improve on the the 12- and 24-hour duration estimates.

The first question with respect to short-term impacts is what is the shortest time that would be reasonable to consider? While visibility is a short-term effect it does involve spatial averaging of the optical effects of pollutants between the viewer and the objects being viewed. Consider that a view with an object at 50 km will not be as impacted by looking through a 1km distribution of polluted air as with the same pollution concentration over the entire sight-path. Generally speaking, the average wind speed relates an air parcel's size to the time it takes to pass a fixed point. In other words a short-term peak measured at a site would be expected to be associated with a polluted air parcel with relatively small dimensions or with a larger parcel and higher wind speed. At typical wind speeds (~7 m/s) two hours corresponds to a dimension of about 50 km. Therefore the shortest time that should be considered to correspond to viewing scenic objects is an hour or two.

Estimates of MPP contribution to haze have been presented as 12-hour (7am – 7pm and 7pm – 7am) for all methods except for TAGIT which is restricted to 24-hour estimates. This was done because many of the assessment methods required tracer, particulate sulfate, SO$_2$ and/or elemental data which are only available on 12-hour (receptor sites) and 24-hour duration sampling schedule. The air quality models used for assessing MPP contributions including CALPUFF, HAZEPUFF, and ROME make short-term predictions that were averaged to 12-hours so that their results could be compared with the measurements and with the other assessment methods. Another reason for averaging to 12 and 24 hours is that in practice the shorter time period predictions of any air quality model are less comparable to measurements than the longer-term averaged predictions.

The process selected to explore short-term impacts is to develop and use a simple adjustment factor (or range of factors) to estimate the magnitude of the highest short-term impacts from the 12- and 24-hour estimated impacts. This allows adjustment to the estimates from any of the methods as presented above. Two approaches were used to develop adjustment factors. Both were only applied to the Meadview site during the summer intensive period for the MPP estimates of fractional light extinction coefficient. One approach uses the limited short-time resolution tracer data set, while the other uses CALPUFF predictions of hourly tracer concentrations. Application of the two approaches is described in Appendix B. Adjustment factors developed by the two approaches range from less than 2 to greater than 5 for adjusting the 24-hour duration estimated MPP impacts and range from less than 1.5 to 4 for adjusting the 12-hour duration estimated impacts.

From the large ranges of possible adjustment factors generated by the two approaches, it must be concluded that there is substantial uncertainty in estimates of short-term MPP contributions to light extinction coefficient at Meadview from the 12-hour and 24-hour results of the various models. This is not surprising considering the lack of data gathered specifically to address short-term impacts and the limitations of air quality models for high time resolution predictions. However, one conclusion is certain. The short-term impacts are generally greater than the long-term average estimates because every day there are periods with very little or no impact that are incorporated into the average. While the true adjustment factor probably varies from one sample period to another, it cannot be determined very well with the available methods and data. Given the range of results for the two approaches as shown above, for the purposes of this report the maximum short-term impact will be assumed to be twice the 12-hour or 24-hour impact estimates from the various methods.

9.8 How noticeable are the changes in haze that correspond to various fractional changes in light extinction?

Two major challenges in assessing the effects that changes in light extinction will have on perceived visual air quality are to link the optical properties of aerosols and gases to the visual appearance of the scene and to link various depictions of these changes to human perception. It is possible, with varying degrees of accuracy, to model or monitor the effect that optical properties of pollutants have on various visual parameters such as deciview, contrast, equivalent contrast, chromaticity, color difference, modulation transfer function, or just-noticeable-change (JNC). Yet it is difficult for scientists, let alone decision makers and lay persons, to "visually interpret" changes in any of these parameters that are presented in tabular or graphical form. Photography is a method that is ideally suited to present this information in a constant and reproducible form. In principle, if the ambient atmosphere was completely characterized by an intense spatial and temporal network of aerosol and optical measurements concurrent with high quality color photographs of a vista contained in the monitoring network, it should be possible to establish a data base that would show pictorially the correspondence between measured values and the appearance of the scenic resource. In reality, this approach requires an extensive, long-term monitoring program for a specific scene under a wide variety of meteorological, illumination and pollution conditions. Even then, experience has shown that the collected data usually will not be able to answer questions concerning various control or growth strategies that may be contemplated to mitigate existing visual air quality impacts or predict future visibility conditions. An alternative strategy, that was used for this project, is to collect photographs of

extremely clean periods and employ radiative transfer models and digital image processing techniques to create synthetic imagery simulating the various extinction scenarios. The process used was described in section 8.4.

Accordingly, the CD-ROM included at the end of this report provides images of vistas from Desert View and Tuweep in GCNP, each at 13 visibility levels. The baseline extinction level simulated in the images is the summertime transmissometer measured median extinction at Meadview for the Tuweep scene and at Hopi Point for the Desert View scene. In addition, visibility levels spanning from 0.5 to 1.5 times the baseline extinction level are portrayed.

To further explore the perceptibility of various changes in haze levels, the WinHaze program on the CD-ROM can be used to simulate any extinction level on several scenic vistas. For reference purposes, the median extinction measured at Meadview by the transmissometer during the summer intensive sampling period was 32.5 Mm^{-1}. At Hopi Point during the summer intensive sampling period, the median extinction was 35.5 Mm^{-1} in the canyon and 22.7 Mm^{-1} on the rim. Differences between the images are most perceptible when comparing the fine detail and color of medium and long range visual targets.

9.9 Level of confidence in the Project MOHAVE Findings

The findings that deal with the fractional contribution of MPP to light extinction coefficient (F_{MPP}) are the most applicable to the primary goal of Project MOHAVE. Those dealing with the sulfate concentration and fraction of sulfate contribution by MPP are merely the results of necessary intermediate steps in the assessment, and the computer imaging is just a tool to aid in judging the significance of the findings. The chain of reasoning needed to produce the light extinction findings can be subdivided into four basic steps: (1) MPP impact potential (same as Tracer Potential in section 8.5); (2) particulate sulfate yield from MPP emitted SO_2; (3) sulfate extinction efficiency; and (4) measured extinction coefficient. These are shown conceptually as the four factors on the right in Equation 9-1 and are discussed further in the text below.

$$F_{MPP} \equiv \frac{b_{SO_4,MPP}}{b_{ext}} = \frac{T\left(\dfrac{SO_X}{T}\right)_{MPP} \times \dfrac{SO_4}{SO_X} \times \dfrac{b_{SO_4}}{SO_4}}{b_{ext}} \qquad (9-1)$$

Though it incorporates a serious temporal resolution limitation, the ambient tracer concentration, T, is thought to provide a very reliable measure of the primary MPP impact at any of the monitoring sites. The uncertainty in the MPP impact potential is only a function of the tracer measurement uncertainty and the stability of the SO_x to tracer ratio, $(SO_X/T)_{MPP}$, in the plume at the stack. The net effect of these factors is relatively small ($\sigma < 15\%$) at Meadview, but is larger at Hopi Point, where the tracer concentrations are smaller. Had there not been tracer data, the uncertainty for this step would be considerably larger. This can be readily appreciated by considering the much larger range of results estimated by the source contribution methods employed prior to release of the tracer data to the analysts.

Without question the largest cause of uncertainty and reason most responsible for the range of the findings among the various methods is the lack of credible information concerning the time and space variation of the yield of particulate sulfate produced from MPP. The yield can be

expressed as the ratio SO_4/SO_x. Much is known about the processes involved in a hypothetical sense. Dry conversion rates during daylight hours range from about 0.5% to 5% per hour with the lower end of the range more appropriate to a relatively clean desert environment. Wet conversion can be much faster but requires plume cloud interaction, is limited by the availability of oxidizing compounds, and probably stops well short of 100% conversion in any case. Finally, depositional losses of particulate sulfate and SO_2 between MPP and the monitoring site, especially the substantial washout that would be caused by rain events, can further change the yield.

The problem is not a lack of understanding of the processes as much as far too little information of the type needed to apply our understanding. For example, consider a day with clouds that could interact with MPP emissions. The yield could range from less than 5% to 50% or greater depending on whether the MPP emissions entirely missed or encountered clouds in a wet chemistry efficient manner. The factor of 10 range of uncertainty for sulfate yield for this example is directly translated to a factor of 10 uncertainty in the estimated MPP contribution to light extinction (F_{MPP}). Fortunately many days did not have a high probability for cloud interaction so the range of uncertainty is smaller. However, even under dry/cloudless conditions, the uncertainty is as much as a factor of 2 due to uncertainty in effective transport duration and number of daylight hours during transport (caused by not knowing the MPP impact timing better than the 12-hour sample period resolution). The combined range of uncertainty in yield depends on the true mixture of dry and wet conversion sample periods, which is unknown.

The method for converting the estimated MPP contributed sulfate concentration to extinction coefficient is to multiply by a relative humidity dependent extinction efficiency term (in equation 10-1, b_{SO4}/SO_4). The extinction efficiency term that was used was 2 m^2/g times f(RH). The value of 2 was determined from first principle model calculations using the sulfate particle size distribution. The relative humidity function, f(RH), is adapted from laboratory measurements of water vapor growth data for sulfate aerosol. Sulfate particle size distribution data were available for many of the summer intensive days but not generally for other periods. The average and standard deviation of the calculations of dry particle efficiency is 2.2 ± 0.5 m^2/g, with a range from about 1.5 to 4.1 m^2/g. In other words there is about a 10% negative bias and roughly 25% uncertainty in the use of the rounded off value of 2 m^2/g. The uncertainty in the relative humidity function is smaller than the uncertainty in the dry efficiency for the relative humidity conditions experienced during all of the summer intensive period and much of the winter intensive period (RH < 90%).

The greatest confidence limit issue with respect to the extinction coefficient measurement (b_{ext}) is the possibility of a positive bias in the transmissometer measurements for Meadview during the summer intensive (discussed further in Section 5). To assess the magnitude of the effects of this possible bias on the findings concerning the MPP contributions to light extinction coefficient, particle calculated light extinction coefficient values were used in a separate calculation of the findings (Figure 9-6and Meadview during the summer where the range is larger by about one third to one half using the calculated values.

Table 9-5). The calculated extinction coefficients are more likely to underestimate the true light extinction coefficient than to overestimate it. Using the calculated extinction increased the 90th percentile values at Meadview during the summer by about one third to one half. The random

measurement error for the transmissometer determined light extinction coefficient is about 10% to 15%.

As indicated above, most of the uncertainty in the principal findings of Project MOHAVE is the result of uncertainty in the yield of particulate sulfate from SO_2. The various methods used to estimate the contribution of MPP to visibility at GCNP used a number of approaches from simplistic assumptions to sophisticated meteorological/chemical modeling to attempt to assign the reasonable values and constructive limits (e.g. CALPUFF Dry and Wet). For this report, the ranges of estimate by the various methods at different points in the cumulative frequency distribution are taken as credible ranges for the findings. To examine the plausibility of this approach in light of the uncertainty in the yield, a reconfiguration of the data using the most reliable steps in the process was conducted by solving Equation 9-1 for the yield, *(SO_4/SO_X)*.

Figure 9-22 and Figure 9-23 show time plots of the yield for each 12-hour period that would be required to generate 1% and 10% of the measured light extinction coefficient in summer at the Meadview and Hopi Point sites (i.e. set F_{MPP} = 1% and F_{MPP} = 10%). This information was produced solely from the tracer measurements (*T*) along with the emissions ratio of SO_x to tracer ratio (*SO_x/T*) for MPP, the extinction efficiency (*b_{SO4}/SO_4*) and measured extinction coefficient (*b_{ext}*) as described above. Obviously, a yield greater than 100% is not possible, so any point above 100% yield (horizontal line) is a 12-hour period where MPP could not have contributed 1% or 10% of the light extinction coefficient. While an attainable upper limit is not generally agreed upon, most of the analysts would consider 50% a pretty large fraction even for wet conversion over the distances involved here and 5% to 10% might be considered easily attainable with dry conversion for transport during daylight hours.

These time plots illustrate the potential for MPP to contribute at the 1% and 10% of the light extinction coefficient levels during the summer intensive period. Using any reasonable upper limit (e.g., between 50% and 100%) as a yield criterion, one would say that most of the time MPP doesn't have the potential to contribute as much as 10% of the light extinction coefficient at Meadview and as much as 1% of the light extinction coefficient at Hopi Point. Using any reasonable lower limit as a yield criterion (e.g. between 5% and 10% for daytime transport), one would say that MPP often has the potential to contribute at least 1% of the light extinction coefficient at Meadview.

Yield is the big unknown in the process. However, these time plots demonstrate that the use of any user-selected reasonable limits for conversion generates results that are broadly consistent with the ranges that are the findings shown in Section 9.6. This assessment can not shed any light on which of the methods is more likely to be correct overall or during any particular time period, but it does show that the true values are unlikely to lie outside of the ranges.

Uncertainty necessarily increases for the findings concerning MPP contributions during non-tracer periods. CALPUFF predictions of tracer concentration at Meadview for the period with the augmented upper air wind data are the basis for the assessment of the non-tracer period MPP contributions. CALPUFF tracer estimates are arguably as good at predicting measured tracer as those of any of the other air quality models. There is no way to know whether the agreement would be as good or worse for the periods without tracer and so the result that 'March and April

may have comparable MPP contributions to those found during the summer intensive period' should be treated as semi-quantitative at best.
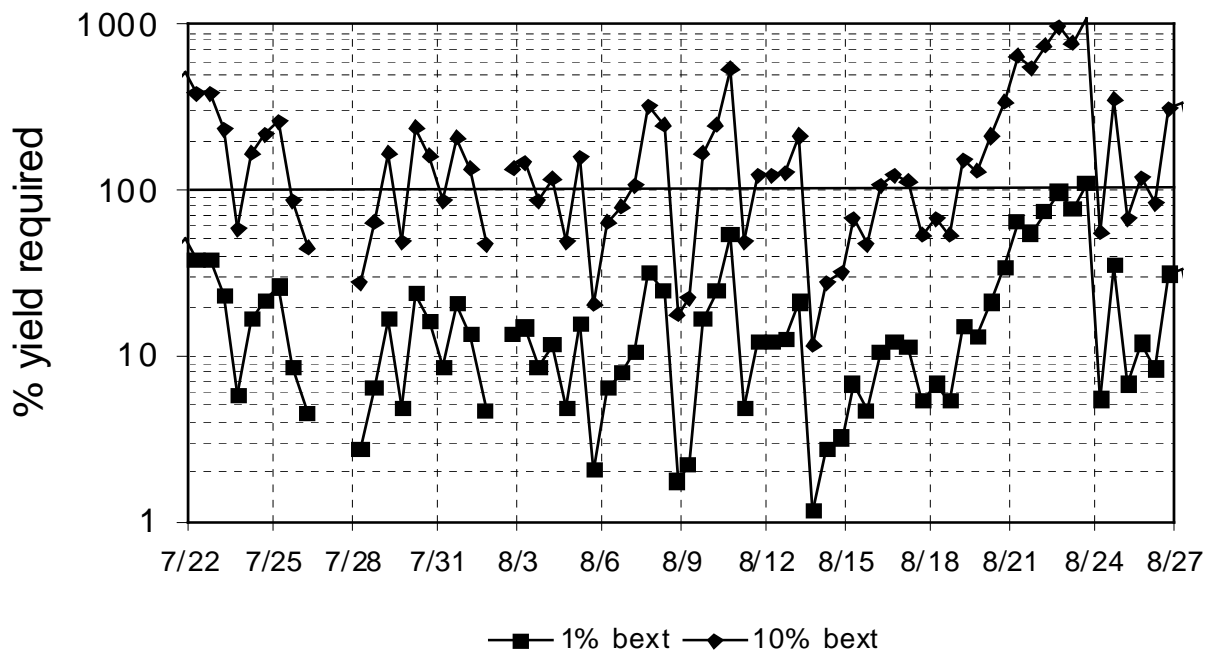
Figure 9-22: Time plots of the particulate sulfate yield for each 12-hour period that would be required to generate 1% and 10% of the measured light extinction coefficient in summer at Meadview.
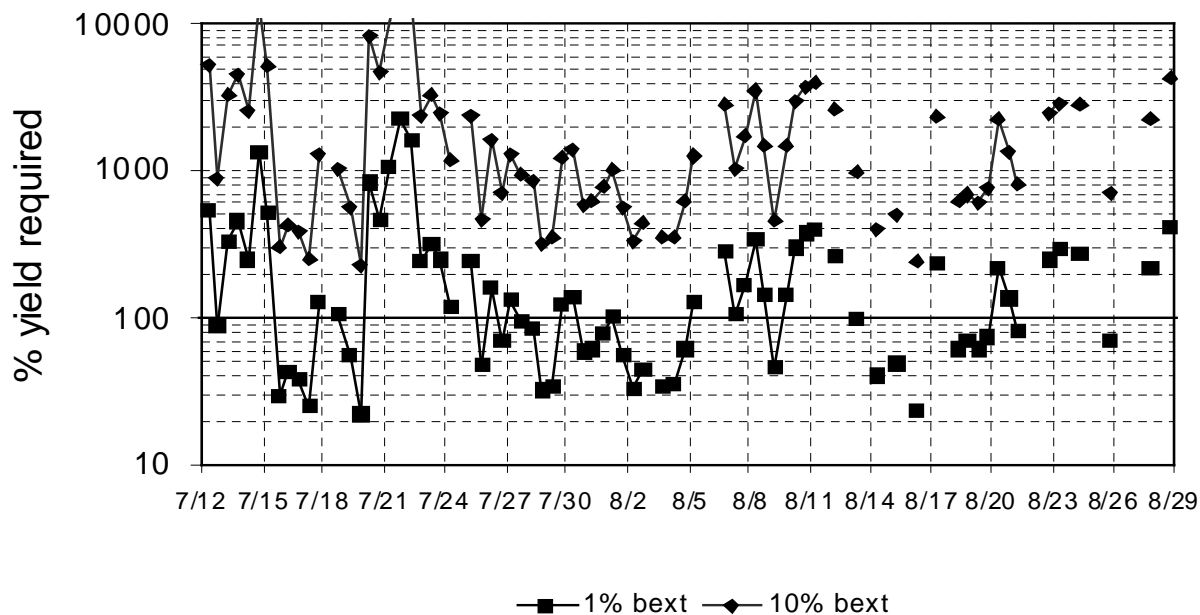
Figure 9-23 Time plots of the particulate sulfate yield for each 12-hour period that would be required to generate 1% and 10% of the measured light extinction coefficient in summer at Hopi Point.

Uncertainty in the adjustment factor to estimate the maximum MPP short-term impacts for any 12-and 24-hour estimate contribution to light extinction coefficient may be best expressed by the ranges of results of the two methods that generated the consensus factor. For the factor to adjust from the 12-hour estimates the range was about 1.5 to 4 and for the factor to adjust from 24-hour estimates the range was about 2 to 8. The consensus value of 2 is near the low end of the range principally because of the concern that this term may be more used to adjust the highest MPP impact estimates which may have involved longer than average impacts. Certainly if the consensus adjustment term were used to adjust all of the 12- or 24-hour predictions the results would be biased too low. However, it was never the intent of the data analysts to use this adjustment so broadly. It was developed solely to give a semi-quantitative sense of how much greater the short-term impact may be than the sample period averaged impacts.

It is useful to view the computer simulated photographs in the CD-ROM accompanying this report when considering whether the ranges of estimated MPP fractional contribution to light extinction coefficient are sufficiently narrow to make judgments concerning MPP impacts. Take for example the 90th percentile range for Meadview summer as shown in Table 9-4 with a range from 1.3% to 5.0%. While the range is a factor of four, it seems unlikely that the difference in these two estimates would be visible. Even if the values were multiplied by 2 to crudely estimate the maximum short-term impacts the differences would be less than 10%.

10.   Summary and Conclusions

Project MOHAVE sponsors and participants designed and operated an air quality monitoring program, including perfluorocarbon tracer studies in the winter and summer of 1992, and conducted extensive data analysis and modeling with the primary goal of characterizing the impact of MPP emissions on visibility at Grand Canyon National Park. The project had five specific objectives to meet in order to achieve its goal:

1.   Evaluate the measurements for applicability to modeling and data analysis activities.

2.   Describe the visibility, air quality and meteorology during the field study period and determine the degree to which these measurements represent typical visibility events at the Grand Canyon.

3.   Further develop conceptual models of physical and chemical processes which affect visibility impairment at the Grand Canyon.

4.   Estimate the contributions from different emissions sources to visibility impairment at the Grand Canyon, and quantitatively evaluate the uncertainties of those estimates.

5.   Reconcile different scientific interpretations of the same data and present this reconciliation to policy-makers.

This section summarizes the results of Project MOHAVE in terms of these objectives and comments on lessons learned during the project.

10.1   Evaluate the measurements for applicability to modeling and data analysis activities.

Project MOHAVE measurements were acquired over the entire 1992 calendar year. In particular, detailed meteorology, visibility, air quality, and tracer measurements were collected during a winter intensive sampling period (1/14/92 to 2/15/92) in a 31 site network and a summer intensive sampling period (7/12/92 to 9/2/92) in a 34 site network. These measurements were organized into a consistent and documented database and subjected to tests to determine their completeness, precision, lower quantifiable limit, and accuracy. Validation tests were applied to address the uncertainties that the data impart to data analysis and mathematical simulations. Where possible, the sensitivity of Project MOHAVE conclusions to measurement uncertainty was evaluated.

10.2   Describe the visibility, air quality and meteorology during the field study period and determine the degree to which these measurements represent typical visibility events at the Grand Canyon.

Measured light extinction (a parameter that is inversely related to the visual range) is lower at Grand Canyon National Park (GCNP) than at most other sites in the United States. Median light extinction levels were lower during the winter intensive sampling period than during the summer period. At Meadview, on the western border of the GCNP, the closest park location to MPP, the light extinction coefficient averaged 27.6 Mm^{-1} in winter and 32.5 Mm^{-1} in summer; at Hopi

Point, on the southern rim toward the eastern end of the canyon, it averaged 20.2 Mm^{-1} in winter and 22.7 Mm^{-1} in summer; and at Indian Gardens, within the canyon near Hopi Point, the values were 33.5 Mm^{-1} in winter and 35.5 Mm^{-1} in summer. Visibility was generally worse within the canyon than on the rim.

At Meadview, median PM_{10} concentrations were 3.9 µg/m^3 in winter and 14 µg/m^3 in summer. Median $PM_{2.5}$ concentrations were 1.6 µg/m^3 in winter and 5.4 µg/m^3 in summer. Rayleigh scattering (the extinction of light due to clean air) accounted for the largest fraction of calculated light extinction: $54 \pm 11\%$ in winter and $42 \pm 8\%$ in summer. Organic material and ammonium sulfate aerosol were major contributors to the calculated light extinction ($15 \pm 4\%$ and $13 \pm 6\%$, respectively) during the winter sampling period. Coarse mass and ammonium sulfate were the major contributors ($21 \pm 8\%$ and $18 \pm 5\%$) to light extinction during the summertime sampling period.

Perfulorocarbon tracer (PFT) measurements indicated that emissions from the Dangling Rope release point, near the eastern end of the canyon, were typically transported downriver within the Grand Canyon during the winter sampling period. Emissions from the MPP were also transported southward down the Colorado river, in winter. In summer, flows were generally reversed from the winter. Tracer released from El Centro was predominantly detected at monitoring stations north and east of the release site. Emissions from Tehachapi Pass were transported east toward Las Vegas. The MPP tracer was transported north over Lake Mead.

These findings are consistent with visibility, air quality, and meteorological observations conducted over a longer time period. Between 1987 and 1994, the summer seasonal median extinction on the rim ranged from 21 to 27 Mm^{-1}. Within the canyon, summer median extinction ranged from 30-36 Mm^{-1}. The winter seasonal median ranged from 17 to 20 Mm^{-1} on the rim. Within the canyon, the median winter time extinction ranged from 25 to 33 Mm^{-1}.

Aerosol sulfate levels measured as part of SCENES (1984 through 1989) and IMPROVE (1987 to 1997) were comparable to those measure during Project MOHAVE study. For the period corresponding to the winter intensive monitoring period (January 14-February 13), the SCENES 50th percentile was 0.22 µg/m^3 compared to Project MOHAVE's 0.19 µg/m^3 at Meadview. Summertime median sulfate concentrations at Meadview were 0.51 µg/m^3 during Project MOHAVE and 0.44 µg/m^3 during SCENES. At Hopi Point, Project MOHAVE summer intensive study median was 0.38 µg/m^3 compared to SCENES 0.40 µg/m^3 and IMPROVE 0.30 µg/m^3.

1992 was a moderate El Niño year in the southwestern United States, which led to above normal precipitation and clouds, particularly during the winter season. Most of this moisture emanated from atypically high "thermal low" patterns (strong westerlies in the desert Southwest) which occurred nearly 40% of the winter compared to the climatological average of 25%.

Tracer transport through the monitoring network was qualitatively consistent with seasonal synoptic scale transport patterns developed from back trajectory calculations for the period 1979 to 1992. The 13 year transport record indicates that in winter there are no prevailing winds at the rim of the canyon at Hopi Point. In summer, transport is usually from the southwest.

10.3   Further develop conceptual models of physical and chemical processes which affect visibility impairment at the Grand Canyon.

Because of the tendency for MPP emissions to be transported in the direction of the Grand Canyon principally in summer, the major focus of project analyses and mathematical simulations of the air quality was the summertime period. During the summer, the dominant contributors to visibility impairment at Meadview were coarse particles, ammonium sulfate, and carbon.

Modeling of MPP emissions indicated that the formation of sulfate particles was small in dry conditions, but was much greater when the plume interacted with liquid water in clouds. Analysis of the optical effects of the size spectrum of sulfate particles in the desert produced the conclusion that they were smaller than the most efficient size, and had a dry scattering efficiency of about 2 m^2/g.

Thus the conceptual model that evolved for determining the impact of MPP emissions on GCNP visibility was the following: (1) MPP emissions were transported toward GCNP mainly when the flow at MPP was from the south, which occurred mostly in the summer; (2) The SO_2 emitted by MPP was converted to sulfate in appreciable amounts only when the plume interacted with clouds; (3) The resulting sulfate particles had a dry scattering efficiency of 2 m^2/g, which is less than the value of 3 m^2/g that is typically used; and (4) The impact of the emissions was greatest at the western end of GCNP, the location closest to MPP.

10.4   Estimate the contributions from different emissions sources to visibility impairment at the Grand Canyon, and quantitatively evaluate the uncertainties of those estimates.

Detailed analysis of field measurements was unable to link elevated sulfate concentrations with MPP emissions. In general, the concentrations of visibility-impairing species seemed to be affected by regional sources and regional meteorology. Several analyses of concentration patterns and of distributions of the PFT and of other natural tracers all concluded that the dominant sources of GCNP visibility impairment were area sources (principally urban) in Southern California, Arizona, and northern Mexico. The Las Vegas urban area was also implicated in some analyses.

Modeling of the MPP contribution by various methods concluded that the 50th percentile impact of MPP emissions to the 12-hour average measured light extinction at Meadview in the summer is between 0.2 and 0.6% with upper bound as high as 1.0%. The 90th percentile impact is between 1.3 and 2.8% with upper bound as high as 5.0%. The shorter term impacts may be, perhaps, twice these values. Contributions at Hopi Point were estimated to be somewhat smaller.

The uncertainties in these values have not been quantified, but the range of results represents the conclusions of four different methods and thus that range can be considered an index of the uncertainty in any particular estimate.

10.5   Reconcile different scientific interpretations of the same data and present this reconciliation to policy-makers.

Initial assessments of the impact of MPP on GCNP extinction differed widely and the models used were not effective at predicting the concentrations of the perfluorocarbon tracer.

Subsequent methods, which relied on the tracer data to provide information on transport and dilution, had better agreement with each other. As the discussion above has indicated, the 50th percentile MPP extinction impact at Meadview was $0.6 \pm 0.4\%$ and the 90th percentile impact was $3 \pm 2\%$. Thus all results were within about 70% of a mean value, which indicates that the methods agreed relatively well in this comparison. Unfortunately, comparisons of results at specific locations at specific times did not agree as well as the comparisons of values at the same percentile level.

In light of the good agreement in contribution statistics, the results of all methods have been included in the presentation of study results in this report, with no effort made to assign more or less credibility to any specific method.

10.6   Technical Lessons Learned as a Result of Project MOHAVE

Project MOHAVE reflects the combined efforts of many investigators in many organizations. Although the project was successful overall, not all approaches that were used were successful and some findings indicated that a different measurement or analysis might have been more appropriate. As an epilogue, it may be useful to review some of these lessons learned.

Perhaps the most important technical lessons learned had to do with the benefits and limitations of using tracer technology. Project MOHAVE demonstrated that, contrary to the experience in several previous studies, high quality tracer data for study of the transport and dispersion characteristics of point source emissions can be practically achieved in a large field program. Some of the more useful features of the tracer component of Project MOHAVE are the extensive background (no tracer released) monitoring with collocated samplers to document background variability and measurement precision near background concentrations, and use of collocated sampling during the entire tracer release period at a few sites. Both of these allowed the quality control performance characteristics of the tracer component of the study to be determined.

Without the tracer data the range of results from various source contribution methods would have been substantially larger, the advocates of the various methods would have been energetically defending their results and there would have been no way to establish the crediblity of any of the methods. This in fact happened as part of the preliminary assessment conducted several years after the field study but prior to the release of the tracer data to the analysts, as described in Section 8.1. Comparison of the preliminary analysis methods' predictions of tracer concentration to the tracer measurements demonstrated the poor performance of those methods. These comparisons did not include any consideration of the transformation of SO_2 to sulfate, because the PFT is inert, a limitation that prevents full evaluation of the performance of all modules of the models.

At the time of the evaluation of the preliminary methods, the very low correlation coefficients between predicted and measured tracer (Table 8.1) were given the greatest attention as indicators of this poor performance of the methods. Subsequent to the comparison of the various post-tracer release assessment method results, use of a range of results from the various models' cumulative frequency distributions was adopted because of the inability to resolve which methods were more likely to be correct for sample periods where there were significant

disagreements. However, agreement among cumulative frequency distribution curves is a much less rigorous criterion than the correlation criterion applied to the pre-tracer release methods.

Could roughly the same findings have been developed using the preliminary assessment methods' predictions of primary transport of MPP instead of the tracer data? Figure 10-1 and Figure 10-2 show frequency distributions of the preliminary assessment methods' predictions of tracer and measured tracer. They show a range of a results at the 90th percentile of about a factor of 10 at Meadview and 6 at Hopi Point that would replace the estimated combined uncertainty of $\pm 15\%$ for the measured tracer and ratio of tracer to SO_2 in the MPP plume. In other words, the MPP potential impact step in the assessment process would have nearly comparable uncertainty with the SO_2 to particulate sulfate yield step, and the overall results would have been much less credible.

Its interesting to note that the only models in the final analysis that came close to reproducing the cumulative frequency distribution of the measured tracer data at Meadview used wind fields developed from a very high spatial resolution model (<1 km grid spacing). However, these only agree well over about 20% of the time periods and substantially under-predict for 40% or more of the time. At Hopi Point the MCMB estimates have a cumulative frequency distribution that is most nearly like the measured tracer, but is still about a factor of two too low on average. It would have been interesting to have compared the results of the higher spatial resolution models for Hopi Point, but computational limitation precluded such high spatial resolution over the larger domain required to include the more distant site.

Reasons for the poor performance vary depending on the type of assessment method. Inadequate resolution of meteorological data and spatial resolution that is inadequate to account for the terrain are thought to be the principal reasons that air quality models performed poorly. Both during the winter and summer intensive periods, spatial patterns of tracer revealed that terrain channeling of flow is an important phenomenon. Models that cannot correctly simulate flow are unlikely to perform well. There are a greater variety of possible causes for poor performance among the empirical models. For those that quantify source influence to an ambient particle sample by using source compositional characteristics, the possible problems arise from inadequate uniqueness and insufficiently known or non-conserved source characteristics. Spatial analysis methods may have performed poorly due to insufficient spatial data (i.e. insufficient numbers of sites) or substantial vertical gradients of pollutants.

Some of the methods used in the preliminary assessment were ultimately used in the final assessment with some method modification or changed input data. It is not clear that any of the method adaptations employed to improve performance can be generalized and transferred to other situations without tracer data to test performance. As an example consider the experience of the CALPUFF modeler, whose results were improved by using upper air wind data from the radar wind profiler. However, the best performance by CALPUFF came using data from only one of several wind profiler sites. In a different modeling domain or with different source and receptor locations the optimal choice of wind data for input might be different. In other words a future source contribution study in complex terrain conducted without tracer data could not apply the lessons learned in Project MOHAVE with any great assurance that they would improve the results.
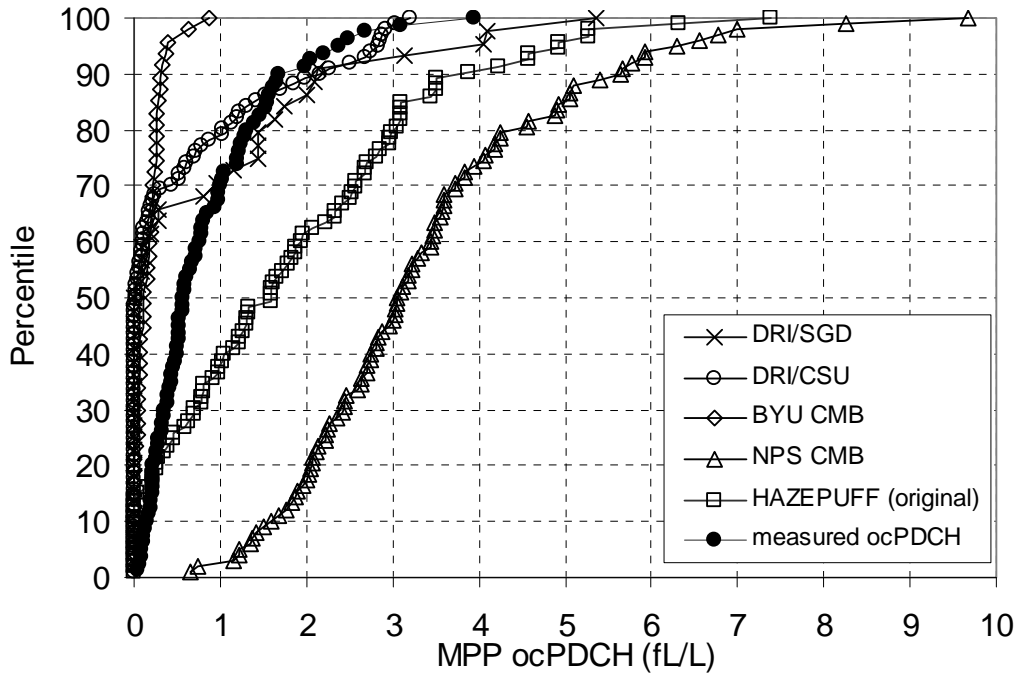
Figure 10-1 Cumulative frequency distributions of predicted and measured ocPDCH concentrations at Meadview for the summer intensive study period. Model predictions were made before the tracer data were available.
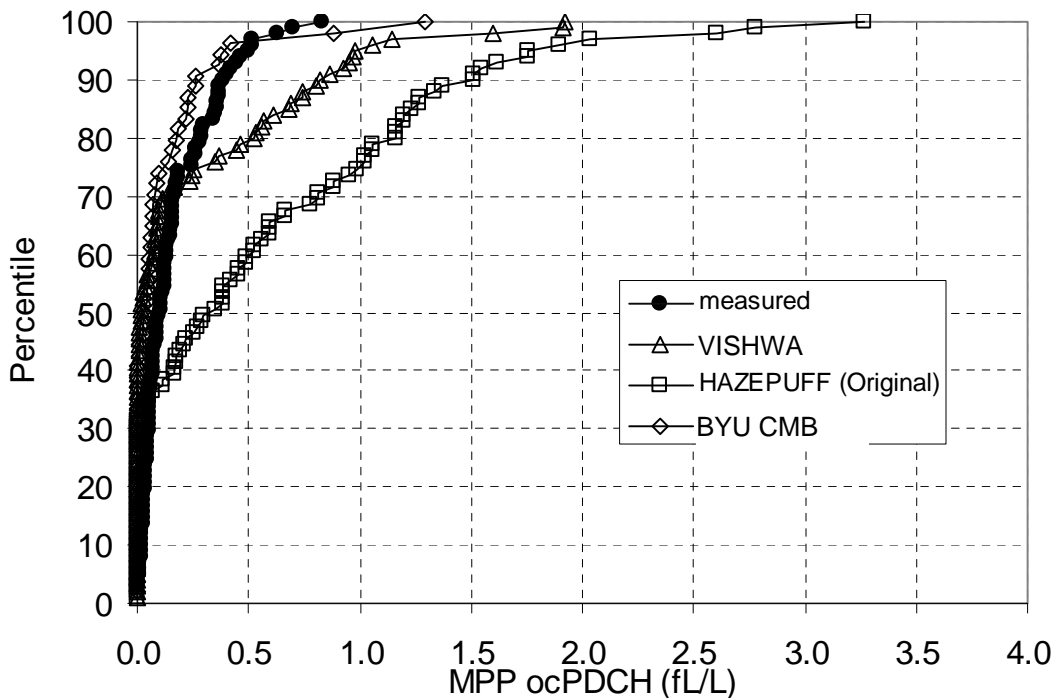
Figure 10-2 Cumulative frequency distributions of predicted and measured ocPDCH concentrations at Hopi Point for the summer intensive study period. Model predictions were made before the tracer data were available.

Availability of tracer data resulted in an expansion of the number of independent contribution assessment methods (i.e., independent assumptions and data requirements) employed. New source contribution methods were developed and applied that used the tracer data as input to account for the primary MPP impact step. The greatest limitation of these methods is the inability to operate except for periods and times with tracer data. The TAGIT assessment method used tracer data in a unique way to merely determine which monitoring locations were being influenced by MPP during any sampling period. To assess the net impact of MPP, TAGIT treated data from the unimpacted sites as background that can be subtracted from the data at MPP impacted sites. Though assessment method results do not agree on a sample period by sample period basis, the use of many independent attribution methods that provided similar distributions of results was an important process for building confidence among the technical analysis team that the range of results was credible.

The dominant cause of the differences between the various methods that were ultimately used for estimating the MPP contribution appears to be the representation of the chemistry of sulfate formation in clouds, and the related parameterization of such factors as amount of time spent in clouds. Project MOHAVE provided little experimental data to use as inputs for such calculations or to use for checking outputs, a limitation that has also been present in several other recent source attribution studies.

Consequently, the particulate sulfate yield from the MPP SO_2 emissions is the greatest source of uncertainty in the findings. Unfortunately, use of tracers did nothing to reduce this uncertainty for Project MOHAVE. If the MPP contributions had been a much larger fraction of the particulate sulfate, it might have been possible to detect a relationship between tracer and sulfate concentrations that could have shed some light on the typical yield. In future studies, high time resolution tracer data might be used to show a relationship to high time resolution SO_2, particulate sulfate and nephelometer data at a receptor site and allow a substantial insight into the conversion issue. By having high time resolution data of that type at several sites near the receptor sites, a TAGIT approach would have a much-improved chance to use spatial gradients to explore particulate sulfate yield.

11. References

AIRS (1998) http://www.epa.gov/airsweb/

Ames R.B. and W.C. Malm (1999). Estimating the Contribution of the Mohave Coal-Fired Power Plant Emissions to Atmospheric Sulfur at Grand Canyon National Park. Submitted to *JAWMA*.

Andrews, E., P. Saxena, S. Musarra, L.M. Hildemann, P. Koutrakis, P.H. McMurry, I. Olmez, and W.H. White (1999). Concentration and Composition of Atmospheric Aerosols from the 1995 SEAVS Experiment and a Review of the Closure between Chemical and Gravimetric Measurements. Accepted by JAWMA.

Angevine W.M. and J.I. MacPherson (1996) Comparison of wind profiler and aircraft wind measurements at Chebogue Point, Nova Scotia, *J. of Atmospheric and Oceanic Technology*, 12, 427-436.

Angevine W.M., P.S. Bakwin, and K.J. Davis (1998) Wind profiler and RASS measurements compared to measurements from a 450-m tower *J. of Atmospheric and Oceanic Technology* (in press).

Bastable H.G., D.E. Schorran, and D.P. Rogers (1990) Tracers of opportunity and pollutant transport in Southern California. *Atmospheric Environment* 24B, 137-51.

Cahill T.A. (1990) Particle-induced x-ray emission. *Metals Handbook Ninth Edition*. American Society for Metals. Kathleen Mills, Editor. Vol. 10, p 102.

Cahill T.A., R.A. Eldred, N. Motallebi, and W.C. Malm (1989) Indirect measurement of hydrocarbon aerosols across the United States by nonsulfate hydrogen-remaining gravimetric mass correlations. *Aerosol Science and Technology*. 10, 421.

Campbell D. S., T. A. Cahill, R. A. Eldred, C. Cahill, J. Vesenka, and T. van Curen (1989) The coefficient of optical absorption of particles deposited on filters: Integrating plate, integrating sphere, and coefficient of haze measurements. *82nd Annual Meeting of the Air and Waste Managment Association*. Anaheim, CA: 1989. 864.

Chow J.C., J.G. Watson, L.C. Pritchett, W.R. Pierson, C.A. Frazier, and R.G. Purcell (1993) The DRI thermal/optical reflectance carbon analysis system: description, evaluation and applications in U.S. air quality studies. *Atmospheric Environment* 27A, 1185.

Cui W., J. Machir, L. Lewis, D. J. Eatough, and N. L. Eatough (1997) Fine particulate organic material at Meadview during the Project MOHAVE Summer Intensive Study. *JAWMA* 47:357-369.

Dietz R.N. (1996) Perfluorocarbon tracer technology. Regional and Long-range Transport of Air Pollution, Lectures of a course held at the Joint Research Center, Ispra, Italy, 15-19 September 1996, Elsevier Publishers B.V. Amsterdam, 215-247.

Department of Energy (DOE) (1995). SO_2 emissions data. Personal Communication from Edward Trexl.

Douglas M.W., R.W. Maddox, K.W. Howard, and S. Reyes, 1993: The Mexican Monsoon, *J. of Climate* 6, 1665-1677.

Eatough D.J. (1993) Determination of endemic tracers for the source apportionment of SO_2 and sulfate in emissions from coal fired power plants for Project MOHAVE. *Project MOHAVE data report*. Brigham Young University.

Eatough D.J., L.J. Lewis, M. Eatough, and E.A. Lewis (1995) Sampling artifacts in the determination of particulate sulfate and $SO_2(g)$ in the desert Southwest using filter pack sampler *Environ. Sci. Tech.*, **29**, 787-791.

Eatough, D.J., A. Du, J.M. Joseph, F.M. Caka, B. Sun, L. Lewis, N.F. Mangelson, M. Eatough, L.B. Rees, N.L. Eatough (1997a). Regional source profiles of sources of SO_X at the Grand Canyon during Project MOHAVE. *JAWMA* 47:101-18.

Eatough N.L., M. Eatough, J.M. Joseph, F.M. Caka, L. Lewis, and D.J. Eatough (1997b). Precision and accuracy in the determination of sulfur oxides, fluoride, and spherical aluminosilicate fly ash particles in project MOHAVE. *JAWMA* 47:455-67.

Eatough D.J., R.J. Farber, and J.G. Watson (1999). Second Generation Chemical Mass Balance Source Apportionment of Sulfur Oxides and Sulfate at Grand Canyon During the Project MOHAVE Summer Intensive. *Accepted by JAWMA*.

Eatough D. and R. Farber (1999) The influence of emissions from Baja California during the August 31 – September 2 episode after the project MOHAVE summer intensive. Presented at the *92nd Annual Meeting of the Air and Waste Managment Association*. St. Louis, MO.

Eldred R.A., T.A. Cahill, M.L. Pitchford, and W.C. Malm (1988) IMPROVE--a new remote area particulate monitoring system for visibility studies. Proceedings of *the Air Pollution Control Association 81st Annual Meeting*. Dallas, TX, June 19-24. Paper No. 88-54.3.

Eldred, R.A., and T.A. Cahill (1994). Trends in elemental concentrations of fine particles at remote sites in the United States of America. *Atmos. Environ*. 28, 1009-1019.

Enger L. (1990) Simulation of dispersion in moderately complex terrain - Parts A-C *Atmospheric Environment* 24A:2431-2471.

Enger L., D. Koracin, and X. Yang (1993) A Numerical Study of Boundary-Layer Dynamics in a Mountain Valley Part 1. Model Validation and Sensitivity Experiments. *Boundary Layer Meteorology* 66:357-94.

Enger L. and D. Koracin (1994) Simulations of dispersion in complex terrain using a higher-order closure model. *Atmospheric Environment*, **29**, 2449-2466.

Farber R.J. (1995) Climatological Representativeness of 1992. Note prepared for the Meteorology Subcommittee of the Grand Canyon Visibility Transport Commission, April 4.

Farber R.J., T.E. Hoffer, M.C. Green, and P.A. Walsh, (1997). Summer transport patterns affecting the Mohave power project emissions. *JAWMA* 47:383-94.

Feeney P., T. Cahill, J. Olivera, and R. Guidara (1984) Gravimetric determination of mass on lightly loaded membrane filters. *JAPCA* 34:376.

Flocchini R.G., T.A. Cahill, M.L. Pitchford, R.A. Eldred, P.J. Feeney, and L.L. Ashbaugh (1981). Characterization of particles in the arid West. *Atmos. Environ.* 15, 2017.

Gabruk R.S., I. Sykes, C. Seigneur, P. Pai, P. Gillespie, R.W. Bergstrom, and P. Saxena (1997) Performance evaluation of the Reactive & Optics Model of Emissions (ROME). *Air & Waste Management Association 90th Annual Meeting*, Toronto, Ontario.

Gaynor J.E. and Y.J. Ping (1992a): Transport patterns in western Arizona monitored by wind profilers. Proc. of *the 4th Arizona Weather Symposium*, 10-12 June 1992, NOAA National Weather Service, Phoenix, AZ, pp. 72-77.

Gaynor J.E. and Y.J. Ping (1992b) Flow in a narrow sloping valley and implications to power plant transport. Preprint volume of *the Tenth Symposium on Turbulence and Diffusion*, 29 Sept.- 2 Oct. 1992, Portland, Oregon. Published by the American Meteorological Society, Boston, Massachusetts.

Gaynor J.E., R.B. Fritz, and Y.J. Ping (1993) Power plant plume transport in a narrow valley in the presence of complex wind and thermal vertical structure. In Proceedings: 86th annual meeting of the Air & Waste Mgmt. Assoc., June 14-18, 1993, pp. 93-TP-49.06, Air & Waste Management Association, Pittsburgh, PA.

Gebhart K.A. and W.C. Malm: (1994) Source attribution and statistical summary of data measured at Grand Canyon National Park during 1989-1991. In Proceedings: Aersosols and Atmospheric Optics: Radiative Balance and Visual Air Quality. September 26-30, 1994, pp. 1098-1124. Air & Waste Management Association, Pittsburgh, PA.

Gebhart K.A. and M.C. Green (1995) Clean Air Corridors. In the report Clean Air Corridors: A framework for identifying regions that influence clean air on the Colorado Plateau. Prepared by the Meteorology Subcommittee of the Grand Canyon Visibility Transport Commission. Available from the Western Governors' Association, Denver, CO.

Gebhart K.A. and W.C. Malm (1997). Spatial and temporal patterns in particle data measured during the MOHAVE Study. *JAWMA* 47:119-35.

Grand Canyon Visibility Transport Commission (1996). Recommendations for Improving Western Vistas. Report of the Grand Canyon Visibiliy Transport Commission to the United States E.P.A. Available for the Western Governors Association, Denver, CO. June, 1996.

Green M.C., L.O. Myrup and R.G. Flocchini (1992) A method for classification of wind field patterns and its application to Southern California. *Int. J. Climatol*. 12, 111-136.

Green M.C. and K.A. Gebhart (1997a) Clean Air Corridors: A geographic and meteorologic characterization. *JAWMA* 47, 403-410.

Green M.C., P. Pai, L. Ashbaugh, and R.J. Farber (1997b) Evaluation of Wind Fields used in the Grand Canyon Visibility Transport Commission Analyses. *Proceedings: Visual Air Quality: Aerosols and Global Radiation Balance*, Bartlett, New Hampshire, September 1997, pp.213-223, Air & Waste Management Association, Pittsburgh, PA.

Green M.C. and I. Tombach (1999). Use of project MOHAVE Perfluorocarbon Tracer Data for Source Attribution Analysis. Accepted by *JAWMA*.

Grell G.A., J. Dudhia, and D.R. Stauffer (1995) A Description of the Fifth-Generation Penn State/NCAR Mesoscale Model (MM5), National Center for Atmospheric Research, Techn. Note TN-398, 122 pp.

Hasan H. and C.W. Lewis (1983) Integrating nephelometer response corrections for bimodal size distributions, *Aerosol Sci. Technol.* **2**, 443-453.

Hasan H. and T. G. Dzubay (1983) Apportioning Light Extinction Coefficients to Chemical Species in Atmospheric Aerosol. *Atmospheric Environment* 17(8):1573-1573.

Heffter J.L. (1980) Air Resources Laboratories Atmospheric Transport and Dispersion Model (ARL-ATAD), Technical Memorandum ERL ARL-81; NOAA, Rockville.

Hegg D.A., P.V. Hobbs, and J.H. Lyons (1985) Field studies of a power plant plume in the arid southwestern United States. *Atmospheric Environment* 19, 1147.

Hegg D.A., J. Livingston, P. Hobbs, T. Novakov, and P. Russell (1997) Chemical apportionment of aerosol column optical depth off the mid-Atlantic coast in the United States. *J. Geophys. Res.* 102, 25293-25303.

Heintzenberg J, R. Charlson, A. Clarke, C. Liousse, V. Ramaswamy, K. Shine, M. Wendisch, and G. Helas (1997) Measurements and modelling of aerosl single-scattering albedo; Progress, problems, and Prospects. *Bietr. Phys. Atmosph.* **70**, 249-263.

Henry R.C. (1997a) Receptor model applied to patterns in space (RMAPS) part I -model description. *JAWMA* 47:216-9.

Henry R.C. (1997b) Receptor model applied to patterns in space (RMAPS) part II - apportionment of airborne particulate sulfur from Project MOHAVE. *JAWMA* **47,** 220-5.

Henry, R.C. (1999) Perception of color in images of simulated haze. Report prepared by R. Henry 24017 Ingomar St., West Hills, CA 91304 for EPRI, January 4, 1999.

Hoffer T.E., D.F. Miller, and R.J. Farber (1981) A case study of visibility as related to regional transport. *Atmospheric Environment* 15, 1935.

Horvath H. (1993). Atmospheric light absorption - A review. *Atmospheric Environment* **27A**, 293-317.

Horvath H. (1996) Experimental calibration for aerosol light absorption measurements using the integrating plate method - summary of the data. *J.Aerosol Sci.* **28(7)** , 1149-1161.

Huffman D. (1996) Comparison of the light absorption coefficient and carbon measures for remote aerosols: an independent analysis of data from the IMPROVE network I and II. *Atmos Environ.*, 30 (1), 73-83 and 85-99.

Iyer H.K., W.C. Malm, and R.A. Ahlbrandt (1987) A mass balance method for estimating the fractional contributions of pollutants from various sources to a receptor site. *APCA Transactions* 10, 861.

Kahl J.D., D. Liu, W.H. White, E.S. Macias, and L. Vasconcelos (1997) The relationship between atmospheric transport and the particle scattering coefficient at the Grand Canyon *JAWMA*, 47, 419-425.

Karamchandani P., Y. Zhang, and C. Seigneur (1999) Simulation of Sulfate Formation in the Mohave Power Plant Plume. Report CP026-98-1, prepared by Atmospheric and Environmental Research, Inc., San Ramon, CA, for EPRI.

Koracin D. and L. Enger (1994) A Numerical Study of Boundary-Layer Dynamics in a Mountain Valley Part 2. Observed and simulated characteristics of atmospheric stability and local flows. *Boundary Layer Meteorology* 69:249-283.

Koracin D., V. Isakov, and J. Frye (1999) A method of evaluating atmospheric models by using tracer measurements. Submitted to *J. of Applied Meteorology*.

Koutrakis P., K. M. Thompson, J. M. Wolfson, J. D. Spengler, G. J. Keeler, and J. L. Slater. (1992) Determination of aerosol strong acidity losses due to interactions of collected particles: Results from laboratory and field studies. *Atmos Environ*. **26A**, 987-995.

Kuhns H., M. Green, M. Pitchford, L. Vasconcelos, W. White, , and V. Mirabella (1999). Attribution of Particulate Sulfur in the Grand Canyon to a Specific Point Source using Tracer-Aerosol Gradient Interpretive Technique (TAGIT). *Accepted by JAWMA*.

Latimer D.A., H.K. Iyer, and W.C. Malm, (1989) Application of a differential mass balance model to attribute sulfate haze in the Southwest. In *Transactions*, *Visibility and Fine Particles*, C.V. Mathai, Ed. A&WMA, Pittsburgh, pp. 819-830.

Latimer D.A. (1993) Development of regional haze screening models. Paper 93-TP-49.04, *86th Annual Meeting of the A&WMA*, Denver, June 13-18.

Lewis E.A., L.J. Lewis, M. Eatough, L.D. Hansen and D.J. Eatough (1991) Filter pack sampler artifacts in particulate sulfate and SO_2 determination in the desert Southwest in *Proceedings, EPA/AWMA Conference on Toxic and Related Air Pollutants*, Air and Waste Management Association, Pittsburgh, PA, pp 872-884.

Lindsey C.G., T.S. Dye, R.A. Baxter (1995) Draft guidelines for the quality assurance and management of PAMS upper-air meteorological data. *Report prepared by Sonoma Technology, Santa Rosa*, *California* for USEPA, Office of Air Quality Planning and Standard, Emissions, Monitoring, and Analysis Division, Research Triangle Park, North Carolina, December.

Lowenthal D. H., C. F. Rogers, P. Saxena, J. G. Watson, and J. C. Chow (1995) Sensitivity of estimated light extinction coefficients to model assumptions and measurement errors. Anonymous. Anonymous. *Atmospheric Environment* 29(7):751-766.

Lu X. and T. Yamada (1998) Numerical simulation of airflows and tracer transport in an arid western mountain area. *Proceedings of AMS Annual Meeting*, Phoenix, January 11-16.

Macias E.S., J.O. Zwicker, and W.H. White (1981) Regional haze case studies in the E.S. southwestern U.S. -- II. Source contributions. *Atmospheric Environment* 15, 1987.

Malm W.C., H.K. Iyer, and K. Gebhart (1989a). Application of tracer mass balance regression to WHITEX data. In Transactions, *Visibility and Fine Particles*, C.V. Mathai, Ed. A&WMA, Pittsburgh, pp. 806-818.

Malm W., K. Gebhart, D. Latimer, T. Cahill, R. Pielke, and J. Watson (1989b) National Park Service Report on the Winter Haze Intensive Tracer Experiment (WHITEX).

Malm W.C. (1992) Characteristics and origins of haze in the continental United States. *Earth-Science Reviews* 33, 1.

Malm, W.C., J. F. Sisler, D. Huffman, R.A. Eldred, and T.A. Cahill (1994). Spatial and seasonal trends in particle concentration and optical extinction in the United States. *J. Geophys. Res.* 99, 1347-1370.

Malm W.C. and S.M. Kreidenweis (1997) The effects of models of aerosol hygroscopicity on the apportionment of extinction. *Atmos. Env*. **31**, 1965-1976.

Malm W.C. (1998) Examining the relationship between aerosol concentration and partial scattering efficiencies near the Grand Canyon. *Annual Meeting of the A&WMA*, San Diego, CA.

Markowski. G. R. (1992) The WHITEX Study and the Role of the Scientific Community: A Critique. *JAWMA* 42(11):1453-1460.

Mathai C. V. (1995) The Grand Canyon Visibility Transport Commission and visibility in Class I areas. *EM* 1(12):20-31.

McMurry P. H., X. Zhang, and C. T. Lee. (1996) Issues in aerosol measurement for optics assessments. *J. Geophys. Res.* 101(D14):19189-19198.

Miller D.F., D.E. Schorran, T.E. Hoffer, D.P. Rogers, W.H. White, and E.S. Macias (1990) An analysis of regional haze using tracers of opportunity. *JAWMA* 40, 757-61.

Mirabella V.A. (1996a). Summary of MPP tracer dispersion modeling simulations, Latimer HAZEPUFF model – Project MOHAVE Summer Experiment. Memorandum to Project MOHAVE technical group, prepared by Southern California Edison. November 12.

Mirabella V.A. (1996b). Supplemental Analysis: Latimer HAZEPUFF model, Project MOHAVE summer experiment. Memorandum to Project MOHAVE technical group, prepared by Southern California Edison. November 14.

Mirabella V. (1997) Relating summer ambient particulate sulfur and sulfur dioxide to gaseous tracer emissions at the Mohave Power Project. Proceedings, Visual Air Quality, Aerosols & Global Radiation Balance, A&WMA, Pittsburgh, pp. 733-753.

Murray L.C., R.J. Farber, M.D. Zeldin, and W.H. White (1990) Using statistical analyses to evaluate modulation in SO2 emissions. In: *Transactions, Visibility and Fine Particles*, edited by Mathai, C.V. Pittsburgh, PA: Air & Waste Management Association, 1990, p. 923-934.

National Research Council (1990) Haze in the Grand Canyon – An evaluation of the Winter Haze Intensive Tracer Experiment. Prepared by the Committeee on Haze in National Parks and Wilderness Areas. National Academy Press, Washington D.C.

Neff W.D. (1990) Remote sensing of atmospheric processes over complex terain. *In Atmospheric Processes over Complex Terrain*. W. Blumen, editor. American Meteorological Society, Boston, MA. 173-228.

Neff W.D. (1994) Mesoscale air quality studies with meteorological remote sensing systems *International Journal of Remote Sensing*, 15, 393-426.

Nelson L. R. (1991) Personal communication. May 8, 1991.

Patterson P., H. Iyer, J. Sisler, and W. Malm (1999). An analysis of the yearly changes in sulfur concentrations at various national parks in the United States for the period 1980-1996. Submitted to *JAWMA*.

Pilinis C., S. N. Pandis, and J. H. Seinfeld (1998) Sensitivity of direct climate forcing by atmospheric aerosols to aerosol size and composition. *J.Geophys.Res.* 100 (D9):18739-18754.

Piringer M., K. Baumann, H. Rotzer, J. Riesing, K. Nodop (1997) Results on perfluorocarbon background concentrations in Austria. *Atmospheric Environment* 31, 515-527.

Pitchford M.L., and W.C. Malm (1994). Development and Application of a Standard Visual Index. *Atmospheric Environment* 28, 1049-1054

Pitchford M. and M. Green, (1997). Analyses of sulfur aerosol size distributions for a forty-day period in summer 1992 at Meadview, Arizona. *JAWMA* 47:136-46.

Raabe O.G., D.A. Braaten, R.L. Axelbaum, S.V. Teague, and T.A. Cahill (1988) Calibration Studies of the DRUM Impactor. *Journal of Aerosol Science*. 19.2:183.

Richards L.W., C.L. Blanchard, and D.L. Blumenthal (1991) Navajo Generating Station Visibility Study: Executive Summary. Sonoma Technology Inc. report STI-90200-1124-FRD2, April 16, 1991. Prepared for Salt River Project, Phoenix AZ.

Seigneur C., X.A. Wu, E. Constantinou, P. Gillespie, R.W. Bergstrom, I. Sykes, A. Venkatram, and P. Karamchandani (1997a). Formulation of a Second-Generation Reactive Plume & Visibility Model. *JAWMA* 47:176-184.

Seigneur C., X.A. Wu, E. Constantinou, P. Gillespie, R.W. Bergstrom, I. Sykes, A. Venkatram, and P. Karamchandani (1997b). Formulation of a Second-Generation Reactive Plume & Visibility Model. *JAWMA* **47:**176-184.

Seigneur C., P. Pai, I. Tombach, C. McDade, P. Saxena, and P. Mueller (1998). Modeling of potential power plant plume impacts on Dallas-Fort Worth visibility. Submitted to *JAWMA*.

Seinfeld J. H. (1986) Atmospheric Chemistry and Physics of Air Pollution. John Wiley & Sons, Inc., New York.

Sheiman D.A., D.D. Doniger, and L.L. Dator (1990) A Who's Who of American Ozone Depleters. Report by National Resources Defense Council, New York.

Sisler J.F. and W.C. Malm (1997). Characteristics of winter and summer aerosol mass and light extinction on the Colorado Plateau. *JAWMA* 47:317-30.

Sisler J.F., W.C. Malm, and M.L. Pitchford (1996) Spatial and seasonal patterns and long term variability of the composition of the haze in the United States: An analysis of data from the IMPROVE Network. CIRA Report, ISSN: 0737-5352-32.

Sloane C. S. (1986) Effect of Composition on Aerosol Light Scattering Efficiencies. *Atmospheric Environment* 20:1025-1037.

Switzer P., L. Enger, T.E. Hoffer, D. Koracin, and W.H. White (1996) Ambient sulfate concentrations near Grand Canyon as a function of fluctuating loads at the Mohave

Power Project: An exploratory analysis of an atmospheric experiment. Atmospheric Environment 30(14), 2551-2564.

Tombach I., P. Karamchandani, and P. Pai (1996). Development, Evaluation, and Application of Transfer Coefficients for Predicting Colorado Plateau Air Quality. Paper 96-TP46.03, *89th Annual Meeting of the A&WMA*, Nashville, June 23-28.

Turpin B.J., P. Saxena, G. Allen, P. Koutrakis, P. McMurry, and L. Hildemann (1997) Characterization of the southwestern desert aerosol, Meadview, AZ. *JAWMA* 47:344-56.

UC Davis (1994) UCD/*AQG* Internal Report: Absorption Coefficient, March 31.

Uliasz M. and R.A. Pielke (1993) Numerical Modeling of Air Pollution Transport in Southwestern United States Using Source- and Receptor-Oriented Techniques. In Proceedings: 86th annual meeting of the Air & Waste Mgmt. Assoc., June 14-18, 1993, pp. 93-TP-49.06, Air & Waste Management Association, Pittsburgh, PA.

U.S.E.P.A. (1991) The Project MOHAVE Study Plan, Septeber 27, 1991, Office of Air Quality Planning and Standards, Research Triangle Park, NC.

Vasconcelos L., J.D.W. Kahl, D. Liu, E.S. Macias, and W.H. White (1996a) A tracer calibration of back trajectory analysis at the Grand Canyon. *J. Geophysical Research* 101, 19329.

Vasconcelos L., J.D.W. Kahl, D. Liu, E.S. Macias, and W.H. White (1996b) Patterns of dust transport to the Grand Canyon. *Geophysical Research Letters* 23, 3187.

Vimont J. C. (1998). Evaluation of the CALMET/CALPUFF Modeling System using Project MOHAVE Tracer and Implications for Sulfate Concentrations. Proceedings, Visual Air Quality, Aerosols & Global Radiation Balance, A&WMA, Pittsburgh, pp. 436-446.

Waggoner A. (1995) Presentation at DOE Extinction Efficiency Workshop, Las Vegas, February 1995.

Wallace J. M. and P. V. Hobbs (1977) *Atmospheric Science, An Introductory Survey* San Diego, CA, Academic Press 467 pages.

Warneck P (1988) *Chemistry of the Natural Atmosphere*. Academic Press, San Diego, CA.

Weiss R.E. (1989) Accuracy Calibration for IPM Optical Absorption on 47 mm Filters, *SCENES Internal Report*.

White W. H. (1986) On the Theoretical and Empirical Basis for Apportioning Extinction by Aerosols: a Critical Review. *Atmospheric Environment* 20(9):1659-1672.

White W.H., E.S. Macias, D.F. Miller, D.E. Schorran, T.E. Hoffer, D.P. Rogers (1990). Regional Transport of the Urban Workweek: Methylchloroform Cycles in the Nevada-Arizona Desert. *Geophysical Research Letters* 17:1081-4.

White W. (1993) Extinction and particle mass measurements at Meadview during the MOHAVE summer intensive. Interim report prepared from Southern California Edison, Dec. 22.

White W.H., E.S. Macias, R.C. Ninger, and D. Schorran (1994a) Size-resolved measurements of light scattering by ambient particles in the southwestern U.S.A. *Atmospheric Environment* 28, 909.

White W.H., E.S. Macias, J.D. Kahl, P.J. Samson, J.V. Molenar, and W.C. Malm (1994b) On the potential for regional-scale emissions zoning as an air quality management tool for the Grand Canyon. *Atmospheric Environment*, 28, 1035-1045.

White W.H. (1997a). Deteriorating air or improving measurements? On interpreting concatenate time series. *J. Geophys. Res.* 102, 6813-6821.

White W.H. (1997b). Phantom Sources from Spatial Correlations: An Example. In Proceedings: Visual Air Quality: Aerosols and Global Radiation Balance, Bartlett, NH, September 1997, pp. 762-767, Air & Waste Management Association, Pittsburgh, PA.

White W.H., R.J. Farber, M.C. Green, E.S. Macias, V.A. Mirabella, M.L. Pitchford, and L.A. Vasconcelos (1999). Tracking Regional Background in a Haze Attribution Experiment. Accepted by *JAWMA*.

Yamada T. (1997). Numerical Simulations of Airflows and Tracer Transport in the Arid Western Mountainous Area. Final Report by Yamada Science & Art Corporation, Santa Fe, NM, to EPRI.

Yamada, T. (1999) Numerical Simulations of Airflows and Tracer Transport in the Western Mountainous Area. Accepted by *J. Appl. Meteor.*

Zeng X, X. Wu, H. Yao, F. Yang, and T. Cahill (1993) PIXE-Induced XRF with Transmission Geometry. *Nuclear Instruments and Methods in Physics Research*, B75, 99-104.

APPENDICES

A. Data Base Contents and Structure

The MOHAVE database has been assembled on a CDROM. The following section describes the structure of the database.

Mohave Database Structure

The Mohave database contains the data collected by the different contractors or data sources involved in this study. In addition, there are several miscellaneous database files that document the sites where the data was collected, the conversions made to the data, and the codes and field names used in this database. The Mohave database is stored in dBASE IV format.

This section describes all aspects of the Mohave database structure, including the organization of the directories, file naming convention, field name characteristics, and relational keys. In addition, it describes in detail the files containing site and database documentation.

Directory Structure

The directory structure used to organize the Mohave database files is the following:

```
    1              2            3            4

                                /arm       ayumip.dbf
                                /ars       arsmhp.dbf
                                /byu       byaabw.dbf
                                /car       casehr.dbf
                                /csu       csincs.dbf
                                /dri       drbshpg.dbf
                                /misc      mofiles.dbf
    /mohave     /dbase          /nid       nitrhs1.dbf
                                /noa       nbrthp.dbf
                                /nws       nwsmhp.dbf
                                /sce       scsehp.dbf
                                /srp       srsmhp.dbf
                                /sti       stacisc.dbf
                                /tab       tbumip.dbf
                                /ucd       udelcs.dbf
```

Column 1 above shows the main directory (mohave) and column 2 shows the dbase subdirectory that stores all dBASE files that form the Mohave database.

The names of the subdirectories on column 3 are abbreviations of the Mohave contractors or data sources that supplied the data (with the exception of the misc subdirectory). Table A-1 describes the abbreviations used for the contractors/data sources. The misc subdirectory shown in column 3 contains miscellaneous dBASE IV files which document the Mohave database and sites. Please refer to Section 2.7 for more details. Finally, column 4 shows examples of the actual dBASE data files which are stored under the subdirectories shown directly to the left of each file. For example, arsmhp.dbf can be found in the /mohave/dbase/arm subdirectory.

Table A-1 Abbreviation for contractors.

Abbreviation	Contractor
arm	Army - Yuma Proving Grounds
ars	Air Resource Specialists
byu	Brigham Young University
car	CARNOT
csu	Colorado State University
dri	Desert Research Institute
nid	NOAA - Idaho Falls
noa	NOAA - Boulder
nws	National Weather Service
sce	Southern California Edison
srp	Salt River Project
sti	Sonoma Technology, Inc.
tab	Technical and Business Systems
ucd	University of California, Davis

File Naming Convention

The database file naming convention used for all dBASE files is described below.

```
            MOHAVE DATABASE FILE NAMING CONVENTION

    FORMAT:  SSTTVPYZ.DBF


        SS   = DATA SOURCE CODE
        TT   = DATA TYPE
         V   = AVERAGING INTERVAL
         P   = TIME PERIOD
        YZ   = ADDITIONAL (if needed)


    DATA SOURCE CODES (CONTRACTORS)


        AR   = AIR RESOURCE SPECIALISTS
        AY   = ARMY - YUMA PROVING GROUNDS
        BY   = BIRMINGHAM YOUNG UNIVERSITY
        CA   = CARNOT
        CS   = COLORADO STATE UNIVERSITY
        DR   = DESERT RESEARCH INSTITUTE
        NI   = NOAA - IDAHO FALLS
        NO   = NOAA - BOULDER
        NW   = NATIONAL WEATHER SERVICE
        SC   = SOUTHERN CALIFORNIA EDISON
        SR   = SALT RIVER PROJECT
        ST   = SONOMA TECHNOLOGIES, INC.
        TB   = TECHNICAL AND BUSINESS SYSTEMS
        UD   = UNIVERSITY OF CALIFORNIA, DAVIS


    DATA TYPE CODES


        AA = ATOMIC ABSORPTION
        AC = AIRCRAFT CONTINUOUS DATA
        AO = AIRBORNE CANISTER ORGANICS
        BS = DRI BASIC STUDY
        DN = ANNULAR DENUDER
```

```
            EL = ELEMENTAL - ELEMENTS, NITRATE, SULFATE
            HA = HALOGENS
            IN = IONS
            OG = SURFACE CANISTER ORGANICS
            PR = PEROXIDES
            RT = RADAR PROFILER - TEMPERATURE
            RW = RADAR PROFILER - WIND
            SE = STACK EMISSIONS
            SM = SURFACE MET DATA
            SP = SONIC PROFILER
            TR = TRACER
            UM = UPPER AIR BALLOON - MET
            UW = UPPER AIR BALLOON - WINDS
            VN = VISIBILITY - NEPHELOMETER
            VT = VISIBILITY - TRANSMISSOMETER

      AVERAGING INTERVAL CODES

            C    = 12 HOUR SAMPLES
            H    = HOURLY
            I    = INSTANTANEOUS
            P    = PARTIAL HOUR (< 60 MIN.)
            O    = 24 HOUR SAMPLES

      TIME PERIOD CODES

            P    = PROJECT PERIOD
            R    = PARTIAL DATA
            S    = SUMMER INTENSIVE
            W    = WINTER INTENSIVE
            1-9  = JAN - SEP
            A-C  = OCT - DEC
```

For example, the filename ayumip.dbf can be decomposed as follows:

```
      ay   =  file provided by Army - Yuma Proving Grounds
      um   = which contains upper air balloon met data
       i   = gathered as instantaneous measurements
       p   = for the project period
```

```
File Extensions
```

The table below shows the file extensions that can be found in the Mohave database:

```
      Extension Description
      .DBF      dBASE IV database file
      .DBT      dBASE IV memo field file
      .TXT      Text file (ASCII)
```

Field Names

These are the general characteristics of the field names:

- The field name is up to 6 characters long and the first character is always alphabetical, and the only other characters used are underscores or digits. This maximizes compatibility with interpretation software.

- The field format (field length and decimal places) reflects the sensitivity (i.e. the lower quantifiable limit) of that measurement.

- Some parameters (i.e. hydrocarbons) were measured by different methods at the same site, so they have different field names.

- For a detailed description of each of the field names used in the Mohave database, refer to the mfldnam.dbf file.

Relational Keys

Each record in the dBASE IV files containing data supplied by the different contractors, is uniquely identified by the following fields:

```
Field Name      Description

VAL             Validation code; indicates the level of
                validation performed on that record.  Values:
                1A = data as received from the contractor, 1B
                = preliminary validation checks were
                executed.

SITE            Site code; identifies the site in which the
                measurements were obtained.

DATE            Sampling date; shown in MM/DD/YY format.

STHR            Indicates the beginning of an hourly average
                or the closest hour to a measurement.  The
                spread is 29 minutes before the hour to 30
                minutes after the hour, inclusive.  For
                example, a time X where 2:30 < X <= 3:30 has
                a start hour of 3.

HR,MIN,SEC      Hour, minutes and seconds in which the sample
                was recorded; used only for samples that are
                recorded more frequently than every hour.
```

The unique key is formed by VAL + SITE + DATE + STHR or by VAL + SITE + DATE + HR + MIN + SEC, depending on the sampling frequency.

Other Considerations

The values of all data fields have been converted to common units, regardless of how they were originally reported by the contractor. Since dBASE IV does not have an inherent way to identify missing data, we chose -99 to represent missing data.

All time (hour) values are shown in Mountain Standard Time (MST).

Site and Database Documentation

The sampling site documentation can be found in the /mohave/dbase/misc subdirectory. This miscellaneous subdirectory contains dBASE IV files with information about all the sampling sites used in the Mohave study. In addition, it contains other database files that document the conversions made to the data, and the codes and field names used in this database. Table A-2 shows a list of the database files stored in the miscellaneous subdirectory along with a brief description of their content.

Table A-2 dBASE IV site documentation files.

Filename	Description
mochange.dbf	Lists changes made to database files.
moconver.dbf	Lists conversion changes made to the measurement data files received from the contractors/data sources before they were incorporated into the database (i.e., converted temperature degree values from Fahrenheit to Celsius).
mofiles.dbf	Lists all the files that form the Mohave database, and includes the date they were received and notes on the contents of the file.
moflags.dbf	Lists the codes (and meaning of codes) used in the MOFLG field in the files containing measurement data.
mofldnam.dbf	Lists all the field names used in the Mohave database and their meaning. It also shows the units for the parameters measured.
mosite.dbf	Lists all sampling sites that participated in the Mohave study. Includes site code, elevation, coordinates, and parameters measured.

The structure of mosite.dbf and mofiles.dbf contains several field names that end with the letter X. These fields represent groups of data collected. For example, the field name NOGX represents the group of oxides of nitrogen measurements, while RHX represents the group of relative humidity measurements. The contents of the fields ending with the letter X is a two letter code that identifies the contractor or data source. This code is the same code used in the Mohave database file naming convention.

B. Approach for Estimating Short-term Impacts of MPP at Meadview

A first step in attempting to estimate the maximum short-term impacts of MPP at Meadview during the summer is to estimate the duration of MPP tracer presents at Meadview using the two weeks of high-time resolution data during the summer intensive period. Determining the duration is complicated by the inability of the high-time resolution tracer monitor to reliably differentiate background tracer levels from those just above background and by the data gaps on many of the days. The method used minimizes the impacts of these problems by considering what fraction of the data collected during a 24-hour period is responsible for a specific fraction of the total tracer measured during that 24-hour period. For example on August 12, 50% of the tracer measured above background arrived in about 17% of the day, which corresponds to just over 4 hours. If we assume that this rate of MPP tracer arrival at Meadview were continued then the duration of the impact would be just over 8 hours (twice the duration corresponding to 50%).

Figure B-1 is a plot showing the range of estimated durations of MPP tracer impacts for each day with sufficient tracer data, calculated for fractions of tracer from 10% to 90%. Using the 50% tracer duration criterion (horizontal line at 50%), 11 of the 14 days have MPP tracer impact durations from about 5 to 10 hours with the other 3 having durations from 12 to14 hours. Selection of a fraction-of-tracer criterion to use is somewhat arbitrary, with larger fractions producing somewhat longer duration estimates. Though better estimates may be reasonably expected when using a higher fraction for the criterion, at some ill-defined day-dependent point the measurements are of sufficiently low concentration that they can no longer be reliably distinguished from background levels. Using a 75% criterion, the duration estimates are from about 6 to 16 hours with most days having values less than 12 hours.
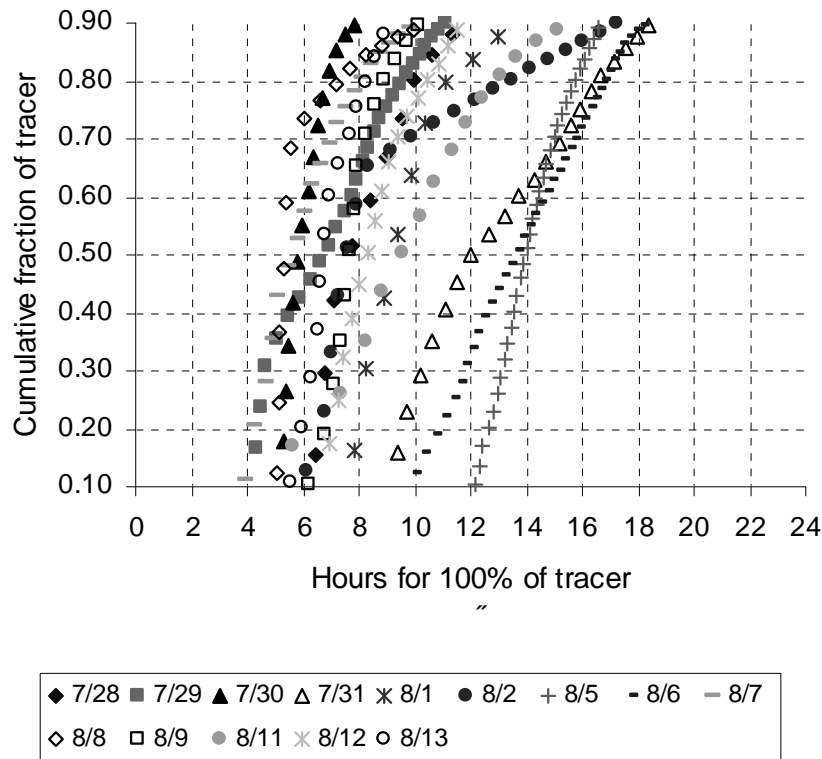
Figure B-1: Estimate time scales for tracer impact of Meadview on various dates.

The process selected to explore short-term impacts is to develop and use a simple adjustment factor (or range of factors) to estimate the magnitude of the highest short term impacts from the 12- and 24-hour estimated impacts. This allows adjustment to the estimates from any of the methods as presented above. Two approaches were used to develop adjustment factors. Both are only applied to the Meadview site during the summer intensive period for the MPP estimates of fractional light extinction coefficient. One approach uses the limited short-time resolution tracer data set, while the other uses CALPUFF predictions of hourly tracer concentrations.

As indicated above the short-term tracer data suggest that MPP impacts at Meadview in the during the summer intensive period tend to be centered on the late afternoon and evening hours with duration typically of about 8 hours. The first approach makes use of the assumptions that MPP impact occurs exclusively during the period of tracer hit and that the MPP impact is uniform even though the tracer levels may be varying. In other words it assumes a step function impact of MPP on the light extinction coefficient with the width of the step equal to the duration of the tracer hit. If the first assumption is substantially correct, which seems reasonable, then the second assumption would be expected to result in an underestimate of the magnitude of the adjustment factor, because it seems unlikely that the impact is in fact uniform. The approach also assumes that the average non-MPP contributions to light extinction coefficient are the same during the short-term impact period as for the entire 12- or 24-hour long-term period. The approach calculates the adjustment factor, the ratio of the short-term to long-term impact, consistent with the assumed step function duration and the magnitude of the long-term impact value. The resulting adjustment factors increase as impact duration decrease and as the magnitude of the long-term impact decrease.

Figure B-2 shows the result of applying the approach to the typical range of MPP tracer duration estimated from the Meadview high time resolution measurements (8.2 ± 3.4 hours duration based on 50% of tracer arriving, see Section 9.3). The resulting adjustment terms to convert 24-hour duration fraction of light extinction coefficient impacts to short term impact range from less than 2 to greater than 5 at the 5% 24-hour duration impact level depending on what impact duration is assumed.

This highlights an important question, whether the duration of the MPP impact is related to the magnitude of the impact. One might assume that the largest 12- or 24-hour average impact results from longer than typical duration of impact over the period. If this were the case then the lower line in Figure B-2 representing 11.6-hour duration out of 24 hours might be the more appropriate one to use. On the other hand, the magnitude of the impact may be unrelated to the length of impact. The problem with addressing these questions is that we do not have any direct way to gauge the magnitude or duration of the MPP contributions to sulfate or light extinction coefficient. The best surrogate that we have, tracer measurements, cannot account for deposition and SO_2 to particulate sulfate conversion processes. For example, tracer data may indicate that MPP emissions are present for 8 hours on a particular day, but the first 4 hours may have involved very little converted sulfate so that the effective period of light extinction impact was closer to 4 hours. The various source contribution models provide the only estimates to gauge the magnitude of the light extinction coefficient impact.
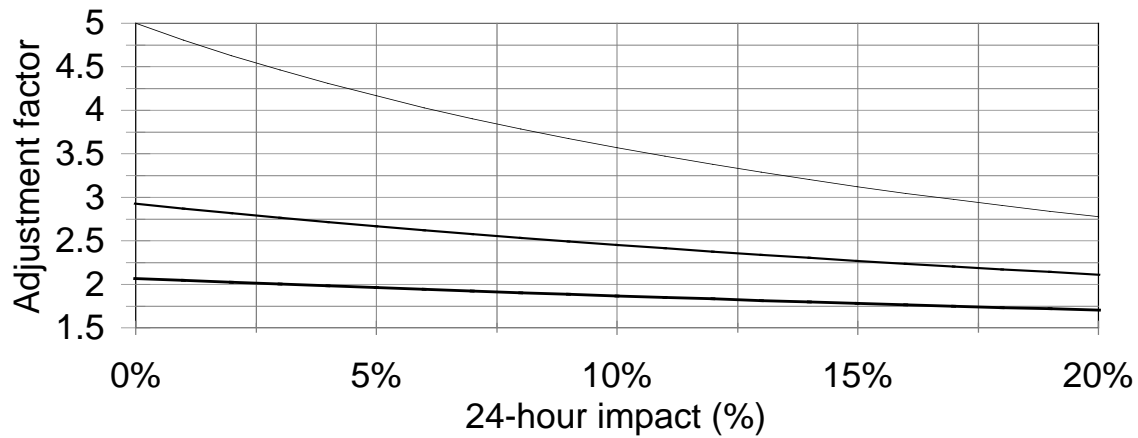
Figure B-2: Adjustment factor for converting 24 hour MPP estimated contribution to light extinction coefficient to short term impact.

Figure B-3 and Figure B-4 contain scatter plots of 24-hour duration MPP tracer concentration versus tracer duration and estimates of MPP particulate sulfate concentration by the various methods versus tracer concentration. There doesn't appear to be any relationship between measured tracer or model estimated tracer and duration. From this it would seem that there is no reason to assume that periods of greatest impact have longer (or shorter) impact duration then average. In other words the uncertainty indicated by the three curves in Figure B-2 would seem to apply regardless of the magnitude of the 24-hour impact that is being adjusted to short-term impact.

Standard deviations of the ratios of short-term to 24-hour extinction coefficient measurements at Meadview were calculated to explore the effects of the assumption of the same contribution of non-MPP sources during the short- and long-term periods. These ranged from about 0.1 for 5-hours to 0.07 for 12-hour short-term periods. These are small compared to the one standard deviation range as shown by the upper and lower curves in Figure B-2 and therefore the contribution to uncertainty is minor from this assumption

The second approach to explore the short-term impacts employs hourly estimates of the MPP tracer concentrations at Meadview by CALPUFF. The method assumes CALPUFF is able to simulate the short-term temporal characteristics of MPP tracer impacts, and that MPP light extinction coefficient impacts are proportional to the tracer concentrations. As in the previous approach, it is assumes that the average non-MPP contributions to light extinction coefficient are the same during the short-term impact period as for the entire 12- or 24-hour long-term period.
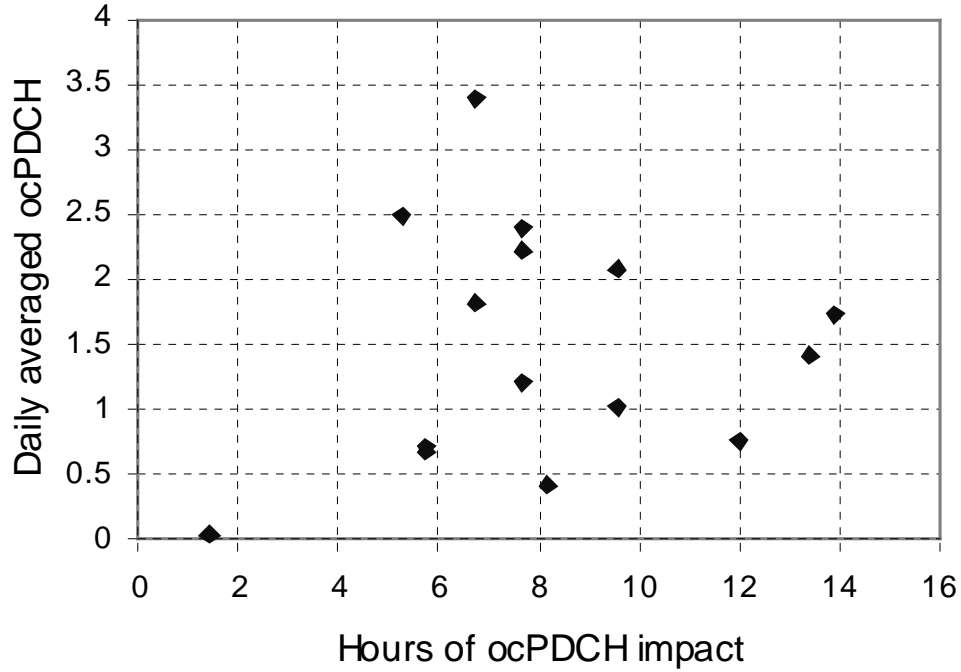
Figure B-3: Daily average ocPDCH tracer concentration at Meadview versus duration of tracer impact. The duration of impact is defined as two times the number of hours needed for 50% of the total daily tracer to arrive.
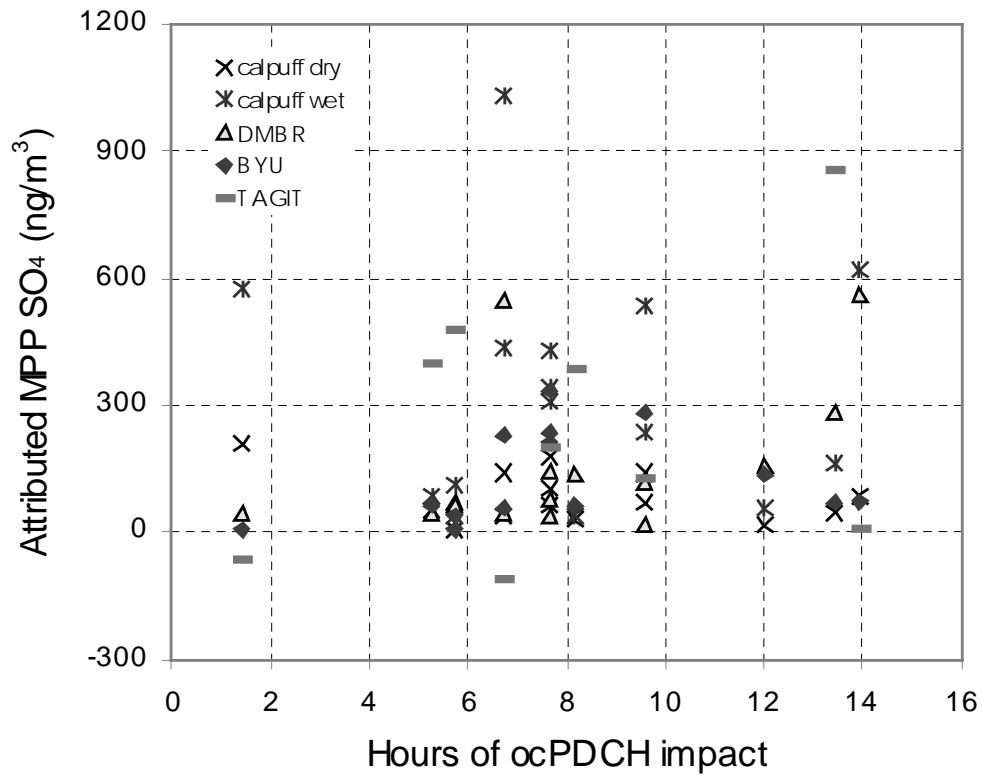
Figure B-4: Estimates of MPP attributed sulfate versus duration of tracer impact.

Unlike the high-time resolution tracer measurements, the CALPUFF hourly tracer estimates at Meadview are complete for the entire summer intensive. This permits the determination of the maximum ratio for each long-term period (12- or 24-hour) of the short-term average tracer to the 12- or 24-hour period average without concerns for missing data or detection limits near background levels. To be useful, these maximum ratios of short-term average to long-term average CALPUFF tracer estimates must be similar to what would have been obtained using short-term tracer data. Model estimates need not predict individual hourly concentrations correctly to meet the needs of this approach, but they must have about the same frequency, magnitude, and shape of peaks on a time plot as would be seen with measurement data. As seen in Figure B-5 where the CALPUFF estimates are shown as negative values to facilitate distinguishing them from the measurements, CALPUFF estimates match the frequency, but tends to have more narrow peaks that are about twice as high as the measurements. A 3-hour averaging of tracer estimates for the short-term value mitigates the problem of the narrow peaks since the peaks are generally only one or two hours long.
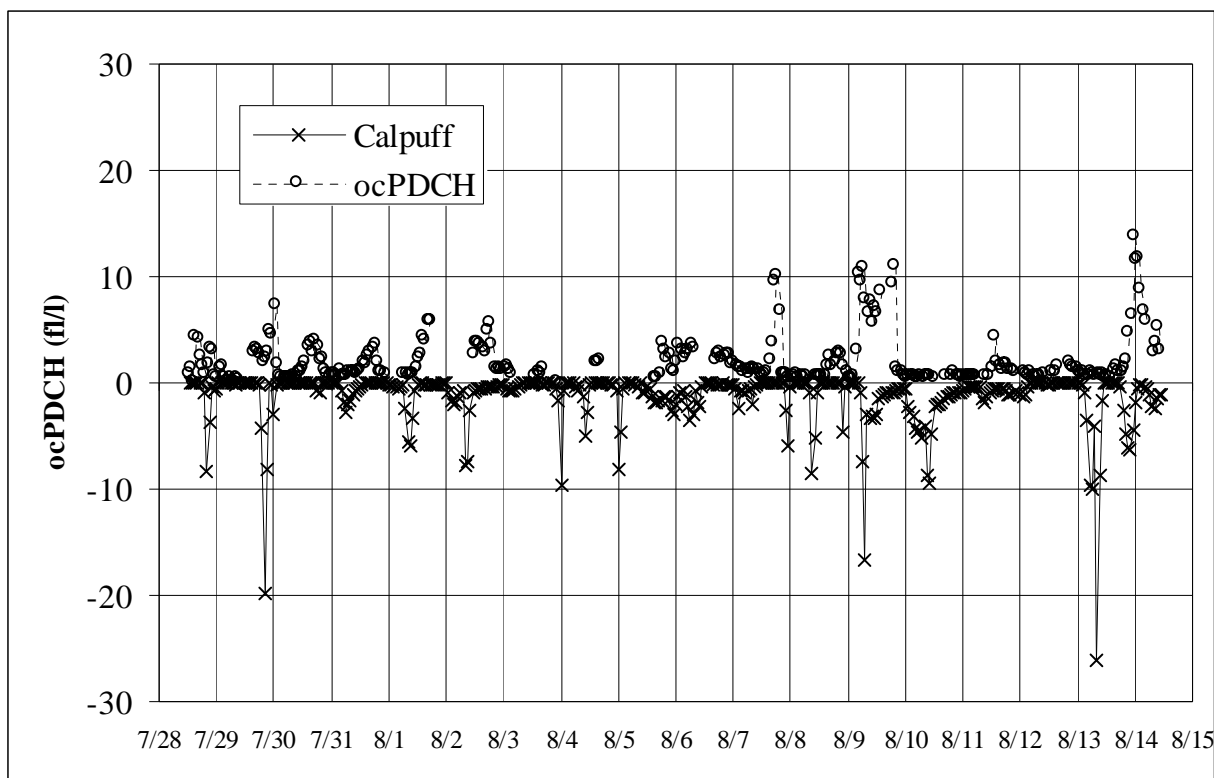
Figure B-5: One hour time series of observed ocPDCH concentration and CALPUFF predicted tracer concentrations (CALPUFF predictions are multiplied by –1 to facilitate comparison).

The second assumption for this approach, that the MPP contribution to light extinction be proportional to the tracer, basically indicates that transport and dispersion are thought to be of prime importance for determining MPP impacts. However, this can not be completely true since it ignores the variable effects of deposition and conversion chemistry. As an example consider that some periods with high tracer concentrations are probably the result of a relatively direct plume hit under moderately high wind speeds and consequently little time for dry conversion. Yet there are significant relationships between the estimate of MPP impact by the various models

(except for TAGIT) and the tracer concentration with correlation coefficients ranging from about 0.5 to 0.6 as shown in Table 9-3.

Scatter plots of the maximum ratios of 3-hour average to 24-hour and to 12-hour average versus the long-term average concentrations are shown in Figure B-6. For the ratios to 24-hour values, the range is from about 2 to 8 for the smallest 24-hour tracer concentrations, and about 2 to 4 for largest tracer concentrations. For the ratios to 12-hour values, the range is from about 1.5 to 4 over the entire range of 12-hour average concentrations. For both the 12-hour and 24-hour periods the high ends of the ranges (8 for 24 hour and 4 for 12 hour) correspond to cases with all of the CALPUFF estimated tracer for the long term period predicted to arrive in three hours or less.

From the large ranges of possible adjustment factors generated by either of the two approaches, it must be concluded that there is substantial uncertainty in estimates of short-term MPP contributions to light extinction coefficient at Meadview from the 12-hour and 24-hour results of the various models. This is not surprising considering the lack of data gathered specifically to address short-term impacts and the limitations of air quality models for high time resolution predictions. However, there is one conclusion that is certain. The short-term impacts are generally greater than the long-term average estimates because every day there are periods with very little or no impact that are incorporated into the average. While the true adjustment factor probably varies from one sample period to another, it cannot be specified very well with the available data. Given the range of results for the two approaches as shown above, for the purposes of this report the maximum short-term impact will be assumed to be twice the 12-hour or 24-hour impact estimates from the various methods.
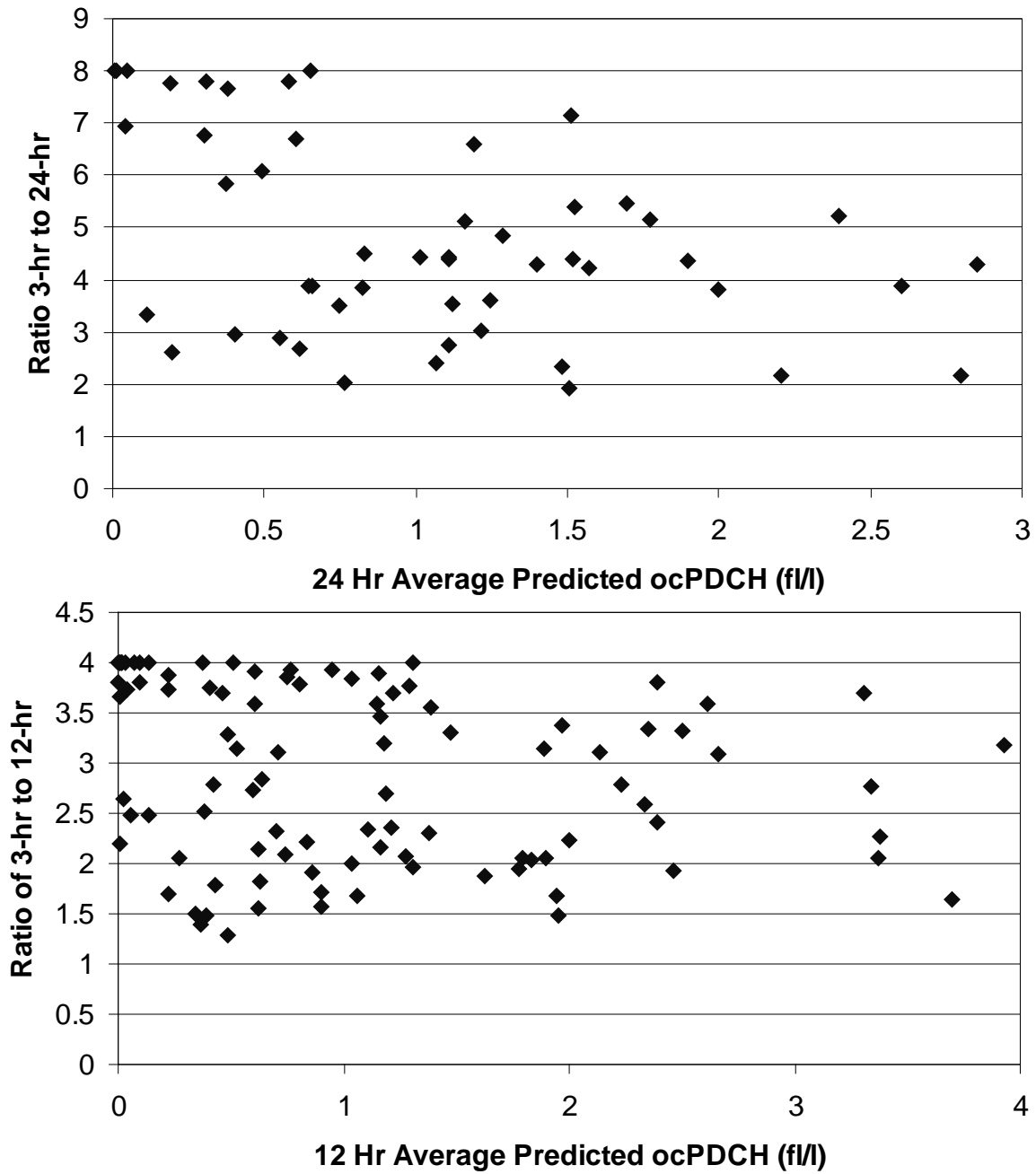
Figure B-6: Ratios of maximum 3 hour CALPUFF predicted tracer concentration to 12 and 24 hour average values.

C. Descriptions of Attribution Methods and their Application

Many of the individual studies used in Project MOHAVE are new enough that their descriptions have not yet been published in the literature and therefore are not readily available.

This appendix contains reprints of manuscripts and brief reports and memoranda that describe the research that have not yet been published in a journal. Additional information about the methods and their application is provided in the published literature and in contractor reports that are cited in the reference section. The contractor reports are available from the authors and their sponsoring organizations.

The following documents, all of which are cited in the body of the report, are contained in this appendix:

Ames, R.B., and W.C. Malm (1999). Estimating the Contribution of the Mohave Coal-Fired Power Plant Emissions to Atmospheric Sulfur at Grand Canyon National Park. Submitted to *JAWMA*.

Eatough, D.J., R.J. Farber, and J.G. Watson (1999). Second Generation Chemical Mass Balance Source Apportionment of Sulfur Oxides and Sulfate at Grand Canyon during the Project MOHAVE Summer Intensive. *Accepted by JAWMA*.

Green, M.C., and I. Tombach (1999). Use of project MOHAVE Perfluorocarbon Tracer Data for Source Attribution Analysis. *Accepted by JAWMA*.

Henry, R.C. (1999) Perception of color in images of simulated haze. Report prepared by R. Henry 24017 Ingomar St., West Hills, CA 91304 for EPRI, January 4, 1999.

Karamchandani, P., Y. Zhang, and C. Seigneur (1999). Simulation of Sulfate Formation in the Mohave Power Plant Plume. Report CP026-98-1, prepared by Atmospheric and Environmental Research, Inc., San Ramon, CA, for EPRI.

Koracin D., J. Frye, and V. Isakov (1999) A method of evaluating atmospheric models using tracer measurements. Submitted to *J. of Applied Meteorology*.

Kuhns, H., M. Green, M. Pitchford, L. Vasconcelos, W. White, and V. Mirabella (1999). Attribution of Particulate Sulfur in the Grand Canyon to a Specific Point Source using Tracer-Aerosol Gradient Interpretive Technique (TAGIT). *Accepted by JAWMA*.

Mirabella, V.A. (1996a). Summary of MPP tracer dispersion modeling simulations, Latimer HAZEPUFF model – Project MOHAVE Summer Experiment. Memorandum to Project MOHAVE technical group, prepared by Southern California Edison. November 12.

Mirabella, V.A. (1996b). Supplemental Analysis: Latimer HAZEPUFF model, Project MOHAVE summer experiment. Memorandum to Project MOHAVE technical group, prepared by Southern California Edison. November 14.

Mirabella, V.A. and R. Farber (1999). Relating summer ambient particulate sulfur, sulfur dioxide, and light scattering to gaseous tracer emissions at the Mohave Power Project. Submitted to *JAWMA*.

Vimont, J. C. (1998). Evaluation of the CALMET/CALPUFF Modeling System using Project MOHAVE Tracer and Implications for Sulfate Concentrations. *Proceedings, Visual Air Quality, Aerosols & Global Radiation Balance*, A&WMA, Pittsburgh, pp. 436-446.

White, W.H., R.J. Farber, M.C. Green, E.S. Macias, V.A. Mirabella, M.L. Pitchford, and L.A. de P. Vasconcelos (1999). Tracking Regional Background in a Haze Attribution Experiment. *Accepted by JAWMA*.

Yamada, T. (1999). Numerical Simulations of Airflows and Tracer Transport in the Western Mountainous Area. *Accepted by J. Appl. Meteor.*